DOPPLER SATELLITE CONTROL

D. E. WELLS

September 1974

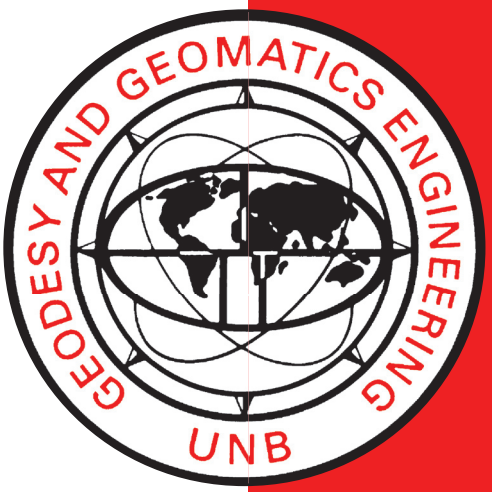

TECHNICAL REPORT
NO. 29

PREFACE

In order to make our extensive series of technical reports more readily available, we have scanned the old master copies and produced electronic versions in Portable Document Format. The quality of the images varies depending on the quality of the originals. The images have not been converted to searchable text.

DOPPLER SATELLITE CONTROL

by

David Ernest Wells

Department of Surveying Engineering

University of New Brunswick

Fredericton, N.B.

September, 1974

Reprinted June, 1975

Reprinted with Corrections April, 1976

Reprinted with Corrections December, 1977

Reprinted September 1981

PREFACE

This report is an unaltered* printing of the author's doctoral thesis, named "Electromagnetic metrology, Hilbert space optimization, and their application to Doppler satellite control", submitted to this department in September, 1974.

The principle thesis adviser for this work was Dr. E.J. Krakiwsky. During the last few months, while Dr. Krakiwsky was abroad on sabbatical leave, Dr. P. Vanicek ably filled in.

Details of financial support and other assistance rendered are given in the Acknowledgement.

*For the April 1976 reprinting, typographical errors on pages 118, 126 and 143, and factual errors on pages 45, 106, 109, 132 and 272 have been corrected.

For the December 1977 reprinting, changes to pages 50, 127, 129 and 131 were made.

ABSTRACT

The application of the Transit Doppler satellite system to geodetic positioning, is investigated, using the operational ephemeris for satellite coordinates, and navigation-type receivers to track the satellites. A set of test data from eight stations in Atlantic Canada is analyzed. Four a priori decisions were to use the shortest possible integration interval (4.6 seconds); to use the technique of translocation to reduce the effect of ephemeris and refraction errors; to allow the satellite trajectory to relax parallel to itself during the adjustment; and to process the data completely automatically.

Transit mathematical models are related to the basic principles of electromagnetic metrology. The assumptions involved in Transit mathematical models are analyzed in detail.

The least squares approximation, least squares spectral analysis and least squares estimation algorithms used here are related to the basic principles of Hilbert space optimization.

The accuracy of the operational ephemeris is investigated by comparing it to the NWL precise ephemeris; by comparison between stale and fresh ephemerides during injection passes; and Guier plane navigation. The operational ephemeris errors are found to be well represented by biases in the along track, radial, and cross track directions which have standard deviations (from pass to pass) of 26, 5, and 10 m respectively.

The shape of the operational ephemeris is investigated by a comparison between Transit and Keplerian orbit elements; time series

analysis of Transit variable orbit parameters; and least squares approximation of the Transit variable orbit parameters. The shape of each of the variable orbit parameters ΔE, Δa, η is well approximated by the base functions $\Phi = \{1, \cos 2nt, \sin 2nt, t\}$ where n is the satellite mean motion and t is time.

The measurement variances of three models of Transit navigation receiver are found to be 1.5, 4.0 and 10.0 counts^2 respectively for the ITT 5001, Marconi 722 and Magnavox 702.

The internal consistency of multipass point positioning station coordinates is found to be 1.3 m. However this is found to be optimistic, since the orbit was held fixed for these computations. The internal consistency of adjusted network coordinates is less than one metre, but again this is found to be optimistic.

The index of external consistency (rms value of Δ/σ_Δ) between independent point positioning solutions at one station are found to be 2.5 to 4.0 for point positioning when the orbit is fixed and 1.2 to 1.5 when the orbit is relaxed. The external consistency between two sets of point positioning solutions using data one year apart is 4.7, attributed principally to uncorrected pole motion effects. The external consistency between an adjusted Transit network and a terrestrial network is 1.6.

TABLE OF CONTENTS

TABLE OF CONTENTS - cont'd

TABLE OF CONTENTS - cont'd

LIST OF TABLES

LIST OF TABLES - cont'd

LIST OF FIGURES

LIST OF FIGURES - cont'd

ACKNOWLEDGEMENT

This work was partially funded by the Geodetic Survey of Canada, the Canadian Defence Research Board, the National Research Council of Canada, Shell Canada Limited, and the University of New Brunswick. I thank the Bedford Institute of Oceanography, and particularly C.S. Mason, for the generous policy of educational leave which permitted me to undertake this work.

The raw Doppler data used in Chapter 5 were provided by the Geodetic Survey of Canada. The precise ephemerides used in Chapter 4 were provided by the U.S. Naval Weapons Laboratory, through the good offices of the Canadian Mapping and Charting Establishment.

I have benefitted from earlier work on Doppler positioning in this department done (in chronological order) by J. Kouba, E.A. Ogunbayo, B.P. Kirkham, M.M. Nassar, D.B. Thomson, R.L. Wade, R.W. Kerslake, I.M. Udoffa, and J.E. Hagglund. Their work is noted in the references. Insights into the functioning of Transit receivers has been provided over the years by discussions with F. Blaha and S. Morvai of Canadian Marconi Company, P.D. Rodgers of JMR Instruments Inc., T.H. Stansell of The Magnavox Company, and A.D. Parsons and his co-workers at the Bedford Institute. Discussions with R.J. Anderle of the U.S. Naval Weapons Laboratory, H.D. Black of The Johns Hopkins University Applied Physics Laboratory, R.W. Smith and C.R. Schwarz of the U.S. Defense Mapping Agency, and particularly and most often J. Kouba of the Geodetic Survey of Canada have helped me to understand many of the more interesting aspects of Doppler positioning. I thank R.J. Anderle, J. Kouba and P. Martin for their critical review of this thesis.

My association with C.L. Merry, D.B. Thomson and M.M. Nassar at U.N.B. and R.M. Eaton and S.T. Grant at the Bedford Institute has been one of friendship and open exchange of ideas and constructive criticism. The self-realization of overwhelming ignorance, in my opinion the purpose of advanced education, is in my case the responsibility of two superb teachers, P. Vaníček and my supervisor, E.J. Krakiwsky.

Assistance beyond sibling responsibilities, including shelter and meals for eight months and her usual faultless typing job, were provided by Wendy Wells.

This work is dedicated to Solveig, whose patience and support, in the face of forced single parenthood, have exceeded what should be expected, even from a student's wife. The way of the sun is my sustenance.

CHAPTER 1

INTRODUCTION

1.1 Statement of the Problem

The purpose of this investigation is to consider the application of the Transit Doppler satellite system (also called the Navy Navigation Satellite System) to geodetic positioning, using the operational ephemeris (predicted satellite orbit parameters broadcast by Transit satellites), and AN/SRN-9 type ("navigation") receiving equipment.

Transit geodetic positioning using the U.S. Naval Weapons Laboratory precise ephemeris (satellite coordinates post-computed by fitting a 48 hour satellite arc to Doppler observations obtained by a worldwide tracking network) and AN/PRR-14 ("Geoceiver") receiving equipment, has demonstrated that control point coordinates can be determined from Transit observations with accuracies of about one metre (DOD, 1972; Hadgigeorge, 1972; Anderle, 1974).

While the NWL precise ephemeris more closely approximates actual satellite positions than the operational ephemeris, its use involves delays and perhaps added expense. A number of specifically geodetic receivers are now available, the measurements from which are superior to navigation receiver measurements. However when the data analyzed here was collected, the Geoceiver was the only geodetic receiver in use, and it is considerably more expensive than navigation receivers, and will provide operational ephemerides only when interfaced to a computer.

Preliminary results using the operational ephemeris and navigation receivers (Krakiwsky, Wells and Kirkham, 1972; Krakiwsky, Wells and Thomson, 1973) indicate that Transit determined interstation distances agree with terrestrially surveyed interstation distances within about two metres on average. However these results were obtained using a Doppler integration interval of two minutes, and assuming the operational ephemeris to perfectly represent the actual satellite trajectory. Also much manual processing and checking of the data was involved, a simplified tropospheric refraction correction was employed, and the effect of polar motion was not taken into account.

1.2 Outline of Treatment

The work reported here is divided into the three parts suggested by the title. Chapter 2 discusses the Doppler measurements made by both navigation and geodetic Transit receivers, and places these measurements in the context of other electromagnetic measurements made in surveying. This discussion is developed beginning with the basic principles of electromagnetic metrology.

Chapter 3 discusses the three applications of least squares optimization used in this work (least squares approximation, least squares spectral analysis, and least squares estimation), developing the algorithms for these three applications from the basic principles of Hilbert space optimization.

Chapters 4, 5 and 6 discuss the application of Transit Doppler measurements to geodetic positioning, using the operational ephemeris and navigation receivers. To minimize the effect of operational ephemeris and navigation receiver deficiencies, four a priori decisions were made:

(a) The quantity of data from a given satellite pass was maximized by

using the shortest possible Doppler integration interval (about 4.6 seconds). This requires the computation of satellite positions in between those provided at two minute intervals by the operational ephemeris. This is treated as a least squares approximation problem in Chapter 4.

(b) The effect of ephemeris and uncorrected refraction errors was reduced by using the technique of translocation (computing the interstation vectors between simultaneously tracking receivers, rather than the position vectors of each).

(c) The satellite trajectory defined by the operational ephemeris was permitted to assume a new position parallel to the orbit defined by the operational ephemeris, in accordance with appropriate bias parameters and their variances, discussed in Chapter 4.

(d) Automatic processing of the data was implemented. Algorithms to automatically correct the data for tropospheric and ionospheric refraction are discussed in Chapter 2. Algorithms to automatically identify each pass and correct for polar motion are discussed in Chapter 4. Algorithms to automatically filter out noisy passes and noisy Doppler measurements within accepted passes, are discussed in Chapter 5. As described in Chapter 4 the plane containing the tracking station and the satellite velocity vector at closest approach for a particular pass is the "natural" coordinate system for Transit measurements, and it was decided to perform much of the Doppler and pass filtering in this coordinate system.

1.3 Summary of Contributions

As a guide to the reader, this section presents the goals set by the author for each of the remaining five chapters, and lists what, in the author's opinion, are the original contributions contained in each chapter.

The goal of Chapter 2 is to relate the navigational and geodetic

Transit mathematical models to the basic principles of electromagnetic metrology. Transit phase measurements are compared to phase measurements made by other electromagnetic surveying systems (2.1, 2.2). The assumptions involved in Transit mathematical models are analyzed in detail (2.2.2, 2.2.3). The computational efficiency obtainable with the Hopfield tropospheric refraction correction model is analyzed (2.3.2). Other models are compared to the Hopfield model (2.3.3).

The goal of Chapter 3 is to relate the least squares optimization algorithms used here to the basic principles of Hilbert space optimization. Least squares estimation is developed from functional analysis principles (3.1, 3.2). Differences between the phased and sequential algorithms for stepwise least squares estimation are analyzed (3.3.3).

The goal of Chapter 4 is a systematic investigation of the accuracy and shape of the operational ephemeris. Guier's theorem is applied to the problem of geodetic position determination (4.2), including the development of an algorithm for obtaining Guier plane coordinates (4.2.1). An algorithm to identify the operational ephemeris was developed (4.3). A simple alert algorithm was developed (4.3.2).

The goal of Chapter 5 is to demonstrate the accuracy of Transit geodetic positioning using the operational ephemeris and navigation receivers. A set of flexible, automatic, reasonably efficient programs providing the facility for complete analysis of Transit data was developed (5.2). The performance and costs involved in using these programs are documented (5.2). The performance of some currently available navigation receivers is analyzed (5.3, 5.4). A test set of Transit data is thoroughly analyzed (5.3, 5.4).

The goal of Chapter 6 is to assess the decisions upon which the results of Chapters 4 and 5 depend. Alternatives to these decisions are

discussed. Conclusions are drawn. Recommendations are made.

CHAPTER 2

ELECTROMAGNETIC METROLOGY

The metric properties of physical space are based on the velocity of propagation of electromagnetic energy in a vacuum, both in Newton's (classical) model and in Einstein's (relativistic) model of physical space.

It is thus natural that the metrology of physical space depend heavily on observations involving electromagnetic propagation. It is also expected that the principal difficulty in electromagnetic metrology arises when the propagation medium is not a vacuum, and its propagation characteristics (refraction characteristics) must be accounted for.

Very few surveying measurements (principally those involving the magnitude, gradient and variations of gravity) do not involve electromagnetic propagation, and therefore the problem of refraction. The two basic electromagnetic survey measurement techniques involve respectively alignment of an optical instrument (measurement of horizontal and vertical angles to terrestrial and extraterrestrial targets, and spirit levelling), and the measurement of the difference in phase between two electromagnetic signals (electromagnetic distance measurements and radio positioning).

Here we are concerned with a particular radio positioning system, the Transit Doppler satellite system. In this chapter we first place the Transit system in perspective by reviewing the basic principles of all electromagnetic survey measurements. Then Transit observations are described, and finally techniques for coping with refractive effects on observations are discussed.

2.1 Electromagnetic Survey Measurements

2.1.1 Basic definitions

In this section we define the terms which we will use to discuss electromagnetic metrology. The source of many of these definitions is (IEEE, 1972).

The base units defined in the International System of Units (CSA, 1973) in terms of adopted values for specific natural phenomena are the base units of metrology. At present these are seven in number: metre, kilogram, second, ampere, Kelvin, mole, candela. We are particularly interested in the metre and the second, presently defined:

> "The metre is the length equal to 1 650 763.73 wavelengths in vacuum of the radiation corresponding to the transition between the levels $2p_{10}$ and $5d_5$ of the $Krypton^{86}$ atom." (CGPM, 1960).

> "The second is the duration of 9 192 631 770 periods of the radiation corresponding to the transition between the two hyperfine levels of the ground state of the $Cesium^{133}$ atom." (CGPM, 1967).

A disturbance which is a function of time or space or both we call a wave. A periodic wave is a wave in which the disturbance is repeated in detail, either at a fixed point after the lapse of time known as the period, P, or at a fixed time after the addition of a distance known as the wavelength, λ, or both. Periods are measured relative to the adopted value for the $Cesium^{133}$ atom, that is in seconds. Wavelengths are measured relative to the adopted value for the $Krypton^{86}$ atom, that is in metres.

The phase of a time-periodic wave is the fractional part t/P of the period P through which time t has advanced relative to an arbitrary time origin. The frequency of a periodic wave is the reciprocal of its period, $f = 1/P$. The angular frequency is $\omega = 2\pi f$. The phase constant is $k = 2\pi/\lambda$.

A periodic wave which has both period and wavelength, that is which is periodic both in time and space, is said to propagate through the medium in which the spatial periodicity is measured. The ratio of the wavelength λ to the period P is the propagation velocity

$$v = \lambda/P = f\lambda = \omega/k \quad .$$

A periodic wave in which the disturbance is adequately modelled by a sinusoidal function of space or time or both is a sinusoidal wave. An example of a plane sinusoidal wave propagated with period P and wavelength λ is

$$y = A \sin 2\pi(t/P + x/\lambda + \theta_o) \qquad (2\text{-}1)$$

where y is the magnitude of the wave (disturbance) at time t after some time origin, and distance x from some space origin; θ_o is the phase of the wave at $t = x = 0$; and A is the amplitude (maximum magnitude) of the wave. The phase at (t,x) is

$$\theta = t/P + x/\lambda + \theta_o \quad .$$

The phase angle at (t, x) is $2\pi\theta$.

A wave may be composed of two or more constituent waves, each having a different frequency. The distribution of the amplitudes of these constituents as a function of frequency is the frequency spectrum of the wave. A wave whose spectrum consists of one or more continuous ranges of frequencies is said to consist of frequency bands. The differences between the limiting frequency values for each band is the bandwidth. A band whose bandwidth is sufficiently narrow that it can be modelled by a single frequency is called a spectral line. A wave whose spectrum consists of a single line is monochromatic.

Electromagnetic waves are waves in which the disturbance is electromagnetic in nature. Metrologically useful electromagnetic waves are sinusoidal and monochromatic or have a small number of spectral

lines, The wavelengths of electromagnetic waves depend on certain properties of the medium in which the wave is propagating, called the refraction properties of the medium. Because the wavelength depends on the refraction characteristics of the medium, so does the velocity. In a vacuum the velocity is

$$c = \lambda_{vac}/P = f\,\lambda_{vac} = \omega/k_{vac} \quad . \qquad (2\text{-}2)$$

The International Scientific Radio Union passed the following resolution at its XIIth General Assembly in 1957 (URSI, 1957):

> "In view of the progress made since the XIth General Assembly in the measurement of the velocity of electromagnetic waves, it is recommended that in radio engineering problems its value in vacuum be taken as 299 792 500 ± 400 m/s."

The International Union of Geodesy and Geophysics subsequently passed a similar resolution (IUGG, 1958). The three adopted values defining the metre, the second, and the vacuum velocity of propagation, are not independent. It has recently been shown (Evenson et al., 1972) that the inconsistency between them, expressed in velocity units, is 44 m/s. This means use of the adopted value for c in scaling electromagnetic time interval measurements into metres results in a world too large by about 0.15 ppm relative to the metre definition. This inconsistency will eventually be resolved by redefinition of the metre, since the Krypton metre standard is now known to have a disadvantage unknown at the time it was accepted as the length standard (Rowley and Hamon, 1963). In June, 1973 the Consultative Committee for the Definition of the Metre (CCDM) recommended that the value 299 792 458 m/s ± 4 parts in 10^9 be used for c; that further work is needed before the metre is redefined; and that even if the metre is eventually redefined in terms of an adopted value for c, that the metre remain a base unit of SI (maintaining dimensional if not physical

independence). These recommendations were approved by the CIPM in October, 1973 (Terrien, 1974a; 1974b).

For propagation media other than a vacuum, the refraction characteristics are usually expressed in terms of the index of refraction

$$n = c/v = \lambda_{vac}/\lambda = k/k_{vac} \qquad (2\text{-}3)$$

or the refractivity

$$N = (n-1)* 10^{6} . \qquad (2\text{-}4)$$

A medium in which the wavelength (and thus the velocity, index of refraction and refractivity) is a function of frequency is a dispersive medium. Dispersion is discussed in Section 2.1.2.

A medium in which the wavelength, velocity, index of refraction and refractivity are functions of position and time is a nonhomogeneous medium. Nonhomogeneity is discussed in Section 2.1.3.

The particular aspect of electromagnetic metrology with which we are concerned involves measurement of phase differences (or equivalently time intervals) between different electromagnetic waves, and the scaling of these measurements into metres, using the propagation velocity as the scaling factor. Phase measurements are discussed in Section 2.1.4.

The particular system with which we are concerned is the Transit Doppler satellite system. Electromagnetic waves propagated between the Transit satellites and tracking receivers involve the Doppler effect, since transmitter and receiver are in relative motion. The Doppler effect is discussed in Section 2.1.5. Transit phase measurements are discussed in Section 2.2. Transit electromagnetic waves propagate through the earth's ionosphere and troposphere, both of which are dispersive and non-homogeneous. Tropospheric effects on Transit measurements are discussed in Section 2.3. Ionospheric effects are discussed in Section 2.4.

2.1.2 Dispersion

Any propagation medium other than a vacuum, be it gas, liquid, solid or plasma, contains charge carriers (electrons and protons) having electric fields which interact with any externally applied field. These charge carriers are in motion (electrons spinning and orbiting around nuclei), causing magnetic moments which interact with any externally applied magnetic field. The existance of such interactions dissipates the external field (attenuation) and the finite interaction time required to change the position or motion of the charge carriers retards the propagation of the external field through the medium. Exceptions to these statements occur when the energy (frequency) of the external field exactly matches the energy (frequency) of an atomic interaction, in which case a phenomenon called resonance occurs. At frequencies close to such a resonance the external field and charged particles interact to such an extent that the propagation velocity is affected, and the medium exhibits dispersion.

On a macroscopic level, the behaviour of a medium in retarding an electric field is characterized by a parameter called the permittivity; the behaviour in retarding a magnetic field by the permeability; and the behaviour in attenuating an electric field by the conductivity. The velocity of propagation through a medium can be expressed as

$$v = 1/\sqrt{\mu\varepsilon} \quad , \tag{2-5}$$

where ε is the permittivity (in Farad/metre) and μ the permeability (in Henry/metre). The permittivity and permeability of free space (a vacuum) are respectively

$$\varepsilon_o \simeq 8.85 \times 10^{-12} \text{ F/m} \quad ,$$

$$\mu_o = 4\pi \times 10^{-7} \text{ H/m} \quad ,$$

so that the refractive index of a medium can be expressed

$$n = c/v = \sqrt{\varepsilon\mu/\varepsilon_o\mu_o} \quad . \tag{2-6}$$

The velocity we have considered so far is the phase velocity. In a dispersive medium we must consider a second propagation velocity called the group velocity. If we superpose two waves of equal amplitude but slightly different period and wavelength, say

$$y = A \sin(\omega t + kx) + A \sin((\omega + \Delta\omega)t + (k + \Delta k)x) \quad , \tag{2-7}$$

then from the identity

$$\sin\alpha + \sin\beta = 2 \sin\frac{1}{2}(\alpha + \beta) \cos\frac{1}{2}(\alpha - \beta) \quad , \tag{2-8}$$

we have

$$y = 2A \sin(\bar{\omega}t + \bar{k}x) \cos(\frac{\Delta\omega}{2} t + \frac{\Delta k}{2} x) \quad , \tag{2-9}$$

where $\bar{\omega} = \omega + \frac{\Delta\omega}{2}$, $\bar{k} = k + \frac{\Delta k}{2}$ are the mean values. This combined wave consists of a wave very much like either of the original waves (the first cosine term) having a velocity (the phase velocity)

$$v_p = \bar{\omega}/\bar{k} \quad , \tag{2-10}$$

and a wave which modulates this original wave (the second cosine term) having a velocity (the group velocity)

$$v_g = \Delta\omega/\Delta k \quad . \tag{2-11}$$

As the two original frequencies approach each other, we obtain, in the limit

$$v_p = \omega/k \qquad \text{and} \qquad v_g = d\omega/dk \quad . \tag{2-12}$$

Setting $\omega = v_p k$ we have

$$v_g = v_p + k \frac{dv_p}{dk} \quad , \tag{2-13}$$

or, from $k = 2\pi/\lambda$

$$v_g = v_p - \lambda \frac{dv_p}{d\lambda} \quad , \tag{2-14}$$

or

$$v_g = v_p/(1 - \frac{1}{\lambda} \frac{dv_p}{df}) \quad , \tag{2-15}$$

from which we see that for a non-dispersive medium $(\frac{dv_p}{dk} = \frac{dv_p}{d\lambda} = \frac{dv_p}{df} = 0)$

we have $v_g = v_p$.

When a transmitter is first turned on in a dispersive medium, it is the group velocity that governs the time of travel of the wavefront, and thus it is the velocity at which energy or information is propagated. The group velocity cannot exceed the vacuum velocity c, however it is possible for the phase velocity to do so. Corresponding to the group and phase velocities are the group and phase indices of refraction

$$n_g = c/v_g, \quad n_p = c/v_p \quad . \tag{2-16}$$

If the dispersive medium has resonances at frequencies f_i, with corresponding vacuum wavelengths $\lambda_i = c/f_i$, then the phase refractive index is given by Sellmeier's Equation

$$(n_p^2 - 1) = \sum_i \frac{A_i \lambda^2}{\lambda^2 - \lambda_i^2} \quad . \tag{2-17}$$

At wavelengths which are sufficiently longer than any resonance wavelengths so that we can ignore higher powers of λ_i/λ we can approximate Sellmeier's Equation by Cauchy's Equation (Jenkins and White, 1957)

$$n_p = A + \frac{B}{\lambda^2} + \frac{C}{\lambda^4} \tag{2-18}$$

Given the phase refractive index we compute the group refractive index from

$$n_g = n_p - \lambda \frac{dn_p}{d\lambda} \quad . \tag{2-19}$$

2.1.3 Nonhomogeneity

Given two points in an electromagnetic propagation medium with refractive index n, we noted at the beginning of the chapter that the two basic electromagnetic measurements involving these points are the path length between them, and the path direction to one point measured at the other (with respect to some coordinate system). Let us define

two electromagnetic path lengths and end point path directions. The path length which would have been measured if the propagation medium had been a vacuum, and assuming the vacuum propagation velocity c, is the geometric distance. The path length measured in the actual (non-vacuum) medium, but still assuming the vacuum velocity c, is the apparent distance. The analogous directions are the geometric direction and apparent direction.

For a homogeneous medium, $n \neq n(x, t)$ the effect on path length is to scale apparent distances larger than geometric distances by the factor n. Geometric distances can be recovered from apparent distances if the single value for n is known. Both geometric and apparent paths are geodesics in Euclidean space. Geometric and apparent directions are identical.

For a non-homogeneous medium, $n = n(\mathbf{x}, t)$ is a scalar field, and the electromagnetic path is a geodesic not in Euclidean space, but in a space for which the metric tensor is $n\delta_i^j$ (where δ_i^j is the unit tensor). This is Fermat's Principle, another statement of which is that the electromagnetic path is that path for which the path length

$$\Lambda = \int n ds \qquad (2\text{-}20)$$

is a minimum. The effect of nonhomogeneity on path length is to introduce a position and time dependent scale difference between geometric and apparent distances. To recover geometric distances from apparent distances we must somehow determine the average propagation velocity over the path being measured. The effect of nonhomogeneity on path direction is to introduce a difference between the geometric and apparent directions.

The physical space of most interest to electromagnetic survey measurements is the earth's troposphere. The primary feature of the tropospheric $n(x, t)$ is its vertical lapse rate, for which adequate

predictive models have been developed (see Section 2.3). The secondary feature of n(x, t) is its horizontal variability which is more difficult to model. The vertical lapse rate introduces a curvature into electromagnetic paths which are nearly horizontal, which is usually represented by the coefficient of refraction

$$K = R/\sigma \qquad (2\text{-}21)$$

where R is the distance to the geocentre and

$$\frac{1}{\sigma} = -\frac{1}{n}\frac{dn}{dh}\cos E \qquad (2\text{-}22)$$

where E is the elevation angle of the path above the horizon, and -dn/dh is the vertical lapse rate of n.

2.1.4 Phase Difference Measurements

In this subsection we consider the phase difference measurements involved for the following: electromagnetic distance measurements; ranging, hyperbolic and rho-rho radio positioning systems; and the Transit system. In all cases measured phase differences are scaled into seconds by the period of the phase comparison signal, which must be known relative to the definition of the second. The oscillator from which this signal is obtained is thus the time standard for the measurement. The observations are then scaled from seconds into "apparent" metres by the vacuum velocity c, and thence into "geometric" metres by some average index of refraction. Of these three scaling operations, it is the last which limits the accuracy of electromagnetic survey measurements.

Given a set of observation points, let us designate those points from which electromagnetic signals are broadcast as transmitters, and those at which electromagnetic signals are detected as receivers. A particular point may be either a transmitter or receiver or both. A

point which detects a signal and retransmits it with zero or constant phase change is a reflector.

EDM involves two combined transmitters/receivers, one of which is a reflector or slave, the other being called the master. The master transmits a signal which propagates along the measured path, is reflected, and is received and phase compared with the transmitted signal.

If we add at least one more slave (reflector), and place the slaves at known locations, then we have a ranging radio positioning system with which the master can be located in a two dimensional coordinate system. If the master transmitter is also placed at a known location then any number of receivers can be positioned by measuring the phase differences between the received master signal and each of the received slave signals, and we have a hyperbolic radio positioning system (lines of equal range difference from a pair of known positions are hyperbolas).

In all the above configurations the transmitted master signal is available at all points and for all measurements, and the oscillator which generates the master signal is the measurement time standard, all receivers (including slaves) being locked in frequency to the master signal.

If we abandon the condition that the master oscillator be the only time standard, then we remove the distinction between master and slaves, and are left only with transmitters (at known locations) and receivers (at unknown locations). Each transmitter and each receiver is provided with its own time standard, and all time standards must be synchronized. Each receiver then measures the phase differences between the phase of its own time standard and the phases of the received signals from each of the transmitters, each such measurement being a range measurement. This configuration is called a rho-rho radio positioning system.

The Transit system embraces aspects of both hyperbolic and rho-rho systems. The known satellite trajectory can be considered as a sequence of known transmitter locations having a common time standard, and therefore generating a set of hyperboloids of position. Some Transit tracking receivers have independent time standards. Either the satellite or receiver time standard may be used as the measurement time standard, and in the latter case, the receiver and satellite time standards must be synchronized (Section 2.2.2).

To put the discussion of Transit timing requirements in perspective (Section 2.2), here we develop an analysis of the time standard precision requirements for rho-rho, ranging and hyperbolic systems.

Consider the phase of the time standards at a transmitter and at a receiver at three epochs which we will call calibration time, transmission time, and reception time.

At calibration time, $t = 0$ let the periods of the time standards be P_T^c and P_R^c respectively, and their phases be ϕ_T^c and ϕ_R^c respectively. Let us express the relative phase in seconds by

$$\alpha = (\phi_R^c - \phi_T^c)\, P_R^c \tag{2-23}$$

and the relative period difference, in fractional parts by

$$\beta = (P_T^c - P_R^c)/P_T^c \tag{2-24}$$

Let us suppose that both the transmitter and receiver time standard frequencies are changing linearly with time at different rates, say

$$\frac{1}{P_T(t)} = \frac{1}{P_T^c}(1 + 2\gamma_T\, t) \tag{2-25}$$

$$\frac{1}{P_R(t)} = \frac{1}{P_R^c}(1 + 2\gamma_R\, t) \tag{2-26}$$

Now at some arbitrary time t the phase of either time standard is given by

$$\phi(t) = \phi^c + \int_o^t \frac{dt}{P(t)} = \phi^c + \frac{t}{P^c} + \frac{\gamma t^2}{P^c} \quad . \tag{2-27}$$

Let us specify that the phase of the signal broadcast by the transmitter at transmission time t_1 be equal to the phase of the same signal detected by the receiver at reception time t_2. Then $(t_2 - t_1)$ is the time of travel of this signal between transmitter and receiver. The measured phase difference between the incoming signal and the receiver time standard then is

$$\begin{aligned}
\Delta\phi &= \phi_R(t_2) - \phi_T(t_1) \\
&= \phi_R^c + \frac{t_2}{P_R^c} + \frac{\gamma_R t_2^2}{P_R^c} - \phi_T^c - \frac{t_1}{P_T^c} - \frac{\gamma_T t_1^2}{P_T^c} \\
&= (\phi_R^c - \phi_T^c) + \left(\frac{t_2}{P_R^c} - \frac{t_1}{P_T^c}\right) + \left(\frac{\gamma_R t_2^2}{P_R^c} - \frac{\gamma_T t_1^2}{P_T^c}\right) \\
&= \frac{1}{P_R^c}\left[(t_2 - t_1) + \alpha + \beta t_1 + \gamma_R t_2^2 - \gamma_T t_1^2 + \beta\gamma_T t_1^2\right] \quad .
\end{aligned} \tag{2-28}$$

Assuming the frequency drift rates and relative period difference are all small (β, γ_R, $\gamma_T \ll 1$) then

$$\Delta\phi = \frac{1}{P_R^c}\left[(t_2 - t_1) + \alpha + \beta t_1 + (\gamma_R - \gamma_T)\, t_1^2\right] \quad . \tag{2-29}$$

Scaling this measured phase difference into seconds using the current receiver time standard period we have

$$P_R(t_2)\,(1 + 2\gamma_R t_2)\Delta\phi = (t_2 - t_1) + \alpha + \beta t_1 + (\gamma_R - \gamma_T)\, t_1^2 . \tag{2-30}$$

This is the observation equation for rho-rho system range measurements. It is evident that an error in the calibration of the relative phase of the two time standards (an error in α) produces a constant error in range (travel time). An error in the calibration of the relative

period difference (an error in β) produces a spurious velocity. An error in the knowledge of the rate at which the relative frequency is changing (an error in $\gamma_R - \gamma_T$) produces a spurious acceleration. An error in the knowledge of the receiver time standard period at calibration time, relative to the definition of the second (an error in P_R^c), or an error in the knowledge of the rate at which the receiver time standard frequency is changing with respect to the definition of the second (an error in γ_R) produces an incorrect scaling of the measured phase difference into seconds. We will be scaling the measured range from seconds to metres using a propagation velocity which is approximately 3×10^8 m/s.

Therefore for example, to maintain a ranging accuracy of 300 metres at ranges of 500 km for up to one day after calibrating, we must know α to within 10^{-6} sec, β to within 1 part in 10^{11}, $(\gamma_R - \gamma_T)$ to within 1 part in 10^{11} per day, P_R^c to within 6 parts in 10^4, and γ_R to within 1 part in 10^6 per day. For this reason both transmitters and receivers in rho-rho systems use Cesium clocks as time standards, for which γ is normally zero, and which are capable of β values of a few parts in 10^{12}. Even so, maintaining an adequate calibration is not simple (Grant, 1973).

To obtain the observation equation for a ranging system, we recall that the master transmitter and receiver use the same time standard, and the slave acts simply as a reflector, so that $\alpha = \beta = 0$ and $\gamma_R = \gamma_T$ and we have

$$P(t)\ (1+2\gamma t_2)\Delta\phi = t_2 - t_1 \qquad (2\text{-}31)$$

where in this case the travel time measures twice the master/receiver to slave range. Now the time standard requirements are that the period at calibration time (P^c) be known relative to the definition of the second, and that the drift rate (γ) be known or be sufficiently small to be ignored. The stability of quartz crystal oscillators is well in excess

of the present limit of precision of radio positioning, which is about 50 ppm, so that γ is usually ignored.

For hyperbolic systems we have the same observation equation as for ranging systems, except that the travel time now measures the difference between the master-receiver and slave-receiver ranges.

The frequency spectrum of electromagnetic waves can be divided into three general divisions: The region in which radiation is best described as particles of energy called photons (gamma and X-rays); the region in which radiation has sensible physiological effects (ultraviolet, visible and infrared regions); and the region in which it is possible to generate and propagate waves electronically (Figure 2-1).

EDM instruments use visible, infrared and microwave frequencies. Radio positioning systems use microwave and radio frequencies. Lower frequency systems in general have longer range and lower accuracy. The Transit system uses 150 MHz (VHF) and 400 MHz (UHF) signals.

2.1.5 The Doppler effect

We have so far assumed that our transmitters and receivers have been stationary with respect to the propagation medium. Let us consider the effect of their motion (Figure 2-2).

Let a transmitter T have a velocity u_T and a receiver R a velocity u_R. Let the propagation medium be a vacuum, with constant propagation velocity c. At transmission time t_1 a signal is emitted from T. Let R be at a distance s from T at t_1. Let this signal be received at R at reception time t_2. If u_R is constant over the interval $t_2 - t_1$ then R will have travelled a distance $u_R(t_2 - t_1)$, and the signal will have travelled a distance $c(t_2 - t_1)$ (Gill, 1965). (For an alternative, perhaps more satisfying derivation, see Moller (1952)).

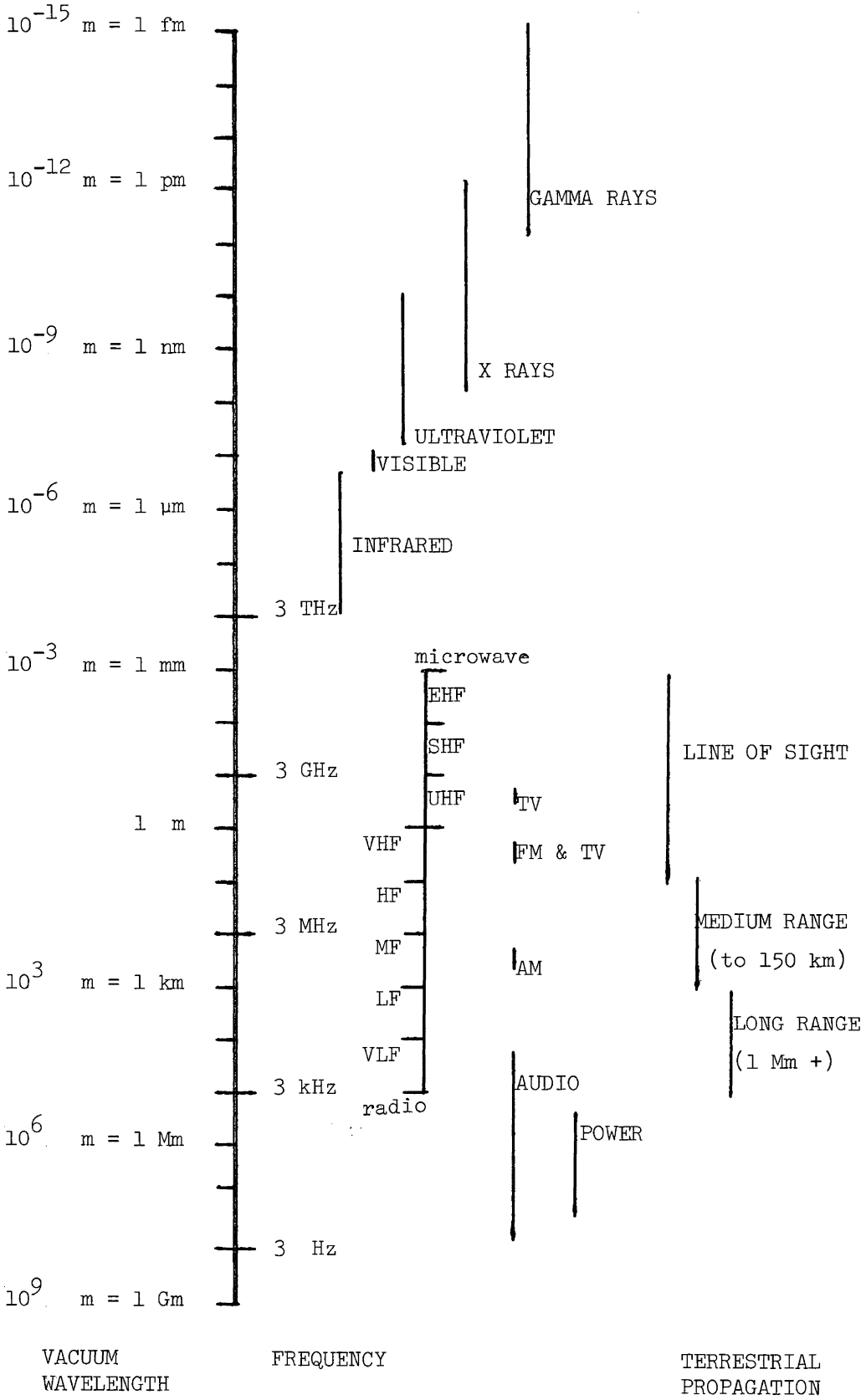

FIGURE 2-1

Electromagnetic Frequency Spectrum

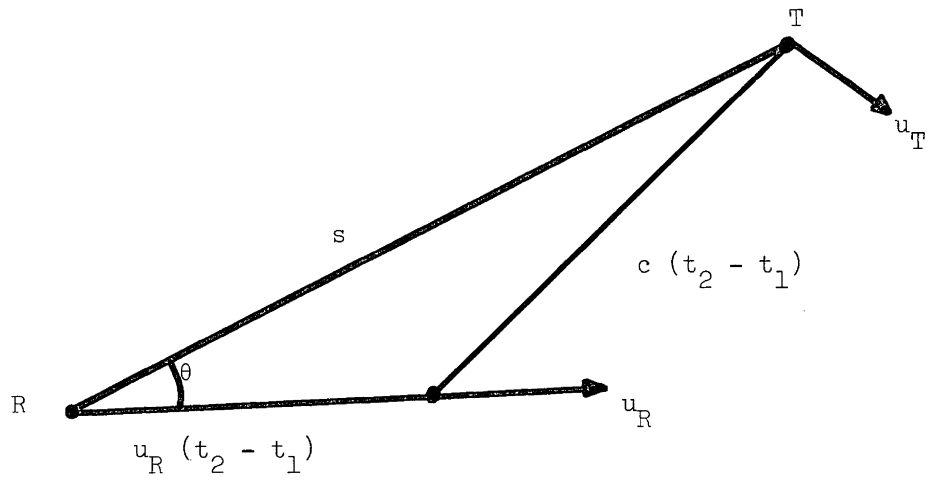

FIGURE 2-2

Doppler Effect Geometry

From the cosine law

$$c^2(t_2-t_1)^2 = u_R^2(t_2-t_1)^2 + s^2 - 2su_R(t_2-t_1)\cos\theta \ , \qquad (2\text{-}32)$$

or

$$t_2-t_1 = \frac{s}{c^2 - u_R^2}\{\sqrt{c^2-u_R^2\sin^2\theta} - u_R\cos\theta\}. \qquad (2\text{-}33)$$

Differentiating with respect to t_1

$$dt_2 = dt_1\{1 + \frac{d}{dt_1}[\frac{s}{c^2-u_R^2}(\sqrt{c^2-u_R^2\sin^2\theta} - u_R\cos\theta)]\} \ . \qquad (2\text{-}34)$$

If the period of the transmitted signal is sufficiently short that s and u_R can be assumed constant over one period then we have

$$P_R = P_T\{1 + \frac{d}{dt_1}[\frac{s}{c^2-u_R^2}(\sqrt{c^2-u_R^2\sin^2\theta} - u_R\cos\theta)]\} \ . \qquad (2\text{-}35)$$

If the receiver velocity u_R is small compared to the propagation velocity c

$$P_R = P_T\{1 + \frac{1}{c}\frac{ds}{dt_1}\} \ , \qquad (2\text{-}36)$$

or in terms of frequency

$$f_R = f_T \left\{ 1 + \frac{1}{c} \frac{ds}{dt_1} \right\}^{-1} . \qquad (2\text{-}37)$$

If the relative velocity ds/dt_1 is small compared to the propagation velocity c

$$f_R = f_T \left\{ 1 - \frac{1}{c} \frac{ds}{dt_1} \right\} . \qquad (2\text{-}38)$$

We have assumed throughout this development that both special and general relativistic effects can be ignored. This is valid if (a) all quantities (f_T, f_R, and ds/dt_1) are measured in the same reference frame or (b) the velocities u_T and u_R are sufficiently small to ignore special relativity effects (time dilation), and the gravity potentials at T and R are sufficiently equal that general relativity effects (gravitational red shift) can be ignored. We will return to this question in section 2.2.3.

2.2 Transit Doppler Positioning

The particular radio positioning system we are concerned with is the Transit Doppler satellite system, also called the U.S. Navy Navigation Satellite System. This has been described in, for example, Guier and Weiffenbach (1960), Newton (1967), and Stansell (1971). In this section we first consider the data made available to the user by the Transit system, then the measurements made by various Transit receivers.

The relationship between any set of measurements and the complete set of parameters from which (if perfectly known) the measured values could be predicted is the mathematical model for those measurements. These parameters fall into three categories, (a) those which can be adequately estimated independently of the measurements, (b) those which can be adequately estimated only from the measurements, and (c) those which cannot be estimated, either because their existance is not suspected, or the form of their contribution to the mathematical model cannot be deduced or analytically expressed. We are powerless to deal with (c). If we separate the treatment of (a) and (b), then the mathematical model including

the measured values and (a) is the reduction equation, the effect of which is to reduce or correct the measurements for the effects of (a). The mathematical model containing the reduced values and (b) is the observation equation, the effect of which is to estimate values for the parameters (b). It is sometimes difficult to decide whether a particular parameter should be included in (a) or (b), and sometimes a parameter is included in both (a) (nominal reduction) and (b) (estimated residual reduction).

In this context, Transit observation equation parameters include the satellite and tracking station coordinates, and usually the frequency difference between the satellite and tracking station reference oscillators. Transit observation equations are discussed in section 2.2.2. Transit reduction equations include corrections for tropospheric and ionospheric refraction. These are discussed in sections 2.3 and 2.4. For work of the highest precision there are several less significant parameters which may be included in either the reduction or observation equations. For example, Brown and Trotter (1969) incorporate additional terms for bias and drift for each of the satellite and receiver oscillators; special relativity; general relativity; residual tropospheric refraction; propagation delay; and nominal and residual interstation timing bias. Many of these terms are applicable only when the receiver oscillator is used to drive a local clock (section 2.2.2). Others of these terms are discussed in section 2.2.3.

2.2.1 Data broadcast by Transit satellites.

Transit satellites broadcast two stable harmonically related carrier frequencies at 150 MHz and 400 MHz. The ground station Doppler satellite receiver measures the amount by which these stable frequencies have been changed owing to the Doppler frequency shift caused by the

relative velocity between satellite and ground station. There are many ways of measuring this Doppler shift. At least three are in current use. The AN/BRN-3 submarine receivers and the original TRANET Doppler satellite tracking network (Dunnell, 1967) receivers measure an "instantaneous" Doppler shift. The AN/SRN-9 and other navigation receivers measure an integrated Doppler count, where the integration interval is gated by timing signals from the satellite. The AN/PRR-14 Geoceiver and other geodetic receivers measure an integrated Doppler count, gated either by satellite timing signals or local clock timing signals. Navigation and geodetic receiver measurements are discussed in section 2.2.2.

Transit satellites also transmit a series of digital signals by imposing balanced digital phase modulations on the carriers. The timing of these phase modulations is controlled by the satellite time standard, so that they can be used as timing signals. The pattern of these digital signals is repeated every 120 seconds, and consists of 6103 binary bits organized into words of 39 bits each and groups of six words (234 bits) each. The duration of one such group then is 234 x 120/6103=4.601015894... seconds. This is the shortest Doppler integration interval currently used with commercial navigation or geodetic receivers. Any multiple of this 4.6 second interval, or 120 seconds, can be used for integration.

Parameters describing the satellite orbit are contained in the last word in each group of six words. There are twenty-five such words in all in each two minute message, and the set of parameters they contain are called the operational ephemeris, which is discussed in more detail in Chapter 4. These parameters are decoded by the receiver and can be used to compute predicted satellite coordinates at two-minute intervals.

During a single pass, a Transit satellite may stay above the horizon for as long as 18 minutes, so that a maximum of nine two-minute integrated Doppler observations, or more than 200 4.6 second integrated

Doppler observations, may be obtained.

2.2.2 Transit Doppler observation equations

In this section we consider the measurements made by Transit receivers, and how these measurements can be incorporated into an observation equation. We consider two classes of receivers, those designed for the navigation and geodetic applications. The difference between the two is that for geodetic receivers the measurement precision is improved by using the receiver reference oscillator to drive a local clock, the output of which becomes part of the measurement process in one of several possible ways. The data analyzed in Chapter 5 was produced by navigation receivers, and we first describe the navigation receiver observation equation and measurements. We then consider the measurements made by three particular geodetic receivers, and some of the possible alternative observation equations. In section 2.2.3 we return to a more detailed consideration of the navigation observation equation used here.

The Transit Doppler observation process attempts to relate measurements recorded at a sequence of epochs τ_i to a set of (known) satellite positions given for a sequence of epochs t_i, and in the case where the receiver is moving, to a set of receiver positions (known relative to one another) for a sequence of epochs T_i. Therefore we could conceivably have three different time scales, τ_i, t_i and T_i. For geodetic positioning we are interested only in stationary receivers so that we will not consider the T_i time scale here.

We can relate the τ_i and t_i time scales via satellite-transmitted time marks, by making two assumptions. Firstly that the measurements are made (the τ_i time scale) at the epochs at which these time marks arrive at the receiver (assumption one). Secondly that the satellite ephemeris positions (the t_i time scale) are given for the epochs at which the time

marks are transmitted (assumption two).

Let the satellite transmit two time marks at times t_1 and t_2 and at these times let the satellite-to-receiver distances be s_1 and s_2 respectively. Assuming the vacuum propagation velocity c (assumption three), these signals will arrive at the receiver at times $\tau_1 = t_1 + s_1/c$ and $\tau_2 = t_2 + s_2/c$. If during the interval t_1 to t_2 the satellite transmits a frequency f_s, and if we assume a non-relativistic Doppler shift on this frequency (assumption four), then the received frequency between times τ_1 and τ_2 is given by (2-38)

$$f_r = f_s \left(1 - \frac{1}{c}\frac{ds}{dt}\right) . \tag{2-39}$$

For convenience f_s is offset from its nominal value of 400 MHz by about -32 kHz, and in the receiver a nominally 400 MHz reference frequency f_g is generated and mixed with f_r to obtain the beat frequency $(f_g - f_r)$ which will always be positive (32 kHz ± 10 kHz). The observed quantity with which we will be concerned is the integrated beat frequency between τ_1 and τ_2

$$D = \int_{\tau_1}^{\tau_2} (f_g - f_r)d\tau = \int_{\tau_1}^{\tau_2} f_g d\tau - \int_{\tau_1}^{\tau_2} f_r d\tau . \tag{2-40}$$

If we assume that both f_s and f_g remain constant during the duration of one pass (20 minutes) (assumption five) then the first integral becomes

$$\int_{\tau_1}^{\tau_2} f_g d\tau = f_g(\tau_2 - \tau_1) = f_g(t_2 + s_2/c - t_1 - s_1/c) , \tag{2-41}$$

and from assumption one, the number of cycles received between τ_1 and τ_2 is equal to the number transmitted between t_1 and t_2, so that the second integral becomes

$$\int_{\tau_1}^{\tau_2} f_r d\tau = \int_{t_1}^{t_2} f_s dt = f_s(t_2 - t_1) , \tag{2-42}$$

and

$$D = (f_g - f_s)(t_2 - t_1) + \frac{f_g}{c}(s_2 - s_1) . \tag{2-43}$$

This is the form of the integrated Doppler observation equation used in Chapter 5. We consider the validity of each of our five assumptions in section 2.2.3. Note that (2-43) can be rewritten in the form

$$(s_2 - s_1) = \frac{c}{f_g} D - c \frac{(f_g - f_s)}{f_g} (t_2 - t_1) , \qquad (2\text{-}44)$$

from which we note, in the context of our discussion of radio positioning (section 2.1.4) that:

(a) the observed quantity D is analogous to a phase difference measurement. It is scaled into seconds by the period $1/f_g$ of the receiver time standard, and therefore any error in our knowledge of the relationship between $1/f_g$ and the definition of the second will cause an incorrect scaling into seconds. D is scaled into (vacuum) metres by the vacuum propagation velocity c. The scaling between geometric and electromagnetic paths lengths is discussed in section 2.2.3.

(b) the measurements are of range differences $(s_2 - s_1)$, and therefore this system is related to hyperbolic radio positioning systems. In this case the hyperbolic pairs are consecutive satellite positions at the epochs of which Doppler integration intervals are gated.

(c) the frequency standards (satellite and receiver reference oscillators) are independent, and therefore this system is also related to rho-rho radio positioning systems. However in this case there are enough redundant measurements to calibrate the frequency offset for each satellite pass.

Let us consider more closely what a navigation receiver actually measures. The satellite signal detected at the antenna consists not only of the Doppler shifted carrier f_r, but also the time marks superimposed on the carrier by phase modulation. These two components, the Doppler signal and the timing signal, have different roles to play in the measurement, and they are handled somewhat differently by the receiver, being processed by

different circuits. The received Doppler frequency f_r is tracked by a phase locked loop tracking filter and mixed with the local frequency f_g to produce the beat frequency $(f_g - f_r)$, positive zero crossings of which generate pulses, which are then used to increment a Doppler count register (actually two sets of such circuits and counters are used, one each for 150 MHz and 400 MHz signals). Time marks are extracted from the received signal phase modulations through demodulator and decoder circuits, from which timing pulses are generated to start and stop the Doppler counters. The observed quantity then is the integral number of positive zero crossing pulses counted between successive readouts of the Doppler counters, and the epochs of these readouts are controlled by successive timing pulses.

We have assumed that the epochs at which satellite transmitted time marks are detected and the epochs between which the beat frequency $(f_g - f_r)$ is integrated are identical (assumption one). However this assumption fails in two ways: The time scale recovered by detecting the time marks is influenced by several sources of noise; the Doppler measurement is an integer number (the number of positive zero crossings counted) therefore the actual integration interval is between the epochs of the first and last positive zero crossing pulses, (let us call this the τ_i^* time scale) not between the epochs of the timing pulses controlling the readout (the τ_i time scale). See Figure 2-3. These two effects are reduced in geodetic receivers by incorporating and using a local clock. We will discuss their effect on navigation receiver observations in section 2.2.3.

We now consider the measurements made by three geodetic receivers. They are the Geoceiver (Magnavox, 1971), the JMR-1 (JMR, 1973), and the CMA-722B (Marconi, 1974). All three make use of the receiver reference oscillator to drive local clocks which are used either to supplement or replace the satellite time marks as the time scale gating the Doppler integration intervals.

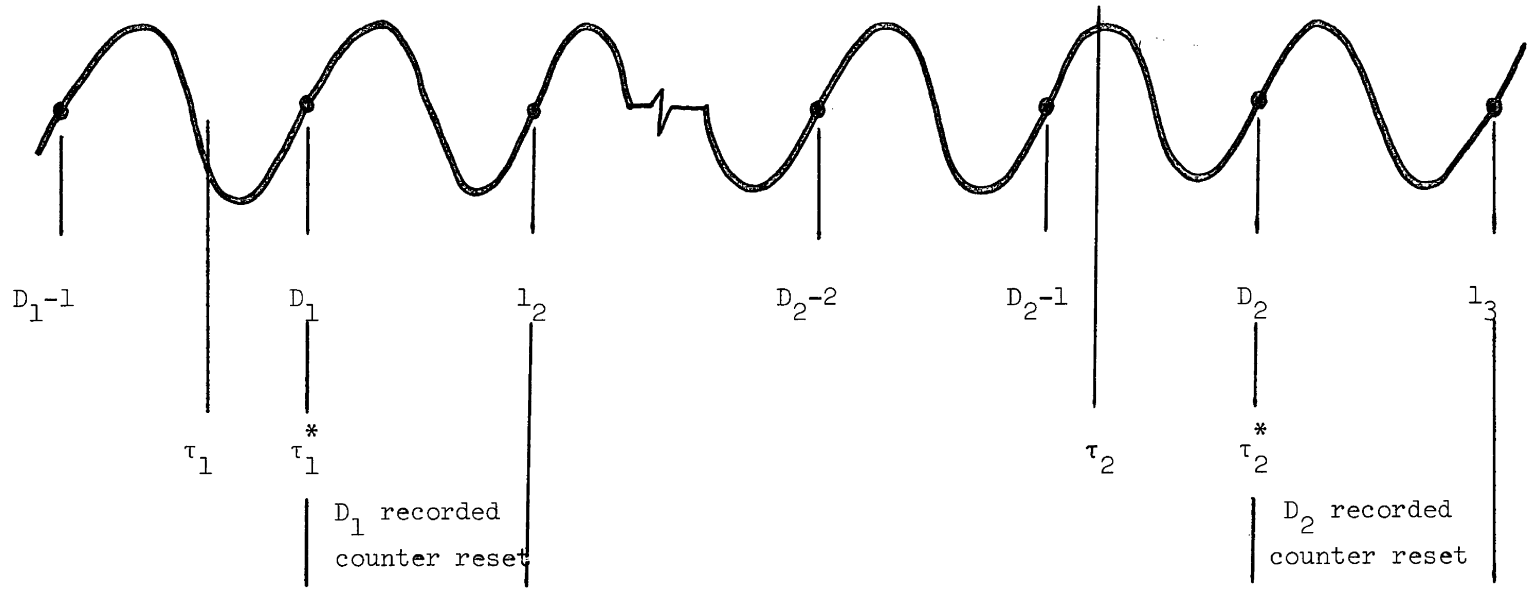

τ_i = epoch at which time signal detected

τ_i^* = epoch of first positive zero crossing of $(f_g - f_r)$ after τ_i

FIGURE 2-3

Doppler Integration Timing

The Geoceiver has 10 operating modes, of which five test the operation of the receiver, two are used to track GEOS satellites, and three (modes 0, 1 and 8) are used to track Transit satellites. The Geoceiver must be operated in mode 1 for at least one Transit pass to start the local clock, before operating in any other mode. The local clock is manually preset to an even two minutes of time, and then starts automatically upon detection of the first two minute time mark from the first Transit satellite pass tracked after the Geoceiver was switched on in mode 1. Thereafter (barring power interruptions) the local clock continues to run independently of the satellite time marks in whichever of the 10 modes (including mode 1) the receiver is operated. In modes 1 (attended operation) and 8 (unattended operation), satellite time marks gate the Doppler counts as for navigation receivers, whereas in mode 0 a simulated satellite bit rate generated from the local clock timing is used to gate the Doppler integrations. In all three modes the recorded data consists not only of an integrated integer Doppler count and integer refraction count, but also the local clock time (with 4 μs resolution) at the epochs of the first beat frequency zero crossing occurring after detection of the gating signal (satellite time mark for modes 1 and 8, receiver time mark for mode 0).

The JMR-1 receiver local clock is re-synchronized for each pass to the first satellite two-minute time mark detected. However to provide clock drift data, just before re-synchronization (1/4 bit period or 4915.6 μs before) the local clock time, based on the previous synchronization, is recorded. Integrated integer Doppler counts are gated by satellite time marks. The two Doppler frequencies are combined in an analogue circuit before incrementing the single Doppler counter. The local clock microsecond counter is sampled and recorded with a resolution of 0.5 μs (a) upon detection of each satellite time mark (τ_i epoch) and (b) upon detection of the first positive zero crossing following each time mark,

including the synchronization time mark (τ_i^* epoch). The latter clock records provide the same information as Geoceiver modes 1 and 8 clock records.

The CMA-722B receiver optionally gates the Doppler integration intervals using satellite time marks (BR mode), or using a bit rate derived from the local clock according to one bit period = $7865000/f_g$ seconds (CBR mode). In the CBR mode the local clock (bit rate counter) is synchronized for each pass to the first satellite two-minute time mark received. The Doppler counters in this receiver are incremented by positive zero crossings of the frequency 100 $(f_g - f_r)$, and optionally neither, one or both of the two least significant digits (the "fractional Doppler count") can be recorded. Using both digits, the maximum delay between time mark detection and first zero crossing of the recorded Doppler count (maximum $\tau_i^* - \tau_i$) is less than 0.5 μs.

Table 2-1 summarizes some of the features of these three geodetic receivers, and the three navigation receivers used in this thesis.

We now consider an alternative observation equation to (2-43) which makes use of geodetic receiver features. Assume as before that the satellite broadcasts a constant frequency f_s during the interval between transmitting time marks at times t_1 and t_2, at which times the satellite to receiver distances are $s(t_1)$ and $s(t_2)$. The received frequency is as before, from (2-38)

$$f_r = f_s \left(1 - \frac{1}{c} \frac{ds}{dt} \right) \quad ,$$

and the beat frequency $(f_g - f_r)$ is counted between the first zero crossing epochs τ_i^* following the time marks τ_i (which now may be generated either by the satellite time marks or by the local clock). However, now we either independently measure the epochs τ_i^* (Geoceiver and JMR-1), or reduce the differences $(\tau_i^* - \tau_i)$ effectively to zero (CMA-722B). Then we can use the τ_i^* epochs as the limits of integration

Navigation Receivers	Resolution of Recorded Data				Satellite Message Recorded	Local Clock Synch	τ_i From Satellite	τ_i From Local Clock	Integration Intervals (bit periods)*
	D_{400} (counts)	D_{150} (counts)	Local τ_i Epochs (μs)	Local τ_i^* Epochs (μs)					
CMA-722	1	1			✓		✓		24 x 234 + 487
ITT-5001	1	1			✓		✓		25 x 234 + 453
Magnavox 702CA	1	1			✓		✓		24 x 234 + 487
Geodetic Receivers									
CMA-722B	.01	.01			✓	each pass	BR mode	CBR mode	24 x 234 + 487
JMR-1	1		.5	.5	✓	each pass	✓		25 x 234 + 453
Geoceiver	1	1		4		each station	modes 1, 8	mode 0	1638, 1404, 1638, 1423

* 234 bit periods = 4.601016 s
253 4.974603
487 9.575619
1404 27.606095
1423 27.979682
1638 32.207111

TABLE 2-1

Receiver Features

$$D = \int_{\tau_1^*}^{\tau_2^*} (f_g - f_r)d\tau^* = \int_{\tau_1^*}^{\tau_2^*} f_g d\tau^* - \int_{\tau_1^*}^{\tau_2^*} f_s(1 - \frac{1}{c}\frac{ds}{dt})d\tau^*$$

$$= (f_g - f_s)(\tau_2^* - \tau_1^*) + \frac{f_s}{c}\int_{\tau_1^*}^{\tau_2^*} \frac{ds}{dt} d\tau^* \quad . \qquad (2\text{-}45)$$

Assuming that the t_i and τ_i^* time scales differ in epoch but negligibly in interval, then $dt = d\tau^*$ and

$$D = (f_g - f_s)(\tau_2^* - \tau_1^*) + \frac{f_s}{c}(s(\tau_2^*) - s(\tau_1^*)) \quad . \qquad (2\text{-}46)$$

Comparing this observation equation with (2-43) two differences are that the t_i time scale is replaced by the τ_i^* time scale, and that f_g is replaced in the second term by f_s.

Since we are given satellite positions at t_i epochs and in (2-46) we require positions at τ_i^* epochs, we must determine the differences in epoch $\Delta t_i = \tau_i^* - t_i$. We will describe two approaches to this problem. It is possible to determine Δt_i to 50 μs (Anderle, 1974). Since Transit satellites move at about 7500 m/s, an error of 50 μs in the determination of Δt_i is equivalent to an along track error of less than 0.5 m in the satellite positions used to compute $s(\tau_i^*)$. Since the error in Δt_i is highly correlated for adjacent satellite positions, the resultant error in $s(\tau_2^*) - s(\tau_1^*)$ will be much less than the error in $s(\tau_i^*)$.

Let $t = t_o$ and $\tau^* = \tau_o^*$ at synchronization time. The t time scale is derived from the satellite oscillator f_s, and the τ^* time scale from the local clock oscillator f_g. We will assume that the period $1/f_s$ is perfectly known relative to the definition of the second (that is any offset and drift in f_s has been corrected for before generating the t_i time marks). We will assume that the relationship between the period $1/f_g$ and the definition of the second is adequately modelled by

$$f_g(t) = f_g(t_o) + \dot{f}(t - t_o) \quad , \qquad (2\text{-}47)$$

where $f_g(t_o)$ and $\dot{f}$ are constants. Then

$$\frac{d\tau^*}{dt} = 1 + \frac{f_g - f_o}{f_o}$$

(where and f_o is the nominal value of f_g, see page 45)

$$\int_{\tau^*_o}^{\tau^*} d\tau^* = \int_{t_o}^{t} [1 + \frac{f_g(t_o) - f_o}{f_o} + \frac{\dot{f}}{f_o}(t - t_o)]dt \ .$$

Integrating

$$\tau^* - \tau^*_o = t - t_o + (\frac{f_g(t_o) - f_o}{f_o})(t - t_o) + \frac{\dot{f}}{2f_o}(t - t_o)^2 \ ,$$

and

$$\Delta t_i = \tau^*_i - t_i = \Delta t_o + (\frac{f_g(t_o) - f_o}{f_o})(t - t_o) + \frac{\dot{f}}{2f_o}(t - t_o)^2 \ . \quad (2\text{-}48)$$

Thus Δt_i is modelled by (2-48) if we can determine the three constants Δt_o, $(f_g(t_o) - f_o)/f_o$ and $\frac{\dot{f}}{f_o}$. The first constant, Δt_o, is the epoch difference at synchronization. Since geodetic receivers synchronize the local clock to received satellite time marks, Δt_o is composed of the propagation delay and the receiver delay, both of which must be determined. The propagation delay s/c varies between 3000 and 13000 μs, depending on the satellite elevation at synchronization. It can be computed with an accuracy of a few μs from the approximate satellite and receiver coordinates, since a 300 m error in s causes a 1 μs error in s/c. The receiver delay is of order 500 to 1000 μs, depending on the receiver used, and the variations for a given receiver are of order 30 to 50 μs. Geoceiver test mode 3 measuresthe receiver delay. For the other receivers it must be determined in the laboratory.

The receiver oscillator offset $(f_g(t_o) - f_o)/f_o$ and drift rate $\dot{f}/f_o$ can be determined by maintaining records from pass to pass of the frequency offset, relative to the satellite oscillator $(f_g - f_s)$, which appears in both (2-43) and (2-46). The offset $(f_g(t_o) - f_o)/f_o$ varies

between 100 and 1000 parts in 10^{10}, and the drift $\dot{f}/f_o$ varies between plus and minus 10 parts in 10^{10} per day, both values depending on the receiver used. The instantaneous frequency offset computed from

$$\frac{f_g(t) - f_o}{f_o} = \frac{f_g(t_o) - f_o}{f_o} + \frac{\dot{f}}{f_o}(t - t_o) \quad ,$$

typically has a standard deviation of 5 parts in 10^{10} (see Chapter 5).

An alternative application of (2-48) is to estimate one or more of the three parameters Δt_o, $(f_g(t_o) - f_o)/f_o$ and $\dot{f}/f_o$ from measurements of the average $\overline{\Delta t}$ for each pass. To "measure" the average $\overline{\Delta t}$, from each recorded τ_i^* value subtract the equivalent t_i value, compute and subtract the propagation delay s_i/c, and subtract a nominal value for the receiver delay d. The average of the results is $\overline{\Delta t}$ for that pass

$$\overline{\Delta t} = \frac{1}{n}\sum_i^n \tau_i^* - t_i - \frac{s_i}{c} - d \quad . \tag{2-49}$$

In general the values averaged will be scattered about $\overline{\Delta t}$ due to variations in d (of order 30 μs) and the delay between the time mark detection and next zero crossing (also of order 30 μs).

It is worth noting that this process of determining the difference in the time scales defined by two independent oscillators is the same problem faced in rho-rho radio positioning (section 2.1.4).

Presuming that we have independently determined Δt_i we can rewrite (2-46)

$$D = (f_g - f_s)(t_2 + \Delta t_2 - t_1 - \Delta t_1) + \frac{f_s}{c}(s(t_2 + \Delta t_2) - s(t_1 + \Delta t_1)) \quad ,$$

or

$$D - \Delta_1 = (f_g - f_s)(t_2 - t_1) + \frac{f_s}{c}(s(t_2) - s(t_1)) \quad , \tag{2-50}$$

where the corrective term Δ_1 is

$$\Delta_1 = (f_g - f_s)(\Delta t_2 - \Delta t_1) + \frac{f_s}{c}(\Delta s_2 - \Delta s_1) \quad , \tag{2-51}$$

and

$$\Delta s_i = s(t_i + \Delta t_i) - s(t_i) \quad . \tag{2-52}$$

We have seen that Transit measurements are analogous to hyperbolic radio positioning system measurements, since a range-difference term appears in the observation equations (2-43) and (2-46). Brown (Brown and Trotter, 1969; Brown, 1970; Brown and Trotter, 1973) argues that the Transit system can alternatively be considered an "asymptotic ranging system". To obtain Brown's observation equation we rewrite (2-46)

$$D_j = (f_g - f_s)(\tau_j^* - \tau_{j-1}^*) + \frac{f_s}{c}(s(\tau_j^*) - s(\tau_{j-1}^*)) \quad .$$

Since no cycle counts are lost between D_j measurements we can define an alternative measurement

$$N_i = \sum_1^j D_j \quad , \tag{2-53}$$

from which

$$N_i = (f_g - f_s)(\tau_i^* - \tau_o^*) + \frac{f_s}{c}(s(\tau_i^*) - s(\tau_o^*)) \quad ,$$

or

$$s(\tau_i^*) = s(\tau_o^*) + \frac{c}{f_s}[N_i - (f_g - f_s)(\tau_i^* - \tau_o^*)] \quad . \tag{2-54}$$

Brown calls this an "asymptotic" ranging observation equation since the bias parameter $s(\tau_o^*)$ common to all measurements must be estimated. Brown argues that D_j observations are serially correlated, since the τ_j^* of one is the τ_{j-1}^* of the next, and that the N_i observations are not correlated in this way. Kirkham (1972) and Krakiwsky, Wells and Kirkham (1972) show that the use of equations (2-46) and (2-54) will give equivalent results only if a serially correlated weight matrix is adopted for the D_j (in (2-46)).

A final alternative is to consider Transit measurements to be frequency measurements (Anderle, 1973). From (2-45)

$$D = \int_{\tau_1^*}^{\tau_2^*} (f_g - f_r) d\tau^* \quad .$$

If $(\tau_2^* - \tau_1^*)$ is sufficiently short that f_r can be considered to change linearly over the interval, then the integration yields

$$D = (f_g - f_r(\frac{\tau_1^* + \tau_2^*}{2}))(\tau_2^* - \tau_1^*) \quad ,$$

and the reduction equation is

$$f_r(\frac{\tau_1^* + \tau_2^*}{2}) = f_g - D/(\tau_2^* - \tau_1^*) \quad . \qquad (2\text{-}55)$$

In this case the observation equation is the Doppler equation (2-38)

$$f_r = f_s(1 - \frac{1}{c}\frac{ds}{dt}) \quad .$$

In fact this is the original Transit observation equation, used with the submarine (AN/BRN-3) and original TRANET receivers.

2.2.3 Parameters of the navigation observation equation

In this section we will be principally interested in the observation equation for the measurements made by navigation receivers, (2-43). We reconsider each of the five assumptions made in deriving (2-43).

Assumption one. We assumed that the epochs at which satellite transmitted time marks arrive at the receiving antenna and the epochs between which the beat frequency $(f_g - f_r)$ is integrated are identical. However the propagation and processing of the Doppler and timing signals through the receiver involves delays, and the Doppler measurement is an integer number, the number of positive zero crossings counted. Therefore the actual integration interval is between the epochs of the first and last positive zero crossing pulses, occurring after detection of the timing pulses controlling the readout.

The Doppler signal from which zero crossings are detected is the output of a voltage controlled oscillator in the phase locked loop tracking filter. This tracking filter continually "hunts" for the received signal it is tracking, and may at any instant lag or lead this signal. If

we can assume that the mean Doppler delay is governed by propagation (cable length) not processing (that is on average the tracking filter neither lags nor leads), then a reasonable estimate for the mean Doppler delay would be of the order of a microsecond. Variations about this mean due to the filter lag and lead excursion are specified for the Geoceiver, for example, to be within 120 degrees of phase (about 10 μs at 32 kHz).

To decode the Transit phase modulations and extract the timing and digital message data requires considerably more processing than for the Doppler signal, consequently the time mark delays are much larger than the Doppler signal delays. As mentioned in section 2.2.2, depending on the receiver used, the mean timing delay is of order 500 to 1000 μs, and the variations about this mean of order 30 to 50 μs. These variations are due to such influences as variations in the strength of the received signal, power supply voltages, and temperature, for example. Often the variations are separated into a long period component (much longer than the integration interval) which together with the mean delay serves to shift the integration interval; and a short period component (less than or of the order of the integration interval, usually called "jitter") which serves to change the length of the integration interval.

With this in mind let us follow through the derivation of (2-43). Let the satellite transmit time marks at t_i which arrive at the receiving antenna at $\tau_i = t_i + s_i/c$. Let the timing delay at τ_i be $\Delta t^c + \Delta t_i^v$ (where Δt^c is the mean delay plus long period component of the variations, and Δt_i^v is the short period variations, differing for each subscript value), and the Doppler delay be Δt_i^d. Then at $\tau_i + \Delta t_i^d$ the Doppler signal is available to increment the Doppler counter, however since the timing delay exceeds the Doppler delay, the time signal is decoded and available to gate the Doppler counter only at $\tau_i + \Delta t^c + \Delta t_i^v$. After the gate pulse,

let the next Doppler positive zero crossing occur Δt_i^z later.

The actual limits of integration in (2-40) are not τ_i but $\tau_i + \Delta\tau_i$ where

$$\Delta\tau_i = \Delta t^c + \Delta t_i^v - \Delta t_i^d + \Delta t_i^z \quad , \tag{2-56}$$

and

$$D = \int_{\tau_1+\Delta\tau_1}^{\tau_2+\Delta\tau_2} (f_g - f_r)d\tau \cong \int_{\tau_1}^{\tau_2} (f_g - f_r)d\tau + \int_{\tau_2}^{\tau_2+\Delta\tau_2} (f_g - f_r)d\tau - \int_{\tau_1}^{\tau_1+\Delta\tau_1} (f_g - f_r)d\tau. \tag{2-57}$$

The first integral results in equation (2-43), and the other two yield correction terms to (2-43). From (2-39)

$$f_r = f_s - \frac{f_s}{c}\frac{ds}{dt} \quad ,$$

so that

$$\int_{\tau_i}^{\tau_i+\Delta\tau_i} (f_g - f_r)d\tau = (f_g - f_s)\Delta\tau_i + \frac{f_s}{c}\frac{ds(\tau_i)}{dt}\Delta\tau_i \quad , \tag{2-58}$$

and (2-57) becomes

$$D = (f_g - f_s)(t_2 - t_1) + \frac{f_g}{c}(s(t_2) - s(t_1)) + \Delta_2 + \Delta_3 \quad , \tag{2-59}$$

where Δ_2 is the correction term due to a changed integration interval length, and Δ_3 is the correction term due to a shift in the integration interval, given by (A. Thorndike, personal communication)

$$\Delta_2 = (f_g - f_s)(\Delta\tau_2 - \Delta\tau_1) \quad , \tag{2-60}$$

$$\Delta_3 = \frac{f_s}{c}\left(\frac{ds(\tau_2)}{dt}\Delta\tau_2 - \frac{ds(\tau_1)}{dt}\Delta\tau_1\right) \quad . \tag{2-61}$$

Assuming Δt_i^v, Δt_i^d and Δt_i^z are uncorrelated between i values, the mean values $\Delta_2 \simeq 0$, $\Delta_3 \simeq \frac{f_s}{c}\Delta t^c \frac{d^2s}{dt^2}(t_2 - t_1)$. For $(t_2 - t_1) = 120s$, $\Delta t^c = 500\mu s$, then for a 60° pass $d^2s/dt^2 \simeq 40$ m/s^2 at closest approach and $\Delta_3 \simeq 3$ counts, and at the horizons $\Delta_3 \simeq 0$. Given that the standard deviations of Δt_i^v, Δt_i^d and Δt_i^z are respectively $\sigma_v = 30$ μs, $\sigma_d = 10$ μs and $\sigma_z = \frac{1}{\sqrt{12}(f_g - f_s)}$,

then

$$\sigma_{\Delta_2} = \sqrt{2}(f_g - f_s)(\sigma_v^2 + \sigma_d^2 + \sigma_z^2)^{1/2} \simeq 1.4 \text{ counts} .$$

Since $\frac{ds}{dt}$ changes from the satellite velocity (7500 m/s) at the horizons to zero at closest approach

$$\sigma_{\Delta_3} = \sqrt{2}\frac{f_s}{c}\frac{ds}{dt}(\sigma_v^2 + \sigma_d^2 + \sigma_z^2)^{1/2} ,$$

will vary from zero at closest approach to 0.45 counts at the horizons. In summary then, Δ_2 introduces no bias, but does introduce noise, whereas Δ_3 introduces noise but no bias at the horizons, and bias but no noise at closest approach.

Assumption two. We assumed that the epochs for which we have satellite positions and the epochs of transmission of time marks by the satellite are identical. Both the ephemeral positions and transmitted time marks from Transit satellites are nominally referred to UTC (Coordinated Universal Time). Because of this the Transit system can be used as a time dissemination system as well as a positioning system. However in the positioning application, only the uniformity of UTC (between different passes and different satellites) is used to calibrate a local clock, when such a clock is employed, as in geodetic receivers. Since the Transit system is self-contained, and need not use time-dependent data from external sources, any uniform time scale would do as well as UTC. When no local clock is employed, as in navigation receivers, then even a non-uniform time scale could in principle be used.

For navigation receivers we are concerned only that the ephemeris and time mark epochs be identical. For every microsecond difference between these epochs, the satellite positions will be in error relative to the time mark, in an along track direction, by 7.5 mm (since Transit satellites move at approximately 7500 m/s). There are three possible

constituents for such errors. First the time mark epochs may differ from the nominal time scale. Second the ephemeris position epochs may differ from the nominal time scale. Third the ephemeral positions may differ from the actual satellite positions at the epoch for which they are given. These last errors are discussed in Chapter 4, and are of order 25 m (3000 μs) in the along track direction for the operational ephemeris.

Considering the first error source, the time mark epochs are synchronized with UTC by introducing 10 μs steps when necessary. A three month comparison between TUA-F (French Atomic Universal Time) and the clock on board Transit satellite 30180 indicated that the offset (UTC - Transit) decreased fairly linearly from about 80 μs to 0 in about 40 days, then changed from 0 to 30 μs and back to 0 during the next 30 days (Laidet, 1972). A typical error of 50 μs might be deduced from these results. This will introduce positioning errors only when the ephemeris epochs do not also differ from UTC by the same amount.

Errors in ephemeris epochs and ephemeris along track positions are indistinguishable from a single pass. However for the operational ephemeris these two effects might in principle be separated over many passes by presuming that the portion which is constant over the time span of an ephemeris computation (12 hours into the future for the operational ephemeris, 48 hours for the precise ephemeris) to be epoch errors, and the portion which varies within these time spans to be position errors (due to inadequate force modelling). For the operational ephemeris there is no reason to believe the ephemeris epoch errors to be much different than the typical 50 μs time mark epoch errors. This would contribute about 2% of the 25 m along track ephemeris errors.

Assumption three. We assumed the propagation velocity was the vacuum velocity c. To maintain consistency with the value for c used in computing satellite ephemerides (assumed to be the old value of 299 792 500 m/s), the new value of 299 792 458 m/s (Terrien, 1974a), was not used in this thesis. We assume, then, that the travel time for a signal from the satellite to the receiver was s/c, or more precisely $\int \frac{ds}{c}$, where

the integration is performed along the geometric path joining the satellite position at time t and the receiver. Due to refraction the actual travel time will be $\int \frac{nds}{c} = \int \frac{dv}{c}$ where the integration is performed along the electromagnetic path rather than the geometric path. If we assume that the electromagnetic and geometric paths are coincident (we ignore refractive bending - this is not a valid assumption for closely horizontal paths), then the refractive contribution to the travel times will be $\frac{1}{c} \int (n-1)ds$ and to the ranges will be

$$\Delta s = \int (n-1)ds. \tag{2-62}$$

The correction to Doppler measurements then is

$$\Delta_4 = \frac{f_g}{c}(\Delta s_2 - \Delta s_1) \quad , \tag{2-63}$$

which can be added either to the observation equation (2-43)

$$D = (f_g - f_s)(t_2 - t_1) + \frac{f_g}{c}(s_2 - s_1) + \Delta_4 \quad , \tag{2-64}$$

or to the reduction equation in which we are converting the observed Doppler measurements into "vacuum" Dopplers $D_{vac} = D_{obs} - \Delta_4$.
We will adopt the reduction equation approach. There are two refraction corrections which must be made, one for tropospheric effects (section 2.3) and one for ionospheric effects (section 2.4).

Assumption four. We assumed that relativistic effects can be ignored. In fact, since for navigation receivers we have no local clock, there is no relativistic consideration. All measurements are with respect to the same reference frame, that of the moving satellite. The basic assumption was that

$$\int_{\tau_1}^{\tau_2} f_r d\tau = \int_{t_1}^{t_2} f_s dt \quad ,$$

that is that the number of cycles of f_r counted between detection of the time marks is equal to the number of cycles of f_s transmitted between transmission of the time marks. This assumption is not affected by the form of

the Doppler shift (relativistic or not) which we assume for f_r.

However for geodetic receivers both local and satellite clocks are used, and the two time scales will be influenced by both special (time dilation) and general (gravitational red shift) relativity effects. According to Gill (1965) and Rindler (1969) the Doppler effect with relativistic satellite velocity v_s is

$$\frac{\lambda_r}{\lambda_s} = \frac{1 + \frac{1}{c}\frac{ds}{dt}}{(1-v_s^2/c^2)^{1/2}} \quad , \tag{2-65}$$

and from $\lambda_r = c/f_r$, $\lambda_s = c/f_s$ we have

$$f_r = f_s(1 + \frac{1}{c}\frac{ds}{dt})^{-1}(1 - \frac{v_s^2}{c^2})^{1/2} \quad . \tag{2-66}$$

Obviously we can no longer assume $(1 + \frac{1}{c}\frac{ds}{dt})^{-1} = 1 - \frac{1}{c}\frac{ds}{dt}$ as in (2-38). In addition Rindler gives the gravitational Doppler effect as

$$f_r = f_s\ (1 + \Delta\phi/c^2) \quad , \tag{2-67}$$

where

$$\Delta\phi = \phi_s - \phi_e \simeq \mu(\frac{1}{r_s} - \frac{1}{r_e}) = -\mu(\frac{r_s - r_e}{r_s r_e}) \quad , \tag{2-68}$$

and ϕ_s, ϕ_e are the gravity potentials at the satellite and receiver respectively, and μ is the earth's gravitation constant ($\mu \simeq 4 \times 10^{14}\ m^3/s^2$). Keeping all terms to order $1/c^2$

$$f_r = f_s - \frac{f_s}{c}\frac{ds}{dt} + \frac{f_s}{c^2}(\frac{ds}{dt})^2 - \frac{f_s}{c^2}\frac{v_s^2}{2} - \frac{f_s}{c^2}\mu(\frac{r_s - r_e}{r_s r_e}) \quad . \tag{2-69}$$

Integrating this expression as in (2-45)

$$D = (f_g - f_s)(\tau_2^* - \tau_1^*) + \frac{f_s}{c}(s(\tau_2^*) - s(\tau_1^*)) + \Delta_5 + \Delta_6 + \Delta_7 \quad , \tag{2-70}$$

where Δ_5, Δ_6, Δ_7 are the corrections respectively due to the approximation $(1 + \frac{1}{c}\frac{ds}{dt})^{-1} \simeq 1 - \frac{1}{c}\frac{ds}{dt}$; the satellite velocity v_s (special relativity time dilation); and the difference in gravity potentials $\Delta\phi$ (general

relativity gravitational red shift). For the circular Transit orbits we can take v_s and r_s as constant. If $\tau_2^* - \tau_1^*$ is sufficiently small we can assume $\frac{ds}{dt}$ to vary linearly with time so that

$$\Delta_5 = -\frac{f_s}{c^2}(\tau_2^* - \tau_1^*)\left(\frac{ds}{dt}\right)^2\Bigg|_{\frac{\tau_1^* + \tau_2^*}{2}} , \qquad (2\text{-}71)$$

$$\Delta_6 = \frac{f_s}{c^2}(\tau_2^* - \tau_1^*)\,\frac{v_s^2}{2} , \qquad (2\text{-}72)$$

$$\Delta_7 = \frac{f_s}{c^2}(\tau_2^* - \tau_1^*)\,\mu\left(\frac{r_s - r_e}{r_s\, r_e}\right) . \qquad (2\text{-}73)$$

For v_s = 7500 m/s, r_s = 7.5 Mm, r_e = 6.4 Mm, $\frac{ds}{dt} \leq v_s$, f_s = 400 MHz, $\tau_2^* - \tau_1^*$ = 120 s

$$|\Delta_5| \leq 30 \text{ counts}$$

$$\Delta_6 \simeq 15 \text{ counts}$$

$$\Delta_7 \simeq 5 \text{ counts}$$

Brown and Trotter (1969) point out that Δ_6 and Δ_7 (their Δr corrections $= \Delta_5$) are additive with the $(f_g - f_s)$ term in (2-70), so that neglecting them will introduce errors principally into the value of f_g which is computed, not in the tracking station coordinates.

Assumption five. We assumed that for the duration of a pass (20 minutes), both the satellite reference frequency f_s and the receiver frequency f_g can be taken as constant. In addition, since f_g appears in the second term of (2-43), then the period $1/f_g$ is used to scale D into seconds, and therefore this period must be known relative to the definition of the second (relative to its nominal value). Let f_o be the nominal value of 400 MHz, common to both f_g and f_s. Then our assumption is that the frequency offsets

$$\delta f_s = \frac{f_s - f_o}{f_o} \qquad \delta f_g = \frac{f_g - f_o}{f_o} \quad , \tag{2-74}$$

are constant during a pass. Rewriting (2-43)

$$D = (\delta f_g - \delta f_s) f_o (\tau_2^* - \tau_1^*) + \frac{f_o}{c}(1 + \delta f_g)(s(\tau_2^*) - s(\tau_1^*)). \tag{2-75}$$

Values for δf_s are given by one of the parameters of the operational ephemeris with a resolution of 5 parts in 10^{10}. Table 2-2 lists sets of average values for these parameters, taken approximately one year apart, and the apparent long term drift, indicating that δf_s may drift by as much as 0.6 parts in 10^{10} per day.

By using the broadcast values of δf_s in (2-75), and treating δf_g as an unknown, the results in Chapter 5 indicate that (a) single pass solutions for δf_g yielded values between 150 and 1500 parts in 10^{10}, (b) the standard deviations of these single pass δf_g solutions is about 2 parts in 10^{10} (however, since δf_s is given only to 5 parts in 10^{10}, each δf_g solution contains a bias due to the residual part of δf_s), (c) multi-pass solutions for δf_g (obtained by fitting a linear trend to a few hundred single pass solutions using all satellites) yielded linear drift values between 1 and 10 parts in 10^{10} per day, and (d) the standard deviation of the linear fits was about 5 parts in 10^{10} (due to the above δf_s biases, and nonlinearities in the actual drift).

If we can infer that these long term drifts in δf_s and δf_g also represent the short term (20 minute) behaviour (a somewhat risky assumption) then we add three corrective terms to (2-75)

$$D = (\delta f_g - \delta f_s) f_o (\tau_2^* - \tau_1^*) + \frac{f_o}{c}(1 + \delta f_g)(s(\tau_2^*) - s(\tau_1^*)) + \Delta_8 + \Delta_9 + \Delta_{10} \tag{2-76}$$

where

$$\Delta_8 = \dot{\delta f_g}(t - t_{ca})\, f_o(\tau_2^* - \tau_1^*) \quad ,$$

Satellite	Frequency Offset Parameter δf_s		Drift $\dot{\delta f}_s$
	Avg Days 162-171, 1972	Avg Days 138-167, 1973	
12	-801345×10^{-10}	-801545×10^{-10}	-0.6×10^{-10}/day
13	-799330	-799315	+0.04
14	-801320	-801440	-0.3
18	-801250	-801430	-0.5
19	-800440	-800550	-0.3

TABLE 2-2

Long Term Satellite Oscillator Drift

$$\Delta_9 = -\delta\dot{f}_s(t - t_{ca})\, f_o(\tau_2^* - \tau_1^*) \quad ,$$

$$\Delta_{10} = \delta\dot{f}_g(t - t_{ca})\, \frac{f_o}{c}(s(\tau_2^*) - s(\tau_1^*)) \quad .$$

Taking the maximum values $(t - t_{ca})$ = 10 minutes, δf_g = 10 parts in 10^{10} per day, δf_s = 0.6 parts in 10^{10} per day, $\tau_2^* - \tau_1^*$ = 120 seconds, $s(\tau_2^*) - s(\tau_1^*) = 10^6$ m, then $\Delta_8 \simeq 0.3$ counts, $\Delta_9 \simeq 0.02$ counts, and $\Delta_{10} \simeq 10^{-5}$ counts. Therefore for most precise work Δ_8, perhaps Δ_9, but definitely not Δ_{10} should be included (either in the reduction equation or observation equation).

For less precise work it is traditional to omit δf_g from the second term of (2-75), that is to use $1/f_o$ instead of $1/f_g$ to incorrectly scale D into seconds. The effect of this is to systematically shift each pass further or closer to the receiver than it really is, depending on the sign of δf_g. For the maximum values δf_g = 1500 parts in 10^{10}, $\tau_2^* - \tau_1^*$ = 120 seconds, and $s(\tau_2^*) - s(\tau_1^*) = 10^6$ m, this introduces an error in D of 0.2 counts. Using a receiver with $\delta f_g \simeq 1500$ parts in 10^{10}, omitting this term shifted the multipass solution vector, computed from over 100 passes, by about 40 cm.

2.3 Tropospheric Refraction Reduction

In this section we discuss a model for the reduction of Doppler measurements for the effects of tropospheric refraction.

The troposphere is an approximately spherical shell of gases extending outward from the earth's surface to about 30 km in height. Its index of refraction is slightly greater than unity ($n \simeq 1.0003$) so that apparent distances are greater than geometrical (vacuum) distances. In the remainder of these introductory notes we consider models for three features of the troposphere: Its constituents, dispersion and nonhomogeneity.

Subsequently we apply these models to obtain a Doppler reduction model.

Constituents. The troposphere contains nitrogen (80%) and oxygen (20%), with small quantities of argon, neon, helium, krypton, xenon, hydrogen, ammonia, carbon dioxide, carbon monoxide, water vapour, and probably other pollutants. The tropospheric phase refractive index is usually assumed to obey the Lorenz-Lorentz equation

$$\frac{n^2 - 1}{n^2 + 2} = \sum_i R_i \rho_i \quad , \tag{2-77}$$

where ρ_i is the partial density of the i^{th} gas in the mixture making up the troposphere, and R_i is the specific refractivity of the gas, which in general depends on the frequency of the electromagnetic radiation. Tropospheric refraction can be adequately modelled by assuming that there are only three constituent gases; carbon dioxide, water vapour, and all other gases aggregated under the title "dry air free from carbon dioxide". The partial density of each of these is related to the temperature and the partial pressure of each constituent. Since the measurement of carbon dioxide content is not a simple field procedure, it is usual to assume the troposphere contains 0.03% carbon dioxide. This is more likely to be true outdoors than indoors, where the concentration may be much higher. At optical frequencies the contribution of water vapour to the refractive index is about 50 times smaller than at radio frequencies. Since the tropospheric index of refraction is close to unity the left side of the Lorenz-Lorentz equation is often approximated by

$$\frac{n^2 - 1}{n^2 + 2} = (n - 1)\left(\frac{n + 1}{n^2 + 2}\right) \approx \frac{2}{3}(n - 1) \quad . \tag{2-78}$$

One empirical formula based on this equation is that of Essen and Froome (1951). The simpler formula used here is that of Smith and Weintraub (1953).

$$N = (n - 1)10^6 = \frac{77.6}{T}(P + \frac{4810\ e}{T}) \quad , \tag{2-79}$$

where N is the refractivity, T is the temperature in kelvins, P is the pressure in millibars, and e is the partial pressure of water vapour in millibars. Separating (2-79) into "dry" and "wet" components we have

$$N = N_d + N_w = 77.6\frac{P}{T} + 77.6(4810)\frac{e}{T^2} \quad . \tag{2-80}$$

While the pressure P and temperature T are directly measured, water vapour pressure e is not. Instead the temperature of a wetted bulb T_w is measured. Given P in mb and T and T_w in K then from the empirical formula of Goff and Gratch (1946) the saturation water vapour pressure e_w in mb is

$$e_w = e_{ws}(\frac{T_s}{T_w})^{5.02808} \exp[-g(T_w)] \quad , \tag{2-81}$$

where T_s is the steam point temperature (373.16 K), e_{ws} is the saturation vapour pressure at T_s(1013.246 mb), and

$$g(T_w) = g_1(T_w) + g_2(T_w) + g_3(T_w) \quad ,$$

where

$$g_1(T_w) = 18.19728(\frac{T_s}{T_w} - 1) \quad ,$$

$$g_2(T_w) = 0.0187265\ \{1 - \exp[-8.03945(\frac{T_s}{T_w} - 1)]\} \quad ,$$

$$g_3(T_w) = 3.1813 \times 10^{-7}\ \{\exp[26.1205(1 - \frac{T_w}{T_s})] - 1\} \quad ,$$

and the empirical formula for the partial pressure e in mb is (Smithsonian, 1971), (noting that $6.6 \times 10^{-4}(1+1.15 \times 10^{-3}(T-273.16)) = 4.5 \times 10^{-4}\ (1 + 1.68 \times 10^{-3}T)$)

$$e = e_w - 4.5 \times 10^{-4}\ (1 + 1.68 \times 10^{-3}T_w)(T - T_w)P \quad . \tag{2-82}$$

For the Transit data analyzed in Chapter 5, the measurements of P, T and T_w which were used were not made at the tracking station but at the nearest airport (up to 75 km away). T and T_w were assumed to be

identical at the airport and tracking station. P was corrected for the difference in height between the airport and tracking station. The airport pressure was reported as an equivalent sea level pressure $P_{s\ell}$ (the airport height having been already taken into account). Then from Smithsonian (1971), given $P_{s\ell}$ in mb, T in K, and h_o, the tracking station orthometric height, in m, the tracking station pressure P in mb is given by the empirical formula

$$P = P_{s\ell} \exp(-h_o/c) \quad , \tag{2-83}$$

where

$$c = 29.2897(T + h_o/400) \quad .$$

Dispersion. In section 2.1.2 we noted that when the frequency of the external field closely matches the frequency of one of the atomic interactions characteristic of one of the constituents of the medium, then resonance occurs and dispersion is exhibited. For the troposphere, the lowest such resonances occur in the microwave region of the spectrum. Water vapour has a weak resonance at 22 GHz and a strong resonance at 300 GHz, and oxygen has a strong resonance at 60 GHz. There are a number of strong resonances in the infrared region. At frequencies below these resonances tropospheric dispersion is so small that it is usually ignored. In the infrared and optical regions tropospheric dispersion is usually assumed to follow Sellmeier's Equation (2-17) (the formula of Edlen, 1966) or Cauchy's Equation (2-18) (the formula of Barrell and Sears, 1939).

Nonhomogeneity. In section 2.1.3 we noted that the two features of the tropospheric index of refraction are its vertical profile and horizontal variability. Pressure and temperature have vertical profiles which can be modelled, but water vapour pressure does not. The horizontal variabilities of all three are more difficult to model. Here we will

develop a vertical profile for the "dry" refractivity from the pressure and temperature profiles. It is usual to assume that the temperature lapse rate is constant

$$\frac{dT}{dh} = - \alpha \quad , \tag{2-84}$$

and that the pressure lapse rate is proportional to density

$$\frac{dP}{dh} = -\rho g \quad , \tag{2-85}$$

where g is the acceleration due to gravity, and from the perfect gas law

$$PV = RT \quad ,$$

or

$$\rho = \frac{1}{V} = \frac{P}{RT} \quad ,$$

where R is the gas constant. Integrating (2-84) from the geoid to height h

$$T = T_o - \alpha h \quad . \tag{2-86}$$

Using this expression and integrating (2-85) from the geoid surface to height h, assuming g to be constant

$$P = P_o \left[\frac{T_o/\alpha - h}{T_o/\alpha}\right]^{g/R\alpha} \quad . \tag{2-87}$$

Putting (2-86) and (2-87) into (2-80) we obtain, for the N_d profile

$$N_d = N_{o_d}\left[\frac{T_o/\alpha - h}{T_o/\alpha}\right]^{g/R\alpha - 1} \quad ,$$

or

$$N_d = K_d(h_d - h)^{\mu} \quad , \tag{2-88}$$

where $\mu = \frac{g}{R\alpha} - 1$, h_d is the height (T_o/α) at which $T = 0$, and K_d depends on surface measurements of T_o and P_o.

2.3.1 The Hopfield model

In this section we discuss the Doppler reduction model derived from (2-88) by Hopfield. In the next section we discuss practical computational considerations when using her model.

Using (2-88), Hopfield (1969) found that the integer value of μ for which computed height derivatives of N_d near the surface best approximate observed N_d profiles is $\mu = 4$, and (Hopfield, 1972) that the value of h_d for which computed zenith integrals of N_d best approximate observed values is given, in metres, by

$$h_d = 40136 + 148.72\ (T_o - 273.16) \quad , \tag{2-89}$$

where T_o is the surface temperature in kelvins. Then

$$K_d = N_{od}/(h_d - h_o)^4 \quad ,$$

and

$$N_d = \frac{N_{od}}{(h_d - h_o)^4}\,(h_d - h)^4 \quad , \quad h \leq h_d \quad , \tag{2-90}$$

where N_{od}, h_o are the dry refractivity and orthometric height (in metres) of the observing station. The gradient of water vapour pressure cannot be so simply modelled as the gradients of T and P, so Hopfield (1969) has simply assumed a relationship analogous to that for the dry refractivity

$$N_w = \frac{N_{ow}}{(h_w - h_o)^4}\,(h_w - h)^4 \quad h \leq h_w \quad , \tag{2-91}$$

where the value of h_w for which computed zenith integrals of N_w best approximate observed values is, in metres (Hopfield, 1972)

$$h_w = 11000 \quad . \tag{2-92}$$

From (2-62), neglecting refractive bending the tropospheric contribution to the path length is

$$\Delta s = \int (n - 1)ds = \int_{r_o}^{r_{tro}} N \times 10^{-6}\,\frac{ds}{dr}\,dr \quad ,$$

integrated along the geometric path, where r_o is the radius to the tracking station and r_{tro} is the radius at which N becomes negligible. Splitting N into dry and wet components

$$\Delta s = \Delta s_d + \Delta s_w \quad .$$

Using (2-90) and (2-91) for N_d and N_w we have

$$\Delta s_i = \int_{r_o}^{r_{tro_i}} N_i \times 10^{-6} \frac{ds}{dr} dr = \frac{No_i \times 10^{-6}}{(h_i - h_o)^4} \int_{r_o}^{r_{tro_i}} (h_i - h)^4 \frac{ds}{dr} dr \quad , \qquad (2\text{-}93)$$

where the subscript values are i = 1, 2 for dry and wet components. Letting

$$h_{tro_i} = r_{tro_i} - r_o = h_i - h_o \quad , \qquad (2\text{-}94)$$

and

$$x = h - h_i = r - r_{tro_i} \quad , \qquad (2\text{-}95)$$

we have

$$\Delta s_i = \frac{No_i \times 10^{-6}}{h_{tro_i}^4} \int_{-h_{tro_i}}^{o} \frac{ds}{dr} x^4 dx \quad .$$

For a path having an elevation angle E we see from Figure 2-4 that

$$r^2 = (r_o \cos E)^2 + (r_o \sin E + s)^2 = \ell_2^2 + (\ell_1 + s)^2 \quad ,$$

or

$$s = \sqrt{r^2 - \ell_2^2} - \ell_1 \quad ,$$

and

$$\frac{ds}{dr} = \frac{r}{\sqrt{r^2 - \ell_2^2}} \quad ,$$

from which we have, using (2-95)

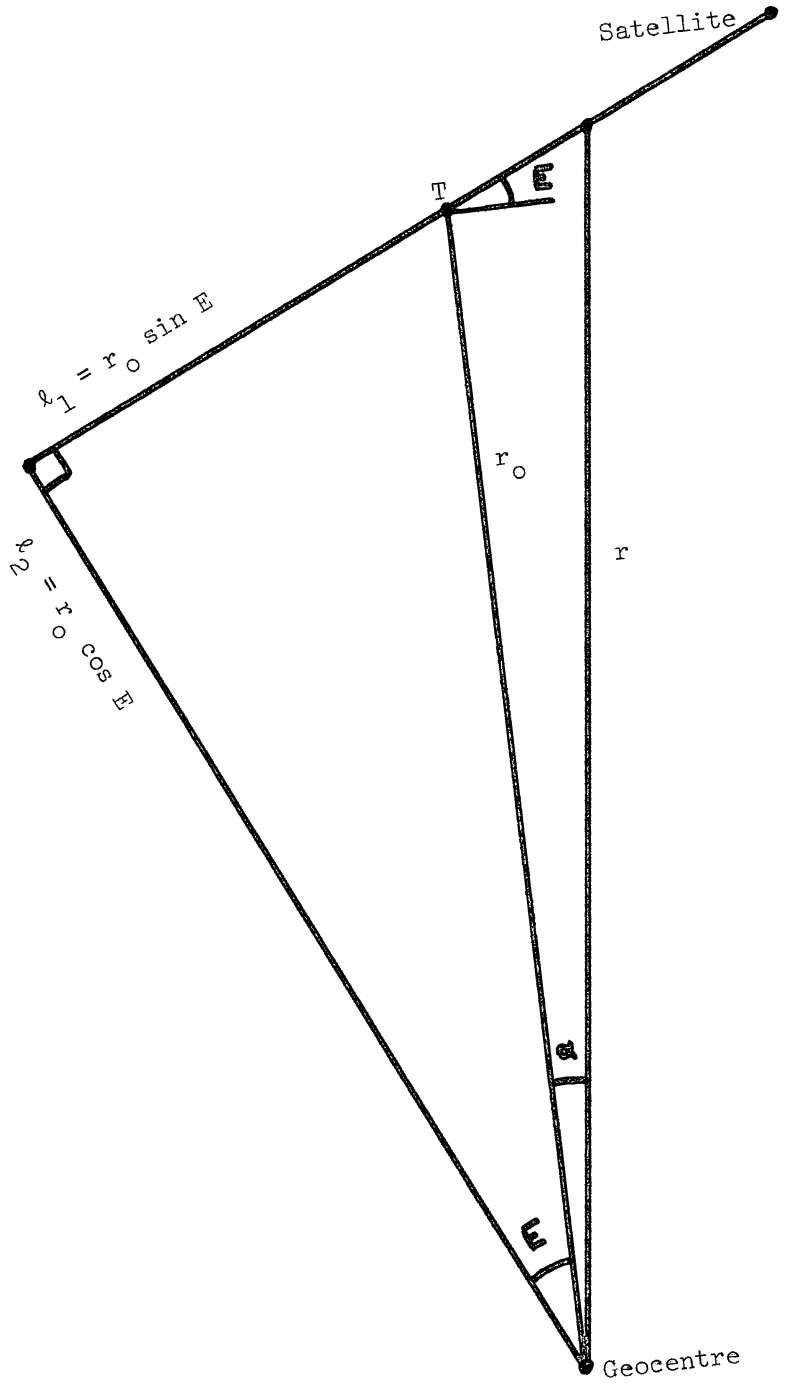

FIGURE 2-4
Tropospheric Refraction Geometry

$$\Delta s_i = \frac{No_i \times 10^{-6}}{h_{tro_i}^4} \int_{-h_{tro_i}}^{o} \frac{(r_{tro_i} + x)\, x^4 dx}{\sqrt{(r_{tro_i} + x)^2 - \ell_2^2}} \quad . \qquad (2\text{-}96)$$

The evaluation of this integral is discussed in section 2.3.2.

The tropospheric contribution to the integrated Doppler count (between data points 1 and 2) then is, from (2-63)

$$\Delta_{11} = D_{obs} - D_{vac} = \frac{f}{c} g (\Delta s_{d_2} + \Delta s_{w_2} - \Delta s_{d_1} - \Delta s_{w_1}) \quad . \qquad (2\text{-}97)$$

A comparison of the results from this model with ray tracing results indicates errors of about 45 cm in range corrections for low satellite elevations, and less than 5 cm above 20° elevations (Hopfield and Utterback, 1973).

2.3.2 Yionoulis algorithm for Hopfield model

While (2-96) can be integrated in closed form, the expressions obtained lead to serious roundoff errors for high elevation angles. Yionoulis (1970) has found two series expansions for the integrand, one for low elevations and one for high elevations, which when integrated term by term eliminate the roundoff problem. His high elevation algorithm is

$$\Delta s_i = No_i \times 10^{-6} \{W_i - \ell_1 - \frac{0.8 h_{tro_i}\, r_{tro_i}}{W_i} - W_i \sum_{p=1}^{NP}$$

$$\frac{1}{p+5} \left(\frac{h_{tro_i}}{V_i}\right)^{p+1} [2G(p+1)\left(1+\left(\frac{V_i}{U_i}\right)^{p+1}\right) - \sum_{n=1}^{p} G(n)\, G(p-n+1) \left(\frac{V_i}{U_i}\right)^{n}]\} \,, \qquad (2\text{-}98)$$

and his low elevation algorithm is

$$\Delta s_i = No_i \times 10^{-6} \{-\ell_1 + 4V_i \left(\frac{V_i}{h_{tro_i}}\right)^4 \left(\frac{U_i}{V_i} - 1\right)^{1/2} \sum_{n=1}^{4} C(n) \left[\frac{2}{2n+1}\right.$$

$$\left[1 - \left(1 - \frac{h_{tro_i}}{V_i}\right)^{n+1/2}\right] + \sum_{p=1}^{NP} (-1)^{p-1} \frac{G(p)}{1+2(p+n)} \left(\frac{U_i}{V_i} - 1\right)^{-p} \left(1-\left(1 - \frac{h_{tro_i}}{V_i}\right)^{p+n+1/2}\right)\right]\} \quad (2\text{-}99)$$

where $U_i = r_{tro_i} + \ell_2$

$V_i = r_{tro_i} - \ell_2$

$W_i = \sqrt{U_i V_i}$

$G(K) = \dfrac{(2K)!}{(K!)^2 2^{2K}(K-1/2)} = \{1, 1/4, 1/8, 5/64, \ldots\}$ for $K = 1,2,3,4,\ldots$

$C(K) = \{1, -3, 3, -1\}$ for $K=1,2,3,4$

and the p-series summations consist of NP terms, NP being chosen sufficiently large to provide convergence of the series to within desired limits.

The convergences of these two series were investigated to determine the optimum changeover elevation angle between them, and the minimum NP values providing convergence with negligible error (taken as being 1 mm). These convergences were evaluated by comparing with Δs_i values computed using an "infinite" value for NP (NP = 10). For equal NP values (2-99) requires at least three times as many arithmetic operations as (2-98). For mid-range elevations (2-98) converges with a smaller NP than (2-99). Consequently it is desirable to maximize the use of (2-98) by choosing as low a changeover elevation angle as possible.

For $T_o \in [273K, 303K]$, $P_o \in [950$ mb, 1050 mb$]$, $e \in [0, 25$ mb$]$, $h_o \in [0, 1000$ m$]$ and $r_o \in [6356$ km, 6378 km$]$, it was found that Δs_1 (dry component) converged to within 1 mm if (a) (2-98) is used at or above 17° and (2-99) below 17°, (b) NP = 3 for (2-98) and NP = 2 for (2-99); and that

Δs_2 (wet component) converged to within 1 mm if (c) (2-98) is used at or above 7° and (2-99) below 7°, and (d) NP = 3 for (2-98) and NP = 1 for (2-99).

Figure 2-5 illustrates the dependence of Δs on E for T_o = 290K, P_o = 1015 mb, e = 15 mb, h_o = 0, r_o = 6365000 m. The Doppler correction is the difference between the range corrections for the integration end point elevations, scaled by f/c.

2.3.3 Simplified models

The tropospheric zenith correction is a particularly simple expression. For example, from (2-96), when $\ell_2 = r_o \cos E = 0$

$$K_i = \Delta s_i(E = 90°) = \int (n-1)dh = \frac{No_i \times 10^{-6}}{h_{tro_i}^4} \int_{-h_{tro_i}}^{0} x^4 dx = \frac{No_i h_{tro_i} \times 10^{-6}}{5} \quad (2\text{-}100)$$

and from (2-80) and (2-94) (Hopfield, 1971)

$$K_d = 77.6 \frac{P_o}{T_o} \frac{(h_d - h_o)}{5} \times 10^{-6} \text{ m} \quad ,$$

$$K_w = 77.6(4810) \frac{e}{T_o^2} \frac{(h_w - h_o)}{5} \times 10^{-6} \text{ m} \quad , \quad (2\text{-}101)$$

where h_d and h_w are given by (2-89) and (2-92), and T_o, P_o, e and h_o are the surface values for temperature, pressure, water vapour pressure and orthometric height.

We can use the zenith corrections (2-101) to scale the corrections for other elevation angles, since for $E \neq 90°$

$$\Delta s_i = \int (n-1) \frac{ds}{dh} dh \quad ,$$

and from Figure 2-4

$$\frac{ds}{dh} = \frac{ds}{dr} = \frac{r}{\sqrt{r^2 - \ell_2^2}} = \frac{1}{\sin(E+\alpha)} \quad ,$$

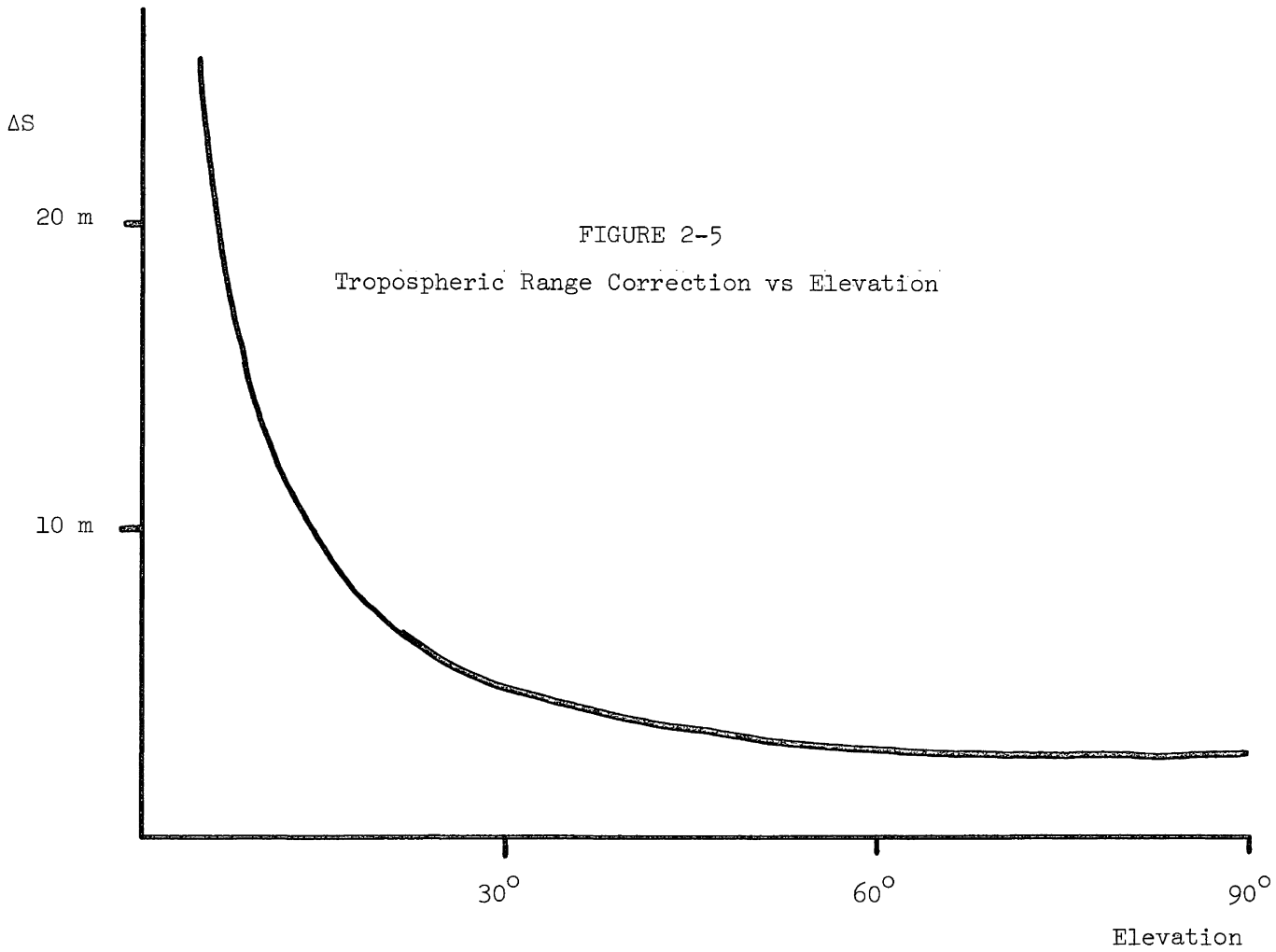

FIGURE 2-5

Tropospheric Range Correction vs Elevation

where E and α are linked by

$$\tan E = \frac{\cos\alpha - r_o/(r_o+h)}{\sin\alpha} \quad .$$

Now since $h_i \leq 40$ km then $\alpha \leq 6^\circ$ so that for high elevations ($E >> 6^\circ$) we can set $E + \alpha \simeq E$ and

$$\Delta s_i = \frac{1}{\sin E} \int (n-1)dh = \frac{K_i}{\sin E} \quad . \qquad (2\text{-}102)$$

For $E > 10^\circ$, Δs_i from (2-102) are within 50 cm of the Δs_i from (2-96). A variety of modifications and correction terms can be introduced to improve this agreement. For example the form prescribed by Hopfield (in Moffett, 1971) is

$$\Delta s_i = K_i/\sin(E^2 + \theta_i^2)^{1/2} \quad , \qquad (2\text{-}103)$$

where $\theta_d = 2.5^\circ$ and $\theta_w = 1.5^\circ$. In this case (2-103) and (2-96) agree to within 20 cm for $E > 3^\circ$, and to within 5cm for $E > 10^\circ$. If surface weather observations are not available, a nominal tropospheric correction can be obtained from (2-103) by using K_i values based on average values for T_o, P_o, e, h_o. For example, for a marine climate (T_o = 273K, P_o = 1014 mb, e = 18 mb, h_o = 0) Moffett (1971) quotes K_d = 2.31 m and K_w = 0.20 m.

An alternative expression to (2-103) is (Saastamoinen, 1973)

$$\Delta s = \frac{0.002277}{\sin E}\left[P_o + \left(\frac{1255}{T_o} + 0.05\right) e - \frac{B}{\tan^2 E}\right] + \delta_R \quad , \qquad (2\text{-}104)$$

where B is a tabulated function of h_o (B is of order unity), and δ_R is used when E is between 10° and 30°, and is a tabulated function of E and h_o, being in the range [0.001 m, 0.121 m]. Saastamoinen recommends this formula for $E > 10^\circ$, and estimates errors to be about 10 to 20 cm. He also gives a formula to correct E for path curvature which is not considered here, and correction terms to 2-104 for latitude and station height.

2.4 Ionospheric Refraction Reduction

The ionosphere extends from about 50 to 400 km in altitude, and consists of electrons and positive ions ionized by ultraviolet radiation from the sun. The profile of ion density as a function of altitude is not monotonic but contains various concentrations or layers, the pattern of which changes from day to night. Below about 30 MHz the ionosphere reflects radiation, thus allowing communications over long distances. In the microwave region propagation through the ionosphere is dispersive, the particular form of Sellmeier's equation often used being the Appleton - Hartree formula (Weiffenbach, 1967) giving the phase refractive index

$$n(r,f,t) = \left[1 - \frac{f_N^2(r,t)}{f^2} \frac{1}{\alpha}\right]^{1/2} \simeq \left[1 - \frac{81N(r,t)}{f^2}\right]^{1/2} , \quad (2\text{-}105)$$

where $f_N(r,t)$ is the electron plasma resonance frequency at position r and time t, which depends on the electron density $N(r,t)$ in electrons/m^3; and α is a complicated function of the value of the earth's magnetic field at position r, the orientation of the magnetic field to the direction of propagation, and the propagation frequency f. The ionospheric phase index of refraction can be expanded in inverse powers of the microwave frequency

$$n = 1 + \frac{c_1}{f^2} + \frac{c_2}{f^4} + \ldots \quad (2\text{-}106)$$

where the c_i are functions of position and time, but not of frequency.

The ionospheric contribution to the path length then is

$$\Delta s = \int (n-1)ds = \frac{b_1}{f^2} + \frac{b_2}{f^3} + \ldots \quad (2\text{-}107)$$

where the b_i are not functions of frequency. The ionospheric contribution to the integrated Doppler count is

$$\Delta_{12} = D_{obs} - D_{vac} = \frac{f_g}{c}(\Delta s_2 - \Delta s_1) = \frac{a_1}{f_g} + \frac{a_2}{f_g^2} + \ldots \qquad (2\text{-}108)$$

where the a_i are not functions of frequency.

2.4.1 The two-frequency model

Transit Doppler measurements are made at both 400 MHz and 150 MHz so that a first order ionospheric refraction correction can be made. The observed values D_{400} and D_{150} are related to the vacuum Doppler D_{vac} by

$$D_{400} = D_{vac} + \frac{a_1}{f_{400}} \quad ,$$

$$D_{150} = \frac{3}{8} D_{vac} + \frac{a_1}{f_{150}} = \frac{3}{8} D_{vac} + \frac{8}{3} \frac{a_1}{f_{400}} \quad .$$

Hence

$$\Delta_{12} = D_{400} - D_{vac} = \frac{24}{55} (D_{150} - \frac{3}{8} D_{400}) \qquad (2\text{-}109)$$

Marconi and Magnavox receivers record not D_{150} but $D_L = \frac{8}{3} D_{150}$

so

$$\Delta_{12} = \frac{9}{55} (D_L - D_{400}) \qquad (2\text{-}110)$$

ITT receivers record not D_{150} but $D_L = (D_{150} - \frac{3}{8} D_{400}) + 2000$

so

$$\Delta_{12} = \frac{24}{55} (D_L - 2000) \qquad (2\text{-}111)$$

Δ_{12} is positive as the satellite approaches, and negative as the satellite recedes.

It has been estimated that the residual effect after the two-frequency correction will be less than 1% of the total ionospheric refraction correction, and will be negligible at night, but may amount to three times the residual tropospheric refraction correction in the afternoon (Willman and Tucker, 1968).

CHAPTER 3

HILBERT SPACE OPTIMIZATION

Physical processes involve operations relating physical objects. A model is a simplified description of the essential properties of physical operations and objects. A mathematical model involves mathematical objects and mathematical relations between these objects.

Given a physical process represented by a mathematical model, we are often faced with making a decision or series of decisions. These may involve only the mathematical model, or may be decisions reached mathematically concerning the physical process.

The fundamental concept of decision theory is that of a best or optimal decision, in which we identify a quantity (representing the "value" of the decision) and optimize it (either maximize or minimize its value). We are free to choose the quantity to be optimized in different ways, and each choice will, in general, produce a different result (decision).

Here we restrict our attention to a family of optimal criteria individually called, for example, the least squares criterion, the minimum variance criterion, and the Gauss-Markov criterion. We refer to these collectively as Hilbert space criteria, and to the associated optimization problem as Hilbert space optimization.

In section 3.1 we synthesize the basic concepts of Hilbert space optimization, using the functional analysis approach. Two applications used in Chapter 4, least squares approximation and least squares spectral

analysis, are also discussed.

The physical operation with which we are primarily concerned is the acquisition of observations. The physical objects related by these observations depend, of course, on what is being observed. In our case the observations are phase measurements, and the physical objects include the constituents of the transmitting satellite, the constituents of the propagation media, and the constituents of the receiving equipment. Mathematical models of these observations and objects, of varying simplicity, have been presented in Chapter 2.

A mathematical model which we assume to exactly represent the physical process we call a reduction equation. A mathematical model which we assume to inexactly represent the physical process, due to unknown components which are present in the physical process but not in the mathematical model, we call an observation equation. The usual treatment of these unknown components (for lack of anything better) is to assume that their influence is random from observation to observation. The inconsistencies between redundant observations which are not resolved by the observation equation are therefore also assumed to be random. The standard method of resolving these inconsistencies in an optimal way is another application of Hilbert space optimization, called Hilbert space estimation. This is the topic of sections 3.2 and 3.3, culminating in the mathematical model used to generate the results described in Chapter 5.

3.1 Basic Concepts

The basic mathematical entity we will require is the scalar product. Therefore the space in which we work must have a scalar product defined. Such a space is a Hilbert space, which is the source of our term Hilbert space optimization.

In the following sections we first define the terms we will need,

then present the basic theorem of Hilbert space optimization. After discussing some applications of this theorem, we discuss various specifications for the scalar product. Finally we discuss some examples of Hilbert space optimization.

The source material consulted in constructing this section includes Cheney (1966), Korn and Korn (1968), Luenberger (1969), Wells and Krakiwsky (1971), and Vaníček and Wells (1972).

3.1.1 Mathematical objects and relations

In this section we define the mathematical objects and the mathematical relations underlying Hilbert space optimization.

Any well defined collection or class of objects is a set. The objects in a set are the elements of the set. Here we will be dealing with numerical sets, the elements of which are numbers. Henceforth by "set" we mean "numerical set". We will be concerned with sets containing two kinds of mathematical objects, scalars and vectors, to be defined below. A set is often defined by listing the properties satisfied by all elements of the set. We call a set which is defined in this way a space.

A mathematical relation is a rule or rules associating two or more mathematical objects. We will be concerned with two kinds of mathematical relations, unitary operations and binary operations. A unitary operation associates one mathematical object (the operand) with another mathematical object (the result). A binary operation associates a pair of mathematical objects (two operands) with another mathematical object (the result).

A function is a unitary operation F which associates one and only one element of a set R (the range of F) to each element of another set D (the domain of F), and for $r \in R$, $d \in D$ is written

$$r = F(d).$$

A function is well defined if and only if $d_1 = d_2$ implies $r_1 = r_2$; single-valued if and only if a unique r corresponds to each d; and regular at a point $d = d_o$ if and only if F(d) is single-valued, and differentiable throughout a neighbourhood of $d = d_o$. Here we will be dealing with well-defined regular functions. Henceforth by "function" we mean "well-defined regular function".

Given a set S and an operation O, then the set S is said to be closed under the operation O, if the results of operating on the elements of S are themselves elements of S.

The mathematical relations we are concerned with include scalar addition, scalar multiplication, vector addition, multiplication of vectors by scalars, scalar multiplication of vectors, and the operations resulting in norms and metrics.

Scalars are the elements of a ring with identity. A ring is a set of elements closed under two binary operations; scalar addition, which associates a scalar $(\alpha + \beta)$ with any two scalars α,β; and scalar multiplication, which associates a scalar $(\alpha \cdot \beta)$ with any two scalars α,β. A ring with identity contains an element (the identity element 1) such that $1 \cdot \alpha = \alpha$ for all α. Scalar addition and scalar multiplication satisfy the following axioms:

0 exists such that $\alpha + 0 = \alpha$; 1 exists such that $\alpha \cdot 1 = \alpha$	identity
$\alpha + (-\alpha) = \alpha - \alpha = 0$	inverse
$\alpha + \beta = \beta + \alpha$	commutative
$\alpha + (\beta + \gamma) = (\alpha + \beta) + \gamma$; $\alpha \cdot (\beta \cdot \gamma) = (\alpha \cdot \beta) \cdot \gamma$	associative
$\alpha \cdot (\beta + \gamma) = \alpha \cdot \beta + \alpha \cdot \gamma$ $(\beta + \gamma) \cdot \alpha = \beta \cdot \alpha + \gamma \cdot \alpha$	distributive

(3-1)

Vectors are the elements of a linear space. A linear space is closed under two binary operations; vector addition, which associates an element (a + b) of the linear space with any two elements a, b of the linear space; and multiplication of vectors by scalars, which associates an element (αa) of the linear space with any element a of the linear space, and any scalar α. Vector addition and multiplication of vectors by scalars satisfy the following axioms:

$$
\begin{array}{lll}
\theta \text{ exists such that } a + \theta = a & & \left.\begin{array}{l}\\ \\ \\ \\ \end{array}\right) \\
 & 0a = \theta & \left.\begin{array}{l}\\ \\ \end{array}\right) \text{ identity} \\
 & 1a = a & \left.\begin{array}{l}\\ \end{array}\right) \\
a + (-a) = \theta & & \text{inverse} \\
a + b = b + a & & \text{commutative} \\
(a + b) + c = a + (b + c) & (\alpha\beta)a = \alpha(\beta a) & \text{associative} \\
 & (\alpha + \beta)a = \alpha a + \beta a & \left.\begin{array}{l}\\ \\ \end{array}\right) \\
 & \alpha(a + b) = \alpha a + \alpha b & \left.\begin{array}{l}\\ \end{array}\right) \text{ distributive}
\end{array}
\tag{3-2}
$$

A unitary space is a linear space in which is defined a binary operation called scalar multiplication of vectors, which associates a scalar $\langle a, b \rangle$, called the scalar product, with any two elements a, b of the unitary space. Scalar multiplication of vectors satisfies the following axioms:

$$
\begin{array}{lll}
\langle a, \alpha b \rangle = \alpha \langle a, b \rangle & & \text{associative} \\
\langle a, b + c \rangle = \langle a, b \rangle + \langle a, c \rangle & & \text{distributive} \\
\langle a, b \rangle = \langle b, a \rangle & & \text{symmetric} \\
\langle a, \theta \rangle = 0 & & \left.\begin{array}{l}\\ \\ \end{array}\right) \\
\langle a, a \rangle \geq 0 & & \left.\begin{array}{l}\\ \end{array}\right) \text{ positive definite} \\
\langle a, a \rangle = 0 \text{ iff } a = \theta & & \left.\begin{array}{l}\\ \end{array}\right)
\end{array}
\tag{3-3}
$$

where α is any scalar.

Every unitary space can be made a normed space. A normed space

is a space in which a unitary operation is defined which associates a scalar $\rho(a)$, called the norm, with each element a of the normed space, satisfying the following axioms:

$$\begin{aligned} &a = b \text{ implies } \rho(a) = \rho(b) \\ &\rho(a + b) \leq \rho(a) + \rho(b) \\ &\rho(\theta) = 0 \\ &\rho(a) \geq 0 \\ &\rho(\alpha a) = |\alpha|\ \rho(a) \end{aligned} \tag{3-4}$$

Let us define the quadratic norm of a as

$$\rho(a) = \langle a, a \rangle \quad . \tag{3-5}$$

The square root of the quadratic norm satisfies all the above axioms, while the quadratic norm itself satisfies all but the last axiom. Since we will not have occasion to invoke the last axiom, we will work with the quadratic norm to preclude the necessity of taking square roots.

From (3-5) and the first three relations of (3-3) we have the identity

$$\rho(a \pm b) = \rho(a) \pm 2 \langle a, b \rangle + \rho(b) \quad . \tag{3-6}$$

Every normed space can be made a metric space. A metric space is a space in which a binary operation is defined which associates a scalar $\rho(a,b)$, called the metric, with each pair of elements a,b of the space, satisfying the following axioms:

$$\begin{aligned} &\rho(a,a) = 0 \\ &\rho(a,b) \leq \rho(a,c) + \rho(b,c) \quad \text{triangle inequality} \end{aligned} \tag{3-7}$$

which imply the additional properties

$$\begin{aligned} &\rho(a,b) = \rho(b,a) \\ &\rho(a,b) \geq 0 \end{aligned}$$

Let us define the mean quadratic distance between a and b as

$$\rho(a,b) = \rho(a-b) = \langle (a-b),(a-b) \rangle \quad . \tag{3-8}$$

This metric satisfies all the above axioms. The quadratic norm and mean quadratic distance are related by

$$\rho(a) = \rho(a,\theta) \quad . \tag{3-9}$$

A metric space is complete if and only if every sequence of elements $a_1, a_2, \ldots$ of the metric space, such that

$$\lim_{\substack{m\to\infty \\ n\to\infty}} \rho(x_m, x_n) = 0$$

converges to an element of the metric space.

A Hilbert space is a complete unitary space, that is a linear space on which a scalar product is defined, and which is complete.

Given some elements a_i of a linear space L and some scalars α_i, the sum $\sum_i \alpha_i a_i$ is called a linear combination. Since L is closed under vector addition and multiplication of vectors by scalars, any such linear combination is also an element of L. A subset of the elements of L which is itself closed under vector addition and multiplication of vectors by scalars is called a subspace S of L. That is, all linear combinations of the elements of S also belong to S. On the opposite extreme, a subset of the elements of L are called a linearly independent set if none of the elements of the set can be expressed as a linear combination of the others. A linearly independent set is called a basis B of L if every element of L can be expressed as a linear combination of the elements of B, in which case B is said to generate or span L, and the number of elements in B is the dimension of L. A space may have many bases, but every basis will have the same number of elements.

Given a subspace $S \subset L$ and an element $v_o \in L$, then a linear variety $V \subset L$ is generated by adding v_o to each element $s \in S$, that is $v = (v_o + s) \in V$.

Given two linear spaces L_1 and L_2 admitting the same ring of

scalars, and elements $a_1, b_1, \ldots \in L_1$ and $a_2, b_2, \ldots \in L_2$, then the direct sum of L_1 and L_2 is the linear space $L = L_1 \oplus L_2$ with elements $[a_1,a_2] = [a_2,a_1]$ closed under vector addition and multiplication of vectors by scalars according to

$$[a_1,a_2] + [b_1,b_2] = [a_1+b_1, a_2+b_2]$$
$$\alpha[a_1,a_2] = [\alpha a_1, \alpha a_2] \quad . \tag{3-10}$$

The dimension of L equals the sum of the dimensions of L_1 and L_2. If L_1 and L_2 are nonintersecting (have no common elements except θ), then they are subspaces of L and $[a_1,a_2] = a_1+a_2$.

3.1.2 The projection theorem

Hilbert space optimization problems are solved by appropriately applying the projection theorem. A simple statement of this theorem is that the shortest distance from a point to a plane is the perpendicular from the point to the plane. The two fundamental concepts here are orthogonality (perpendicularity) and minimum norm (shortest distance). By finding general statements for orthogonality and minimum norm, we can restate the projection theorem with more generality.

Two elements $a,b \neq \theta$ of a Hilbert space H are said to be orthogonal if

$$\langle a,b \rangle = 0 \quad , \tag{3-11}$$

and we denote this by $a \perp b$. If a is orthogonal to each element s of a subset S of H, then a is orthogonal to S ($a \perp S$). In particular if S is spanned by the basis B, then $a \perp S$ if and only if $a \perp B$. The set of all elements of H orthogonal to S is called the orthogonal complement of S and denoted $S^{\perp}$. Then $H = S \oplus S^{\perp}$ is the direct sum of S and $S^{\perp}$. Since S and $S^{\perp}$ are nonintersecting, given an element f of H, and a subspace S of H, then there exists an element s_o of S such that

$f = s_o + (f - s_o)$, where $(f - s_o)$ is an element of $S^{\perp}$. We call s_o the orthogonal projection of f onto S and $(f - s_o)$ the orthogonal projection of f onto $S^{\perp}$. Note that $s_o \perp S^{\perp}$, $(f - s_o) \perp S$, and $s_o \perp (f - s_o)$.

We can now restate the projection theorem (Luenberger, 1969).

Theorem 1. Given an element f and a subspace S of a Hilbert space H, the element s_o of S such that the mean quadratic distance between f and s_o is the minimum of all mean quadratic distances between f and elements of S (that is $\rho(f,s_o) \leq \rho(f,s)$ for all elements s of S), is uniquely given by the orthogonal projection of f onto S (that is by s_o such that $(f - s_o) \perp S$). Figure 3-1 (a) illustrates this theorem in three dimensional geometric Euclidean space.

Note that we can specify a subspace S in two ways. We can specify S by giving a basis $\Phi = \{\phi_i\}$ which generates S, in which case every element s of S is a linear combination of Φ and can be expressed

$$s = \sum_i \alpha_i \phi_i \quad . \tag{3-12}$$

Alternatively we can specify S by giving a basis Ψ which generates its orthogonal complement $S^{\perp}$, in which case every element s of S is orthogonal to Ψ, that is it satisfies the conditions

$$\langle s, \psi_j \rangle = 0 \quad \text{for each } \psi_j \text{ in } \Psi \; . \tag{3-13}$$

We can restate Theorem 1 in terms of the linear variety V where $(v \in V) = (f \in H) + (s \in S)$, (Luenberger, 1969).

Theorem 2. Given an element f and a subspace S of a Hilbert space H, then the unique element v_o of the linear variety $V = f + S$ which has minimum norm (that is $\rho(v_o) \leq \rho(v)$ for all elements v of V), is that element of V which is orthogonal to S (that is v_o is given by $v_o \perp S$).

Figure 3-1 (b) illustrates this theorem in three dimensional geometric Euclidean space.

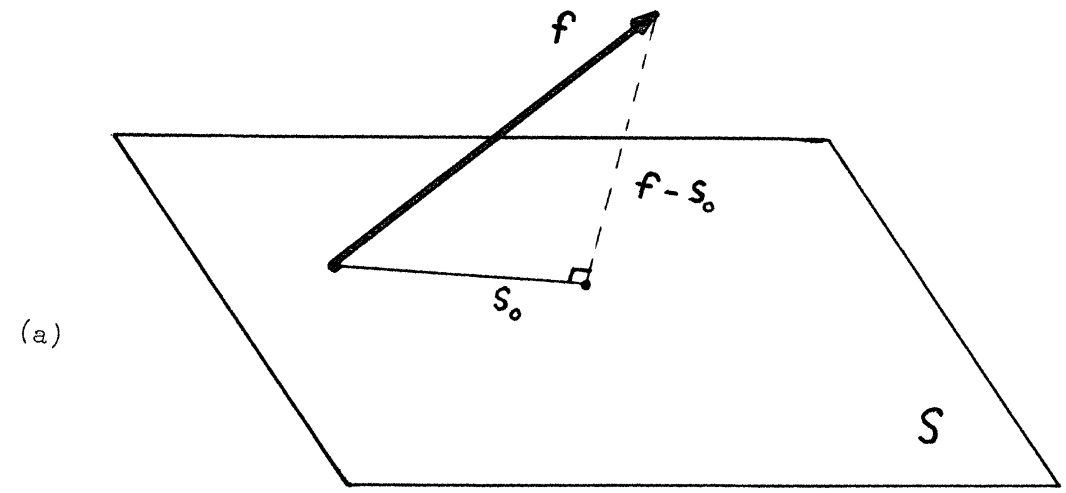

(a)

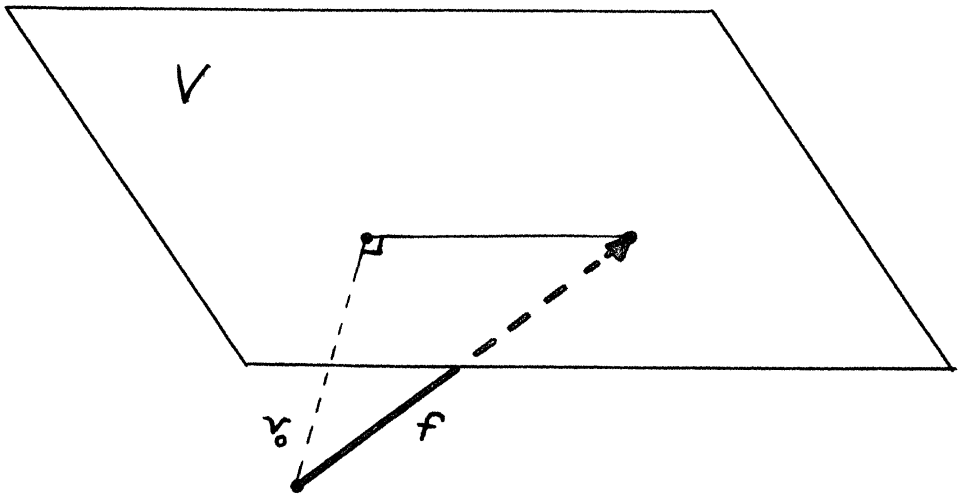

(b)

FIGURE 3-1
The Projection Theorem

Analogous to (3-12) and (3-13) we can specify a linear variety $V = f + S$ in two ways. We can give the fixed vector f and a basis Φ which generates S, in which case every element v of V can be expressed

$$v = f + \sum_i \alpha_i \phi_i \quad . \tag{3-14}$$

Alternatively we can specify V by giving a basis Ψ which generates $S^{\perp}$ and the projections of the fixed vector f onto each of $\{\psi_j\}$ (that is we give the set of scalars $\beta_j = \langle f, \psi_j \rangle$), in which case every element v of V satisfies the conditions

$$\langle v, \psi_j \rangle = \beta_j \quad \text{for each } \psi_j \text{ in } \Psi \ , \tag{3-15}$$

that is, all elements of V have the same projections onto Ψ as has the fixed vector f.

3.1.3 Hilbert space optimization problems

Many Hilbert space optimization problems conform to the projection theorem as stated in Theorem 1. The given element f of H is variously called the known function or observation vector. The given subspace S of H is generated by a given basis Φ, variously called the base, the configuration vectors, or the first order design vectors. The orthogonal projection s_o of f onto S is variously called the approximant, the linear form, and the generalized polynomial, and can be expressed as a linear combination of the basis $\Phi = \{\phi_i\}$, that is

$$s_o = p_m = \sum_i c_i \phi_i \quad .$$

The orthogonal projection

$$r = f - s_o$$

of f onto $S^{\perp}$ is called the residual. The orthogonal relationship $(f - s_o) \perp S$ or equivalently $r \perp \Phi$ generates the normal equations. In detail $r \perp \Phi$ is written $\langle f - s_o, \phi_j \rangle = 0$ for each ϕ_j in Φ, that is

$$\langle f - \Sigma\, c_i\phi_i, \phi_j \rangle = 0 \quad ,$$

and the normal equations are

$$\sum_i \langle \phi_i, \phi_j \rangle c_i = \langle f, \phi_j \rangle \quad \text{for each } \phi_j \text{ in } \Phi \ ,$$

which is a set of linear equations in the unknown coefficients c_i.

Restating this formally, we have:

Theorem 3. (Parametric optimization). Given a known element f and a base $\Phi = \{\phi_1, \phi_2, \ldots, \phi_m\}$ in a Hilbert space H, the mean quadratic distance between f and the approximant $p_m = \sum_{i=1}^{m} c_i\phi_i$ is minimized by the set of coefficients $(c_1, c_2, \ldots, c_m)$ which satisfy the normal equations

$$\sum_{i=1}^{m} \langle \phi_i, \phi_j \rangle c_i = \langle f, \phi_j \rangle \quad j=1,2,\ldots,m \quad . \tag{3-16}$$

In other Hilbert space optimization problems the subspace S is specified using the alternative method of giving conditions. Instead of being given a basis Φ of S we are given a basis Ψ of $S^{\perp}$. Instead of being given the known element f we are given a set of scalars which are the projections of f onto each of the $\{\psi_j\}$, that is we are given the real vector b whose components are $\beta_j = \langle f, \psi_j \rangle$. Since all elements of the linear variety V = f + S (including f itself) have the same projections onto $S^{\perp}$, the following conditions are satisfied

$$\langle v, \psi_j \rangle = \langle f, \psi_j \rangle = \beta_j \quad \text{for all } \psi_j \text{ in } \Psi \ .$$

From Theorem 2, the residual vector v_o of V which has minimum norm is determined by the relationship $v_o \perp S$. But this is equivalent to $v_o \in S^{\perp}$ or $v_o = \sum_i c_i\psi_i$, which when combined with the conditions $\langle v, \psi_j \rangle = \beta_j$ gives the set of normal equations in the unknown coefficients c_i

$$\Sigma \langle \psi_i, \psi_j \rangle c_i = \beta_j \quad .$$

Formally we have

Theorem 4. (Condition Optimization). Given a known vector $b = \{\beta_1, \beta_2, \ldots, \beta_n\}$

and a base $\Psi = \{\psi_1, \psi_2, \ldots, \psi_n\}$ in a Hilbert space H, the norm of the residual vector $r = \sum_{i=1}^{n} c_i \psi_i$ satisfying the conditions $\langle r, \psi_j \rangle = \beta_j$ is minimized by the set of coefficients $(c_1, c_2, \ldots, c_n)$ which satisfy the normal equations

$$\sum_{i=1}^{n} \langle \psi_i, \psi_j \rangle \; c_i = \beta_j \quad j=1,2,\ldots,n \quad . \tag{3-17}$$

Let us consider the more general optimization problem in a linear space $L = H \oplus H^{\perp}$, where H is a Hilbert space and $H^{\perp}$ is not. Given an element f and a subspace S of L, the metric $\rho(f,s)$ is in general no longer defined, and Theorem 1 no longer holds. Optimization is still equivalent to selection of an element s_o of S but s_o is no longer the orthogonal projection of f onto S. Solution of this problem combines features of both parametric and condition optimization. We minimize the norm of a vector v such that, for a given base Ψ each component of the vector $r = f - s_o$ is a projection of v onto Ψ. Interpretation of this problem in terms of Theorem 1 is not straightforward, and requires that we adopt an appropriate specification for the scalar product, as discussed in section 3.1.4. We return to this combined optimization problem in section 3.2.4.

Algorithms for solving the normal equations often involve a transformation from one basis Φ to a new basis Ψ of the subspace S. If the given basis $\{\phi_i\}$ is transformed to an orthonormal basis $\{e_i\}$, that is

$$\begin{aligned} \langle e_i, e_j \rangle &= 0 \quad i \neq j \\ \langle e_i, e_i \rangle &= 1 \quad , \end{aligned} \tag{3-18}$$

then the algorithm is called the Gram-Schmidt Orthogonalization procedure. If $\{\phi_i\}$ is transformed to a basis $\{\psi_i\}$ such that only the first i coordinates of the vector ψ_i are nonzero, and

$$\langle \psi_i, \psi_j \rangle = \langle \phi_i, \phi_j \rangle \quad , \tag{3-19}$$

then the algorithm is called the Choleski decomposition method. We use this

for the computations generating the results of Chapter 5.

3.1.4 Specification of the scalar product

Our results so far are valid in any space in which a scalar product can be defined. However we have not yet defined a specific function for the scalar product.

We have been concerned with a Hilbert space H, a subspace S of H, and the orthogonal complement $S^{\perp}$ of S. We call H observation space S solution space, and $S^{\perp}$ condition space.

Different scalar product definitions are required according to whether H is a discrete or compact space. In the discrete case if H has dimension n, and S has dimension $m < n$, then $S^{\perp}$ has dimension $n - m$.

Considering the discrete case first, let h_{ij} be the metric tensor of H (Vaníček, 1972). Then the scalar product in H can be defined according to tensor calculus practice, that is

$$\langle a,b \rangle = \sum_i \sum_j h_{ij} a^i b^j \quad i,j=1,2,\ldots,n \quad , \tag{3-20}$$

where a^i, b^j are elements of H (n-dimensional vectors). Now, in addition to the value of the known element f and the values of a basis Φ of S or Ψ of $S^{\perp}$, we must also be given the value of the metric tensor at the known point f, before we can proceed to solve the optimization problem. If observation space is locally orthogonal at f, that is if $h_{ij} = 0$ for $i \neq j$ then the scalar product definition becomes

$$\langle a,b \rangle = \sum_i h_{ii} a^i b^i \quad i=1,2,\ldots,n \quad , \tag{3-21}$$

and if observation space is locally Euclidean at f, that is if $h_{ij} = \delta_i^j$ then

$$\langle a,b \rangle = \sum_i a^i b^i \quad . \tag{3-22}$$

We can consider the elements of H to be functions, and H therefore to be a functional space. If H has finite dimension n, each element f of H is a function of an argument t which can take on only n discrete values, that is f is defined on the discrete set $T = \{t_1, t_2, \ldots, t_n\}$. If H has infinite dimension, then each element f of H is defined on a compact set, say $T = [t_a, t_b]$. Analogously to the metric tensor for the discrete case, we introduce a symmetric positive semi-definite weight function $W(t,t')$ with arguments $t,t' \in T$. In the discrete case the metric tensor and the weight function are synonomous. In the compact case we cannot interpret the weight function as a metric tensor, since metric tensors are not usually considered to have infinite dimension. However the scalar product definition is analogously

$$\langle a,b \rangle = \int_T \int_T W(t,t')a(t)b(t')dtdt' \quad . \tag{3-23}$$

Analogous to the metric tensor of a locally orthogonal space, if

$$W(t,t') = \begin{cases} 0 & \text{if } t \neq t' \\ W(t) \geq 0 & \text{if } t = t' \end{cases}$$

then

$$\langle a,b \rangle = \int_T W(t)a(t)b(t)dt \quad , \tag{3-24}$$

and analogous to the metric tensor of a locally Euclidean space, if

$$W(t,t') = \begin{cases} 0 & \text{if } t \neq t' \\ 1 & \text{if } t = t' \end{cases}$$

then

$$\langle a,b \rangle = \int_T a(t)b(t)dt. \tag{3-25}$$

In either the discrete or compact case, if we are given a basis Φ for solution space S, then the metric tensor s_{ij} of S is given by

$$s_{ij} = \langle \phi_i, \phi_j \rangle \quad . \tag{3-26}$$

If Φ is an orthogonal basis, that is if

$$\langle \phi_i, \phi_j \rangle = 0 \quad \text{for } i \neq j \quad ,$$

then solution space is orthogonal, that is

$$s_{ij} = 0 \quad \text{for } i \neq j \quad . \tag{3-27}$$

If Φ is orthonormal, that is if

$$\langle \phi_i, \phi_j \rangle = \begin{cases} 0 & \text{if } i \neq j \\ 1 & \text{if } i = j \end{cases} \quad ,$$

then solution space is Euclidean, that is

$$s_{ij} = \delta_i^j \quad . \tag{3-28}$$

We have seen that optimization involves minimizing a norm or a distance. In Hilbert space the quadratic norm and mean quadratic distance are defined in terms of the scalar product, and lead to expressions which are the sum or integral of squared terms. Therefore optimization problems in Hilbert space are often called least squares optimization problems. On the other hand the term least squares optimization is often reserved for what we have called a locally Euclidean Hilbert space. Here we accept the former, broader connotation of least squares.

3.1.5 Least squares approximation

Least squares approximation problems are problems in parametric optimization (Theorem 3):

Theorem 5. (Least Squares Approximation). Given a Hilbert space H, a function to be approximated f which is an element of H and which is defined on the set T, a weight function W defined and non-negative on T x T, and a basis Φ of a subspace S of H, then the mean quadratic distance between the function to be approximated f, and the approximating polynomial

$$p_m = \sum_i c_i \phi_i \quad , \tag{3-29}$$

is minimized by those values for the set of coefficients $\{c_i\}$ which satisfy the normal equations

$$\sum_i \langle \phi_i, \phi_j \rangle \; c_i = \langle f, \phi_j \rangle \quad , \tag{3-30}$$

where the scalar product is defined

$$\langle a,b \rangle = \begin{cases} \sum_T \sum_T W(t,t')a(t)b(t') & \text{if T is discrete} \\ \int_T \int_T W(t,t')a(t)b(t')dtdt' & \text{if T is compact} \end{cases} . \tag{3-31}$$

The polynomial p_m is then said to be the best <u>least squares approximation,</u> or <u>best least squares fit</u> of Φ to f.

3.1.6 <u>Nonlinear optimization problems</u>

Least squares optimization is a linear process, that is the least squares approximant p_m to the given f is a linear combination of the given base Φ, so that the normal equations are linear. However many nonlinear problems can be solved by transforming them to a sequence of linear problems.

For example, suppose we wish to approximate the known function f(t) by a function $g(t, x_i)$ which is nonlinear in the parameters x_i, i=1,2,...,m. That is, we want to find those values of the parameters x_i for which the mean quadratic distance $\rho(f,g)$ is a minimum. Under certain conditions, this nonlinear problem may be solved by solving the following sequence of linear problems.

Given a set of initial values x_i^o, we can linearize $g(t,x_i)$ by replacing it by the Taylor's series linear approximation

$$g(t,x_i) \simeq g(t,x_i^o) + \left.\frac{\partial g}{\partial x_i}\right|_{x_i^o} (x_i - x_i^o)$$

$$= g(t,x_i^o) + p_m^o \quad , \tag{3-32}$$

where $$p_m^o = \sum_{i=1}^{m} c_i \phi_i^o \tag{3-33}$$

$$c_i = x_i - x_i^o \tag{3-34}$$

$$\phi_i^o = \left.\frac{\partial g}{\partial x_i}\right|_{x_i^o} . \tag{3-35}$$

Applying the (linear) least squares approximation we find those values $c_i = c_i^o$ which minimize the mean quadratic distance $\rho(f - g(t,x_i^o),p_m^o)$. We can now generate the sequence of approximations to x_i

$$x_i^n = x_i^{n-1} + c_i^{n-1} \quad n=1,2,3,... \tag{3-36}$$

the sequence of base functions

$$\phi_i^n = \left.\frac{\partial g}{\partial x_i}\right|_{x_i^n} \tag{3-37}$$

and the sequence of best fitting approximants

$$p_m^n = \sum_{i=1}^{m} c_i^n \phi_i^n \quad , \tag{3-38}$$

such that $\rho(f - g(t,x_i^n),p_m^n)$ is a minimum. Provided that the sequences converge (the coefficients $c_i^n < c_i^{n-1}$) then the nonlinear approximation problem is solved by continuing the iteration until the values of the coefficients c_i^n have become negligible. Then the values $x_i = x_i^{n+1}$ are those for which $\rho(f,g)$ is a minimum.

Note that if the function $g(t,x_i)$ is not monotonic between the initial values x_i^o and the correct solution, then either the sequence of linear solutions will converge to a wrong solution, or will not converge at all. Convergence to the correct solution is more likely to occur the closer the initial values are to the correct solution. If they are sufficiently close, it may be that adequate convergence is obtained after only one iteration.

3.1.7 Least squares spectral analysis

Least squares spectral analysis (Vaníček, 1971) is a nonlinear example of least squares approximation (Theorem 5), in which the function to be approximated is a time series $\{f_i,t_i\}$, the weight function is taken to be orthonormal, and the basis $\Phi_n = \{\phi_1,\phi_2,\ldots,\phi_n\}$ consists of m = n - 2 elements Φ_m representing known constituents of the time series (datum bias, linear trend, known frequencies, etc.) and the two elements

$$\phi_{m+1} = \phi_{n-1} = \cos\omega t \ , \tag{3-39}$$

$$\phi_{m+2} = \phi_n = \sin\omega t \ , \tag{3-40}$$

where ω is the spectral frequency.

A (normalized) least squares spectrum is obtained by finding, for each desired spectral frequency ω, the spectral value

$$\sigma(\omega) = 1 - \frac{\rho(f,p_n)}{\rho(f,\theta)} \ , \tag{3-41}$$

where p_n is the orthogonal projection of f onto the subspace S_n spanned by Φ_n. The optimum least squares spectrum (in the sense that differences in spectral values are most pronounced) is obtained by finding, for each desired spectral frequency ω, the spectral value

$$\sigma^*(\omega) = 1 - \frac{\rho(f,p_n)}{\rho(f,p_m)} \ , \tag{3-42}$$

where p_m is the orthogonal projection of f onto the subspace S_m spanned by Φ_m.

For time series of appreciable length, the computations are extensive, but can be made reasonably efficient, especially for equally spaced time series (Wells and Vaníček, 1975).

3.1.8 Matrix notation

In this section we relate the notation of approximation theory

(which we have used so far) with the notation of least squares estimation (which we will use in the next sections). We have seen that to define a least squares optimization problem we must define:

(a) an expression for the scalar product. Using the specification of section 3.1.4 this is equivalent to defining the metric tensor h_{ij} of observation space.

(b) either solution space S or condition space $S^{\perp}$. In Theorems 3 and 4 respectively we have defined solution space by a basis Φ and condition space by a basis Ψ.

(c) a known element of observation space. In Theorems 3 and 4 respectively the known element is the observation vector f and the condition vector b.

In matrix notation we call the metric tensor of observation space h_{ij} the weight matrix (or second order design matrix) P. Then the scalar product between two vectors X,Y is known as a bilinear form

$$\langle X,Y \rangle = X^T P Y = Y^T P X \quad . \tag{3-43}$$

The vectors of the basis Φ become the column vectors of the configuration matrix (or first order design matrix) A. The vectors of the basis Ψ become the row vectors of the configuration matrix B. Because S and $S^{\perp}$ are orthogonal, then $\Phi \perp \Psi$ and

$$B A = 0 \quad , \tag{3-44}$$

(Note, $A B \neq 0$.)

The observation vector f becomes the vector L, and the condition vector b becomes the vector W. Restating Theorems 3 and 4 in matrix notation:

Theorem 3a. (Parametric Optimization). Given an observation vector L with weight matrix P and a configuration matrix A, the norm $V^T P V$ is minimized by the vector X satisfying the normal equations $A^T P A X = A^T P L$.

Theorem 4a. (Condition Optimization). Given a condition vector W with

weight matrix P and a configuration matrix B, the norm $V^T P V$ (where $P V = B^T K$ and $B V = W$) is minimized by the vector K satisfying the normal equations $B P^{-1} B^T K = W$.

3.2 Least Squares Estimation

Least squares optimization problems to which a statistical interpretation is given are called problems in least squares estimation. Here we consider only problems in discrete finite dimensional Hilbert space. To describe this statistical interpretation we first introduce the concept of expected values, and then discuss the role of covariance and weight matrices. Explicit mathematical models (in which observables can be expressed as an explicit function of the unknown parameters) and implicit mathematical models (in which they cannot) are then discussed.

3.2.1 Expected values

Given a random variable $x \varepsilon T$ (T being a discrete set), and having probability density function Φ, then the expected value of a function f of x is

$$E[f(x)] = \sum_{x \varepsilon T} f(x)\Phi(x) \quad . \tag{3-45}$$

Given the random vector X (a vector for which each component x_i is a random variable, $x_i \varepsilon T_i$, T_i discrete) having a joint probability density function Φ, then the expected value of a function f of X is

$$E[f(X)] = \sum_{x_1 \varepsilon T_1} \sum_{x_2 \varepsilon T_2} \cdots \sum_{x_n \varepsilon T_n} f(x_1, x_2, \ldots, x_n)\, \Phi(x_1, x_2, \ldots, x_n) \tag{3-46}$$

We are interested in the mean E[x] and the variance $E[(x-E(x))^2]$ of a random variable x, and the vector of means E[X] and covariance matrix $E[(X-E[X])(X-E(X))^T]$ of a random vector X. Note that the variance is the statistical equivalent of a mean quadratic distance

$$\rho(x,E(x)) = \langle (x-E(x)),(x-E(x)) \rangle \quad , \tag{3-47}$$

consequently the covariance matrix can be thought of as a parallel to the concept of a quadratic distance.

3.2.2 Covariance and weight matrices

The parameters involved in a least squares estimation problem consist of observables, constants and unknowns. These can be identified according to the variances assigned to them (explicitly or implicitly) prior to the estimation process. Constants have zero variance; unknowns have variances which exceed all limits (are infinite); and observables have variances in between. These variances specify that the values of constants are known with certainty; that we have no a priori knowledge about the values of unknowns; and that we have an uncertain knowledge about the values of observations, this uncertainty being expressed in terms of the variances we assign to the observation. Actually, in general we are able only to assign relative values among the variances we attribute to the observables, that is we know the relative variances, but not the variance scale factor.

Since variances which exceed all limits are inconvenient to deal with, we define the weight of a parameter as the reciprocal of its relative variance. Hence unknowns have zero weights; and observables have finite weights.

In any least squares estimation problem we can arrange the parameters into a vector or set of vectors. Corresponding to parameter relative variances or to parameter weights, we can then specify for each such vector a relative covariance matrix Q or its inverse, the corresponding weight matrix $P = Q^{-1}$. If a vector consists of constants, its Q = 0 and its P is undefined. If a vector consists of unknowns, its a priori P = 0

and its Q is undefined. If a vector consists of observables its a priori $P = Q^{-1} \neq 0$, and P and Q contain not only information on the relative variance (or weight) of each observable in the vector (diagonal elements) but also information on the correlation or covariance between observables (off-diagonal elements). A relative covariance matrix Q is related to its covariance matrix Σ by the variance factor σ_o^2

$$\Sigma = \sigma_o^2 \, Q \quad . \tag{3-48}$$

If two vectors X and Y are linearly related

$$X = A \, Y \quad , \tag{3-49}$$

and the relative covariance matrix of Y is Q^Y, (note this superscript notation does not indicate exponentiation) then from section 3.2.1 it can be shown

$$Q^X = A \, Q^Y \, A^T \quad , \tag{3-50}$$

and similarly if the covariance matrix of Y is Σ^Y, then

$$\Sigma^X = A \, \Sigma^Y \, A^T \quad . \tag{3-51}$$

This is the Covariance Law.

Note that the weight matrix P considered here can be identified with the weight matrix (or metric tensor of observation space) earlier considered in defining the scalar product. In this context the relative covariance matrix $Q = P^{-1}$ can be identified with the associated metric tensor of observation space.

Considering two random vectors X, Y with relative covariance matrices Q^X, Q^Y we have not completely specified the relevant covariance information until we have specified the covariance matrix of the vector $\begin{bmatrix} X \\ Y \end{bmatrix}$ that is

$$Q = \begin{bmatrix} Q^X & Q^{XY} \\ Q^{XY} & Q^Y \end{bmatrix} \quad , \tag{3-52}$$

and if we compute the weight matrix P (the weight matrix in our specification of the scalar product)

$$P = Q^{-1} = \begin{bmatrix} P^X & P^{XY} \\ P^{XY} & P^Y \end{bmatrix} \quad , \tag{3-53}$$

we can form the scalar products (in matrix notation called quadratic forms)

$$\rho(X) = \langle X,X \rangle = X^T P^X X \tag{3-54}$$

$$\rho(Y) = \langle Y,Y \rangle = Y^T P^Y Y \tag{3-55}$$

$$\langle X,Y \rangle = \langle Y,X \rangle = X^T P^{XY} Y = Y^T P^{XY} X \quad . \tag{3-56}$$

We recall that X and Y are said to be orthogonal if

$$\langle X,Y \rangle = 0 \quad , \tag{3-57}$$

or equivalently from the above if

$$P^{XY} = Q^{XY} = 0 \quad , \tag{3-58}$$

which from the statistical point of view means that the random vectors are uncorrelated. Therefore we can say that uncorrelated observables are orthogonal in observation space.

Finally, in practice it will be the rare occasion when we do not have some a priori knowledge about what values the "unknown" parameters will have. In fact, when the mathematical model is nonlinear (see section 3.1.6), efficient iterative convergence depends upon good initial estimates for the values of the "unknown" parameters. We may or may not choose to express this knowledge by specifying an a priori $P \neq 0$ for the "unknowns". This blurs the distinction between unknowns and observables, so far as their a priori P or Q matrices are concerned. However, there is a more fundamental distinction between unknowns and observables, considered in section 3.2.4.

3.2.3 Explicit mathematical models

Reconsidering Theorem 3a, the mathematical model implied is the linear model

$$L = A X \quad , \tag{3-59}$$

and the normal equations for that X which minimizes $V^T P^L V$, where

$$V = A X - L \quad , \tag{3-60}$$

and P^L is the weight matrix of L are

$$A^T P^L A \hat{X} = A^T P^L L \quad . \tag{3-61}$$

Considering this to be a least squares estimation problem, we are interested in a least squares estimate for X and the covariance matrix of that estimate. The solution to the normal equations is the least squares estimate $\hat{X}$ of X, which, providing the inverse exists, is

$$\hat{X} = (A^T P^L A)^{-1} A^T P^L L \quad , \tag{3-62}$$

and the least squares estimate $\hat{V}$ of V is

$$\hat{V} = A \hat{X} - L \quad , \tag{3-63}$$

so that the estimate of $V^T P^L V$ is

$$\hat{V}^T P^L \hat{V} = (A \hat{X} - L)^T P^L (A \hat{X} - L) = L^T P^L L - L^T P^L A \hat{X} \quad . \tag{3-64}$$

Since $Q^L = (P^L)^{-1}$ then by the covariance law

$$Q^{\hat{X}} = (A^T P^L A)^{-1} A^T P^L Q^L P^L A (A^T P^L A)^{-1} = (A^T P^L A)^{-1} \quad , \tag{3-65}$$

and

$$P^{\hat{X}} = A^T P^L A \quad . \tag{3-66}$$

An estimate $\hat{x}$ is said to be <u>unbiased</u> if $E[\hat{x}] = x$. It can be shown (Wells and Krakiwsky, 1971) that $\hat{X}$ is unbiased if $E[V] = 0$; that an unbiased estimate for the variance factor is

$$\hat{\sigma}_o^2 = \hat{V}^T P^L \hat{V} / \nu \tag{3-67}$$

(where ν is the number of degrees of freedom, that is the dimension of condition space $S^{\perp}$); and finally that an unbiased estimate for the covariance matrix of $\hat{X}$ is

$$\hat{\Sigma}_{\hat{X}} = \hat{\sigma}_o^2 Q^{\hat{X}} \quad . \tag{3-68}$$

Let us now consider the nonlinear mathematical model

$$L = F(X^a) \quad . \tag{3-69}$$

As in section 3.1.6 we apply the Taylor's series linear approximation, expanded about the initial estimates X^o

$$F(X^a) \simeq F(X^o) + \frac{\partial F}{\partial X}\Big|_{X^o} (X^a - X^o) \quad , \tag{3-70}$$

and we wish to minimize the quadratic norm $V^T P^L V$ where

$$V = F(X^a) - L = F(X^o) - L + \frac{\partial F}{\partial X}\Big|_{X^o} (X^a - X^o) \quad , \tag{3-71}$$

or

$$V = A X + W \quad , \tag{3-72}$$

where $X = X^a - X^o$ is the vector of corrections to be applied to the initial estimates X^o. Identifying the misclosure vector W as the analogue of -L in the linear model we have the normal equations

$$A^T P^L A \hat{X} + A^T P^L W = 0 \quad , \tag{3-73}$$

and the least squares estimate $\hat{X}$ for the vector of corrections X is

$$\hat{X} = - (A^T P^L A)^{-1} A^T P^L W \quad , \tag{3-74}$$

$$Q_{\hat{X}} = (A^T P^L A)^{-1} \quad , \tag{3-75}$$

$$\hat{V}^T P^L \hat{V} = W^T P^L W - W^T P^L A \hat{X} \quad , \tag{3-76}$$

$$\hat{\Sigma}_{\hat{X}} = \frac{\hat{V}^T P^L \hat{V}}{\nu} Q_{\hat{X}} \quad , \tag{3-77}$$

$$\hat{V} = A \hat{X} + W \quad . \tag{3-78}$$

Because we are considering a nonlinear model, as in section 3.1.6 we compute a new estimate

$$X^1 = X^o + \hat{X} \quad , \tag{3-79}$$

and iterate the estimation process until the vector of corrections is sufficiently small. Often X^o can be chosen close enough to the final estimate that one iteration is enough. The least squares estimate of X^a is the sum of the initial estimate X^o and the estimated corrections $\hat{X}$ from each iteration. The estimated covariance matrix of $\hat{X}^a$ is the estimated

covariance matrix of the corrections $\hat{X}$ from the last iteration.

Both the linear and nonlinear models of this section are explicit, in the sense that the vector of observables L can be explicitly expressed as a function of the vector of unknown parameters X. In section 3.1.3 we referred to a more general model in which this is not the case, which we will call an implicit mathematical model.

3.2.4 Implicit mathematical models

Given the implicit mathematical model

$$F(X^a, Y^a) = 0 \quad , \tag{3-80}$$

and a set of initial estimates X^o, Y^o for the parameters X and Y we apply the Taylor's series linear approximation to obtain

$$F(X^a, Y^a) \simeq F(X^o, Y^o) + \frac{\partial F}{\partial X}\Big|_{X^o, Y^o} (X^a - X^o) + \frac{\partial F}{\partial Y}\Big|_{X^o, Y^o} (Y^a - Y^o)$$

$$= W + A\,X + B\,Y = 0 \quad . \tag{3-81}$$

Given the relative covariance matrix Q^Y of Y then

$$M = Q^{BY} = B\,Q^Y\,B^T \quad . \tag{3-82}$$

Identifying B Y with -V in the explicit models, it can be shown (Vaníček and Wells, 1972) that the normal equations for that X which minimizes $Y^T P^Y Y$ are

$$A^T P^{BY} A\,\hat{X} + A^T P^{BY} W = 0 \quad , \tag{3-83}$$

or

$$A^T M^{-1} A\,\hat{X} + A^T M^{-1} W = 0 \quad , \tag{3-84}$$

and the least squares estimate $\hat{X}$ for the corrections X to X^o is

$$\hat{X} = -(A^T M^{-1} A)^{-1} A^T M^{-1} W \quad , \tag{3-85}$$

$$Q^{\hat{X}} = (A^T M^{-1} A)^{-1} \quad , \tag{3-86}$$

$$\hat{Y}^T P^Y \hat{Y} = W^T M^{-1} W - W^T M^{-1} A\,\hat{X} \quad , \tag{3-87}$$

$$\hat{\Sigma}_{\hat{X}} = \frac{\hat{Y}^T P^Y \hat{Y}}{\nu} Q^{\hat{X}} \quad , \tag{3-88}$$

and it can be shown (Wells and Krakiwsky, 1971) that

$$\hat{Y} = -Q^Y B^T M^{-1} (W + A \hat{X}) \quad , \tag{3-89}$$

$$Q^{\hat{Y}} = Q^Y B^T M^{-1} (BQ^Y - A(A^T M^{-1} A)^{-1} A^T M^{-1} BQ^Y) \quad , \tag{3-90}$$

$$\hat{\Sigma}_{\hat{Y}} = \frac{\hat{Y}^T P^Y \hat{Y}}{\nu} Q^{\hat{Y}} \quad . \tag{3-91}$$

Again, the estimation process is iterated until the final correction $\hat{X}$ is sufficiently small.

The parameters of this model have been separated into two sets, the elements of X and the elements of Y. The usual distinction is that X consists of "unknown" parameters and Y of "observed" parameters. As discussed in section 3.2.2 we need not make any such distinction on the basis of the P or Q matrices assigned to X and Y prior to the estimation process - from that point of view both X and Y can be considered as two partitions of a single "observable" vector. However in that case we should be minimizing $X^T P^X X + Y^T P^Y Y$, but because X consists of unknowns we have seen in section 3.2.2 that $P^X = 0$, so that the weight matrix of $\begin{bmatrix} X \\ Y \end{bmatrix}$ is singular

$$P = \begin{bmatrix} P^X & 0 \\ 0 & P^Y \end{bmatrix} = \begin{bmatrix} 0 & 0 \\ 0 & P^Y \end{bmatrix} \quad ,$$

and the covariance matrix of $\begin{bmatrix} X \\ Y \end{bmatrix}$ is undefined. We then have the situation described in section 3.1.3 in which the "observation" space in which $\begin{bmatrix} X \\ Y \end{bmatrix}$ is an element is the direct sum of a Hilbert space (in which Y is an element) and a non-Hilbert space (in which X is an element). To solve this problem we have recognized that $X^T P^X X$ is automatically minimized since $P^X = 0$, and consequently we need only (and can only) minimize the Hilbert space

component $Y^T P^Y Y$. One way to distinguish between X and Y then is that $P^X = 0$ and $P^Y \neq 0$. An equivalent distinction is that X contains those parameters which are not to be subjected to minimization, and Y contains those parameters which are to be subjected to minimization.

This model is often called the "combined adjustment" model. The model in which all parameters are to be subjected to minimization is called the "condition adjustment" model; is related to Theorem 4a;and its solution can be regarded as a special case of the combined model solution where terms containing the A matrix are omitted. The explicit models of the previous section are called "parametric adjustment" models; are related to Theorem 3a; and their solution can be regarded as a special case of the combined model solution where the B matrix is -I.

3.3 Stepwise Estimation

Least squares estimates resulting from the simultaneous solution of a large system of equations are equivalent to the estimates obtained by processing the equations in a number of stages, only if the effect of previous stages on the solution vector and its covariance matrix is somehow transmitted from stage to stage. The solution vector can be transmitted either by

(a) updating the a priori estimate to be used in the next stage, or

(b) accumulating a sum of corrections to the a priori estimate used in the first stage.

The covariance matrix can be transmitted by transmitting all the following

(a) accumulated sum of residual norms from each stage

(b) accumulated sum of degrees of freedom from each stage

(c) the weight matrix of the solution vector (or its inverse) obtained from the previous stage, used as an a priori weight matrix in the next stage.

The residuals for the current stage are also easily obtained. In general residuals from previous stages are affected by subsequent stages, and can in principle be re-evaluated using a form of back substitution. However this procedure will not be considered here. Although the residuals themselves are affected by subsequent stages, the residual norm is not. That is, the accumulated sum of the residual norms from each stage is equal to the residual norm obtained from the simultaneous solution of all stages.

In this section we derive an algorithm for stepwise estimation for a model in which the parameters X (not subjected to minimization) are common to all stages and the parameters Y (subjected to minimization) each appear in a single stage.

3.3.1 Summation of normal equations

Let us consider two sets of equations having common parameters X but different parameters Y. Then

$$F_1(X^a,Y_1^a) \simeq F_1(X^o,Y_1^o) + \left.\frac{\partial F_1}{\partial X}\right|_{X^o,Y_1^o} (X^a-X^o) + \left.\frac{\partial F_1}{\partial Y_1}\right|_{X^o,Y_1^o} (Y_1^a - Y_1^o)$$

$$= W_1 + A_1 X + B_1 Y_1 = 0 \quad , \tag{3-92}$$

$$F_2(X^a,Y_2^a) \simeq F_2(X^o,Y_2^o) + \left.\frac{\partial F_2}{\partial X}\right|_{X^o,Y_2^o} (X^a-X^o) + \left.\frac{\partial F_2}{\partial Y_2}\right|_{X^o,Y_2^o} (Y_2^a -Y_2^o)$$

$$= W_2 + A_2 X + B_2 Y_2 = 0 \quad . \tag{3-93}$$

We can obtain the model of section 3.2.4, that is

$$W + A X + B Y = 0 \quad , \tag{3-94}$$

by setting

$$W = \begin{bmatrix} W_1 \\ W_2 \end{bmatrix}, A = \begin{bmatrix} A_1 \\ A_2 \end{bmatrix}, Y = \begin{bmatrix} Y_1 \\ Y_2 \end{bmatrix}, B = \begin{bmatrix} B_1 & 0 \\ 0 & B_2 \end{bmatrix} \quad . \tag{3-95}$$

If and only if Y_1 and Y_2 are orthogonal, in the sense that

$$Q^Y = \begin{bmatrix} Q^{Y_1} & 0 \\ 0 & Q^{Y_2} \end{bmatrix} \quad , \tag{3-96}$$

then

$$M = B\, Q^Y\, B^T = \begin{bmatrix} B_1 Q^{Y_1} B_1^T & 0 \\ 0 & B_2 Q^{Y_2} B_2^T \end{bmatrix} = \begin{bmatrix} M_1 & 0 \\ 0 & M_2 \end{bmatrix} \quad , \tag{3-97}$$

from which it is easily seen that, for example

$$A^T M^{-1} A = A_1^T M_1^{-1} A_1 + A_2^T M_2^{-1} A_2 \quad . \tag{3-98}$$

More generally, defining the augmented matrices

$$\tilde{A}_j = [A_j \,\vdots\, W_j] \text{ and } \tilde{A} = \begin{bmatrix} A_1 & \vdots & W_1 \\ A_2 & \vdots & W_2 \\ \cdot & \vdots & \cdot \\ \cdot & \vdots & \cdot \\ \cdot & \vdots & \cdot \\ A_i & \vdots & W_i \end{bmatrix} \quad , \tag{3-99}$$

then we have, for i stages (i sets of equations)

$$\tilde{A}^T M^{-1} \tilde{A} = \sum_{j=1}^{i} \tilde{A}_j^T M_j^{-1} \tilde{A}_j \quad . \tag{3-100}$$

Introducing the symbols

$$N_i = \sum_{j=1}^{i} A_j^T M_j^{-1} A_j \tag{3-101}$$

$$U_i = \sum_{j=1}^{i} A_j^T M_j^{-1} W_j \tag{3-102}$$

$$\rho(W)_i = \sum_{j=1}^{i} W_j^T M_j^{-1} W_j \tag{3-103}$$

$$(\nu)_i = \sum_{j=1}^{i} \nu_j \quad , \tag{3-104}$$

then given (from the previous stage)

$$N_{i-1} \ , \ U_{i-1} \ , \ \rho(W)_{i-1} \ , \ (\nu)_{i-1} \ ,$$

and (from the current stage)

$$A_i \ , \ B_i \ , \ W_i \ , \ Q^{Y_i} \ , \ \nu_i \ ,$$

we have

$$M_i = B_i \ Q^{Y_i} \ B_i^T \tag{3-105}$$

$$\left.\begin{aligned} N_i &= N_{i-1} + A_i^T \ M_i^{-1} \ A_i \\ U_i &= U_{i-1} + A_i^T \ M_i^{-1} \ W_i \\ \rho(W)_i &= \rho(W)_{i-1} + W_i^T \ M_i^{-1} \ W_i \\ (\nu)_i &= (\nu)_{i-1} + \nu_i \end{aligned}\right\} \text{ transmitted to next phase} \tag{3-106}$$

The current estimate of X is

$$\hat{X} = X^O - N_i^{-1} \ U_i \tag{3-107}$$

$$Q^{\hat{X}} = N_i^{-1} \tag{3-108}$$

$$\hat{Y}^T \ P^Y \ \hat{Y} = \rho(W)_i - U_i^T \ \hat{X} \tag{3-109}$$

$$\hat{\Sigma}_{\hat{X}} = \frac{\hat{Y}^T \ P^Y \ \hat{Y}}{(\nu)_i} \ Q^{\hat{X}} \quad . \tag{3-110}$$

The estimate of the residuals for the current stage is

$$\hat{Y}_i = -Q^{Y_i} \ B_i^T \ M_i^{-1} \ (W_i + A_i \ \hat{X}) \tag{3-111}$$

$$Q^{\hat{Y}_i} = Q^{Y_i} \ B_i^T \ M_i^{-1} \ (B_i \ Q^{Y_i} - A_i \ (A_i^T \ M_i^{-1} \ A_i)^{-1} \ A_i^T \ M_i^{-1} \ B_i \ Q^{Y_i}) \tag{3-112}$$

$$\hat{\Sigma}_{\hat{Y}_i} = \frac{\hat{Y}^T P^Y \hat{Y}}{(\nu)_i} Q^{\hat{Y}_i} \quad . \tag{3-113}$$

3.3.2 Two matrix identities

Given nonsingular matrices ${}_nR_n$ and ${}_mS_m$ and rectangular matrix ${}_nA_m$ (where the subscripts n,m denote row and column dimensions respectively)then

$${}_mI_m A^T = A^T {}_nI_n \quad , \tag{3-114}$$

$$S S^{-1} A^T = A^T R R^{-1} \quad , \tag{3-115}$$

adding $A^T R A S^{-1} A^T$

$$S S^{-1} A^T + A^T R A S^{-1} A^T = A^T R R^{-1} + A^T R A S^{-1} A^T \tag{3-116}$$

$$(S + A^T R A) S^{-1} A^T = A^T R (R^{-1} + A S^{-1} A^T) \tag{3-117}$$

postmultiplying by $(R^{-1} + A S^{-1} A^T)^{-1}$ and premultiplying by $(S + A^T R A)^{-1}$

$$\boxed{S^{-1} A^T (R^{-1} + A S^{-1} A^T)^{-1} = (S + A^T R A)^{-1} A^T R} \quad . \tag{3-118}$$

Premultiplying by A and subtracting from I

$$I - A S^{-1} A^T (R^{-1} + A S^{-1} A^T)^{-1} = I - A (S + A^T R A)^{-1} A^T R \tag{3-119}$$

$$(R^{-1}+AS^{-1}A^T)(R^{-1}+AS^{-1}A^T)^{-1} - AS^{-1}A^T(R^{-1}+AS^{-1}A^T)^{-1} = I-A(S+A^TRA)^{-1}A^TR \tag{3-120}$$

$$R^{-1} (R^{-1} + A S^{-1} A^T)^{-1} = I - A(S + A^T R A)^{-1} A^T R \tag{3-121}$$

premultiplying by R

$$\boxed{(R^{-1} + A S^{-1} A^T)^{-1} = R - R A (S + A^T R A)^{-1} A^T R} \quad . \tag{3-122}$$

3.3.3 Phased and sequential expressions

The least squares estimate expressions given in section 3.3.1 are often called the "phased adjustment" (Tienstra, 1956; Ying, 1970; Kouba, 1972).

They involve the inversion of a matrix whose rank is equal to the number of elements in the vector X. In this section we use the matrix identities (3-118) and (3-122) of section 3.3.2 to modify these expressions and obtain new expressions involving the inversion of a matrix whose rank is equal to the number of elements in Y. These new expressions are often called the "sequential adjustment" (Schmid and Schmid, 1965; Krakiwsky, 1968). It is evident that the phased adjustment is advantageous for problems involving fewer "unknown" parameters per stage, whereas the sequential adjustment is advantageous for problems involving fewer "observable" parameters per stage.

From section 3.3.1 we can write the phased expressions

$$\hat{X}_i = X^o - N_i^{-1} U_i \quad , \tag{3-123}$$

$$Q^{\hat{X}_i} = N_i^{-1} \quad , \tag{3-124}$$

where

$$N_i = N_{i-1} + A_i^T M_i^{-1} A_i \quad , \tag{3-125}$$

$$U_i = U_{i-1} + A_i^T M_i^{-1} W_i \quad . \tag{3-126}$$

Then

$$\begin{aligned} \hat{X}_i &= X^o - Q^{\hat{X}_i} (U_{i-1} + A_i^T M_i^{-1} W_i) \\ &= X^o - Q^{\hat{X}_i} U_{i-1} - Q^{\hat{X}_i} A_i^T M_i^{-1} W_i \quad . \end{aligned} \tag{3-127}$$

From (3-122)

$$Q^{\hat{X}_i} = (N_{i-1} + A_i^T M_i^{-1} A_i)^{-1} = N_{i-1}^{-1} - N_{i-1}^{-1} A_i^T (M_i + A_i N_{i-1}^{-1} A_i^T)^{-1} A_i N_{i-1}^{-1} \quad . \tag{3-128}$$

From (3-118)

$$Q^{\hat{X}_i} A_i^T M_i^{-1} = (N_{i-1} + A_i^T M_i^{-1} A_i)^{-1} A_i^T M_i^{-1} = N_{i-1}^{-1} A_i^T (M_i + A_i N_{i-1}^{-1} A_i^T)^{-1} \quad (3\text{-}129)$$

Hence

$$\hat{X}_i = X^o - N_{i-1}^{-1} U_{i-1} - N_{i-1}^{-1} A_i^T (M_i + A_i N_{i-1}^{-1} A_i^T)^{-1} (W_i - A_i N_{i-1}^{-1} U_{i-1}) \quad (3\text{-}130)$$

$$Q^{\hat{X}_i} = N_{i-1}^{-1} - N_{i-1}^{-1} A_i^T (M_i + A_i N_{i-1}^{-1} A_i^T)^{-1} A_i N_{i-1}^{-1} \quad . \quad (3\text{-}131)$$

However

$$\hat{X}_{i-1} = -N_{i-1}^{-1} U_{i-1} \quad , \quad (3\text{-}132)$$

$$Q^{\hat{X}_{i-1}} = N_{i-1}^{-1} \quad . \quad (3\text{-}133)$$

Hence

$$\hat{X}_i = X^o + \hat{X}_{i-1} - Q^{\hat{X}_{i-1}} A_i^T (M_i + A_i Q^{\hat{X}_{i-1}} A_i^T)^{-1} (W_i + A_i \hat{X}_{i-1}) \quad , \quad (3\text{-}134)$$

$$Q^{\hat{X}_i} = Q^{\hat{X}_{i-1}} - Q^{\hat{X}_{i-1}} A_i^T (M_i + A_i Q^{\hat{X}_{i-1}} A_i^T)^{-1} A_i Q^{\hat{X}_{i-1}} \quad , \quad (3\text{-}135)$$

which are the sequential expressions.

3.3.4 Partitioning the Y vector

Let us partition the Y vector into observables L and quasi-observables Z such that

$$Y = \begin{bmatrix} L \\ Z \end{bmatrix}, \quad B = \begin{bmatrix} -I, D \end{bmatrix}, \quad Q^Y = \begin{bmatrix} Q^L & 0 \\ 0 & Q^Z \end{bmatrix} \quad . \quad (3\text{-}136)$$

Then the linearized equations for the i^{th} stage are

$$W_i + A_i X - L_i + D_i Z_i = 0 \quad , \quad (3\text{-}137)$$

so that

$$M_i = Q^{L_i} + D_i \, Q^{Z_i} \, D_i^T \quad . \tag{3-138}$$

The expressions for the updating of N, U, $\rho(W)$, ν and for the estimates $\hat{X}$ and $\hat{\Sigma}_{\hat{X}}$ remain unchanged, from section 3.3.1 however the estimated residuals for the current stage are now

$$\hat{Z}_i = -Q^{Z_i} \, D_i^T \, M_i^{-1} \, (W_i + A_i \, \hat{X}) \quad , \tag{3-139}$$

$$\hat{L}_i = W_i + A_i \, \hat{X} + D_i \, \hat{Z}_i \quad . \tag{3-140}$$

3.3.5 Avoiding explicit inversion of matrix M

In the case where the number of observables is different from the number of quasi-observables, the rank of the matrix to be inverted can be reduced to the minimum of the two. If there are more quasi-observables than observables, then matrix M has minimum rank. If there are more observables than quasi-observables, then we can use the matrix identities to reduce the rank of the matrix to be inverted. We have

$$M = P^{L^{-1}} + D \, P^{Z^{-1}} \, D^T \quad . \tag{3-141}$$

From (3-122) we see

$$M^{-1} = P^L - P^L \, D \, (P^Z + D^T \, P^L \, D)^{-1} \, D^T \, P^L \quad , \tag{3-142}$$

and for the expression for $\hat{Z}_i$ we see from (3-118) that

$$P^{Z^{-1}} \, D^T \, M^{-1} = (P^Z + D^T \, P^L \, D)^{-1} \, D^T \, P^L \quad . \tag{3-143}$$

Then, given

$$N_{i-1} \; , \; U_{i-1} \; , \; \rho(W)_{i-1} \; , \; (\nu)_{i-1} \quad , \tag{3-144}$$

and

$$A_i \; , \; D_i \; , \; W_i \; , \; P^{Z_i} \; , \; P^{L_i} \; , \; \nu_i \tag{3-145}$$

we have

$$M_i^{-1} = P^{L_i} - P^{L_i} D_i \left(P^{Z_i} + D_i^T P^{L_i} D_i\right)^{-1} D_i^T P^{L_i} \tag{3-146}$$

$$\left.\begin{aligned} N_i &= N_{i-1} + A_i^T M_i^{-1} A_i \\ U_i &= U_{i-1} + A_i^T M_i^{-1} W_i \\ \rho(W)_i &= \rho(W)_{i-1} + W_i^T M_i^{-1} W_i \\ (\nu)_i &= (\nu)_{i-1} + \nu_i \end{aligned}\right\} \text{ to next stage} \tag{3-147}$$

$$\hat{X} = X^o - N_i^{-1} U_i \tag{3-148}$$

$$\hat{\Sigma}_{\hat{X}} = \frac{\rho(W)_i + U_i^T X_i}{(\nu)_i} N_i^{-1} \tag{3-149}$$

$$\hat{Z}_i = \left(P^{Z_i} + D_i^T P^{L_i} D_i\right)^{-1} D_i^T P^{L_i} \left(W_i + A_i \hat{X}\right) \tag{3-150}$$

$$\hat{L}_i = W_i + A_i \hat{X} + D_i \hat{Z}_i \quad . \tag{3-151}$$

CHAPTER 4

IDENTIFICATION, ACCURACY AND SHAPE OF THE OPERATIONAL EPHEMERIS

The Doppler observation equation (2-43) contains terms S(t), the slant range between satellite and receiver at epoch t. If we are using the Doppler observations to position the receiver, we must be given satellite coordinates for all epochs t at which we make measurements. In this chapter we consider one source for these satellite coordinates, the operational ephemeris; the set of parameters broadcast by Transit satellites as part of their transmission. In section 4.1 we describe the operational ephemeris and how satellite coordinates can be obtained from it.

An important theorem concerning the operational (or any other) ephemeris is presented in section 4.2 We will make extensive use of this theorem elsewhere in the chapter and in Chapter 5.

The remainder of the chapter deals with three basic problems concerning the operational ephemeris:

(a) how to automatically identify exactly which satellite pass has been tracked,

(b) how accurate is the operational ephemeris, and

(c) how can we obtain satellite positions interpolated between those provided by the operational ephemeris.

4.1 The Operational Ephemeris

The operational ephemeris consists of parameters broadcast by Transit satellites from which earth-fixed satellite positions can be

computed (Moffett, 1971). These parameters are divided into 14 fixed orbit parameters (see Table 4-1) whose values change only twice each day, and four sets of variable orbit parameters (see Table 4-2) whose values change every two minutes. The operational ephemeris is computed for each satellite by fitting 36-hour orbital arcs to Doppler data from four tracking stations (in Maine, Minnesota, California, and Hawaii), and extrapolating this arc 16 hours beyond the time of the last data used (Piscane et al, 1973). Parameters describing this extrapolated arc are then determined by computing a best fitting set of eleven mean orbit parameters (the parameters of Table 4-1 for which symbols are listed) and resolving the residuals of this fit at even minute intervals into the two sets of variable orbit parameters $\Delta E(t)$, $\Delta a(t)$ and at four minute invervals into the set $\eta(t)$ (Table 4-2).

There are at present (July, 1974) six operational Transit satellites. The identification numbers for each of these are summarized in Table 4-3. Values for selected parameters from the operational ephemerides for June 23, 1974 are given in Table 4-4. All Transit satellites follow circular polar trajectories of approximately the same altitude and period. Table 4-5 based on the parameter values from Table 4-4 indicates that the fixed orbit parameters define trajectories which are circular (equal semi-major and semi-minor axes) within 1200 metres, are polar (inclinations of 90°) to within better than one degree, have equal altitudes (semi-major axes equal to the mid-range value of 7430 km) within 40 km, and have equal periods (equal to the mid-range value of 106.25 minutes) within less than one minute. Figure 4-1 based on the parameter values from Table 4-4, shows the right ascensions of the ascending nodes, and their precession rates, as of June 23, 1974.

Symbol	Definition	Broadcast Units (Current Resolution)*
tp	Time of first satellite perigee after last satellite injection	10^{-4} min UT
n	Mean motion (only fractional part is broadcast)	10^{-7} deg/min
$\omega(tp)$	Argument of perigee at tp	10^{-4} deg
$\lvert\dot{\omega}\rvert$	Absolute value of precession rate of perigee	10^{-7} deg/min
e	Eccentricity of orbit ellipse	10^{-6}
$\bar{a}$	Mean semi-major axis of orbit ellipse	10 metres
$\Omega(tp)$	Right ascension of ascending node at tp	10^{-4} deg
$\dot{\Omega}$	Precession rate of ascending node	10^{-7} deg/min
cos i	Cosine of inclination	10^{-6}
GAST(tp)	Greenwich apparent sidereal time at tp	10^{-4} deg
-	Satellite identification number	-
-	Day number and time of last satellite data injection	2 min UT
sin i	Sine of inclination	10^{-6}
-	Fractional satellite frequency offset $(f_o - f_s)/f_o$	parts in 10^9

* For each of these parameters there is a trailing zero digit which is not currently used, and which could be used to increase the resolution (the frequency offset has four trailing zeroes).

TABLE 4-1

Fixed Orbit Parameters

Symbol	Definition	Broadcast Units
t	Time in even minutes of UT, modulus one half hour	2 min UT
$\Delta E(t)$	Correction to eccentric anomaly at time t	10^{-4} deg
$\Delta a(t)$	Correction to semi-major axis at time t	10 metres
$\eta(t)$	Out of plane orbit component at time t*	10 metres

* $\eta(t)$ values are available only at four minute intervals (for times which when expressed in minutes UT are divisible by 4). $\Delta E(t)$ and $\Delta a(t)$ values are available at two minute intervals (for even minutes UT).

TABLE 4-2

Variable Orbit Parameters

Launch Date	Apr 14 1967	May 18 1967	Sep 25 1967	Mar 2 1968	Aug 27 1970	Oct 30 1973
Code Names	0-12 OSCAR 12	0-13 OSCAR 13	0-14 OSCAR 14	0-18 OSCAR 18	0-19 OSCAR 19	0-20 OSCAR 20
International Number	1967-034A	1967-048A	1967-092A	1968-012A	1970-067A	1973-081A
NASA Number	2754	2807	2965	3133	4507	6909
APL Number	30120/36	30130/40	30140/56	30180/52	30190/28	30200/16
Operational Ephemeris Identification Number	30120	30130	30140	30180	30190	30200
Used Here	12	13	14	18	19	20

TABLE 4-3

Transit Satellite Identification Numbers

Satellite	n(deg/min)	e	a(km)	Ω(deg)	$\dot{\Omega}$(deg/min)	cos i
12	3.3813608	.002137	7438.10	10.9708	+.0000147	-.003652
13	3.3661988	.002044	7460.44	334.1076	-.0000254	+.006365
14	3.3726972	.004840	7450.85	6.7239	-.0000524	+.013083
18	3.3670756	.007956	7459.14	277.2435	-.0000013	+.000316
19	3.3654875	.017802	7461.49	245.9560	+.0000067	-.001682
20	3.4103203	.016842	7395.90	112.4926	+.0000127	-.003088

TABLE 4-4

Values for Selected Operational Ephemeris Parameters for June 23, 1974

Satellite	a-b * $= a(1-\sqrt{1-e^2})$	(i-90°)	a-7430	(Period-106.25 min) = (360°/n-106.25)
12	17 m	+ 13 arcmin	8 km	13 sec
13	16	- 22	30	42
14	87	- 45	21	29
18	236	- 1	29	40
19	1182	+ 6	31	43
20	1049	+ 11	-34	-41

*The apogee-perigee radial difference is 2ae (see Figure 4-2). For satellites 12, 13, 14, 18, 19 and 20, 2ae is respectively 32, 31, 72, 119, 266 and 249 km.

TABLE 4-5

Transit Orbit Geometry

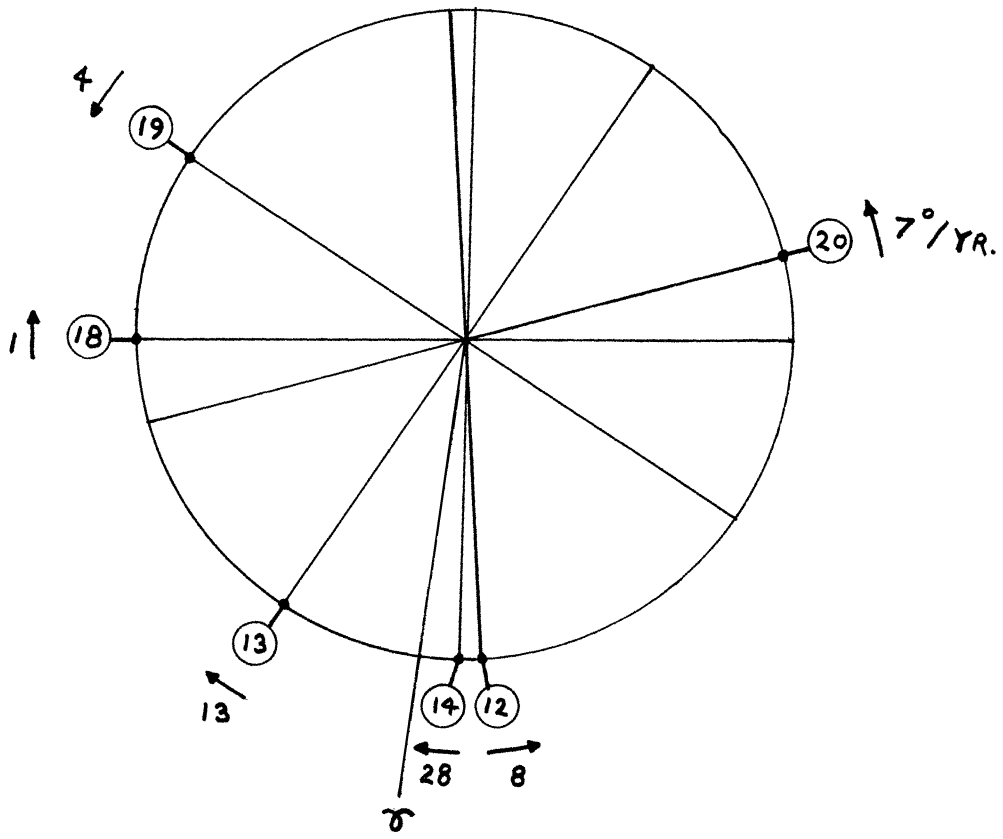

FIGURE 4-1
Transit Orbit Ascending Node Right Ascensions
and Precessions for June 23, 1974.

4.1.1 Earth fixed satellite coordinates

To obtain the transformation between the parameters of the operational ephemeris and earth fixed coordinates, let us first consider the geometry of the orbital ellipse (Figure 4-2) and the position of this ellipse in an earth fixed coordinate system (Figure 4-3).

The size and shape of the ellipse is defined by its semi-major axis, a, and eccentricity, e. Transit ellipses are considered to have time-varying semi-major axes

$$a(t) = \bar{a} + \Delta a(t) \quad . \tag{4-1}$$

The position of the satellite with respect to the perigee point can be described in terms of the mean anomaly

$$M(t) = n(t - tp) \quad , \tag{4-2}$$

or in terms of the eccentric anomaly, which for Transit satellites is defined (see section 4.5.1 for another definition)

$$E(t) = M(t) + e \sin M(t) + \Delta E(t) \quad , \tag{4-3}$$

or in terms of the true anomaly

$$f(t) = \arctan \left[\frac{\sin E(t)}{\cos E(t) - e}\right] \quad . \tag{4-4}$$

Then the satellite coordinates with respect to the orbital coordinate system are, for the Transit system

$$X_o(t) = \begin{bmatrix} x_o(t) \\ y_o(t) \\ z_o(t) \end{bmatrix} = \begin{bmatrix} a(t)(\cos E(t) - e) \\ a(t) \sin E(t) \\ n(t) \end{bmatrix} \quad . \tag{4-5}$$

These orbital coordinates are related to earth fixed (terrestrial) coordinates by three rotations

$$X_T(t) = \begin{bmatrix} x_T(t) \\ y_T(t) \\ z_T(t) \end{bmatrix} = R(t)X_o(t) \quad , \tag{4-6}$$

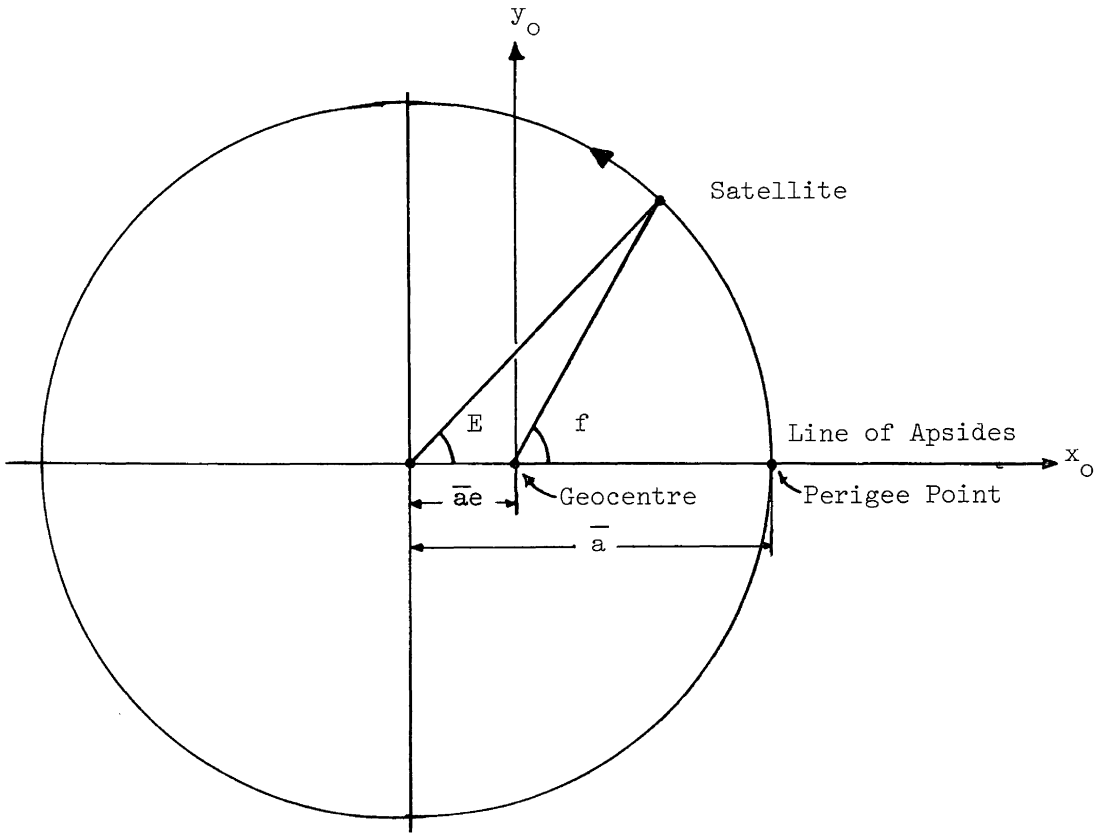

FIGURE 4-2

Transit Orbit Ellipse

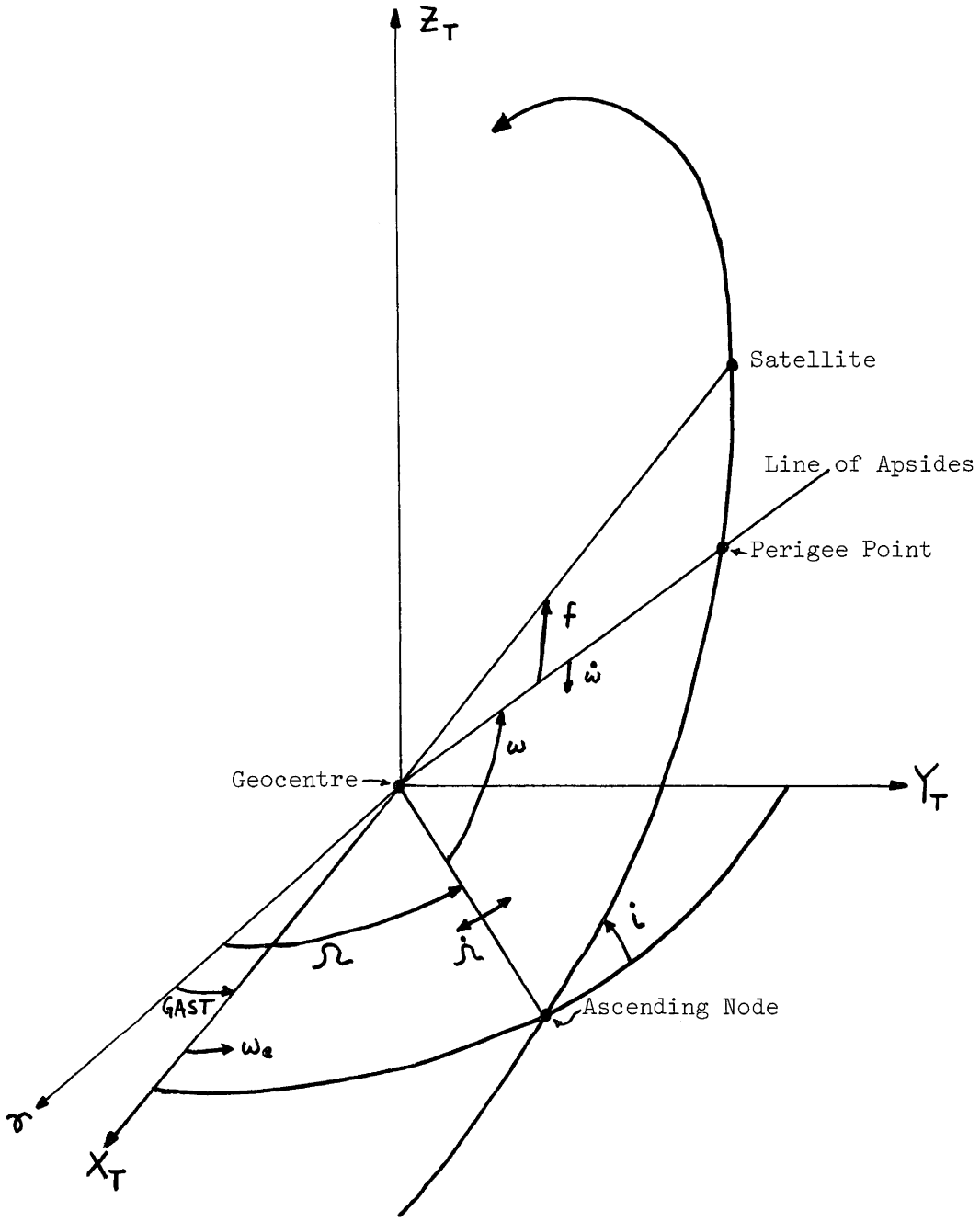

FIGURE 4-3

Position of Orbit Ellipse in an Earth Fixed Coordinate System

where

$$R(t) = R_3(\alpha_3(t))R_2(\alpha_2)R_3(\alpha_1(t)) \tag{4-7}$$

$$\alpha_1(t) = -\omega(t) = -\omega(tp) + |\dot{\omega}|(t - tp) \tag{4-8}$$

$$\alpha_2 = -i = -\arctan(\sin i/\cos i) \tag{4-9}$$

$$\alpha_3(t) = -\Omega(t) + GAST(t) = -\Omega(tp) + GAST(tp) + (\omega_e - \dot{\Omega})(t - tp) \tag{4-10}$$

$$\omega_e = \text{earth's rotation rate} = 4.3752695 \text{ milliradians/minute} \tag{4-11}$$

and the

R_i = the rotation matrices for rotations about axis i (Krakiwsky and Wells, 1971).

Equations (4-1) to (4-11) can be considered to define the eleven constants tp, n, $\omega(tp)$, $|\dot{\omega}|$, e, $\bar{a}$, $\Omega(tp)$, $\dot{\Omega}$, cos i, GAST(tp) and sin i (the fixed orbit parameters of Table 4-1), and the three functions $\Delta E(t)$, $\Delta a(t)$ and $\eta(t)$ (the variable orbit parameters of Table 4-2). In section 4.5.2 we compare these definitions with the definitions of parameters describing unperturbed and perturbed Keplerian orbits.

We have not yet stated precisely which terrestrial coordinates are obtained from the operational ephemeris. The two usual possibilities are instantaneous terrestrial coordinates (for which the Z_T axis is directed towards the earth's instantaneous axis of rotation), and average terrestrial coordinates (for which the Z_T axis is directed towards the Conventional International Origin, or CIO pole) (Krakiwsky and Wells, 1971). Since the location of the instantaneous pole with respect to the earth's crust varies by about 10 m (polar motion), it is preferable to express the location of tracking stations on the earth's crust in terms of average coordinates.

Since January 27, 1974 the operational ephemeris is claimed to yield average terrestrial coordinates (Piscane et al, 1973). However,

prior to that date (particularly for the data analyzed in Chapter 5), it appears that the operational ephemeris yielded coordinates which were neither average nor instantaneous. Evidence discussed in section 4.4.1 and in Chapter 5 indicates, however, that the coordinates were closer to instantaneous than average, in which case it is beneficial to apply the correction which transforms instantaneous into average coordinates (polar motion correction). In this case equation (4-7) becomes

$$R(t) = R_1(\frac{-y_p}{r})\ R_2(\frac{-x_p}{r})\ R_3(\alpha_3(t))\ R_1(\alpha_2)\ R_3(\alpha_1(t)) \qquad (4\text{-}12)$$

where r is the earth's radius and (x_p, y_p) are the coordinates of the instantaneous pole relative to the CIO pole (Krakiwsky and Wells, 1971), all in metres.

4.2 Guier's Theorem

Guier's theorem is based upon two principles. First, when the error in the satellite trajectory is small, the actual and estimated trajectories are nearly parallel (Guier, 1965). Second, the three parameters most fully representing the information contained in a set of satellite Doppler observations from a single pass (Figure 4-4) are the time of closest approach (the time, t_{ca} at which the slope of the Doppler curve is a maximum), the receiver to satellite range at closest approach (related to the maximum value of the slope, $(df/dt)_{ca}$), and the frequency offset between satellite and receiver oscillators (related to the Doppler frequency, f_{ca} at maximum slope). The first two parameters are dependent upon the tracking station to satellite geometry (they are geometrical parameters), while the third is independent of geometry (it is a nuisance parameter).

Guier's theorem relates to the geometrical parameters, and has been stated as follows (Guier, 1965):

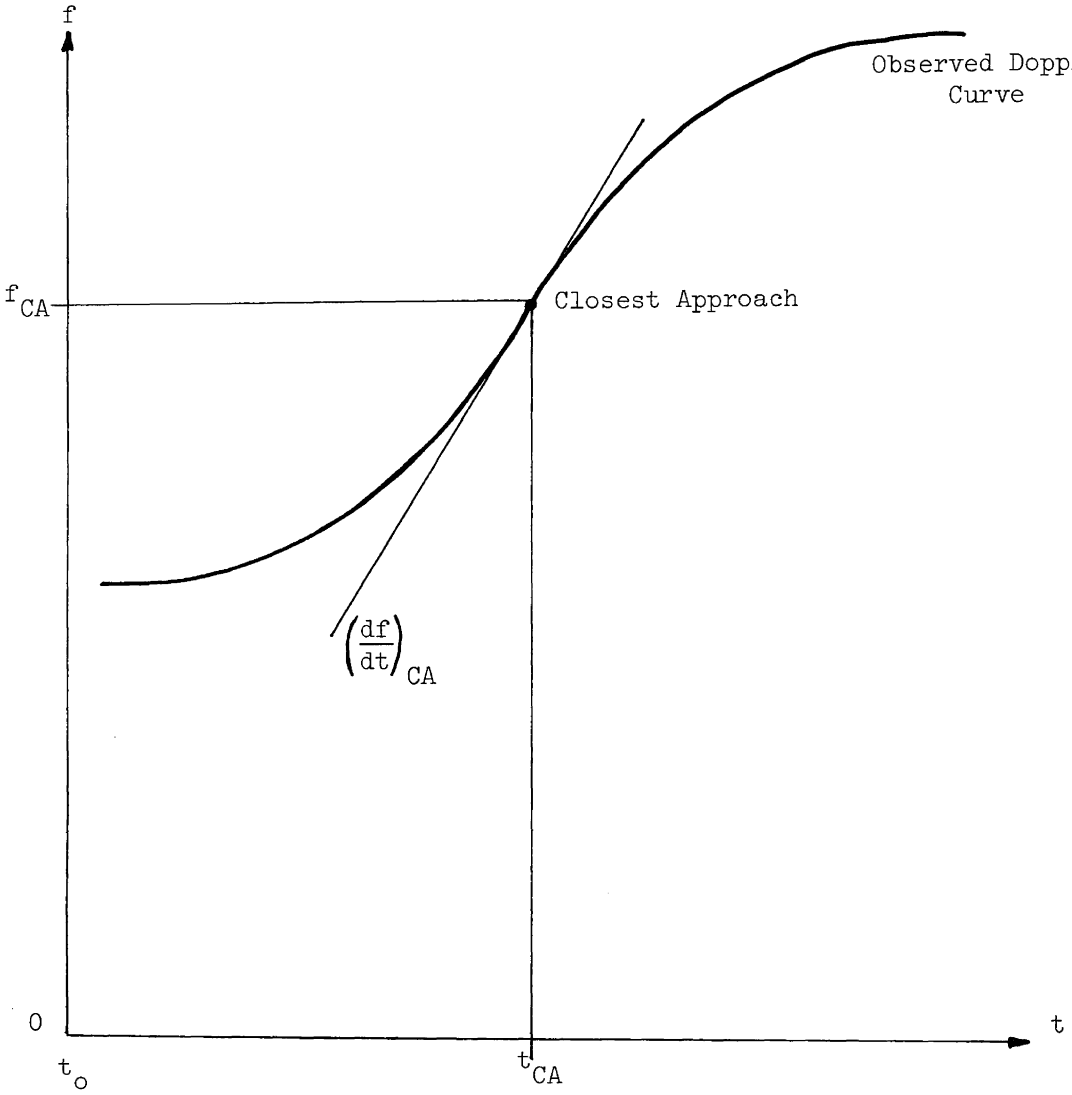

FIGURE 4-4

Parameters Describing a Doppler Curve

Guier's Theorem (A): To first order, Doppler residuals can be reduced to their experimental noise level by so adjusting the satellite position at closest approach that the range and time of closest approach agree with their experimental values.

These two geometrical parameters (closest approach time and range) are equivalent to the closest approach satellite coordinates, expressed in the coordinate system with origin at the tracking station, x axis aligned to the a priori estimate of the closest approach range vector, y axis parallel to the a priori estimate of the closest approach satellite velocity vector, and z axis forming a right hand triad, (Figure 4-5). Provided that the tracking station coordinates with respect to the origin of the coordinate system implied by the Transit operational ephemeris are reasonably well known (say within a few tens of metres), and given geocentric satellite coordinates and velocities, it is possible to compute satellite coordinates referred to this coordinate system (section 4.2.1).

Guier's theorem can then be restated as follows (Guier, 1965):

Guier's Theorem (B): To first order, Doppler residuals can be reduced to their experimental noise level by appropriately adjusting the satellite position at closest approach in the plane defined by the closest approach range and velocity vectors.

By so adjusting only the satellite position at closest approach we are in effect performing parallel translations of the trajectory in the range (x_G) and along track (y_G) directions. This is equivalent to a translation (with opposite sign) of the tracking station coordinates away from the origin (that is away from their initial values), constrained to the xy plane. Henceforth we shall refer to this xy plane as the Guier plane.

Hence we can restate Guier's theorem again as follows (Newton, 1967):

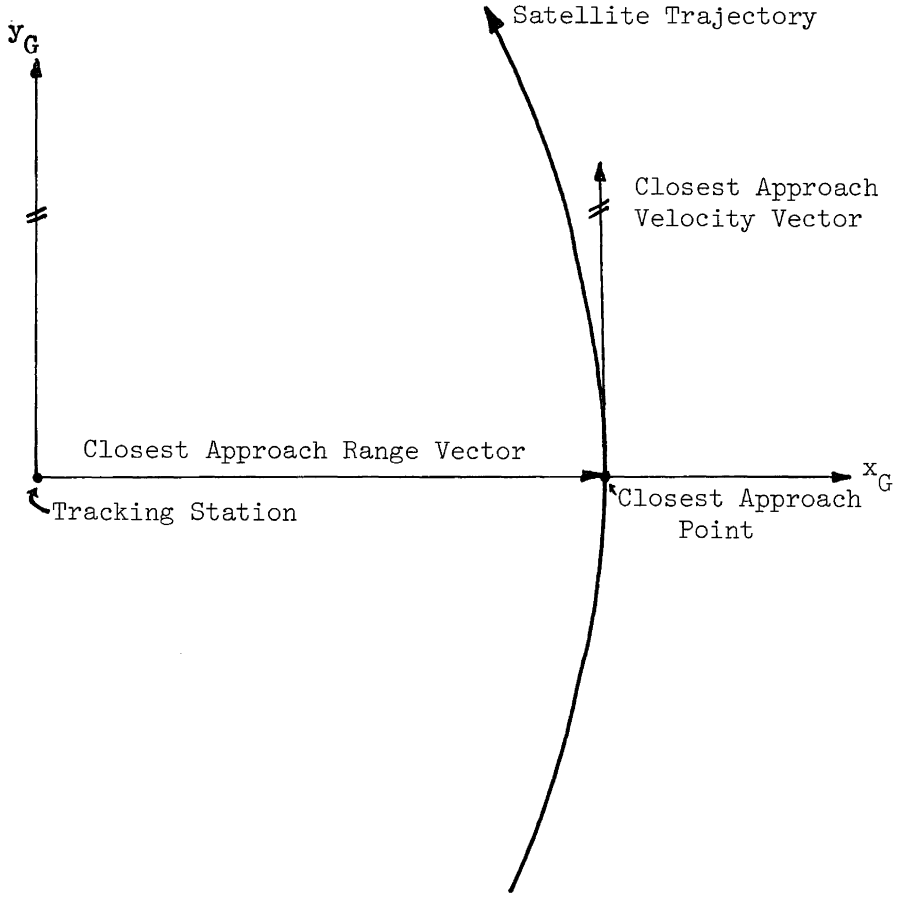

FIGURE 4-5

Guier Plane Geometry

Guier's Theorem (C): The three quantities which can be determined with accuracy using the data from a single pass are the frequency offset, the navigator's coordinate parallel to the satellite velocity vector and the shortest distance from the navigator to the satellite.

In summary, a final restatement of Guier's theorem using the terminology of adjustment calculus is as follows:

Guier's Theorem (D): An adjustment in which the observations are Doppler data from a single pass, and the unknown parameters are the closest approach range and time (and the frequency offset), or equivalently the coordinates of the satellite at closest approach in the Guier plane (and the frequency offset), or equivalently the navigator's coordinates in the Guier plane (and the frequency offset), will result in an estimated variance factor which is, to first order, uncontaminated by satellite orbit errors, and a solution vector expressing the satellite orbit errors resolved into range (x) and along track (y) components.

These two properties of navigation in the Guier plane (uncontaminated variance factor, and estimates of orbit errors) make it eminently suitable for editing and filtering both Doppler observations and satellite orbit parameters. In addition, the solution for frequency offset in the Guier plane is also less contaminated by other effects than the solution for frequency offset in any other coordinate system. We will make use of, and further discuss these applications of Guier plane navigation in Chapter 5.

4.2.1 Guier plane coordinates

To compute satellite coordinates in the Guier plane, we must be given

(a) the parameters of the operational ephemeris, discussed in section 4.1;

(b) an algorithm for interpolating between the satellite positions defined (at two minute intervals) by the operational ephemeris, discussed in section 4.5;

(c) the time of closest approach, t_{ca}, computation of which is discussed in section 4.3; and

(d) an initial estimate of the tracking station coordinates, X_R, within a few tens of metres of the "true" values. (In practice X_R can usually be obtained to within a few km either from existing maps, or if necessary, astronomic observations. This rough estimate can then be refined to within a few tens of metres from a preliminary processing of several Transit passes.)

Two of the axes of the Guier plane are the closest approach satellite range vector

$$x_G = (X_T(t_{ca}) - X_R) \quad , \tag{4-13}$$

and the closest approach satellite velocity vector

$$y_G = \dot{X}_T(t_{ca}) \quad . \tag{4-14}$$

To transform terrestrial coordinates to Guier plane coordinates we first translate the origin from the geocentre to the tracking station, then rotate the terrestrial axes to align with the Guier plane axes. In general given two coordinate systems with a common origin C and $\tilde{C}$, and the three unit vectors $\hat{U}_i$ of the $\tilde{C}$ axes expressed in the C system, then the transformation from C coordinates to $\tilde{C}$ coordinates is

$$X_{\tilde{C}} = R\, X_C \quad , \tag{4-15}$$

where the orthogonal transformation (product rotation) matrix row vectors are $\hat{U}_i$, that is

$$R = \begin{bmatrix} \hat{U}_1^T \\ \hat{U}_2^T \\ \hat{U}_3^T \end{bmatrix} \quad . \tag{4-16}$$

In our case

$$X_G(t) = R(X_T(t) - X_R) \quad , \tag{4-17}$$

where the row vectors of R are

$$\hat{U}_1 = \frac{X_T(t_{ca}) - X_R}{|X_T(t_{ca}) - X_R|} \quad , \tag{4-18}$$

$$\hat{U}_2 = \frac{\dot{X}_T(t_{ca})}{|\dot{X}_T(t_{ca})|} \quad , \tag{4-19}$$

$$\hat{U}_3 = \hat{U}_1 \times \hat{U}_2 \quad . \tag{4-20}$$

We need now only compute $X_T(t_{ca})$ and $\dot{X}_T(t_{ca})$. From (4-6)

$$X_T(t_{ca}) = R(t_{ca})\, X_o(t_{ca}) \quad , \tag{4-21}$$

and

$$\dot{X}_T(t_{ca}) = R(t_{ca})\, \dot{X}_o(t_{ca}) + \dot{R}(t_{ca})\, X_o(t_{ca}) \quad . \tag{4-22}$$

From (4-5)

$$\dot{X}_o(t) = \begin{bmatrix} \dot{a}(t)(\cos E(t) - e) - \dot{E}(t)\, a(t) \sin E(t) \\ \dot{a}(t) \sin E(t) + \dot{E}(t)\, a(t) \cos E(t) \\ \dot{\eta}(t) \end{bmatrix} \quad , \tag{4-23}$$

where from (4-1), (4-2) and (4-3)

$$\dot{a}(t) = \dot{\Delta a}(t) \tag{4-24}$$

$$\dot{E}(t) = \dot{M}(t)(1 + e \cos M(t)) + \dot{\Delta E}(t) \tag{4-25}$$

$$\dot{M}(t) = n \quad , \tag{4-26}$$

and $\dot{\Delta E}(t)$, $\dot{\Delta a}(t)$ and $\dot{\eta}(t)$ are discussed in section 4.5.4. From (4-7)

$$\dot{R}(t) = \dot{R}_3(\alpha_3(t))\, R_1(\alpha_2)\, R_3(\alpha_1(t)) + R_3(\alpha_3(t))\, R_1(\alpha_2)\, \dot{R}_3(\alpha_1(t)), \tag{4-27}$$

where in general

$$\dot{R}_i(\alpha) = \dot{\alpha}[R_i(\alpha + \pi/2) - \tfrac{1}{2}(P_{i+1} + P_{i+2})] \quad , \tag{4-28}$$

and (i+1), (i+2) are modulus 3, the P_i matrices being reflection matrices (Krakiwsky and Wells, 1971). In our case, from (4-8) and (4-10)

$$\dot{\alpha}_3(t) = \omega_e - \dot{\Omega} \quad , \tag{4-29}$$

$$\dot{\alpha}_1(t) = |\dot{\omega}| \quad . \tag{4-30}$$

4.2.2 Guier plane navigation

In this section we combine the Doppler observation equation (2-43), the parametric adjustment of section 3.2.3, and the Guier plane coordinate system, to provide an algorithm for navigating in two dimensions on the Guier plane. Guier plane navigation results are discussed in section 4.4.3 and in Chapter 5.

From Chapter 2, the observation equation for a refraction-corrected Doppler count integrated between times t_1 and t_2 is

$$D = (\Delta f_g - \Delta f_s) f_o (t_2 - t_1) + \frac{f_o}{c}(1 + \Delta f_g)\,(S(t_2) - S(t_1)) \quad , \tag{4-31}$$

where c is the vacuum velocity of light, f_o is the nominal reference frequency (400 MHz),

$$\Delta f_g = \frac{f_g - f_o}{f_o} \quad \text{and} \quad \Delta f_s = \frac{f_s - f_o}{f_o} \quad , \tag{4-32}$$

are the relative frequency offsets of the receiver and satellite reference oscillators from f_o, and S(t) is the slant range at time t. In the Guier plane coordinate system

$$S(t) = [(x_G(t) - x_R)^2 + (y_G(t) - y_R)^2 + (z_G(t) - z_R)^2]^{1/2} \quad , \tag{4-33}$$

where $x_G(t)$, $y_G(t)$, $z_G(t)$ are the Guier plane satellite coordinates at time t, from section 4.2.1, and in the Guier plane the initial approximation for the receiver position vector is $x_R = y_R = z_R = 0$.

In the two-dimensional fix computation used here c, f_o, $(t_2 - t_1)$, $x_G(t)$, $y_G(t)$, $z_G(t)$, Δf_s and $z_R(=0)$ are all assumed to be perfectly known (have a priori variances of zero) and x_R, y_R and Δf_g are assumed to be completely unknown (have a priori weights of zero). The Doppler counts have

an a priori weight matrix P.

In the notation of section 3.2.3 we can write the observation equation as

$$L = F(X^a) \quad , \tag{4-34}$$

where L is the vector of Doppler observations D, and X^a is the solution vector, containing final values for (x_R, y_R and Δf_g), given the initial values (x_R^o, y_R^o, Δf_g^o) as the elements of X^o. Letting

$$V = L - F(X^a) \quad , \tag{4-35}$$ *

and linearizing $F(X^a)$ we have

$$V = W - A\,X \quad , \tag{4-36}$$

where the residual vector V and correction vector $X = X^a - X^o$ are to be determined, the i^{th} element of the misclosure vector W has the form

$$W_i = L_i - F_i(X^o) \quad , \tag{4-37}$$

and the i^{th} row of the design matrix A has the form

$$A_i = \left[\frac{\partial F_i}{\partial x_R}\bigg|_{X^o} , \frac{\partial F_i}{\partial y_R}\bigg|_{X^o} , \frac{\partial F_i}{\partial \Delta f_g}\bigg|_{X^o}\right] \tag{4-38}$$

where from the observation equation (4-31)

$$\frac{\partial F}{\partial x_R} = \frac{f_o}{c}(1 + \Delta f_g)\left(\frac{\partial S(t_2)}{\partial x_R} - \frac{\partial S(t_1)}{\partial x_R}\right) \quad , \tag{4-39}$$

$$\frac{\partial F}{\partial y_R} = \frac{f_o}{c}(1 + \Delta f_g)\left(\frac{\partial S(t_2)}{\partial y_R} - \frac{\partial S(t_1)}{\partial y_R}\right) \quad , \tag{4-40}$$

$$\frac{\partial F}{\partial \Delta f_g} = f_o(t_2 - t_1) + \frac{f_o}{c}(S(t_2) - S(t_1)) \quad , \tag{4-41}$$

and

$$\frac{\partial S(t)}{\partial x_R} = -\frac{x_G(t) - x_R}{S(t)} \, , \quad \frac{\partial S(t)}{\partial y_R} = -\frac{y_G(t) - y_R}{S(t)} \, . \tag{4-42}$$

Forming the normal equations

* Note that in 4-35 V has opposite sign to V in 3-71.

$$A^T P A X = A^T P W \quad , \tag{4-43}$$

the correction vector is

$$X = (A^T P A)^{-1} A^T P W \quad , \tag{4-44}$$

the residual vector is

$$V = W - A X \quad , \tag{4-45}$$

the quadratic norm of V is

$$\rho(V) = V^T P V \quad , \tag{4-46}$$

and the covariance matrix of X is

$$\Sigma_X = \frac{\rho(V)}{n-3} (A^T P A)^{-1} \quad , \tag{4-47}$$

where n is the dimension of W (the number of Doppler observations). The solution vector is

$$X^a = X^o + X \quad . \tag{4-48}$$

The process of forming A and W and solving for X and V is iterated, with X^a from each iteration becoming X^o for the next iteration, until the correction vector X is negligibly small.

Provided that sufficiently accurate initial estimates for the receiver coordinates are used, the first two elements of the final solution vector X^a are an indication of the slant range and along track errors in the operational ephemerides for that pass, and the elements of the final residual vector V are an indication of the measurement noise on the individual Doppler measurements. This partitioning of the orbit errors from the measurement noise is a unique feature of the Guier plane coordinate system. In other coordinate systems orbit errors affect and are inseparable from the estimates of measurement noise. The Guier plane is the optimum coordinate system in which to examine and filter both orbit errors and measurement noise. Use of this feature is made later in this chapter, in considering the accuracy of the operational ephemeris, and in Chapter 5, in analyzing data used to compute receiver coordinates.

4.3 Identification of the Operational Ephemeris

From Table 4-2 we see that part of each variable orbit parameter word is a time parameter that only partially defines the epoch to which that word refers. This time parameter gives the number of two minute intervals since the previous even half hour of U.T., but does not specify which hour, or whether the epoch falls in the first or second half hour. That is, we know only that the variable orbit parameters for that epoch refer either to time 2n or to time 2n + 30 minutes past some unknown hour, where n is an integer in the range [0, 14].

Determining which half hour of U.T. is the correct one is a problem which must be solved externally to the data provided by the operational ephemeris. Two solutions are currently implemented. For attended operation of the Transit receiver, the watchkeeper can manually log the times of satellite passes, this manual log being later merged with the automatically recorded data to identify which pass was being tracked. Geodetic receivers, or receivers having real-time computer processing of the data, automatically record local clock time in some form or other, which is used to identify the half hour in which the pass is tracked.

In this section an alternative method of identifying the satellite pass is presented which requires neither attended operation nor local clock records.

As a first step the ambiguity between first or second half hours can be resolved by examining the complete set of out of plane variable orbit parameters $\eta(t)$. Each $\eta(t)$ comprises two digits, only one of which is given in each variable word, therefore it takes a pair of variable words to define each value of $\eta(t)$. Correct values of $\eta(t)$ result if the first of the words in such pairs refer to epochs divisible by four. Given a set of variable words, two possible sets of $\eta(t)$ (one correct and one incorrect)

can be computed by taking the odd words as the first of the $\eta(t)$ pairs, and by taking the even words as the first of the $\eta(t)$ pairs. The correct set of $\eta(t)$ values will be smoothly varying, while the incorrect set will not, so that we can identify the correct set as the one having the smallest variance about the mean. We then know that the odd (or even) variable words refer to epochs divisible by four. Since only one of the possibilities 2n or 2n + 30 can be divisible by four, we have determined the epoch of each variable word to modulus one hour.

In section 4.2 we noted that the Doppler count, slope of the Doppler curve, and the time (all measured when the slope is maximum, that is at closest approach) are the three significant properties of an observed set of Doppler counts. In section 4.3.1 and 4.3.2 we describe algorithms to compute the closest approach time and slope in two ways:

(a) observed values from a set of 4.6 second Doppler counts and

(b) predicted values from the operational ephemeris.

From Table 4-1 we see that one of the fixed parameters defines the day and time of the last data injection. Since we know that these injections occur approximately every twelve hours, we realize that the tracked pass must occur somewhere between, say, injection time minus ten minutes and injection time plus 800 minutes. For each visible pass within this time span the predicted and observed values of closest approach time and slope are compared by evaluating the parameter

$$\Delta = |TCA_{pred} - TCA_{obs}| + |SLOPE_{pred} - SLOPE_{obs}| ,$$

where TCA_{pred} has been reduced to modulus one hour. The pass for which Δ is a minimum identifies the pass. The value of $|TCA_{pred} - TCA_{obs}|$ for correctly identified passes is typically less than 0.3 minutes, and the value of $|SLOPE_{pred} - SLOPE_{obs}|$ for correctly identified passes is typically less than one m/s^2. If Δ is greater than five units the

comparison is presumed to have failed and the pass is rejected. In a test of 940 tracked passes, three were rejected on this criterion, and all of the accepted passes had been correctly identified.

4.3.1 Observed values of closest approach time and slope

At closest approach the Doppler shift is zero by definition (closest approach occurs when the satellite velocity vector is orthogonal to the tracking-station-to-satellite slant range vector). Therefore a Doppler count, the integration interval of which is centred about closest approach, is from (4-31)

$$D_{ca} = (\Delta f_g - \Delta f_s) f_o \, \Delta t \quad , \tag{4-49}$$

where Δt is the length of the integration interval (approximately 4.6 seconds). If we have good estimates for Δf_g and Δf_s then we can compute a good estimate for D_{ca} from (4-49).

The observed Doppler counts can then be scanned to find the two values D_1 and D_2 between which the estimated value D_{ca} falls. The epochs t_1 and t_2 of the centres of the integration intervals of D_1 and D_2 can be interpolated from the known (modulus one hour) two minute epochs.

In the interval $[t_1, t_2]$, typically of five or ten seconds duration, the time variation of the Doppler frequency can be adequately modelled as a linear function. Therefore we can linearly interpolate D_{ca} between D_1 and D_2 to obtain the observed time of closest approach (in minutes past the hour)

$$TCA_{obs} = t_2 - (D_2 - D_{ca}) * (t_2 - t_1)/(D_2 - D_1) \quad . \tag{4-50}$$

The observed slope at closest approach in metres/sec^2 is

$$SLOPE_{obs} = [c/(f_g * \Delta t)] * (D_2 - D_1)/(t_2 - t_1) \quad , \tag{4-51}$$

where now t_1, t_2 are in seconds. This equation scales D_1, D_2 from counts

per 4.6 seconds to counts per second by dividing by Δt, and from counts per second into metres per second by dividing by the wave number f_g/c.

If the final loss of lock occurs before closest approach, or if the initial lock-on occurs after closest approach, then this algorithm fails, and the pass must be rejected or identified by some other means.

4.3.2 Predicted values of closest approach time and slope

The computation of time and slope at closest approach, predicted from the operational ephemeris, is essentially an alert computation. The alert algorithm described here is based on an earlier algorithm (Wells, 1972), modified for greater accuracy and for use at high latitudes. The algorithm is based on three simplifying assumptions:

(a) the satellite orbit is assumed polar and circular. We have seen (Table 4-5) that current satellite orbits are polar within one degree and circular within about one kilometre.

(b) satellites can be assumed to move at the constant angular velocity given by the mean motion parameter (an eccentricity of 0.02 will cause variations from this constant velocity which result in differences of up to 20 seconds in the time at which the satellite is at a particular orbit position).

(c) a first approximation for the orbit radius (used in determining whether a particular pass is visible from the tracking station or not) is simply the semi-major axis, that is

$$R_{orbit} = \bar{a} \quad . \tag{4-52}$$

A second order approximation for the orbit radius (used to compute the satellite acceleration relative to the tracking station at closest approach - that is the predicted slope of the Doppler curve at closest approach scaled into metres/second^2) can be derived from (4-5)

$$\begin{bmatrix} x_o \\ y_o \end{bmatrix} = a \begin{bmatrix} \cos E - e \\ \sin E \end{bmatrix} , \tag{4-53}$$

where

$$E = M + e \sin M \quad , \tag{4-54}$$

$$M = n(t_{ca} - tp) \quad . \tag{4-55}$$

We have

$$R_{orbit} = \sqrt{x_o^2 + y_o^2} = a\sqrt{1 + e^2 - 2e \cos E}$$

$$\simeq a(1 - e \cos E) \simeq a(1 - e \cos M) \quad . \tag{4-56}$$

Assumptions (a) and (b) together imply that we can ignore the variable orbit parameters (for example ΔE corrections are up to 0.2 seconds of time along track), and three of the fixed orbit parameters sin i, cos i, e. We can then resolve seven of the remaining eight fixed orbit parameters into four nodal crossing parameters (Wells, 1972)

$$P = \text{period} = 2\pi/(n - |\dot{\omega}|) \tag{4-57}$$

$$WM = \text{westward motion} = (\omega_e - \dot{\Omega}) * P \tag{4-58}$$

$$TN = \text{time of nodal crossing} = tp - \omega(tp)/(n + |\dot{\omega}|) \tag{4-59}$$

$$LN = \text{longitude of nodal crossing} = \Omega(tp) - GAST(tp) + \omega(tp) * (\omega_e - \dot{\Omega})/(n + |\dot{\omega}|) \tag{4-60}$$

and for subsequent revolutions of the satellite

$$TN_i = TN_{i-1} + P \quad , \tag{4-61}$$

$$LN_i = LN_{i-1} - WM \quad , \tag{4-62}$$

where ω_e is the rotation rate of the earth, and all parameters are scaled into radians, minutes or radians/minute. Typically P = 106.25 minutes and WM = 26° for current satellites. The satellite subpoint latitude and longitude then vary linearly with time as

$$\phi_{SUB}(t) = \begin{cases} \frac{2\pi}{P}(t - TN) & \text{Northgoing pass} \\ \pi - \frac{2\pi}{P}(t - TN) & \text{Southgoing pass} \end{cases} \tag{4-63}$$

$$\lambda_{SUB}(t) = \begin{cases} LN - \frac{WM}{P}(t - TN) & \text{Northgoing pass} \\ LN - \frac{WM}{P}(t - TN) - \pi & \text{Southgoing pass} \end{cases} \tag{4-64}$$

where for a northgoing pass $(-\frac{P}{4} < (t - TN) < \frac{P}{4})$ and for a southgoing pass $(\frac{P}{4} < (t - TN) < \frac{3}{4}P)$.

Let us now derive the conditions at closest approach. From Figure 4-6 we have

$$\Delta\lambda = \lambda_{SUB} - \lambda_{OBS} \quad , \tag{4-65}$$

and on the unit sphere

$$\vec{R}_{OBS} = \begin{bmatrix} \cos\phi_{OBS} \\ o \\ \sin\phi_{OBS} \end{bmatrix}, \quad \vec{R}_{SUB} = \begin{bmatrix} \cos\Delta\lambda & \cos\phi_{SUB} \\ \sin\Delta\lambda & \cos\phi_{SUB} \\ & \sin\phi_{SUB} \end{bmatrix} . \tag{4-66}$$

The subpoint-to-observer vector is

$$\Delta\vec{R} = \vec{R}_{SUB} - \vec{R}_{OBS} = \begin{bmatrix} \cos\Delta\lambda & \cos\phi_{SUB} - \cos\phi_{OBS} \\ \sin\Delta\lambda & \cos\phi_{SUB} \\ \sin\phi_{SUB} - \sin\phi_{OBS} & \end{bmatrix} . \tag{4-67}$$

The subpoint velocity vector is

$$\vec{V}_{SUB} = \frac{d\vec{R}_{SUB}}{dt} = \frac{\partial\vec{R}_{SUB}}{\partial\phi_{SUB}}\frac{d\phi_{SUB}}{dt} + \frac{\partial\vec{R}_{SUB}}{\partial\Delta\lambda}\frac{d\Delta\lambda}{dt}$$

$$= \begin{bmatrix} -\cos\Delta\lambda & \sin\phi_{SUB} \\ -\sin\Delta\lambda & \sin\phi_{SUB} \\ & \cos\phi_{SUB} \end{bmatrix}\frac{d\phi_{SUB}}{dt} + \begin{bmatrix} -\sin\Delta\lambda & \cos\phi_{SUB} \\ \cos\Delta\lambda & \cos\phi_{SUB} \\ 0 & \end{bmatrix}\frac{d\Delta\lambda}{dt} \quad . \tag{4-68}$$

We define closest approach as occurring when $\Delta\vec{R} \cdot \vec{V}_{SUB} = 0$. However, since $\vec{R}_{SUB} \cdot \vec{V}_{SUB} = 0$ always, this becomes

$$\vec{R}_{OBS} \cdot \vec{V}_{SUB} = 0 \quad , \tag{4-69}$$

that is

$$(\cos\Delta\lambda \sin\phi_{SUB} \cos\phi_{OBS} - \sin\phi_{OBS} \cos\phi_{SUB})\frac{d\phi_{SUB}}{dt} + \sin\Delta\lambda \cos\phi_{SUB} \cos\phi_{OBS}\frac{d\Delta\lambda}{dt} = 0 \tag{4-70}$$

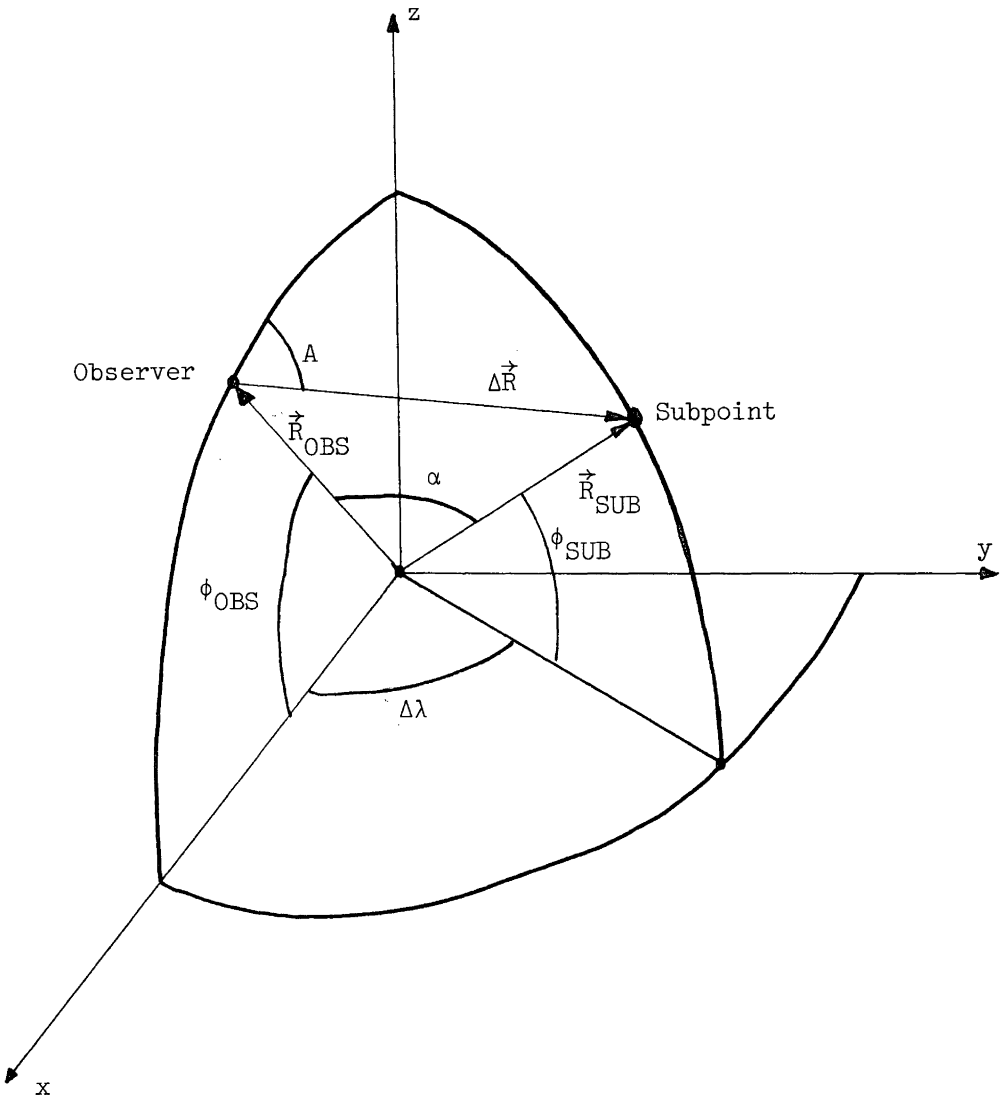

FIGURE 4-6

Alert Computations on the Unit Sphere

Close to the poles we must solve 4-70 iteratively for ϕ_{SUB}. Elsewhere we divide by cos ϕ_{SUB} cos ϕ_{OBS} to get

$$(\cos \Delta\lambda \tan \phi_{SUB} - \tan \phi_{OBS}) \frac{d\phi_{SUB}}{dt} + \sin \Delta\lambda \frac{d\Delta\lambda}{dt} = 0 \quad , \tag{4-71}$$

or

$$\tan \phi_{SUB}(t_{ca}) = \frac{\tan \phi_{OBS} - \sin \Delta\lambda(t_{ca}) \frac{d\Delta\lambda}{dt} / \frac{d\phi_{SUB}}{dt}}{\cos \Delta\lambda(t_{ca})} \quad . \tag{4-72}$$

Now

$$\frac{d\Delta\lambda}{dt} / \frac{d\phi_{SUB}}{dt} = \frac{d\lambda_{SUB}}{dt} / \frac{d\phi_{SUB}}{dt} = \begin{cases} - WM/2\pi & \text{Northgoing} \\ + WM/2\pi & \text{Southgoing} \end{cases} \quad . \tag{4-73}$$

Letting

$$x = \frac{2\pi}{P} (t_{ca} - TN) \quad , \tag{4-74}$$

$$y = LN - \frac{WM}{2\pi} x - \lambda_{OBS} \quad , \tag{4-75}$$

we have

$$\phi_{SUB}(t_{ca}) = \begin{cases} x & \text{Northgoing} \\ \pi - x & \text{Southgoing} \end{cases} \tag{4-76}$$

$$\Delta\lambda(t_{ca}) = \begin{cases} y & \text{Northgoing} \\ y - \pi & \text{Southgoing} \end{cases} \tag{4-77}$$

and for both northgoing and southgoing tracks we have

$$\tan x = \frac{\tan \phi_{OBS} + \sin y \frac{WM}{2\pi}}{\cos y} \quad , \tag{4-78}$$

which can be solved iteratively for x using the initial approximation

$$x_o = \phi_{OBS} \quad . \tag{4-79}$$

Then the time at which

$$\vec{R}_{SUB} \cdot \vec{V}_{SUB} = 0 \tag{4-80}$$

for the current pass is

$$TCA_{pred} = TN + \frac{P}{2\pi} x \quad . \tag{4-81}$$

Our next task is to find a test to determine whether the satellite

is above the observer's horizon at closest approach. The angle α between the position vectors of the observer and subpoint is given by

$$\cos\alpha = \frac{\vec{R}_{OBS} \cdot \vec{R}_{SUB}}{|R_{OBS}|\,|R_{SUB}|} = \cos\Delta\lambda\,\cos\phi_{SUB}\,\cos\phi_{OBS} + \sin\phi_{SUB}\,\sin\phi_{OBS} \quad . \tag{4-82}$$

At closest approach we have, from (4-76) and (4-77)

$$\cos\alpha_{CA} = \cos y\ \cos x\ \cos\phi_{OBS} + \sin x\ \sin\phi_{OBS} \quad . \tag{4-83}$$

The maximum visible α is, from Figure 4-7, obtained where the elevation angle E = 0, that is when

$$\cos\alpha_{max} = R_{earth}/R_{orbit} \quad , \tag{4-84}$$

where $R_{orbit} = \bar{a}$ and R_{earth} is the radial distance from the geocentre to the observer. The condition for visibility is that

$$\alpha_{CA} < \alpha_{max} \quad , \tag{4-85}$$

or equivalently that

$$\cos\alpha_{CA} > \cos\alpha_{max} \quad . \tag{4-86}$$

To compute the Doppler curve slope at closest approach we see from Figure 4-7 and from the law of cosines that

$$S^2 = R_{orbit}^2 + R_{earth}^2 - 2R_{orbit}\,R_{earth}\cos\alpha_{CA} \quad , \tag{4-87}$$

or

$$S = R_{orbit}(1 + \cos^2\alpha_{max} - 2\cos\alpha_{max}\cos\alpha_{CA})^{1/2} \quad , \tag{4-88}$$

so that

$$\frac{dS}{dt} = -\frac{R_{orbit}\,R_{earth}}{S}\frac{d\cos\alpha_{CA}}{dt} \quad , \tag{4-89}$$

and the slope at closest approach is

$$\frac{d^2S}{dt^2} = -\frac{R_{orbit}\,R_{earth}}{S}\left\{\frac{d^2\cos\alpha_{CA}}{dt^2} + \frac{R_{orbit}\,R_{earth}}{S^2}\left[\frac{d\cos\alpha_{CA}}{dt}\right]^2\right\} \quad , \tag{4-90}$$

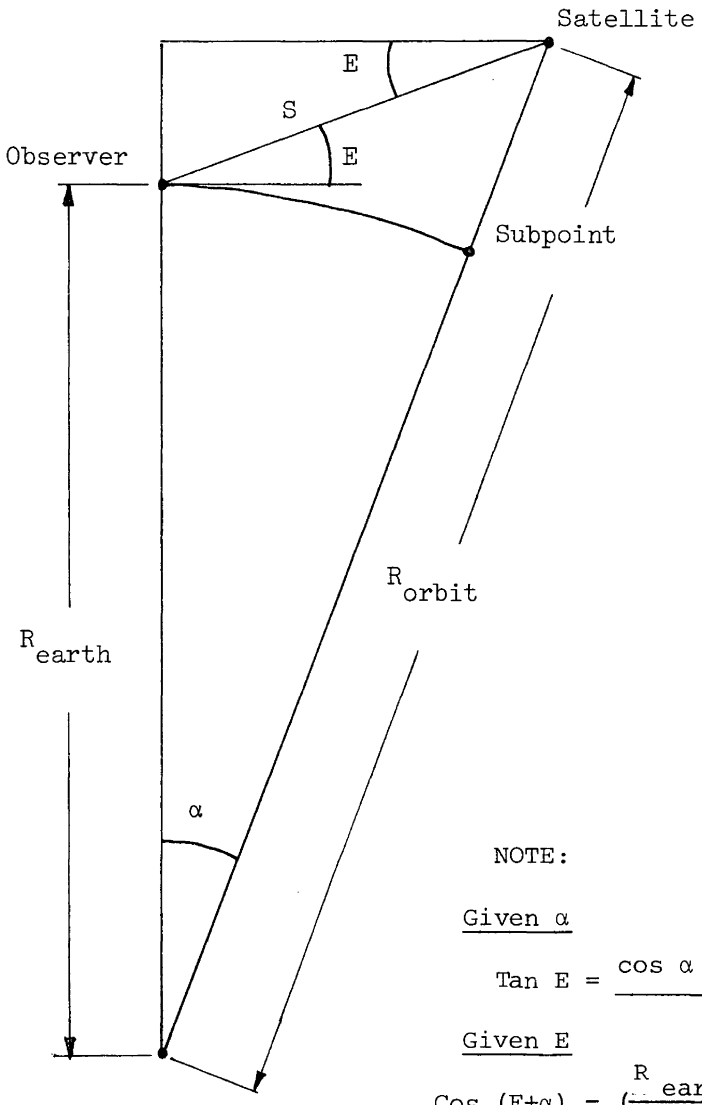

NOTE:

Given α

$$\text{Tan } E = \frac{\cos \alpha - R_{earth}/R_{orbit}}{\sin \alpha}$$

Given E

$$\text{Cos } (E+\alpha) = \left(\frac{R_{earth}}{R_{orbit}}\right) \cos E$$

FIGURE 4-7

Elevation Angle Geometry

where from (4-83) we have

$$\frac{d\cos\alpha_{CA}}{dt} = (-\cos y \sin x \cos\phi_{OBS} + \cos x \sin\phi_{OBS}) \frac{2\pi}{P} + \sin y \cos x \cos\phi_{OBS}(\frac{WM}{P}) \quad (4\text{-}91)$$

(note from 4-91 and 4-78 $d \cos\alpha_{CA}/dt = 0$), and

$$\frac{d^2\cos\alpha_{CA}}{dt^2} = - \cos\alpha_{CA} (\frac{2\pi}{P})^2 - \cos y \cos x \cos\phi_{OBS}(\frac{WM}{P})^2 \quad . \quad (4\text{-}92)$$

Finally the satellite elevation and azimuth at closest approach can easily be computed. From Figure 4-7

$$\tan E_{CA} = \frac{R_{orbit} \cos\alpha_{CA} - R_{earth}}{R_{orbit} \sin\alpha_{CA}} = \frac{\cos\alpha_{CA} - \cos\alpha_{max}}{\sin\alpha_{CA}} \quad , \quad (4\text{-}93)$$

and from Figure 4-6 and the law of cosines for spherical triangles we have

$$\cos(\frac{\pi}{2} - \phi_{SUB}) = \cos\alpha_{CA} \cos(\frac{\pi}{2} - \phi_{OBS}) + \sin\alpha_{CA} \sin(\frac{\pi}{2} - \phi_{OBS}) \cos A \quad , (4\text{-}94)$$

or

$$\cos A = \frac{\sin\phi_{SUB} - \sin\phi_{OBS} \cos\alpha_{CA}}{\cos\phi_{OBS} \sin\alpha_{CA}}$$

$$= \frac{\sin x - \sin\phi_{OBS} \cos\alpha_{CA}}{\cos\phi_{OBS} \sin\alpha_{CA}} \quad . \quad (4\text{-}95)$$

For observer's latitudes below about 70° it makes sense to distinguish between northgoing and southgoing passes and passes passing to the east of the observer, and passes passing to the west. Above 70° it is possible to track a pass whose point of closest approach occurs as the satellite passes over the pole, so that these distinctions are no longer relevant. For lower latitudes however, the satellite tracking quadrant (east, south to north; west, north to south; etc.) is related to the quadrant of $(LN - \lambda_{OBS})$, according to Table 4-6.

A simple test for side is the sign of $\tan(LN - \lambda_{OBS})$ (positive for east) and for direction is the sign of $\cos(LN - \lambda_{OBS})$ (positive for south to north).

	Side	Direction
$0 < LN - \lambda_{OBS} < \pi/2$	E	SN
$\pi/2 < LN - \lambda_{OBS} < \pi$	W	NS
$\pi < LN - \lambda_{OBS} < \frac{3\pi}{2}$	E	NS
$\frac{3\pi}{2} < LN - \lambda_{OBS} < 2\pi$	W	SN

TABLE 4-6

Satellite Quadrants

4.4 Accuracy of the Operational Ephemeris

The accuracy of the operational ephemeris is the accuracy with which the variable orbit parameters $\Delta E(t)$, $\Delta a(t)$ and $\eta(t)$ represent the departures of the actual satellite trajectory from the mean orbit defined by the fixed orbit parameters of Table 4-1.

From Table 4-2, $\Delta a(t)$ and $\eta(t)$ are broadcast to users in units of 10 m, and $\Delta E(t)$ is broadcast in units of 10^{-4} degrees, which is the angle subtended by 13 m at the orbit radius of 7430 km. Because these broadcast values have been rounded rather than truncated, then the roundoff error in each lies with equal likelihood between -0.5 and +0.5 broadcast units. The standard deviation for this equal probability distribution is $0.5/\sqrt{3} = 0.3$ broadcast units, or 3 m for each of $\Delta a(t)$ and $\eta(t)$, and 4 m for $\Delta E(t)$. The precision (but not necessarily the accuracy) of the satellite positions which together they define then has a standard deviation of 6 m. Therefore we cannot expect the accuracy of the operational ephemeris to exceed 6m.

According to one error budget (Piscane et al, 1973) incorrectly modelled geopotential forces likely cause errors of 10 to 20 m; incorrectly modelled drag and radiation pressure likely cause errors of 10 to 25 m; and previously to January 27, 1974 (that is, for all data considered here) use of the incorrect rotation pole caused apparent errors of order 10 m.

In this section we consider evidence from three sources pertaining to the accuracy of the operational ephemeris. First we compare the operational and precise ephemerides for a number of satellite passes. Second we look at the differences between two operational ephemerides for the same pass, each computed from somewhat different tracking data. Third we consider Guier plane navigation in which orbit biases are computed, resolved into along track and slant range components, having assumed that the tracking

station coordinates are perfectly known.

4.4.1 Comparison with the precise ephemeris

The NWL precise ephemeris (Sims, 1972) is a set of Average Terrestrial positions and velocities at one minute intervals, computed for each satellite by fitting a 48 hour orbital arc to Doppler data from the TRANET worldwide tracking network (Dunnell, 1967). The positions are given in units of metres. The velocities are given in units of mm/sec. The residuals of the fit of the Doppler data to the 48 hour arc are about three metres (Anderle, 1974), which we will assume represents the accuracy of the precise ephemeris.

Two data sets were used to compare operational and precise ephemerides provided by NWL. Both sets consisted only of passes of Transit satellite 14. The first data set consisted of 99 passes obtained between days 278 and 315, 1970, and the second data set consisted of 126 passes obtained between days 162 and 207, 1972.

For each pass the operational ephemeris values for $\Delta E(t)$, $\Delta a(t)$ and $\eta(t)$ were compared with equivalent values $\tilde{\Delta E}(t)$, $\tilde{\Delta a}(t)$ and $\tilde{\eta}(t)$ computed from the precise ephemeris coordinates. The latter were computed by inverting (4-6) to obtain

$$\tilde{X}_o(t) = R^T(t)\, X_T(t) \quad , \tag{4-96}$$

where $R(t)$ is given by (4-7) and $X_T(t)$ are the precise ephemeris coordinates, and then inverting (4-5) to obtain

$$\tilde{\Delta a}(t) = \tilde{a}(t) - \bar{a} \quad , \tag{4-97}$$

$$\tilde{\Delta E}(t) = \tilde{E}(t) - M(t) - e \sin M(t) \quad , \tag{4-98}$$

$$\tilde{\eta}(t) = \tilde{z}_o(t) \quad , \tag{4-99}$$

where $M(t)$ is given by (4-2) and

$$\tilde{a}(t) = [e\, \tilde{x}_o(t) + (\tilde{x}_o(t)^2 + \tilde{y}_o(t)^2(1 - e^2))^{1/2}]/(1 - e^2) \tag{4-100}$$

$$\tilde{E}(t) = \arctan\left(\tilde{y}_o(t)/(\tilde{x}_o(t) + \tilde{a}(t)\, e)\right) \quad . \qquad (4\text{-}101)$$

The comparison was made in broadcast units.

Since the precise ephemeris is referenced to the CIO pole and the operational ephemeris is not, tests were run to see whether or not $X_T(t)$ in (4-96) should first be transformed from average to instantaneous coordinates (that is, to see whether the operational ephemeris is closer to instantaneous or average coordinates). As summarized below, these tests indicated the operational ephemeris to be closer to the instantaneous pole, therefore the $X_T(t)$ in (4-96) were first transformed to instantaneous coordinates, using the pole coordinates computed by NWL simultaneously with their computation of the precise ephemeris (Anderle, 1972; 1973b).

A typical pass involved the comparison of eight values for $\Delta E(t)$ and $\Delta a(t)$ and of four values for $\eta(t)$. Table 4-7 shows the results for such a typical pass. The aggregated results for all passes are shown in Table 4-8. The following conclusions can be drawn.

(a) The trajectories represented by the operational and precise ephemerides are nearly parallel. That is, for each pass the set of differences for each of the three variable orbit parameters is well described by a mean value (the bias between the operational and precise ephemerides). The scattering about such mean values, represented by the single pass standard deviations in Tables 4-7 and 4-8, is in general small compared to the resolution of the operational ephemeris (that is, the standard deviations are generally less than one broadcast unit).

(b) The operational and precise ephemerides place the satellite on geopotential surfaces which are coincident, within the resolution of the operational ephemeris. The bias in Δa (bias in the radial direction) between the two trajectories is masked by the resolution with which Δa is broadcast.

2 Hours Plus	Operational Ephemeris			Precise Ephemeris			Precise-Operational		
Min	ΔE	Δa	η	$\tilde{\Delta E}$	$\tilde{\Delta a}$	$\tilde{\eta}$	$(\tilde{\Delta E}-\Delta E)$	$(\tilde{\Delta a}-\Delta a)$	$(\tilde{\eta}-\eta)$
30	15	14							
31									
32	4	28	6	5.7	27.4	6.9	1.7	-0.7	0.9
33				1.2	36.9	7.1			
34	- 4	48		- 2.7	47.8	7.2	1.3	-0.2	
35				- 5.9	60.2	7.4			
36	-10	74	7	- 8.5	73.6	7.5	1.5	-0.4	0.5
37				-10.2	88.0	7.8			
38	-13	104		-11.3	103.1	8.0	1.7	-1.0	
39				-11.6	118.7	8.3			
40	-13	135	8	-11.0	134.8	8.6	2.0	-0.2	0.6
41				- 9.6	150.8	8.9			
42	- 9	167		- 7.5	166.8	9.2	1.6	-0.2	
43				- 4.5	182.3	9.5			
44	- 3	198	9	- 0.8	197.5	9.9	2.2	-0.6	0.9
45				3.6	211.7	10.2			
46	7	226		8.7	225.0	10.5	1.7	-1.0	
47				14.4	237.2	10.8			
48	18	249	10	20.6	248.0	11.2	2.6	-1.0	1.2
49				27.4	257.4	11.4			
50	32	266							
					Mean		1.8	-0.6	0.8
					Std Dev		0.4	0.3	0.3

TABLE 4-7

Typical Comparison in Broadcast Units between Operational and Precise Ephemerides (Satellite 14, Day 162, 1972)

			ΔE				Δa				η			
			Single Pass Mean Values		Single Pass Std Dev'ns		Single Pass Mean Values		Single Pass Std Dev'ns		Single Pass Mean Values		Single Pass Std Dev'ns	
Data Set	Sat #	# Passes	RMS	Worst Case	AVG	Worst Case	RMS	Worst Case	AVG	Worst Case	RMS	Worst Case	AVG	Worst Case
1970	14	99	2.4(31)	5.7(74)	0.4	0.9	0.4(4)	1.2(12)	0.4	0.8	1.1(11)	2.8(28)	0.6	1.7
1972	14	126	1.6(20)	4.1(53)	0.4	0.8	0.4(4)	1.1(11)	0.4	0.6	1.1(11)	2.7(27)	0.5	1.8
1973	12	9	1.4(18)	2.7(35)			0.3(3)	0.5(5)			0.7(7)	1.1(11)		
	13	16	1.0(13)	2.0(26)			0.2(2)	0.4(4)			0.7(7)	1.4(14)		
	14	19	0.9(12)	2.3(30)			0.2(2)	0.3(3)			0.7(7)	1.3(13)		
	18	25	0.9(12)	1.5(20)			0.2(2)	0.5(5)			0.7(7)	2.0(20)		
	19	25	1.0(13)	2.4(31)			0.2(2)	0.6(6)			0.5(5)	1.0(10)		
	All	94	1.0(13)	2.7(35)	0.4	0.7	0.2(2)	0.6(6)	0.4	0.7	0.6(6)	2.0(20)	0.4	1.0

TABLE 4-8

Results of Ephemeral Comparisons

Given in broadcast units (numbers in parentheses are in metres).

The 1970 and 1972 results compare the operational and precise ephemerides.

The 1973 compare fresh and stale operational ephemerides.

(c) The bias in the cross track direction (bias in η) is typically about one broadcast unit (10 metres).

(d) The bias in the along track direction (bias in ΔE) is typically about two broadcast units (25 metres).

As expected, the bias in ΔE is the only bias to be affected by neglecting the effect of polar motion. Without first converting $X_T(t)$ in (4-96) to refer to the instantaneous pole, the 1972 data set rms bias in ΔE increased from 1.6 to 1.8 broadcast units, and the worst case from 4.1 to 5.1 units. The biases in Δa and η were unaffected.

4.4.2 Comparison between fresh and stale operational ephemerides

Operational ephemerides are computed twice daily for each satellite, and "injected" into the satellite memory to be broadcast to users. If a user happens to be tracking a satellite at the time such an injection occurs, he receives both the old (or "stale") and the new (or "fresh") operational ephemeris parameters for that pass.

In comparing these two sets of parameters we are essentially comparing two long arcs, each computed using the same force model, and each fitted to 36 hours of tracking data from the same four stations. However, only 24 hours of this data is common to both arcs, the fresh arc being fitted to data which is 12 hours fresher than the stale arc. Hence in this comparison we eliminate differences in the force model and tracking station configuration which were involved in comparing the operational and precise ephemerides. We should then obtain some measure of the extrapolation error, that is how well the drag and radiation pressure forces in particular can be predicted. We should expect the fresh and stale trajectories to be closer to coincidence than the operational and precise ephemeris trajectories.

The data set used in this comparison consisted of 94 injection passes tracked at Fredericton between days 139 and 178, 1973. Injection

passes for all five satellites then operational were obtained, although not evenly distributed among them.

For each pass the fresh orbit parameters were used to compute geocentric Cartesian coordinates. Variable orbit parameters referred to the stale mean orbit, corresponding to these Cartesian coordinates were then computed, as described for the precise ephemeris coordinates in the previous section. The stale and equivalent fresh variable orbit parameters were then compared in broadcast units. Every pass involved the comparison between seven values for ΔE and Δa and three values for η. Aggregated results are shown in Table 4-8. The following conclusions can be drawn.

(a) The fresh and stale orbits are nearly parallel.

(b) They place the satellite on closely coincident geopotential surfaces. The rms value of the Δa biases was only 0.2 broadcast units.

(c) The bias in the cross track direction (η bias) is typically less than one broadcast unit.

(d) The bias in the along track direction (ΔE bias) is typically one broadcast unit.

(e) No significant differences between satellites was revealed. The large value for the ΔE bias shown in Table 4-8 for satellite 12 is due to one pass, and would have less influenced the rms value had the sample size been larger. The rms value of the ΔE bias for the other eight passes of satellite 12 is 1.1 units.

We can interpret the results in Table 4-8 from this and the previous section as representing the following error budget, in metres. Note that Piscane et al (1973) quote 10 - 25 m for (a) and 10 - 20 m for (b):

	ΔE	Δa	η	rms	
Surface force model errors (section 4.4.2)	13	2	6	14	(a)
Broadcast rounding errors (section 4.4)	4	3	3	6	
Geopotential model errors (to result in totals below)	15	2	9	17	(b)
Totals (section 4.4.1)	20	4	11	23	

4.4.3 Guier plane navigation results

In this section we briefly summarize results which are discussed in detail in section 5.3.2.

Treating 2877 pairs of Guier plane coordinates obtained from passes tracked at eight stations in 1972 and 1973 as statistical samples, sample standard deviations for the slant range (x_G) and along track (y_G) coordinates are respectively about 12 m and 39 m. The standard deviations of the best fitting normal distributions to these samples are respectively about 9 m and 16 m. Assuming the station coordinates to be perfectly known, then for each pass, y_G samples the ΔE bias, and x_G samples components of the Δa and η biases according to $\Delta a \sin(E+\alpha) + \eta\cos(E+\alpha)$ (where E is the closest approach elevation and α the subtended geocentric angle as shown in Figure 4-7). If we assume that other systematic errors will affect the sample standard deviations, but not the best fitting normal standard deviations, then we should expect the rms slant range orbit bias to be less than 9 m,and rms along track orbit bias (ΔE) to be of order 16 m. From Table 4-8 we find that these biases are more consistent with the results of the fresh and stale ephemeris comparison than with the results of the precise ephemeris comparison. As mentioned in section 5.3.2, the existance and effect of other systematic sources of error should be isolated and evaluated

before making firm conclusions about orbit errors on the basis of these results.

4.5 Shape of the Operational Ephemeris

Satellite positions can be computed from the operational ephemeris only for even minutes of Universal Time. If Doppler integration intervals shorter than two minutes are to be used, positions in between the two minute broadcast positions must be computed. There are many ways of computing such positions. Here we treat this as a problem in least squares approximation (section 3.1.5). For each satellite pass, we want to best fit curves, in the least squares sense, to each of the three sets of variable orbit parameters $\Delta E(t)$, $\Delta a(t)$ and $\eta(t)$.

However, to apply the least squares approximation we must first choose appropriate base functions. In this case appropriate functions are those which represent the shape of the functions we wish to approximate.

To establish the shape of $\Delta E(t)$, $\Delta a(t)$ and $\eta(t)$, and hence the choice of base functions, we first relate the operational ephemeris parameters to the parameters which describe a linearly perturbed Keplerian orbit (sections 4.5.1 and 4.5.2). We next analyze a multipass sequence of values for the functions $\Delta E(t)$, $\Delta a(t)$ and $\eta(t)$ as three time series (section 4.5.3). These two investigations suggest appropriate base functions to be $\{1, \cos 2nt, \sin 2nt, t\}$ where n is the satellite mean motion. The fit of these base functions to single pass sets of values for $\Delta E(t)$, $\Delta a(t)$ and $\eta(t)$ is investigated in section 4.5.4.

4.5.1 Unperturbed and linearly perturbed Keplerian orbit parameters

An unperturbed Keplerian orbit can be described by the six parameters (degrees of freedom) (Kaula, 1966) a, e, i, ω, Ω, M, where all are

constant with respect to time except the last

$$M(t) = n(t - t_p) \quad , \tag{4-102}$$

where t_p is the time of perigee passage, and from Kepler's third law

$$n^2 a^3 = \mu \quad , \tag{4-103}$$

where μ is the earth's gravitational constant. The transformation from Keplerian orbital elements to terrestrial Cartesian coordinates is

$$X_T(t) = R_3(-\Omega + GAST)\, R_1(-i)\, R_3(-\omega) \begin{bmatrix} a\,(\cos E(t) - e) \\ a\sqrt{1 - e^2}\,\sin E(t) \\ 0 \end{bmatrix} \tag{4-104}$$

where GAST (Greenwich Apparent Sidereal Time) is a function of Universal Time and from Kepler's equation

$$E(t) - e \sin E(t) = M(t) = n(t - t_p) = \sqrt{\frac{\mu}{a^3}}\,(t - t_p) \quad . \tag{4-105}$$

The <u>perigee period</u> (time interval between successive perigee passages) and the <u>nodal period</u> (time interval between successive nodal crossings) are equal and constant,

$$P_p = P_N = \frac{2\pi}{n} = 2\pi \sqrt{\frac{a^3}{\mu}} \quad . \tag{4-106}$$

A Keplerian orbit to which the linear part of the perturbations due to the oblateness of the earth has been added is described by the same six parameters, a, e, i, ω, Ω, M, however now

$$\omega(t) = \omega(t_p) + \dot{\omega}(t - t_p) \quad , \tag{4-107}$$

$$\Omega(t) = \Omega(t_p) + \dot{\Omega}(t - t_p) \quad , \tag{4-108}$$

$$M(t) = \dot{M}\,(t - t_p) \quad , \tag{4-109}$$

where (Kaula, 1966)

$$\dot{\omega} = -\frac{3\,n}{4\,a^2(1 - e^2)^2}\,(1 - 5\cos^2 i)(a_e^2\,J_2) \quad , \tag{4-110}$$

$$\dot{\Omega} = -\frac{3\,n}{4\,a^2(1-e^2)^2}(2\cos i)(a_e^2 J_2) \quad , \tag{4-111}$$

$$\dot{M} = n - \frac{3\,n}{4\,a^2(1-e^2)^2}(1-e^2)^{1/2}(1-3\cos^2 i)(a_e^2 J_2) \quad , \tag{4-112}$$

where a_e is the earth's equatorial radius, and J_2 is the second degree zonal harmonic coefficient of the earth's gravity field. Note that t_p is now the time of a specific perigee passage, and hence defines a point stationary with respect to the earth, so that $\dot{M}$ is the nodal mean motion, and the nodal period is

$$P_N = \frac{2\pi}{\dot{M}} \quad . \tag{4-113}$$

However since the perigee point is precessing at the rate $\dot{\omega}$, the perigee (anomalistic) mean motion is now $(\dot{M} - \dot{\omega})$ and the perigee period is

$$P_p = \frac{2\pi}{\dot{M}-\dot{\omega}} \quad . \tag{4-114}$$

there are two possibilities for the transformation to terrestrial coordinates. Either we can refer the mean motion $M(t)$ to the perigee position at t_p, in which case the transformation is

$$X_T(t) = R_3(-\Omega(t) + GAST(t))\, R_1(-i)\, \underline{R_3(\omega(t_p))} \begin{bmatrix} a\,(\cos E(t) - e) \\ a\sqrt{1-e^2}\,\sin E(t) \\ 0 \end{bmatrix} \tag{4-115}$$

where

$$E(t) - e\sin E(t) = \dot{M}(t - t_p) \quad , \tag{4-116}$$

or we can refer the mean motion to the perigee point at t, in which case the transformation is

$$X_T(t) = R_3(-\Omega(t) + GAST(t))\, R_1(-i)\, \underline{R_3(\omega(t))} \begin{bmatrix} a\,(\cos E(t) - e) \\ a\sqrt{1-e^2}\,\sin E(t) \\ 0 \end{bmatrix} \tag{4-117}$$

where

$$E(t) - e \sin E(t) = (\dot{M} - \dot{\omega})(t - t_p) \quad . \tag{4-118}$$

Actually the difference $E(t) - M(t)$ is a function of angle with respect to the current perigee position, so that the second alternative is the correct one.

Consider the Keplerian orbit on which the above linear perturbations have been superimposed, after which all other perturbations have been resolved into three functions $\delta E(t)$, $\delta a(t)$, $Z(t)$.* Then the transformation to terrestrial coordinates is

$$X_T(t) = R_3(-\Omega(t) + GAST(t))R_1(-i)R_3(\omega(t)) \begin{bmatrix} (a+\delta a(t))\{\cos[E(t)+\delta E(t)]-e\} \\ (a+\delta a(t))\sqrt{1-e^2}\,\sin(E(t)+\delta E(t)) \\ Z(t) \end{bmatrix} \quad . \tag{4-119}$$

4.5.2 Comparison between Keplerian and operational ephemeris parameters

As described in section 4.1, the operational ephemeris parameters are not based on a Keplerian orbit analysis, but are the parameters of a least squares fit to a set of known terrestrial Cartesian coordinates for the satellite (which have first been precisely determined by numerical integration of the equations of motion, rather than by applying a general orbit theory). These parameters then are defined by equations (4-1) to (4-11).

Comparing these definitions for the operational ephemeris parameters, with the definitions for the equivalent linearly perturbed Keplerian parameters embodied in (4-119), we note the following differences

*In general perturbations are resolved into 3 coordinates and 3 momenta. Here we are concerned only with the 3 coordinates.

Operational Ephemeris	Perturbed Keplerian	
$E(t) - e \sin M(t) = M(t)$	$E(t) - e \sin E(t) = M(t)$	(4-120)
$y_o(t) = (a + \Delta a(t)) \sin(E(t) + \Delta E(t))$	$y_o(t)=(a+\delta a(t))\sqrt{1-e^2} \sin(E(t)+\delta E(t))$	(4-121)
$GAST(t) = GAST(t_p) + \omega_e(t - t_p)$	$GAST(t) = GAST(t_p) + \omega_e(t-t_p)+h.o.t.$	(4-122)

From this comparison we see that the operational ephemeris functions $\Delta E(t)$, $\Delta a(t)$ and $\eta(t)$ will contain

(a) the nonlinear oblateness, other geopotential, and surface force perturbations contained in the Keplerian functions $\delta E(t)$, $\delta a(t)$ and $Z(t)$, and

(b) the effects of the differences represented by (4-120) to (4-122) between the definitions of the Keplerian (theoretical) parameters and the definitions of the operational ephemeris parameters.

Several of these perturbations in (a) have frequencies close to twice the orbit frequency. Satellites with nonzero inclinations cross the equator twice per revolution, hence the residual (nonlinear) oblateness perturbation has twice the orbit frequency. For a polar orbit with a period short compared to one day, the direct and indirect lunar and solar effects also have frequencies close to twice the orbit frequency. The oblateness of the atmosphere will cause a variation in the air drag for polar satellites which has twice the orbit frequency. It can be shown that to first order, the effect of the differences in the expressions for $E(t)$ and $y_o(t)$ has a frequency which is twice the orbit frequency. These considerations suggest that the shape of the functions $\Delta E(t)$, $\Delta a(t)$, $\eta(t)$ will have terms of the form $\cos(2nt)$ and $\sin(2nt)$ where n is the mean motion parameter.

Some of these perturbations, notably solar radiation pressure, and lunar and solar attractions, are known to produce secular and long-

period effects on the motion of satellites (Brouwer, 1963). The effect of second order tesseral harmonics on Transit satellites has a 12 hour period and of order one km magnitude (Anderle, personal communication). Over the duration of one pass (20 minutes) this can be represented by a linear trend, t.

Including a bias term, likely candidates for base functions representing the shape of each of $\Delta E(t)$, $\Delta a(t)$ and $\eta(t)$ are the set $\{1, \cos 2nt, \sin 2nt, t\}$.

4.5.3 Time series analysis of precise ephemeris variable orbit parameters

To further investigate the implications of section 4.5.2, each of the three variable orbit parameters from a number of consecutive passes were treated as a time series. Because the precise ephemeris more closely represents the actual satellite trajectory than the operational ephemeris, and is provided at one minute intervals rather than two and four minute intervals, the sets of variable orbit parameters used were $\tilde{\Delta E}(t)$, $\tilde{\Delta a}(t)$ and $\tilde{\eta}(t)$ (given by (4-97), (4-98) and (4-99)) derived from precise ephemeris Cartesian coordinates. The data set used consisted of 125 passes of satellite 13 between days 183 and 207, 1972. These 125 sets of precise ephemerides were referred to a sequence of 32 operational ephemeris mean orbits, producing time series in $\tilde{\Delta E}(t)$, $\tilde{\Delta a}(t)$ and $\tilde{\eta}(t)$, each of which were 34515 minutes in duration, consisting of 2057 values at one minute intervals grouped in one pass segments typically of 16 values. These segments were separated by gaps which accounted for 94% of the time series duration. The first few segments for each of $\tilde{\Delta E}(t)$, $\tilde{\Delta a}(t)$ and $\tilde{\eta}(t)$ are shown in Figures 4-8a, 4-9a, and 4-10a respectively. In these figures the gaps have been omitted.

These time series were analyzed in two ways. First the initial segments shown in the above figures were subjected to least squares spectral

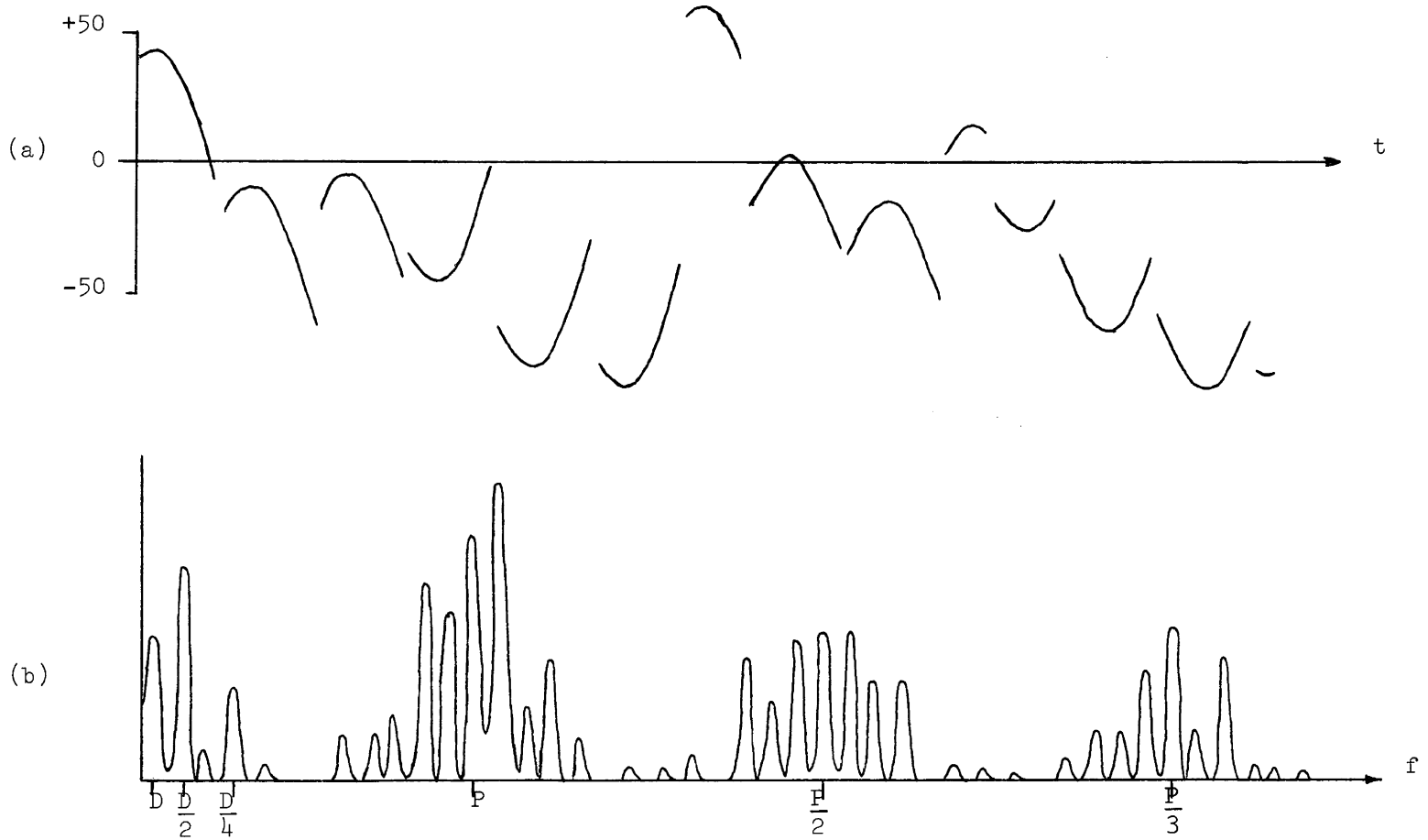

FIGURE 4-8

Time Series and Spectrum for $\Delta\tilde{E}(t)$

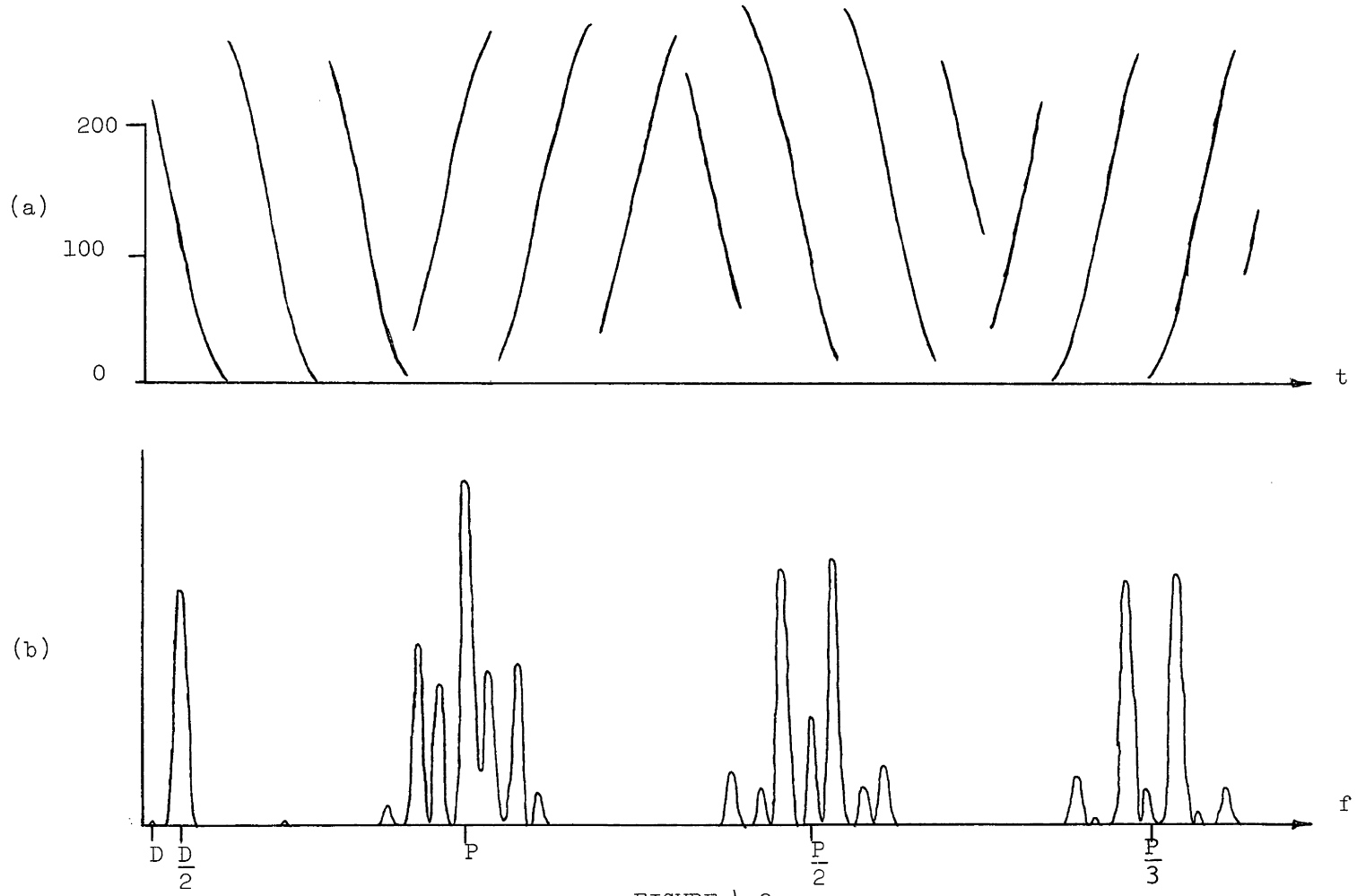

FIGURE 4-9

Time Series and Spectrum for $\Delta\tilde{a}(t)$

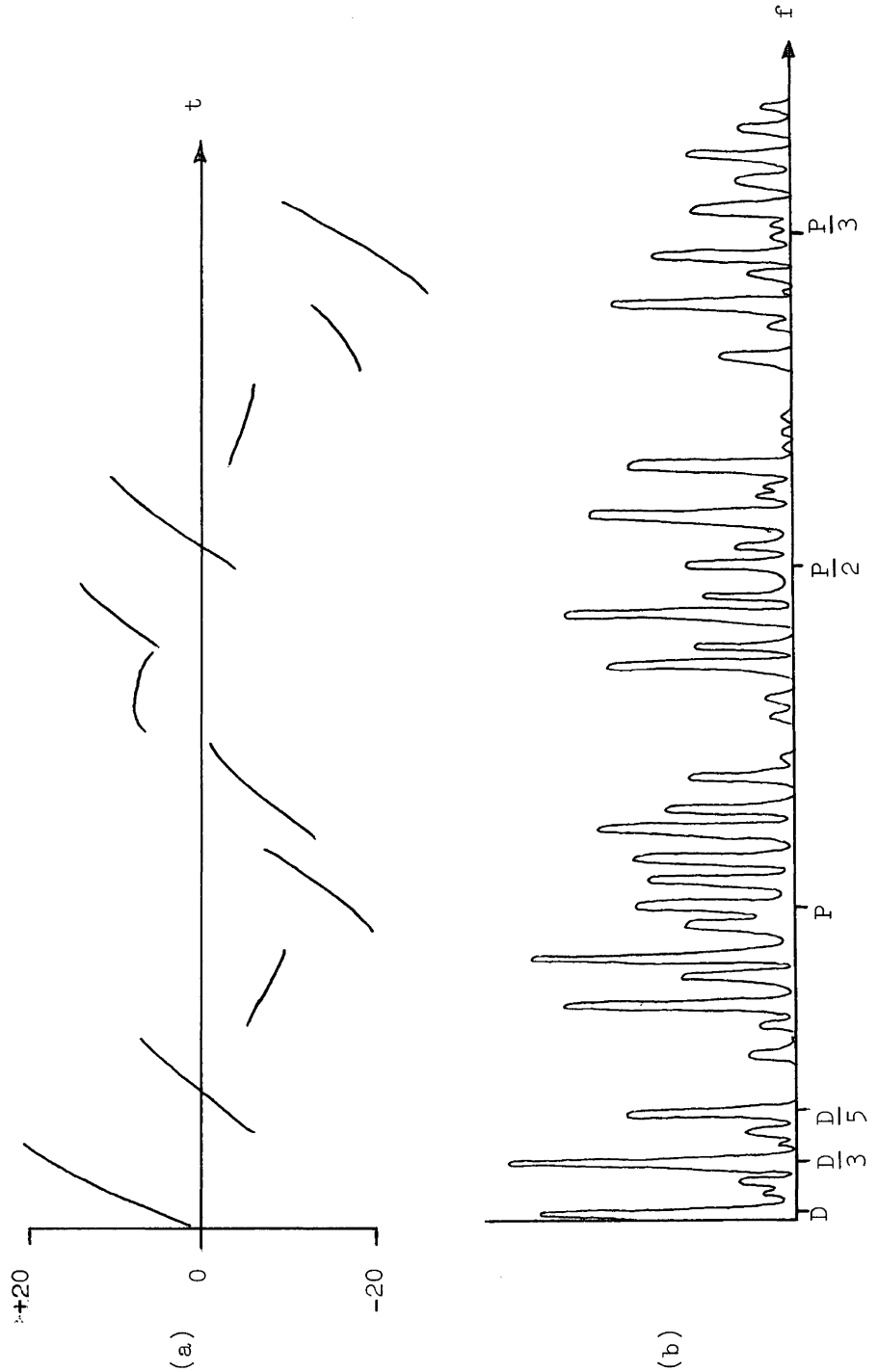

FIGURE 4-10

Time Series and Spectrum for $\tilde{n}(t)$

analyses (section 3.1.7). In this case the $\tilde{\Delta E}(t)$ and $\tilde{\Delta a}(t)$ time series contain 220 values spread over 2439 minutes, and the $\tilde{\eta}(t)$ time series 191 values spread over 2236 minutes. The spectral analysis results are shown in Figures 4-8(b), 4-9(b), and 4-10(b). In each case the low frequency part of the spectrum is shown (periods from 20P out to beyond P/3, where P is the period of the satellite). The $\tilde{\Delta a}(t)$ spectrum is the simplest, containing a barely discernable diurnal peak (D), a strong semi-diurnal peak (D/2), and families of seven peaks centred about P, P/2, P/3, etc. The three pairs of side lobes in each of these "P families" are the beat frequencies between the central (P/n) peak and, moving outward, D, D/2 and D + D/2 respectively. The $\tilde{\Delta E}(t)$ spectrum has a stronger D peak, and has a D/4 peak as well, which adds more side lobes on the P families. The $\tilde{\eta}(t)$ spectrum has a weak D/2 peak, strong D/3 and D/5 peaks, and even more side lobes in the P families. It is clear from all three spectra that the principal periods are D and P and harmonics thereof.

The second time series analysis was to superpose the values for each of the 125 passes according to time since perigee passage, that is on the time interval [0,P]. Figure 4-11 shows the three time series averaged in this way. For $\tilde{\Delta E}(t)$ and $\tilde{\Delta a}(t)$ the principal period is clearly P/2. It would appear that $\tilde{\eta}(t)$ is not sufficiently correlated from pass to pass to reveal a principal period in this way. However, since the $\tilde{\eta}(t)$ spectrum does not markedly differ from the other two, we will assume that the shape of $\tilde{\eta}(t)$ also has a principal period of P/2, even though it may not be correlated over many passes.

It is concluded from these results that the shape of $\tilde{\Delta E}(t)$, $\tilde{\Delta a}(t)$ and $\tilde{\eta}(t)$ are not markedly different (that is the same base functions can be used to approximate them), and that for purposes of approximation over a single pass (20 minutes) the principal frequency is as deduced in section

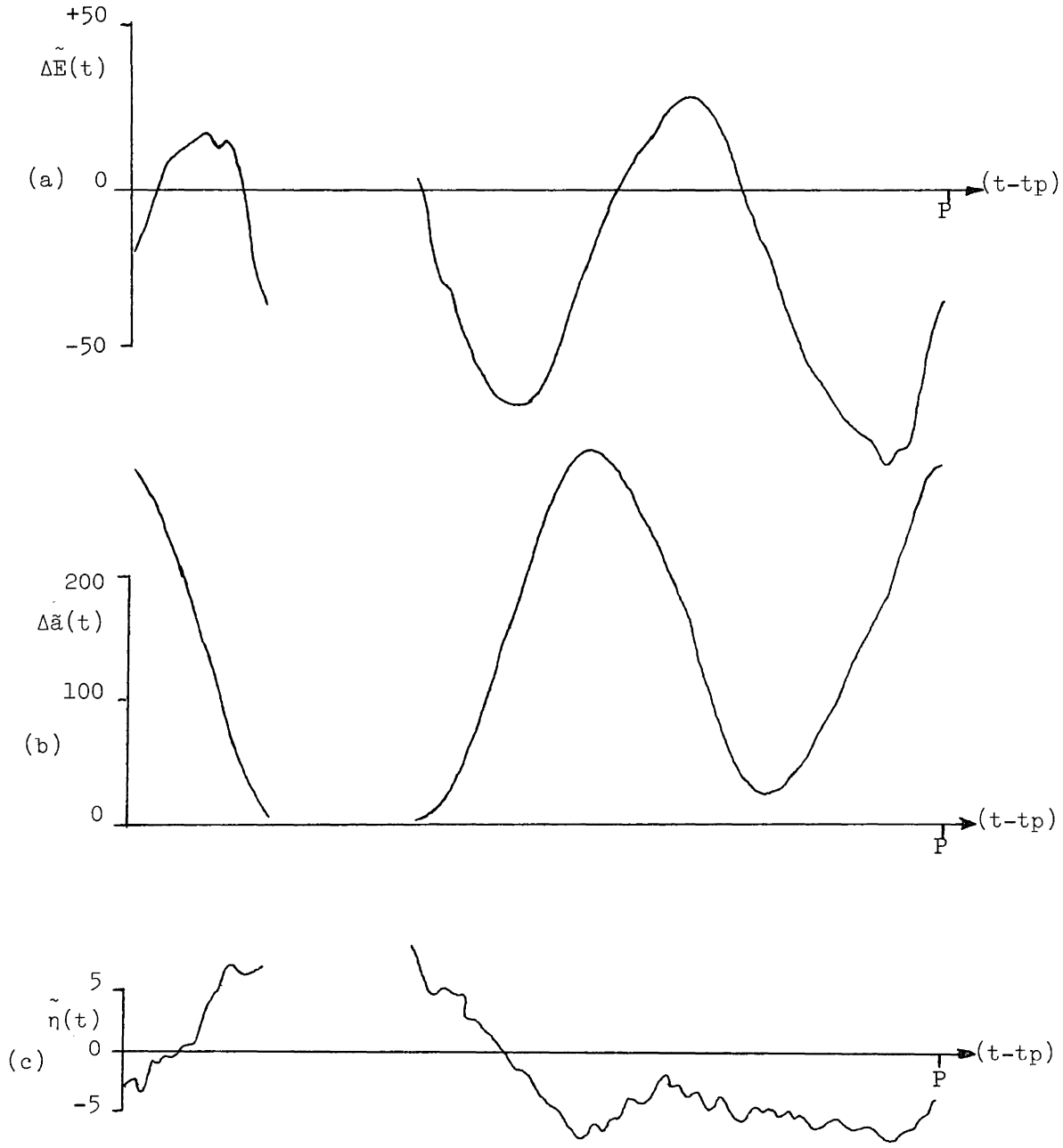

FIGURE 4-11
Averaged Time Series for $\tilde{\Delta E}(t)$, $\tilde{\Delta a}(t)$ and $\tilde{\eta}(t)$
in broadcast units

4.5.2, that is twice the orbit frequency. For single pass approximation, the diurnal frequency will be absorbed by a linear trend base function.

4.5.4 Least squares approximation of precise and operational ephemeris variable orbit parameters

In this section we investigate the fit of the base functions $\Phi = \{1, \cos 2nt, \sin 2nt, t\}$ to

(a) the variable orbit parameters $\Delta\tilde{E}(t)$, $\Delta\tilde{a}(t)$, $\tilde{\eta}(t)$ computed from the precise ephemeris, and

(b) the variable orbit parameters $\Delta E(t)$, $\Delta a(t)$, $\eta(t)$ given by the operational ephemeris. We also investigate

(c) whether the differences between $\Delta\tilde{E}(t)$, $\Delta\tilde{a}(t)$, $\tilde{\eta}(t)$ and the approximants to $\Delta E(t)$, $\Delta a(t)$, $\eta(t)$ are substantially the same as the differences between $\Delta\tilde{E}(t)$, $\Delta\tilde{a}(t)$, $\tilde{\eta}(t)$ and $\Delta E(t)$, $\Delta a(t)$, $\eta(t)$ obtained in section 4.4.1.

Since the precise ephemeris consists of $X_T(t)$ and $\dot{X}_T(t)$, then for (a) and (c) we investigate not only fits of Φ to $X_T(t)$, but also fits of $\dot{\Phi} = \{0, -2n \sin 2nt, 2n \cos 2nt, 1\}$ to $\dot{X}_T(t)$. If

$$P_4 = \sum_{i=1}^{4} C_i \phi_i \qquad (4\text{-}123)$$

best fits $X_T(t)$, (that is best fits $\Delta\tilde{E}(t)$, $\Delta\tilde{a}(t)$, $\tilde{\eta}(t)$),then

$$\dot{P}_4 = \sum_{i=1}^{4} C_i \dot{\phi}_i \quad , \qquad (4\text{-}124)$$

where the C_i are unchanged, should also best fit $\dot{X}_T(t)$ (that is $\dot{\Delta\tilde{E}}(t)$, $\dot{\Delta\tilde{a}}(t)$, $\dot{\tilde{\eta}}(t)$). Given $X_T(t)$ and $\dot{X}_T(t)$ and a set of mean orbit parameters, we derive $\dot{\Delta\tilde{E}}(t)$, $\dot{\Delta\tilde{a}}(t)$, $\dot{\tilde{\eta}}(t)$ from (4-96)

$$\dot{\tilde{X}}_o(t) = \dot{R}(t)^T X_T(t) + R(t)^T \dot{X}_T(t) \quad . \qquad (4\text{-}125)$$

From (4-24), (4-25) and (4-26)

$$\dot{\tilde{\Delta a}}(t) = \dot{\tilde{a}}(t) \tag{4-126}$$

$$\dot{\tilde{\Delta E}}(t) = \dot{\tilde{E}}(t) - n(1 + e \cos M(t)) \tag{4-127}$$

$$\dot{\tilde{\eta}}(t) = \dot{\tilde{z}}_o(t) \quad , \tag{4-128}$$

where the inversion of (4-23) yields

$$\dot{\tilde{a}}(t) = \tilde{a}(t) \left[\frac{(\tilde{x}_o(t) + e\,\tilde{a}(t))\dot{\tilde{x}}_o(t) + \tilde{y}_o(t)\,\dot{\tilde{y}}_o(t)}{(\tilde{x}_o(t) + e\,\tilde{a}(t))\,\tilde{x}_o(t) + \tilde{y}_o(t)^2} \right] \tag{4-129}$$

$$\dot{\tilde{E}}(t) = \left[\frac{\dot{\tilde{a}}(t)\,\tilde{x}_o(t) - \tilde{a}(t)\,\dot{\tilde{x}}_o(t)}{\tilde{a}(t)\,\tilde{y}_o(t)} \right] \tag{4-130}$$

Values for $\dot{\tilde{\Delta E}}(t)$, $\dot{\tilde{\Delta a}}(t)$, $\dot{\tilde{\eta}}(t)$ were expressed in broadcast units/minute.

In these investigations three data sets were used: The 1970 data set described in section 4.4.1 (sets of both precise and operational ephemerides for 99 passes of satellite 14 between days 278 and 315, 1970); the 1972 data set described in section 4.4.1 (sets of both precise and operational ephemerides for 126 passes of satellite 14, between days 162 and 207, 1972); and a 1973 data set consisting of 741 sets of operational ephemerides only, for satellites 12 (125 passes), 13 (144 passes), 14 (147 passes), 18 (158 passes) and 19 (167 passes), obtained between days 139 and 178, 1973.

To investigate the fit of Φ to the precise ephemeris, the 1970 and 1972 data sets were used. For each pass $\tilde{\Delta E}(t)$, $\tilde{\Delta a}(t)$ and $\tilde{\eta}(t)$ were computed from (4-97), (4-98), (4-99) and $\dot{\tilde{\Delta E}}(t)$, $\dot{\tilde{\Delta a}}(t)$ and $\dot{\tilde{\eta}}(t)$ were computed from (4-126), (4-127), (4-128). Then Φ was fitted to each of $\tilde{\Delta E}(t)$, $\tilde{\Delta a}(t)$, $\tilde{\eta}(t)$ using the least squares approximation of section 3.1.5, with unit weighting function.

Taking $\tilde{\Delta E}(t)$ as an example, coefficients CE_i were found which

minimized $\rho(\tilde{\Delta E}(t), PE_4(t))$ where

$$PE_4(t) = \sum_{i=1}^{4} CE_i \, \phi_i(t) \quad , \tag{4-131}$$

is the approximating polynomial, or approximant. The fit of $PE_4(t)$ to $\tilde{\Delta E}(t)$ was then characterized by

$$\hat{\sigma}_o = \left[\frac{\rho(\tilde{\Delta E}(t), PE_4(t))}{n-4}\right]^{1/2}$$

$$= \left[\frac{\sum_{j=1}^{n} (\tilde{\Delta E}(t_j) - PE_4(t_j))^2}{n-4}\right]^{1/2} \tag{4-132}$$

Differentiating (4-131), keeping CE_i constant,

$$\dot{PE}_4(t) = \sum_{i=1}^{4} CE_i \, \dot{\phi}_i(t) \quad . \tag{4-133}$$

The fit of $\dot{PE}_4(t)$ to $\dot{\tilde{\Delta E}}(t)$ was characterized by

$$\hat{\sigma}_o = \left[\frac{\rho(\dot{\tilde{\Delta E}}(t) - \dot{PE}_4(t))}{n-4}\right]^{1/2} \quad . \tag{4-134}$$

Similar computations were made for each pass for $\tilde{\Delta a}(t)$ and $\tilde{\eta}(t)$. The results for a typical pass are shown in Table 4-9.

The rms and worst case values of $\hat{\sigma}_o$ for the 99 passes from 1970, and the 126 passes from 1972 are shown in Table 4-10. The precise ephemeris $X_T(t)$ and $\dot{X}_T(t)$ are given in units of m, and mm/s respectively. Assuming rounding rather than truncation, the roundoff errors in $X_T(t)$ and $\dot{X}_T(t)$ (and hence in $\tilde{\Delta E}(t)$, $\tilde{\Delta a}(t)$, $\tilde{\eta}(t)$ and $\dot{\tilde{\Delta E}}(t)$, $\dot{\tilde{\Delta a}}(t)$, $\dot{\tilde{\eta}}(t)$) will have standard deviations in each coordinate of $0.5/\sqrt{3}$ m = 0.3 m $\simeq$ 0.03 broadcast units, and $0.5/\sqrt{3}$ mm/s = 0.3 mm/s $\simeq$ 0.002 broadcast units/minute respectively. The rms values of $\hat{\sigma}_o$ in Table 4-10 are about 0.03 broadcast units, and 0.02 broadcast units/minute respectively, indicating that

(a) Φ can be fitted to $X_T(t)$ to within the roundoff error in $X_T(t)$ and

2 Hours Plus Min	Precise Ephemeris $\tilde{\Delta E}$	$\tilde{\Delta a}$	$\tilde{\eta}$	Approximant to Precise Ephemeris PE	PA	PN	Differences $\tilde{\Delta E}$-PE	$\tilde{\Delta a}$-PA	$\tilde{\eta}$-PN
32	5.69	27.35	6.94	5.68	27.35	6.95	0.02	0.01	-0.01
33	1.23	36.91	7.12	1.23	36.87	7.06	0.01	0.04	0.06
34	- 2.67	47.83	7.22	- 2.66	47.86	7.20	-0.01	-0.03	0.03
35	- 5.89	60.22	7.36	- 5.90	60.15	7.36	0.01	0.07	-0.01
36	- 8.49	73.61	7.54	- 8.45	73.58	7.55	-0.03	0.03	-0.01
37	-10.23	87.97	7.77	-10.27	87.96	7.77	0.04	0.02	-0.00
38	-11.31	103.05	8.02	-11.31	103.09	8.02	0.01	-0.03	-0.00
39	-11.55	118.74	8.26	-11.56	118.75	8.28	0.02	-0.02	-0.02
40	-10.96	134.77	8.58	-11.00	134.74	8.57	0.05	0.03	0.01
41	- 9.64	150.79	8.88	- 9.63	150.83	8.87	-0.01	-0.03	0.01
42	- 7.45	166.76	9.16	- 7.45	166.79	9.19	0.01	-0.03	-0.03
43	- 4.53	182.34	9.54	- 4.49	182.40	9.52	-0.04	-0.06	0.01
44	- 0.81	197.45	9.88	- 0.78	197.45	9.86	-0.03	0.00	0.02
45	3.63	211.69	10.18	3.64	211.73	10.20	-0.02	-0.04	-0.01
46	8.71	225.04	10.54	8.73	225.03	10.54	-0.01	0.01	0.01
47	14.39	237.17	10.84	14.41	237.18	10.88	-0.02	-0.01	-0.04
48	20.63	248.00	11.20	20.62	248.01	11.21	0.01	-0.00	-0.01
49	27.38	257.37	11.42	27.29	257.35	11.53	0.10	0.02	-0.11
						$\hat{\sigma}_o$	0.04	0.04	0.04

Φ	Approximant Coefficients CE	CA	CN
1	41.87	142.44	9.13
cos2nt	-36.19	-115.09	-2.17
sin2nt	-46.22	74.92	0.05
t	0.73	- 0.07	0.09

TABLE 4-9(a)

Typical Fit of Φ

To the Precise Ephemeris (Satellite 14, Day 162, 1972).

2 Hours Plus Min	Precise Ephemeris $\dot{\Delta E}$	$\dot{\Delta a}$	$\dot{\eta}$	Approximants to Precise Ephemeris $\dot{P}E$	$\dot{P}A$	$\dot{P}N$	Differences $\dot{\Delta E}-\dot{P}E$	$\dot{\Delta a}-\dot{P}A$	$\dot{\eta}-\dot{P}N$
32	-4.74	8.69	0.10	-4.72	8.75	0.09	-0.02	-0.05	0.01
33	-4.19	10.23	0.13	-4.18	10.28	0.12	-0.01	-0.05	0.01
34	-3.57	11.62	0.17	-3.57	11.67	0.15	0.00	-0.05	0.02
35	-2.90	12.85	0.20	-2.91	12.89	0.18	0.00	-0.04	0.02
36	-2.18	13.88	0.24	-2.19	13.94	0.21	0.01	-0.05	0.03
37	-1.43	14.73	0.27	-1.44	14.79	0.23	0.01	-0.06	0.04
38	-0.64	15.37	0.30	-0.65	15.43	0.26	0.01	-0.06	0.04
39	0.16	15.80	0.33	0.16	15.86	0.28	0.00	-0.07	0.05
40	0.96	16.01	0.35	0.97	16.07	0.30	-0.00	-0.06	0.05
41	1.77	15.99	0.37	1.78	16.06	0.31	-0.01	-0.07	0.06
42	2.56	15.76	0.38	2.57	15.82	0.32	-0.01	-0.06	0.06
43	3.33	15.31	0.39	3.34	15.37	0.33	-0.01	-0.06	0.06
44	4.07	14.65	0.39	4.08	14.70	0.34	-0.01	-0.05	0.05
45	4.77	13.78	0.39	4.76	13.82	0.34	0.00	-0.04	0.05
46	5.41	12.72	0.38	5.39	12.76	0.34	0.02	-0.04	0.04
47	5.99	11.47	0.37	5.96	11.51	0.34	0.03	-0.04	0.03
48	6.51	10.06	0.35	6.45	10.11	0.33	0.06	-0.04	0.03
49	6.94	8.51	0.32	6.87	8.56	0.32	0.08	-0.05	0.00
						$\hat{\sigma}_o$	0.03	0.05	0.04

TABLE 4-9(b)

			Fits of Φ to $X_T(t)$						Fits of $\dot{\Phi}$ to $\dot{X}_T(t)$					
			$\tilde{\Delta E}(t)$		$\tilde{\Delta a}(t)$		$\tilde{\eta}(t)$		$\dot{\tilde{\Delta E}}(t)$		$\dot{\tilde{\Delta a}}(t)$		$\dot{\tilde{\eta}}(t)$	
Data Set	Sat #	# Passes	RMS	Worst Case	RMS	Worst Case	RMS	Worst Case	RMS	Worst Case	RMS	Worst Case	RMS	Worst Case
1970	14	99	0.03	0.06	0.04	0.14	0.03	0.07	0.02	0.06	0.02	0.09	0.01	0.03
1972	14	126	0.03	0.05	0.03	0.06	0.03	0.05	0.01	0.03	0.02	0.04	0.02	0.03

TABLE 4-10

Summary of Fits of Φ to Precise Ephemeris

RMS and worst case values of $\hat{\sigma}_o$ in broadcast units for fits of Φ to $X_T(t)$, and of $\hat{\sigma}_o$ in broadcast units/minute for fits of $\dot{\Phi}$ to $\dot{X}_T(t)$.

(b) when Φ is fitted to $X_T(t)$, then $\dot{\Phi}$ is fitted to $\dot{X}_T(t)$ to within ten times the roundoff error in $\dot{X}_T(t)$.

To investigate the fit of Φ to the operational ephemeris, the 1970, 1972 and 1973 data sets were all used. For each pass $\Delta E(t)$, $\Delta a(t)$, $\eta(t)$ as given by the operational ephemeris were compared to their approximants (computed as for the precise ephemeris) and the fit characterized by a scalar of the form (4-132). The results for a typical pass are shown in Table 4-11. The rms and worst case values of $\hat{\sigma}_o$ for each of the 1970, 1972 and 1973 data sets are given in Table 4-12. For the 1973 data set, rms values of $\hat{\sigma}_o$ for each satellite are also shown. From section 4.4 we recall that the roundoff standard deviations for each of $\Delta E(t)$, $\Delta a(t)$ and $\eta(t)$ are 0.3 broadcast units. The rms values of $\hat{\sigma}_o$ in Table 4-12 are generally about 0.3 broadcast units, indicating that Φ can usually be fitted to $\Delta E(t)$, $\Delta a(t)$, $\eta(t)$ to within the roundoff error of the operational ephemeris.

To investigate whether approximants to the operational ephemeris represent the precise ephemeris any differently than does the operational ephemeris itself, the 1970 and 1972 data sets were used. For each pass approximants to the operational ephemeris $\Delta E(t)$, $\Delta a(t)$, $\eta(t)$ (computed as in (4-131)) were compared with $\tilde{\Delta E}(t)$, $\tilde{\Delta a}(t)$, $\tilde{\eta}(t)$ computed from the precise ephemerides using (4-97), (4-98), (4-99). Also the derivatives of the operational ephemeris approximants were compared with $\dot{\Delta E}(t)$, $\dot{\Delta a}(t)$, $\dot{\eta}(t)$ computed from the precise ephemeris using (4-126), (4-127), (4-128). The mean (bias) and standard deviation (scatter) for each of the six sets of differences for each pass were computed. The results for a typical pass are shown in Table 4-13. The rms and worst case values for the biases, and the average worst case values for the scatter are shown in Table 4-14. A comparison between this table and Table 4-8, which compares the

2 Hours Plus Min	Operational Ephemeris ΔE	Δa	η	Approximants to Operational Ephemeris PE	PA	PN	Differences ΔE-PE	Δa-PA	η-PN
30	15	14		14.86	13.98		0.14	0.02	
32	4	28	6	4.33	27.93	6.00	-0.33	0.07	0.00
34	- 4	48		- 4.16	48.31		0.16	-0.31	
36	-10	74	7	-10.07	73.97	7.00	0.07	0.03	0.00
38	-13	104		-13.02	103.47		0.02	0.53	
40	-13	135	8	-12.78	135.17	8.00	-0.22	-0.17	0.00
42	- 9	167		- 9.30	167.30		0.30	-0.30	
44	- 3	198	9	- 2.73	198.09	9.00	-0.27	-0.09	0.00
46	7	226		6.65	225.80		0.35	0.20	
48	18	249	10	18.37	248.90	10.00	-0.37	0.10	0.00
50	32	266		31.85	266.09		0.15	-0.09	
						$\hat{\sigma}_o$	0.31	0.28	0.00

Φ	Approximant Coefficients CE	CA	CN
1	40.31	144.55	5.50
cos2nt	-25.45	-130.58	0.00
sin2nt	-52.89	45.67	0.00
t	0.55	- 0.15	0.25

TABLE 4-11

Typical fit of Φ to the Operational Ephemeris
(Satellite 14, Day 162, 1972).

Data Set	Sat #	# Passes	ΔE(t) RMS	ΔE(t) Worst Case	Δa(t) RMS	Δa(t) Worst Case	η(t) RMS	η(t) Worst Case
1970	14	99	0.31	0.47	0.28	0.44	0.33	0.71
1972	14	126	0.28	0.47	0.29	0.46	0.27	0.68
1973	12	125	0.30		0.29		0.27	
	13	144	0.31		0.29		0.26	
	14	147	0.29		0.29		0.26	
	18	158	0.29		0.30		0.28	
	19	167	0.29		0.42		0.26	
	All	741	0.30	0.58	0.33	0.79	0.27	0.73

TABLE 4-12

Summary of Fit of Φ to Operational Ephemeris
RMS and worst case values of $\hat{\sigma}_o$ in broadcast units for fits of
Φ to ΔE(t), Δa(t) and η(t).

2 Hours Plus Min	Approximants to Operational Ephemeris			Precise Ephemeris - Approximant			Approximants to Operational Ephemeris			Precise Ephemeris - Approximant		
	PE	PA	PN	$\tilde{\Delta E}$-PE	$\tilde{\Delta a}$-PA	$\tilde{\eta}$-PN	$\dot{P}E$	$\dot{P}A$	$\dot{P}N$	$\dot{\tilde{\Delta E}}$-$\dot{P}E$	$\dot{\tilde{\Delta a}}$-$\dot{P}A$	$\dot{\tilde{\eta}}$-$\dot{P}N$
32	4.33	27.93	6.00	1.37	-0.58	0.94	-4.80	8.67	0.25	0.07	0.03	-0.15
33	- 0.21	37.38	6.25	1.44	-0.47	0.87	-4.25	10.21	0.25	0.07	0.02	-0.12
34	- 4.16	48.31	6.50	1.49	-0.48	0.72	-3.64	11.62	0.25	0.07	0.00	-0.08
35	- 7.46	60.56	6.75	1.57	-0.35	0.61	-2.96	12.86	0.25	0.06	-0.01	-0.05
36	-10.07	73.97	7.00	1.58	-0.35	0.54	-2.24	13.92	0.25	0.06	-0.04	-0.01
37	-11.93	88.33	7.25	1.70	-0.36	0.52	-1.48	14.78	0.25	0.05	-0.05	0.02
38	-13.02	103.47	7.50	1.71	-0.41	0.52	-0.69	15.44	0.25	0.05	-0.07	0.05
39	-13.30	119.15	7.75	1.76	-0.41	0.51	0.12	15.89	0.25	0.04	-0.09	0.08
40	-12.78	135.17	8.00	1.82	-0.39	0.58	0.93	16.11	0.25	0.03	-0.10	0.10
41	-11.44	151.29	8.25	1.81	-0.50	0.63	1.74	16.11	0.25	0.03	-0.11	0.12
42	- 9.30	167.30	8.50	1.86	-0.54	0.66	2.53	15.88	0.25	0.03	-0.12	0.13
43	- 6.39	182.97	8.75	1.86	-0.63	0.79	3.29	15.43	0.25	0.03	-0.12	0.14
44	- 2.73	198.09	9.00	1.92	-0.63	0.88	4.02	14.76	0.25	0.05	-0.11	0.14
45	1.64	212.43	9.25	1.99	-0.74	0.93	4.70	13.89	0.25	0.07	-0.11	0.14
46	6.65	225.80	9.50	2.07	-0.76	1.04	5.32	12.82	0.25	0.09	-0.11	0.13
47	12.25	238.01	9.75	2.14	-0.84	1.09	5.87	11.58	0.25	0.12	-0.11	0.12
48	18.37	248.90	10.00	2.26	-0.90	1.20	6.35	10.17	0.25	0.15	-0.11	0.10
49	24.93	258.30	10.25	2.45	-0.94	1.17	6.76	8.62	0.25	0.19	-0.10	0.07
		Mean		1.82	-0.57	0.79				0.07	-0.07	0.05
		Std Dev.		0.29	0.19	0.23				0.04	0.05	0.10

TABLE 4-13

Typical Comparison between the Precise Ephemeris and Approximants to the Operational Ephemeris

(Satellite 14, Day 162, 1972).

Data Set	Sat #	# Passes	Single Pass Mean Values		Single Pass Std Dev'ns		Single Pass Mean Values		Single Pass Std Dev'ns		Single Pass Mean Values		Single Pass Std Dev'ns	
			RMS	Worst Case	AVG	Worst Case	RMS	Worst Case	AVG	Worst Case	RMS	Worst Case	AVG	Worst Case
			ΔE				Δa				η			
1970	14	99	2.38	5.76	0.27	0.83	0.43	1.21	0.32	1.74	1.17	2.82	0.58	1.56
1972	14	126	1.56	4.01	0.28	0.98	0.41	1.13	0.29	0.81	1.04	2.73	0.52	1.80
			$\dot{\Delta} E$				$\dot{\Delta} a$				$\dot{\eta}$			
1970	14	99	0.05	0.14	0.06	0.14	0.06	0.14	0.07	0.27	0.10	0.28	0.10	0.40
1972	14	126	0.06	0.21	0.07	0.28	0.10	0.24	0.07	0.21	0.14	0.48	0.11	0.40

TABLE 4-14

Summary of Comparisons between Precise Ephemeris and Approximants to Operational Ephemeris

operational ephemeris itself with the precise ephemeris, reveals that the coordinate biases are unchanged, but that the average coordinate scatter is slightly reduced, and worst case coordinate scatter increased when the approximant to the operational ephemeris is used. The velocity scatter in this case is three to five times that shown in Table 4-10.

4.6 Covariance matrix of the operational ephemeris

If the operational ephemeris (or any other ephemeris) is assumed to perfectly model the actual satellite trajectory, then in the solution for receiver coordinates, any errors in the ephemeris will result in a spurious increase in the size of the observation residuals. On the other hand it is possible to consider the orbit as only approximately modelled by the ephemeris. If we can assume that the differences between the trajectory and ephemeris have zero mean (that is we assume that over many passes ephemeris errors are balanced in sign), then the ephemeris errors can be represented by an appropriately chosen covariance matrix (section 3.2.2).

In this chapter we have seen that the accuracy of the operational ephemeris is bound up with how well the variable orbit parameters represent the differences between the actual trajectory and the mean orbit defined by the fixed orbit parameters. This has been discussed in section 4.4. There is another consideration. If we compute least squares approximations to the variable orbit parameters as described in section 4.5, then we are no longer using the variable orbit parameters. They are replaced by the polynomial coefficients resulting from the approximations. Therefore the covariance matrix of the operational ephemeris should represent

(a) how well the variable orbit parameters represent the orbit, and

(b) how well the polynomial coefficients represent the variable orbit parameters.

From the results of section 4.4 (and Guier's theorem) we recall that the ephemeris errors are well represented by biases (the ephemeris and trajectory are closely parallel). Coincidentally one of our approximating base functions is a bias. Therefore the ephemeris errors are well represented by assigning variances of 4, 0.25 and 1 broadcast units^2 respectively to the $\Delta E(t)$, $\Delta a(t)$ and $\eta(t)$ bias coefficients resulting from the approximations.

From the results of section 4.5, we recall that the rms residual difference between the variable orbit parameters and their approximants is about 0.3 broadcast units, which from section 4.1 is the standard deviation of the roundoff error in the variable orbit parameters. From this we infer that the contribution to the covariance matrix of the approximation error can be ignored. This is the approach taken here.

The operational ephemeris covariance matrix then is the covariance matrix of the three bias coefficients. Since the least squares approximations yielding these coefficients are performed independently, we have no basis on which to assign correlations between these three coefficients, hence in broadcast units^2 we have

$$\Sigma_{\text{ephemeris}} = \Sigma_{\text{biases}} = \begin{bmatrix} 4 & 0 & 0 \\ 0 & 0.25 & 0 \\ 0 & 0 & 1 \end{bmatrix} . \qquad (4\text{-}135)$$

CHAPTER 5

TEST DATA RESULTS

In this chapter we analyze a set of test data from eight Transit tracking stations in Atlantic Canada. This analysis is in two parts. First (section 5.3) we attempt to detect any systematic components of the physical process (the Transit observation process) not accounted for in the mathematical model of this process (the Transit navigation observation equation (2-43)). The input data for this first analysis are the results generated by Guier plane navigation using the observed test data (section 4.2.2). Second (section 5.4) we analyze the tracking station coordinates computed from the test data.

In section 5.1 we list the decisions upon which the computation of the results rests. In section 5.2 we summarize the data processing required to generate the results.

5.1 Summary of Assumptions and Decisions

The a priori assumptions and decisions made in the course of generating the results of this chapter are listed here under four headings: the measurement and correction of the Doppler counts; the satellite ephemeris; filtering of noisy measurements and passes; and computation of station coordinates. The items listed under each of these headings will be re-examined and more fully discussed in Chapter 6, in the light of the results described in this chapter.

5.1.1 Doppler measurements and corrections

Nine assumptions and decisions which affect Doppler measurements and their correction are:

(a) to use navigation-type Transit receivers (section 2.2.2),

(b) to use the Transit navigation observation equation (2-43)

$$D = (f_g - f_s)(t_2 - t_1) + \frac{f_g}{c}(S_2 - S_1) \quad , \qquad (5\text{-}1)$$

(c) to correct for tropospheric and ionospheric refraction using reduction equations (sections 2.3 and 2.4) rather than incorporating this as part of the observation equation,

(d) to use the Hopfield tropospheric refraction correction model (section 2.3.1),

(e) to use the two-frequency ionospheric refraction correction model (section 2.4.1),

(f) to use the shortest possible Doppler integration interval (about 4.6 seconds),

(g) to assume individual Doppler measurements are uncorrelated,

(h) to assume all Doppler measurements made with the same model receiver have equal variances, and

(i) to assume that the Doppler measurement variances for the three models used here are

ITT 5001	1.5 count^2
Marconi 722	4.0 count^2
Maganvox 702	10.0 count^2

5.1.2 Satellite ephemerides

Four decisions pertaining to the satellite ephemerides were

(a) to use the operational ephemeris (section 4.1),

(b) to approximate the variable orbit parameters by the base functions

of section 4.5,

(c) to allow the satellite trajectory defined by the operational ephemeris to undergo a parallel translation during adjustment (section 4.6),

(d) to apply the pole motion correction computed by Anderle (1972; 1973b) to transform the operational ephemeris coordinates into a closer approximation of the average terrestrial coordinate system (section 4.1.1).

5.1.3 Data filtering

Decisions concerning data filtering are

(a) to examine and edit the observed data as thoroughly as possible prior to accepting it for use in computing station coordinates,

(b) to use the majority-voting process (section 5.2.2) as the first main data examination method,

(c) to use Guier plane navigation (sections 4.2.2 and 5.3) as the second main data examination method,

(d) to examine Doppler counts both individually, and together in single pass sets,

(e) to make as minute an examination of the Doppler measurements as possible by using the shortest Doppler integration interval possible (4.6 seconds),

(f) to reject a piece of data if the results for any test on that data fall below specified threshold values,

(g) to use as threshold values for rejecting individual Doppler counts the following:

(i) one or more non-numeric characters occur in either 150 or 400 MHz data channel,

(ii) loss of lock in either Doppler channel,

(iii) one or more noise characters occur in the message word occupying the same row,

(iv) the satellite elevation is less that 8° when the Doppler count is measured,

(v) the Doppler count is not balanced about closest approach by another Doppler count equidistant and on the other side of closest approach,

(vi) the misclosure (observed Doppler count minus that computed from the right hand side of equation (5-1) using a priori values for the unknown parameters) exceeds 100 counts,

(vii) the Doppler residual fails a 95% confidence level normality test (section A.1),

(h) to use the following threshold values in rejecting an entire satellite pass,

(i) the pass contains less than 600 recorded data characters,

(ii) one or more of the fixed orbit words exceed normal limits, or fails in the majority voting,

(iii) less than three two-minute data messages contain nonzero Doppler counts,

(iv) the number of 4.6 second Doppler counts surviving the tests in (g) is less than 75,

(v) the satellite elevation at closest approach is less than 10°,

(vi) a satisfactory approximation to the variable orbit words (section 4.5) cannot be computed,

(vii) a satisfactory alert cannot be computed (the pass cannot be identified using the algorithm of section 4.3),

(viii)the Guier plane navigation results are unsatisfactory (the tracking station Guier plane coordinates exceed 100 m; the standard deviations of these coordinates exceed 100 m; the standard deviation of the receiver frequency offset exceeds 10 parts in 10^{10}; the estimated a

variance factor fails a 95% chi-square test (section A.2); or convergence requires more than 5 iterations).

5.1.4 Coordinate computation

The decisions relevant to the computation of tracking station coordinates are

(a) to compute the final tracking station coordinates in three steps consisting of:

(i) compute the position vector for each tracking station and its covariance matrix,

(ii) compute the interstation vector between each pair of tracking stations for which passes were tracked simultaneously and its covariance matrix,

(iii) combine these position vectors (x_i and x_j for stations i and j) and interstation vectors (Δx_{ij} between stations i and j) and their covariance matrices into a network adjustment using the model

$$\Delta x_{ij} = x_i - x_j \quad , \tag{5-2}$$

(b) in computing a position vector all the data at the station (after data rejections of section 5.1.3) are used in the multipass model of section 3.3.5,

(c) in computing interstation vectors all the data from both of the pair of stations (after data rejections of section 5.1.3) are used in the multipass model of section 3.3.5,

(d) in computing position vectors the orbit is held fixed,

(e) in computing interstation vectors the orbit is relaxed parallel to itself consistently with the observations from both stations.

5.2 Summary of Data Processing

5.2.1 Input data

The data analyzed in this chapter were collected in May, June and July of 1972 and in May and June of 1973.

Two receivers were used to collect the 1972 data. These were an International Telephone and Telegraph Corporation receiver, model 5001, serial C002, belonging to the Surveying Engineering Department of the University of New Brunswick (henceforth designated simply as the ITT receiver), and a Magnavox Company receiver, model 702CA, serial 005, belonging to the Earth Physics Branch of the Department of Energy, Mines and Resources (henceforth designated simply as the MVX receiver).

Five receivers were used to collect the 1973 data. These were the ITT receiver used in 1972, and four Canadian Marconi Company receivers, model CMA-722. One of these, serial 101, belongs to the Bedford Institute of Oceanography. The other three, serials 102, 103 and 104, belong to the Geodetic Survey of Canada. Henceforth these four receivers are designated

simply MAR101, MAR102, MAR103, MAR104.

Data from five stations occupied in 1972 is used. Data from these same five stations plus three others occupied in 1973 is used. The 1972 data was acquired mainly by U.N.B. students under a contract with the Geodetic Survey of Canada. The 1973 data was acquired by the Geodetic Survey of Canada and was generously made available for the purposes of this thesis. A preliminary analysis of the 1972 data has been presented in Krakiwsky, Wells and Thomson (1973).

Figure 5-1 locates the eight stations occupied. Table 5-1 summarizes the data acquired at each station.

All data was collected on punched paper tape. To convert this to magnetic tape, a 600 character/second paper tape reader was purchased and installed on the U.N.B. IBM/370 computer. The interfacing and software driver for this reader were developed by Mr. Bernd Kurz of the U.N.B. Computer Centre. The conversion process required approximately one manhour per 1400 feet of paper tape to manually feed the tape reader and rewind the paper tape, and approximately 23 seconds ($4.15) in computer charges per 1000 feet of tape. A total of 150 manhours and 4875 jobcharge seconds ($880) were required.

The model used to correct observed Doppler counts for tropospheric refraction (section 2.3.1) requires values for surface pressure, temperature, and partial pressure of water vapour at the receiver location for the time the pass was tracked. These values were approximated from hourly surface weather observations made at the nearest weather station (usually the nearest airport) by the Canadian Atmospheric Environment Service, and contained on a magnetic tape purchased from them.

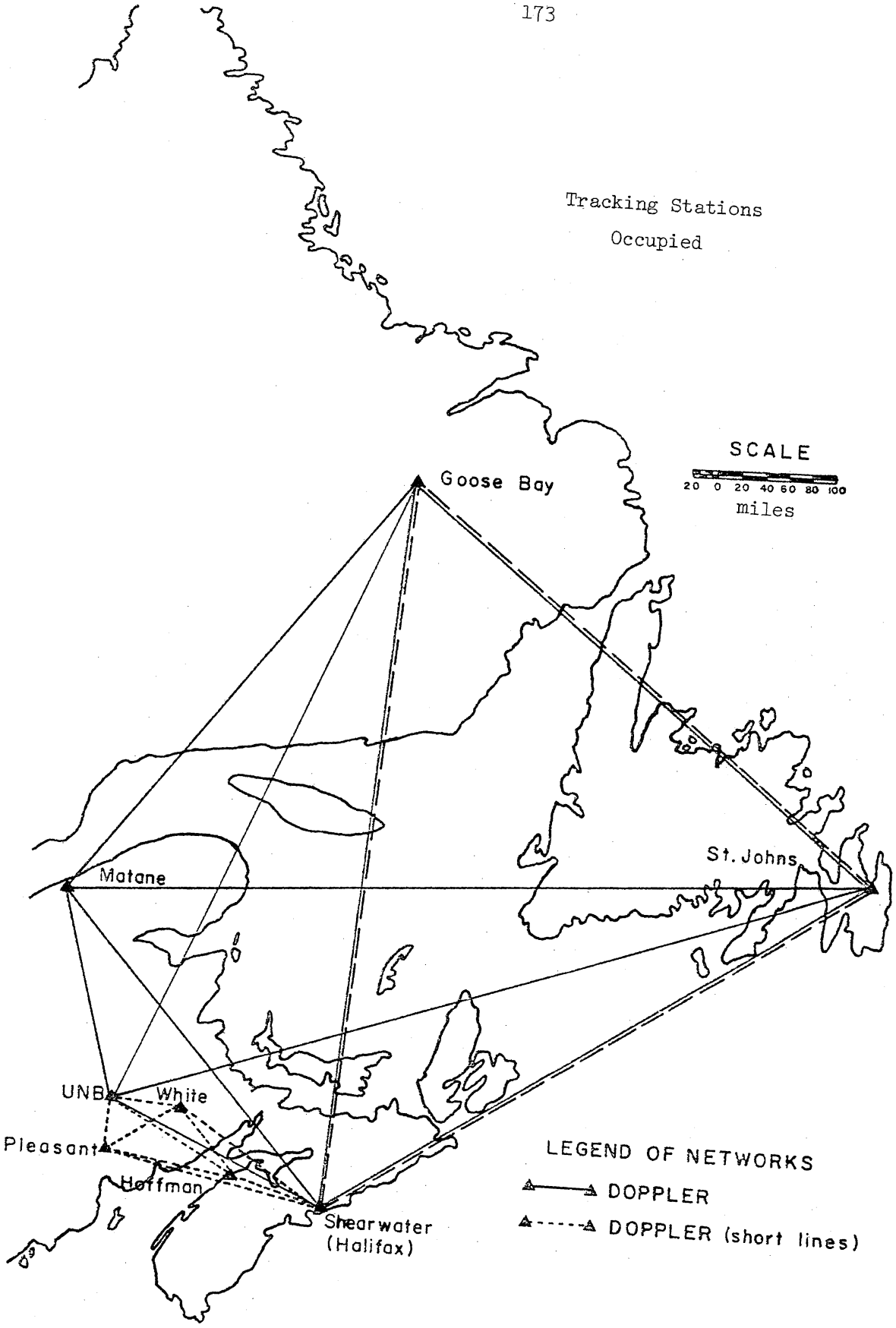
Tracking Stations
Occupied
SCALE
20 0 20 40 60 80 100
miles
Goose Bay
St. Johns
Matane
UNB
White
Pleasant
Hoffman
Shearwater
(Halifax)
LEGEND OF NETWORKS
DOPPLER
DOPPLER (short lines)

FIGURE 5-1

Station	Receiver	Observing Period	Days On Stn	Down Time (hr)	Days of Data	No. of Tapes	Feet of Paper Tape
1973							
Fredericton	ITT	138-179	42	12	38	64	43,000
Halifax	MAR101	138-156	19		16	27	16,990
Pleasant	MAR102	138-145	8		7	12	6,330
St. John's	MAR102	148-163	16		15	25	15,920
Hoffman	MAR103	138-145	8		7	12	6,990
Matane	MAR103	147-163	17	132	10	17	11,260
White	MAR104	139-145	7		6	10	4,250
Goose Bay	MAR104	148-161	14		13	22	15,870
Subtotal			131	144	112	189	120,610
1972							
Fredericton	MVX	161-190	30		27	64	27,430
Halifax	MVX	192-207	16	14	14	31	13,530
Pleasant	ITT	162-172	11		10	32	13,840
Hoffman	ITT	182-199	18	12	14	30	17,100
White	ITT	(173-181) (200-208)	18		16	36	19,680
Subtotal			93	26	81	193	91,580
Total			224	170	193	382	212,190
ITT			89	24	78	162	93,620
MAR			89	132	74	125	77,610
MVX			46	14	41	95	40,960

TABLE 5-1

Summary of Tracking Data Obtained

5.2.2 Processing programs

Data processing was in two stages, data filtering and coordinate computation. A total of six FORTRAN programs were used (Figure 5-2), three for data filtering (programs MAJORITY, PREPARE and ANALYSIS), and three for coordinate computation (ONESTN, TWOSTN and NETWORK). Details of the structure, algorithms, and coding of these programs will appear elsewhere (Wells, 1975). Each program (except TWOSTN and NETWORK) is run once to process all the data acquired at a single station.

Program MAJORITY accepts raw data in the form of paper tape images obtained from any one of the Marconi CMA-722, ITT 5001 or Magnavox 702CA receivers. It processes the data pass by pass, detecting the beginning and ending of passes; formatting the input character stream into the NNSS data matrix; sensing satellite data injections; majority voting the operational ephemerides; and converting the two-minute and intermediate accumulated Doppler counts into 4.6 second accumulated Doppler counts. A particular Doppler is rejected if a non-numeric character appears in either the 150 MHz or 400 MHz channel; if either channel loses lock; or if there is a noise character in the message word occupying the same row in the data matrix. A pass is rejected if it contains less than 600 characters; if there is a majority vote failure for any digit of any fixed orbit parameter word, or if any fixed orbit parameter word has a numerical value outside designated limits; or if there are less than three two-minute messages containing nonzero short Dopplers.

Program PREPARE applies ionospheric and tropospheric refraction corrections; identifies the satellite pass by computing a set of possible alert times and Doppler curve slopes, and then finding the best match between the computed times and slopes and the time and slope obtained from the observed short Doppler counts; computes satellite positions at 4.6

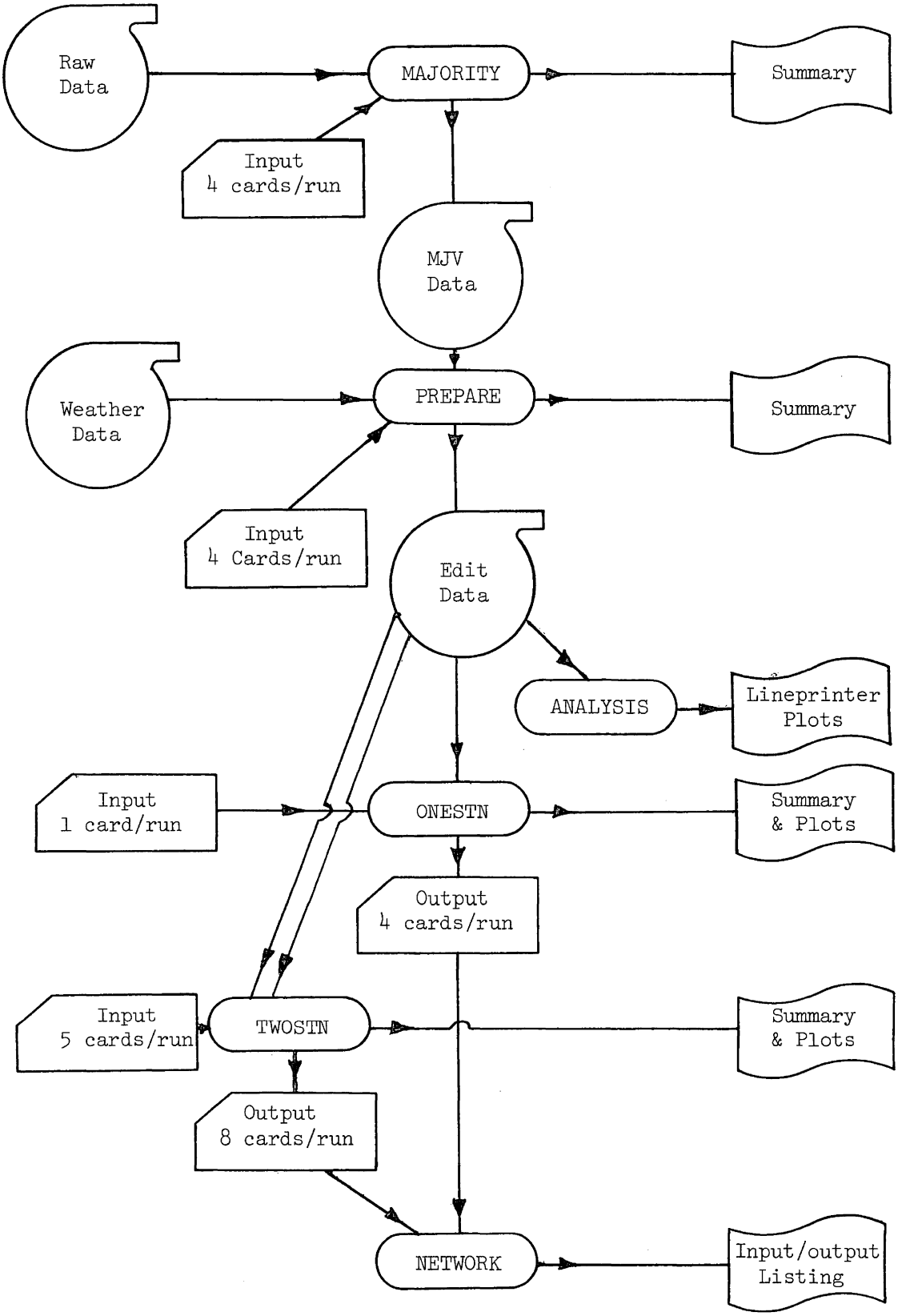

FIGURE 5-2
Processing Flow Diagram

second intervals by fitting polynomials to the broadcast values of ΔE, Δa and η using the base functions {1, cos 2 nt, sin 2 nt, t} where n is the mean motion; rejects low elevation Dopplers and trims the Doppler data to be balanced about closest approach; and computes a two-dimensional, single pass, "filtering fix" in the Guier plane. A pass is rejected if there are too few short Dopplers after balancing about closest approach; if a satisfactory polynomial fit cannot be made to the variable orbit parameters; if a satisfactory pass identification cannot be made; if the satellite elevation at closest approach is too low; or if the filter fix results are unsatisfactory (that is the fix coordinates or their standard deviations are too large, or the estimated variance factor fails a χ^2 test (section A.2) or too many iterations are required for convergence). During the filter fix iterations, individual Doppler counts are rejected if their misclosure is too large, or if their residual value fails a normality test (section A.1).

Program ANALYSIS computes and plots sample statistics from the data accepted after filtering. The Guier plane navigation residuals are analyzed as a function of elevation and magnitude; the Guier plane coordinates, frequency offset, and estimated variance factor resulting from the filter fix are all analyzed as a function of pass elevation, number of Dopplers in the pass, time of day, day of the year, time since injection, satellite number, satellite quadrant, and magnitude. For the frequency offset, the drift of the receiver oscillator is computed by a least squares linear fit.

Program ONESTN computes a three dimensional, single station, multi-pass fix using the phased algorithm of section 3.3.5. Possible quasi-observables are three orbit biases and the receiver frequency offset, although for the results reported here, the orbit was held fixed, and the

frequency offset was held fixed at the value obtained in the filter fix. Each pass is weighted inversely to the estimated variance factor resulting from the filter fix. Passes are processed in chronological order. A pass is rejected if its contribution to the accumulated estimated variance factor fails a χ^2 test (section A.2).

Program TWOSTN computes a six dimensional, two station, multipass fix using the phased algorithm of section 3.3.5. Passes from the two stations are first compared and non-simultaneous passes rejected. For simultaneous passes, the arrays containing the Doppler data are aligned; the arrays containing the variable orbit parameter data are aligned and combined; and the base functions {1, cos 2 nt, sin 2 nt, t} are newly fitted to the combined set of variable orbit parameters. Possible quasi-observables are three orbit biases and two receiver frequency offsets, although for the results reported here the frequency offsets were held fixed at the values obtained in the filter fixes. For each pass, the data from each station was weighted inversely to the estimated variance factor resulting from the respective filter fix. Passes were processed in non-chronological order based on balancing between different satellites and different quadrants. A pass is rejected if its contribution to the accumulated estimated variance factor fails a χ^2 test (section A.2).

Program NETWORK is actually a more general program than required here, developed for other investigations by Mr. D.B. Thomson (Thomson and Krakiwsky, 1974). As used here it was equivalent to a simple condition adjustment in which the mathematical model is

$$F(L) = \Delta x_{ij} - x_i + x_j = 0 \quad , \tag{5-3}$$

where x_i and x_j are point positioning observations (program ONESTN output) and Δx_{ij} is a translocated interstation vector observation (derived from program TWOSTN output). The adjusted network coordinates, interstation

vectors, interstation distances, and their standard deviations, together with the adjusted network covariance matrix and the network correlation coefficient matrix, are all computed.

5.2.3 Data rejection

In this section we review the amount and causes for data rejection. Table 5-2 lists the passes alerted and detected, and those rejected and accepted by programs MAJORITY, PREPARE and ONESTN. Table 5-3 normalizes these figures into passes per day. Table 5-4 lists the numbers of passes available from both stations, and simultaneous passes and the passes accepted by program TWOSTN.

In general about two-thirds of the alerted passes (65%) were rejected before point positioning coordinates were computed by program ONESTN. This percentage can be broken down into the following categories:

Not tracked or not detected by MAJORITY		24%
Fixed orbit parameter majority vote failure	8%	
Pass too short (less than 3 two-minute messages)	2	
Total MAJORITY rejections		10
Low elevation (less than 10°)	10	
Too few Dopplers (less than 75)	10	
Too few variable orbit parameters to fit curve	3	
Unsatisfactory filter fix results	2	
Could not identify pass	1	
Total PREPARE rejections		26
ONESTN chi-square failures		6

Two of the major reasons for completely missing or obtaining degraded passes are low elevation angle at closest approach (at latitude

		MAJORITY				PREPARE						ONESTN	
Station	Alert-ed	Detect-ed	Bad Fixed Params	LT 3 Msgs	Accept-ed	Low Elev	Too Few Dops	Bad Var Params	Bad Filter Fix	No Alert	Accept-ed	χ^2 Failed	Accept-ed
1973													
Fred'ton	1370	1080	124	16	940	174	64	38	2	3	659	195	464
Halifax	560	401	29	7	365	56	23	12	17	2	255	7	248
Pleasant	250	171	18	10	143	18	39	3	10	1	72	1	71
StJohn's	570	402	18	11	373	25	49	13	22	0	264	12	252
Hoffman	250	178	11	11	156	26	26	6	7	0	91	5	86
Matane	380	267	8	6	253	48	30	7	13	1	154	10	144
White	220	128	28	5	95	1	22	11	4	0	57	9	48
GooseBay	600	423	15	13	395	55	60	15	16	2	247	9	238
Sub-Total	4200	3050	251	79	2720	403	313	105	91	9	1799	248	1551
1972													
Fred'ton	970	712	85	15	612	37	209	36	47	17	266	31	235
Halifax	490	340	16	5	319	36	119	21	13	8	122	10	112
Pleasant	360	337	64	2	271	51	13	16	1	2	188	36	152
Hoffman	490	435	45	2	388	82	29	13	5	6	253	46	207
White	580	511	88	5	418	82	26	26	1	34	249	52	197
Sub-Total	2890	2335	298	29	2008	288	396	112	67	67	1078	175	903
Total	7090	5385	549	108	4728	691	709	217	158	76	2877	423	2454
ITT	2800	2363	321	25	2017	389	132	93	9	45	1349	329	1020
MAR	2830	1970	127	63	1780	229	249	67	89	25	1140	53	1087
MVX	1460	1052	101	20	931	73	328	57	60	6	388	41	347

TABLE 5-2
Pass Rejections During Processing

PASSES/DAY (with 5 satellites)

Station	Alerted	Identified	Accepted by MAJORITY	Accepted by PREPARE	Accepted by ONESTN
1973					
Fredericton	36	28	25	17	12
Halifax	35	25	23	16	16
Pleasant	36	24	20	10	10
St. John's	38	27	25	18	17
Hoffman	35	25	22	13	12
Matane	38	27	25	15	14
White	36	21	16	10	8
Goose Bay	46	33	30	19	18
Subtotal	37	27	24	16	14
1972					
Fredericton	36	26	23	10	9
Halifax	35	24	23	9	8
Pleasant	36	34	27	19	15
Hoffman	35	31	28	18	15
White	36	32	26	16	12
Subtotal	36	29	25	13	11
Total	37	28	24	15	13
ITT	36	30	26	17	13
MAR	38	27	24	15	15
MVX	36	26	23	9	8

TABLE 5-3

Accepted Passes Per Day During Processing

Stn 1	Stn 2	Stn 1 Passes	Stn 2 Passes	Simultaneous Passes	Accepted Passes
1973					
Fredericton	Pleasant	109	72	55	55
Fredericton	White	89	57	40	39
Hoffman	White	70	57	39	38
Halifax	Hoffman	95	90	66	65
Pleasant	White	65	56	35	34
Pleasant	Hoffman	71	89	53	53
Fredericton	Hoffman	110	91	73	73
Halifax	White	78	53	38	37
Halifax	Pleasant	96	72	50	50
Fredericton	Halifax	280	253	190	183
Fredericton	Matane	273	173	109	106
Halifax	Matane	75	81	46	46
Matane	Goose Bay	113	142	58	58
St. John's	Goose Bay	227	247	150	150
Halifax	St. John's	146	145	98	97
Fredericton	Goose Bay	222	247	140	138
Halifax	Goose Bay	141	156	101	99
Fredericton	St. John's	254	264	150	145
St. John's	Matane	263	155	83	83
Subtotal		2777	2500	1574	1549
1972					
Fredericton	Pleasant	107	188	82	81
Fredericton	White	86	102	39	39
Halifax	Hoffman	62	104	43	43
Fredericton	Hoffman	78	147	66	66
Halifax	White	58	128	40	39
Subtotal		391	669	270	268
Total		3168	3169	1844	1817

TABLE 5-4

Passes Accepted by TWOSTN

45°, 15% of alerted passes are below 5° elevation; 27% below 10°; and 38% below 15°), and overlapping passes (at latitude 45° with five satellites up to 40% of passes rise before the previous satellite has set). These two causes have three main effects on the processing

(a) either the pass will not be tracked at all,

(b) it will be tracked obtaining noisy data causing MAJORITY to reject it, or

(c) it will have too low an elevation angle. The sum of these three rejection categories is 44%, leaving 22% for all other causes.

Six significant departures or anomalies from the above percentages can be seen from a close examination of Table 5-2. The 1973 White data has rejection percentages of 42% for passes not detected; 13% for bad fixed orbit parameters; 2% for passes too short; and 0% for low elevation, a total of 57% (rather than 44% mentioned above). These anomalies may have been due to the fact that this was the first field use for this receiver, or the inexperience of the operating team (for example attempting to manually screen out low elevation passes - indicated by the fact that only one pass is so rejected for this data), or some environmental influence on reception at the antenna (the accepted passes are split 60% to 40% in favour of satellite subtracks lying to the east, which might indicate some westward antenna shading), or a combination of these three reasons.

The second anomaly is that for the 1972 ITT data (from Pleasant, Hoffman and White) a higher percentage of alerted passes were detected (only 10% not detected), but the MAJORITY and low elevation rejection rates were also higher (15% each), indicating that the receiver was more efficient in obtaining low elevation and noisy passes, but their degraded quality was still reason for rejection.

The third anomaly is that 22% of the Magnavox receiver passes are

rejected because of too few Dopplers. This is probably due in part to the high starting value of the auto acquisition frequency sweep for this receiver.

The fourth anomaly is the difference between the Marconi receivers at Pleasant, Hoffman and White (total 72% rejection) and the same receivers at St. John's,Matane and Goose Bay (total 59% rejection). This again may be due to the first field experience with these receivers and their operators being at the former stations.

The fifth anomaly is the 1972 White rejections due to no pass identification (6%). The reason for this is that an inaccurate estimate of the receiver frequency offset was chosen for the 1972 ITT processing using program PREPARE (+310 parts in 10^{10} instead of -190 parts in 10^{10}), and this caused the time of closest approach as determined from the observed Doppler counts to be in error.

The sixth anomaly is the ITT chi-square rejection rate (12%), particularly for 1973 Fredericton (14%). A discussion of this point is made in section 5.4.1.

Usually reasons can be found for the last three PREPARE rejection categories. For example for 1973 Fredericton, of the 38 passes rejected because of bad variable parameters, 21 lost lock during the pass, 13 were injection passes, 8 had elevation angles less than 15°, and only 6 were none of these. One of the two bad filter fix passes had an 11° elevation angle. Of the three passes for which no alert could be matched, two were injection passes (one also losing lock during the pass), and the other was being tracked when the receiver ran out of paper tape.

From Table 5-4 the TWOSTN results indicate that about 60% of the passes accepted by PREPARE can be expected to be simultaneous with at least one other station. The chi-square rejection rate is very low (1%).

5.2.4 Processing costs

In this section we give the costs of processing Transit data using the methods described in section 5.2.2.

All processing was done on the U.N.B. IBM 370/158J computer under OS/360/MVT release 21.7. The programs were all written in FORTRAN and compiled using the IBM FORTRAN IV G and H compilers. The costs quoted in this section are the costs which would have had to be paid, if the processing was done at the external user rate.

The U.N.B. external user rate is $650 per jobcharge hour ($0.18 per second). The U.N.B. charging algorithm is

Jobcharge time(sec) = CPU time(sec) * (1 + core used(K-bytes)/400)
+ 1 sec/100 disk and tape I/O operations
+ 1 sec/500 card I/O operations
+ 3 sec/1000 lines printed.

Table 5-5 lists the CPU times, jobcharge times, and external user costs of running MAJORITY, PREPARE, ANALYSIS, ONESTN, and TWOSTN. The cost of running NETWORK was negligible, taking 15 CPU seconds, 27 jobcharge seconds, and $7 to run the entire 1973 network.

The total cost of processing the 1973 data was $4,005 (4 hours CPU time), and for the 1972 network it was $2023 (2 hours CPU time). A breakdown by program in terms of cost per edited pass (accepted by PREPARE) cost per observing day, cost per station and cost per interstation line is given in Table 5-6.

The higher costs per pass and per day for the 1973 data is mainly due to the greater number of translocation lines observed (19 vs 5), which serve to increase the internal consistency of the network, as well as the processing costs. The number of translocation lines in a network depends on the number of receivers in simultaneous use (5 in 1973 vs 2 in 1972), which again increases the cost of field data collection.

	MAJORITY			PREPARE			ANALYSIS			ONESTN			TOTAL
Station	CPU Time (sec)	Job Charge Time (sec)	Cost ($)	CPU Time (sec)	Job Charge Time (sec)	Cost ($)	CPU Time (sec)	Job Charge Time (sec)	Cost ($)	CPU Time (sec)	Job Charge Time (sec)	Cost ($)	Cost ($)
1973													
Fred'ton	1281	1841	332	1555	2241	405	59	121	22	754	1028	186	945
Halifax	493	708	128	621	896	162	30	59	11	341	465	84	385
Pleasant	189	272	49	214	309	56	12	24	4	97	132	24	133
StJohn's	466	670	121	668	963	174	29	58	10	339	462	83	388
Hoffman	205	295	53	263	379	68	14	27	5	120	163	29	155
Matane	344	495	89	491	708	128	18	36	7	225	307	55	279
White	126	181	33	137	198	36	11	21	4	71	97	18	91
GooseBay	467	672	121	632	911	164	27	54	10	309	422	76	371
Sub-Total	3571	5134	926	4581	6605	1193	200	400	73	2256	3076	555	2747
1972													
Fred'ton	823	1188	215	755	1088	196	24	48	9	257	351	63	483
Halifax	394	567	102	358	516	93	14	27	5	115	157	28	228
Pleasant	420	603	109	489	705	127	22	45	8	234	319	58	302
Hoffman	532	766	138	644	929	168	24	49	9	309	421	76	391
White	614	883	159	628	907	164	25	53	10	315	429	77	410
Sub-Total	2783	4007	723	2874	4145	748	109	222	41	1230	1677	302	1814
Total	6354	9141	1649	7455	10750	1941	309	622	114	3486	4753	857	4561
ITT	2847	4093	738	3316	4782	864	130	268	49	1612	2197	397	2048
MAR	2290	3293	594	3026	4364	788	141	279	51	1502	2048	369	1802
MVX	1217	1755	317	1113	1604	289	38	75	14	372	508	91	711

TABLE 5-5(a)

Processing Costs

TWOSTN

Stn 1	Stn 2	CPU Time (secs)	Jobcharge Time (sec)	Cost $
1973				
Fredericton	Pleasant	154	250	45
Fredericton	White	108	176	32
Hoffman	White	108	176	32
Halifax	Hoffman	182	295	53
Pleasant	White	96	156	28
Pleasant	Hoffman	146	237	43
Fredericton	Hoffman	200	324	59
Halifax	White	103	169	31
Halifax	Pleasant	139	226	41
Fredericton	Halifax	518	835	151
Fredericton	Matane	295	480	87
Halifax	Matane	129	214	39
Matane	Goose Bay	155	255	46
St. John's	Goose Bay	400	646	117
Halifax	St. John's	272	441	80
Fredericton	Goose Bay	365	593	107
Halifax	Goose Bay	275	446	81
Fredericton	St. John's	400	649	117
St. John's	Matane	234	381	69
Subtotal		4279	6949	1258
1972				
Fredericton	Pleasant	211	343	62
Fredericton	White	100	165	30
Halifax	Hoffman	113	186	34
Fredericton	Hoffman	175	287	52
Halifax	White	104	172	31
Subtotal		703	1153	209
Total		4982	8102	1467

TABLE 5-5(b)

Processing Costs

	1973		1972	
MAJORITY	$0.51/pass	$ 8/day	$0.67/pass	$ 9/day
PREPARE	0.66	11	0.69	9
ANALYSIS	0.04	1	0.04	1
ONESTN	0.31	5	0.28	4
TWOSTN	0.70	11	0.19	3
TOTAL	2.23	36	1.88	25
	$343.00/station $ 66.00/line		$363.00/station $ 42.00/line	

TABLE 5-6

Costs per Pass, Day, Station and Line

5.3 Guier Plane Navigation Results

In this section we analyze the characteristics of the filtered data (that data surviving programs MAJORITY and PREPARE). The analysis tool is program ANALYSIS, which computes various sample statistics, using as input data the Doppler residuals, Guier plane coordinates, frequency offsets and estimated variance factors for all of the filtered data from a single tracking station. Some of the results of ANALYSIS do not indicate any systematic influences. Other results indicate what may or may not be systematic effects, the source of which has not been identified. However here we will describe only those results which indicate systematic effects of identifiable (or hypothesized) origin. Because the quantity of data accumulated at 1973 Fredericton far exceeds that at other stations, the sample statistics there are smoothest. For that reason, the "typical" examples illustrated in this section are from 1973 Fredericton. Numerical results for other stations are also given.

5.3.1 Doppler residuals

In the Guier plane filter fixes, the covariance matrix of the Doppler observations is the unit matrix, that is the observations are assumed to be uncorrelated and of equal weight, the a priori variance factor being one count^2 (for statistical testing other a priori variance factors are assumed). The histogram of the residuals so produced from a set of many passes (all passes at a particular tracking station) is computed and plotted by ANALYSIS, and a best fitting normal curve (section A.4) is computed (Figure 5-3 and Table 5-7). The standard deviation of this normal curve is found to be

(a) very close to the computed residual sample standard deviation;

(b) consistent between data from different stations, but using the same model receiver; and

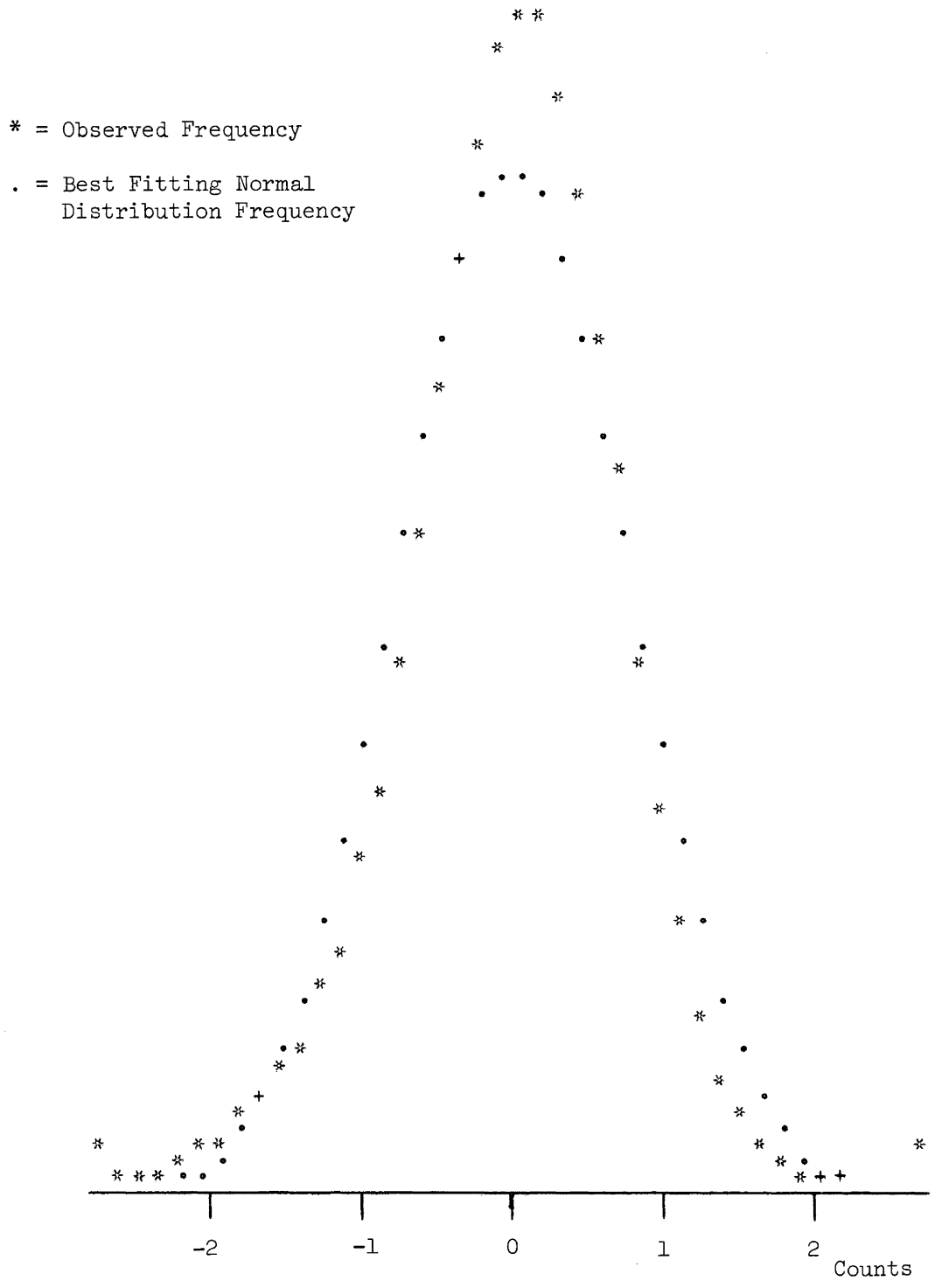

FIGURE 5-3

Typical Histogram of Doppler Residuals

Station	Receiver	Number of Residuals	Sample mean $\bar{x}$ (counts)	Sample Standard Deviation s (counts)	Standard Deviation of best fitting σ (counts) normal curve	Skewness	Kurtosis
1973							
Fredericton	ITT	88805	0.00	0.8	0.8	-0.26	5.0
Halifax	MAR101	37477	0.05	1.6	1.6	0.02	4.2
Pleasant	MAR102	10532	0.05	1.7	1.6	-0.01	3.8
St. John's	MAR102	37329	0.05	1.6	1.5	0.04	4.0
Hoffman	MAR103	13011	0.05	1.6	1.5	0.01	3.8
Matane	MAR103	24314	0.05	1.6	1.5	-0.13	4.1
White	MAR104	7608	0.05	1.6	1.6	-0.27	3.3
Goose Bay	MAR104	34472	0.05	1.5	1.5	-0.15	3.3
1972							
Fredericton	MVX	27558	0.06	2.1	2.0	0.05	5.2
Halifax	MVX	12335	0.06	1.9	1.7	0.01	5.3
Pleasant	ITT	26971	0.00	0.9	0.9	-0.19	4.8
Hoffman	ITT	36389	0.00	0.9	0.8	-0.19	4.9
White	ITT	34245	0.00	0.9	0.8	-0.23	5.0
Averages	ITT		0.00	0.9	0.8		4.9
	MAR		0.05	1.6	1.5		3.8
	MVX		0.06	2.0	1.9		5.3

TABLE 5-7

Doppler Residual Sample Statistics

(c) markedly variable between receiver models, indicating differences in the noise contributions for each receiver. These values (for both s and σ) form one indicator for appropriate scales for the Doppler covariance matrix. (The other important indicator is the χ^2 rejection rate for different assumed a priori variance factors (section 5.2.3).)

The <u>skewness</u> (or moment coefficient of skewness)

$$a_3 = \frac{\sum_{i=1}^{N} (x_i - \bar{x})^3}{N S^3} \quad , \tag{5-4}$$

and <u>kurtosis</u> (or moment coefficient of kurtosis)

$$a_4 = \frac{\sum_{i=1}^{N} (x_i - \bar{x})^4}{N S^4} \quad , \tag{5-5}$$

for each multipass set of residuals were also computed. For a normal distribution $a_3 = 0$ and $a_4 = 3$ (Hamilton, 1964). The histogram in Figure 5-3 is both skewed and leptokurtic, with $a_3 = -0.26$ (indicating the negative or left side of the curve has a longer tail than the positive or right side - that is there are more negative than positive residuals beyond, say, the 2σ level), and $a_4 = 5.0$ (indicating that a higher proportion of the residuals are within, say, the 2σ level, than for a purely normal distribution). From Table 5-7 we see that the residuals from other stations have both positive and negative skewness, but all are leptokurtic. Romanowski (1970) claims that leptokurtosis is frequently found among measurements of the highest quality and homogeneity. Hald (1952) demonstrates that heterogeneous distributions of the form

$$\Phi(t) = \Sigma \frac{\alpha_i}{\sigma_i} \phi\left(\frac{t - \mu_i}{\sigma_i}\right) \quad , \tag{5-6}$$

where $\Sigma\alpha_i = 1$ and in general the μ_i, σ_i are all different, will be

(a) leptokurtic if the μ_i are nearly equal

(b) platykurtic if the μ_i are less equal

(c) multimodal if the μ_i are even further apart, and

(d) skewed if the α_i are unequal.

In Figure 5-3 we have lumped together 659 sets of residuals averaging about 130 residuals per set. Each set is a single element drawn from a multivariate normal distribution, and in general, the covariance matrix of this distribution will not be a scalar matrix. In general, different sets are drawn from different multivariate normal distributions. Therefore we are examining a heterogeneous distribution in which each of the approximately 88,000 residuals is drawn from its own population, in principle different from all the others. The leptokurtic nature of this histogram indicates that the means are nearly equal (and nearly zero).

The residuals were also examined by analyzing their dependence on one of the parameters on which the observation noise level is most likely to depend, that is the satellite elevation angle at which the observation was made. The sample statistics (mean and standard deviation) of the residuals were computed and plotted, after sorting the residuals according to elevation angle (Figure 5-4). For every station the sample standard deviation exhibited a characteristic parabolic dependence on elevation angle. The peak at the low elevation end is interpreted as being due to residual refraction. The peak at the high elevation end is interpreted as being due to increased noise because of decreased antenna sensitivity (the antennas used all are of dipole design with overhead nulls). Plots of the range of these parabolic curves for each receiver are given in Figure 5-5. Another contribution to these results which may be present is movement of the antenna phase centre as a function of the angle of incidence of the incoming waves (satellite elevation angle). The magnitude

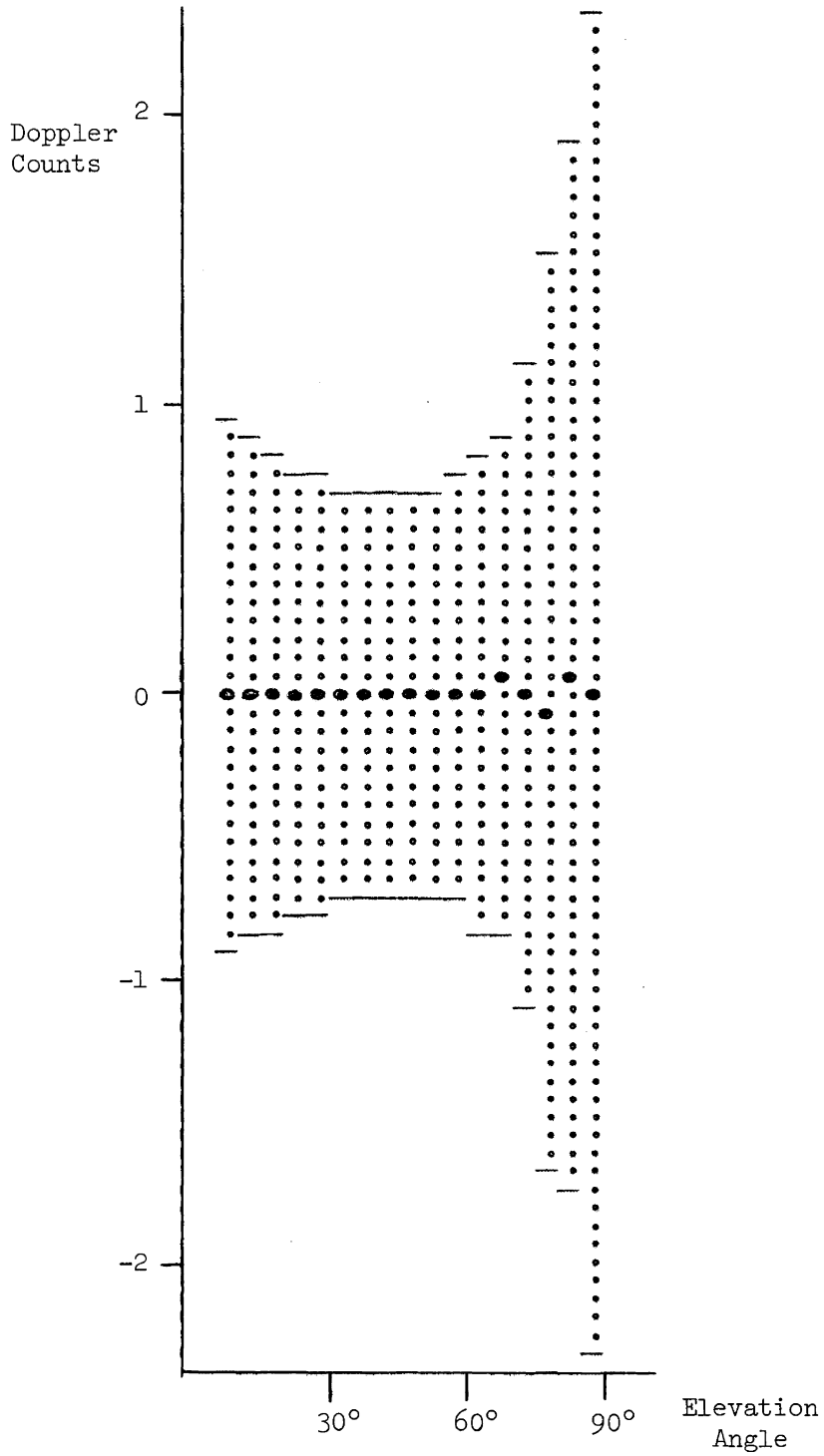

FIGURE 5-4

Analysis of Residuals as a Function of Elevation

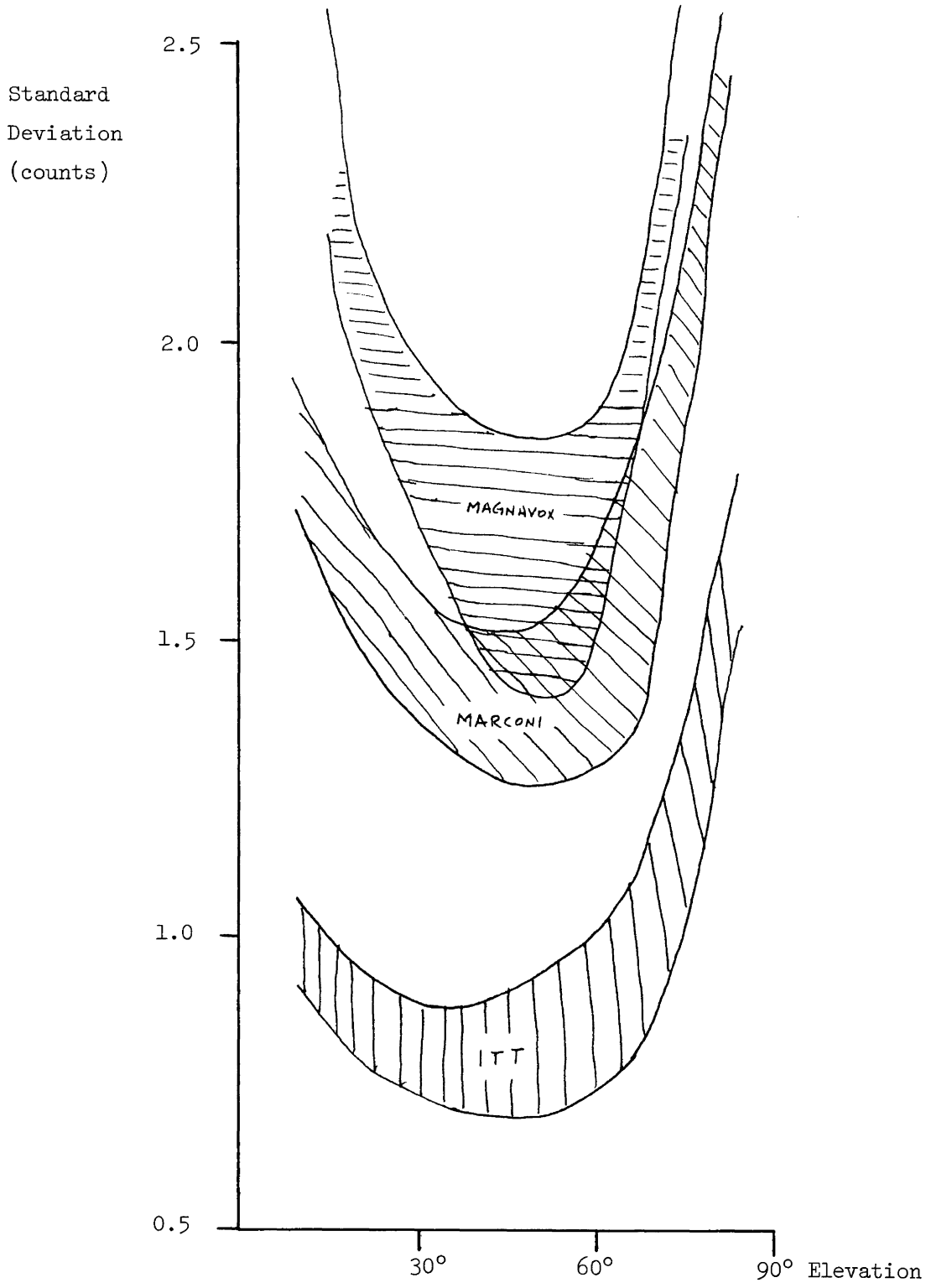

FIGURE 5-5

Standard Deviation of Doppler Observations as Function of Elevation

of this movement is an unresolved question at present.

5.3.2 Guier plane coordinates

The Guier plane for each pass is different than that for all other passes, so that the aggregate of a set of Guier plane coordinates is not simply related to any optimum receiver coordinates. However, providing the approximate receiver coordinates are within a few metres of the finally computed coordinates (see Table 5-12), then what is mainly represented by the Guier plane coordinates are measurement errors, including orbit errors, residual refraction, and other possible systematic effects. A set of Guier plane coordinates can then be analyzed for systematic components of these measurement errors. The parameters of the analysis used here are: satellite tracked; satellite quadrant (travelling northward passing to the east, etc.); satellite elevation at closest approach; day of the year; hour of the day; time since last injection; and number of Doppler observations in the pass. As already mentioned, not all these analyses yielded significant or interpretable results.

One of the two Guier plane coordinates is aligned along the closest approach slant range vector (x_G) and the other is parallel to the closest approach satellite velocity vector (y_G). We will denote these coordinate values respectively as the SR and VEL coordinates.

As for the residuals, histograms and best fitting normal curves were computed for each of the SR and VEL coordinates. Table 5-8 gives the sample mean ($\bar{x}$), sample standard deviation (s) and standard deviation of the best fitting normal curve (σ) for SR and VEL at each station.

Let us assume that the SR and VEL values are principally due to orbit errors. Recall that in section 4.6 we assigned standard deviations of 2, 0.5 and 1 broadcast units, or 26, 5 and 10 metres to the along track, radial and out of plane components of the orbit errors. In the Guier

	SR			VEL		
Station	$\bar{x}$(m)	s(m)	σ(m)	$\bar{x}$(m)	s(m)	σ(m)
1973						
Fredericton	-1	14	10	-6	46	21
Halifax	-3	13	10	-5	36	15
Pleasant	0	11	8	-2	32	14
St. John's	-2	10	7	-10	38	16
Hoffman	-1	11	7	-1	38	11
Matane	-1	13	11	-4	49	6
White	-2	11	7	0	42	26
Goose Bay	-2	10	8	-6	38	16
1972						
Fredericton	-4	14	12	-8	33	26
Halifax	-6	15	10	-4	38	24
Pleasant	-3	12	8	-10	39	12
Hoffman	-3	14	8	-3	50	12
White	6	14	12	-1	45	13
Averages		12	9		40	16

TABLE 5-8

Sample mean ($\bar{x}$), sample standard deviation (s), and standard deviation of best fitting normal curve (σ) for Guier plane coordinates.

plane, VEL measures the along track error, and SR samples components of both radial and out of plane errors. Therefore if the standard deviations of section 4.6 are correct, (26, 5 and 10 metres along track, radially and cross track) we should expect orbit error contributions to VEL and SR of 26 metres and less than 11 = $\sqrt{5^2 + 10^2}$ respectively. Examination of Table 5-8 shows that in general $s_{SR} > 11 > \sigma_{SR}$ and $s_{VEL} > 26 > \sigma_{VEL}$. Since the sample standard deviations likely contain other systematic effects, we should expect them to exceed the orbit error contribution. The fact that the best fitting normal standard deviations are less than the expected orbit error contributions may mean that the orbit error standard deviations are too pessimistic (more so for along track than the other two), however the other systematic effects should be identified and accounted for and new best fitting normal curves computed before assigning new values to the orbit error standard deviations.

Let us now consider the effect of residual ionospheric and tropospheric refraction on the SR values, if we assume that residual refraction is

(a) proportional to total refraction (modelled by scaling total refraction), and

(b) has consistent positive sign from pass to pass.

In the ionosphere the optical path length is less than the geometric path length, therefore as the residual refraction increases, the SR value should become more positive. Since the ion density is higher during the sunlight hours we should expect the SR values at local noon to be more positive (closer to the satellite track) than at local midnight. In the troposphere the optical path length is greater than the geometrical path length, therefore as the residual refraction decreases, the SR value should become more positive. Since the total refraction decreases as temperature increases, and daytime temperatures are generally higher than at night, then as for

the ionospheric case we should expect SR values at local noon to be more positive than at local midnight. In summary we should expect the SR plot against time of day to have the form

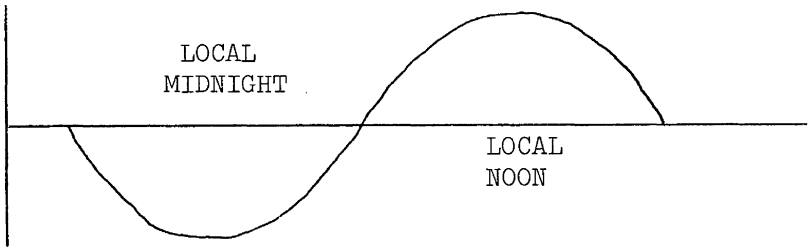

This is indeed the case (see for example the data for a typical station shown in Figure 5-6), with peak to peak amplitudes of approximately 5 m. Therefore the two assumptions we have made about residual refraction are consistent with the observed data. However these assumptions are not well grounded in physics, so that Figure 5-6 may be exhibiting some other phenomenon altogether.

We have investigated the sum of the two residual refractions above, from which we have inferred that the effect may exist, but could not identify whether the dominant source is ionospheric or tropospheric. We can also investigate the difference of the two residual refractions, since as the path length increases, residual tropospheric refraction should push SR away from the satellite (more negative SR values), and residual ionospheric refraction should push SR towards the satellite (more positive SR values). Plots of SR against elevation angles (Figure 5-7), show SR increasing with elevation angle (decreasing as path length increases) hence tropospheric refraction is the dominant source of residual refraction (again only if both assumptions are valid).

As mentioned in section 4.1.1 the broadcast ephemeris (prior to early 1974) was not referred either to the average terrestrial or instan-

taneous terrestrial systems. Therefore the application of the usual transformation from I.T. to A.T. (which was made here) is not sufficient to account for the effects of polar motion. The residual polar motion effect should impose a diurnal variation on the tracking station latitude (the VEL coordinate). Plots of VEL against hour of day (Figure 5-8) indicate the presence of this effect (this data was collected over a 40 day period). However, two other possible sources for this effect might be errors in first order tesseral coefficients (Anderle, personal communication) and a combination of neglecting the receiver timing delay and a pattern of north and south going passes which repeats with a daily period (Kouba, personal communication).

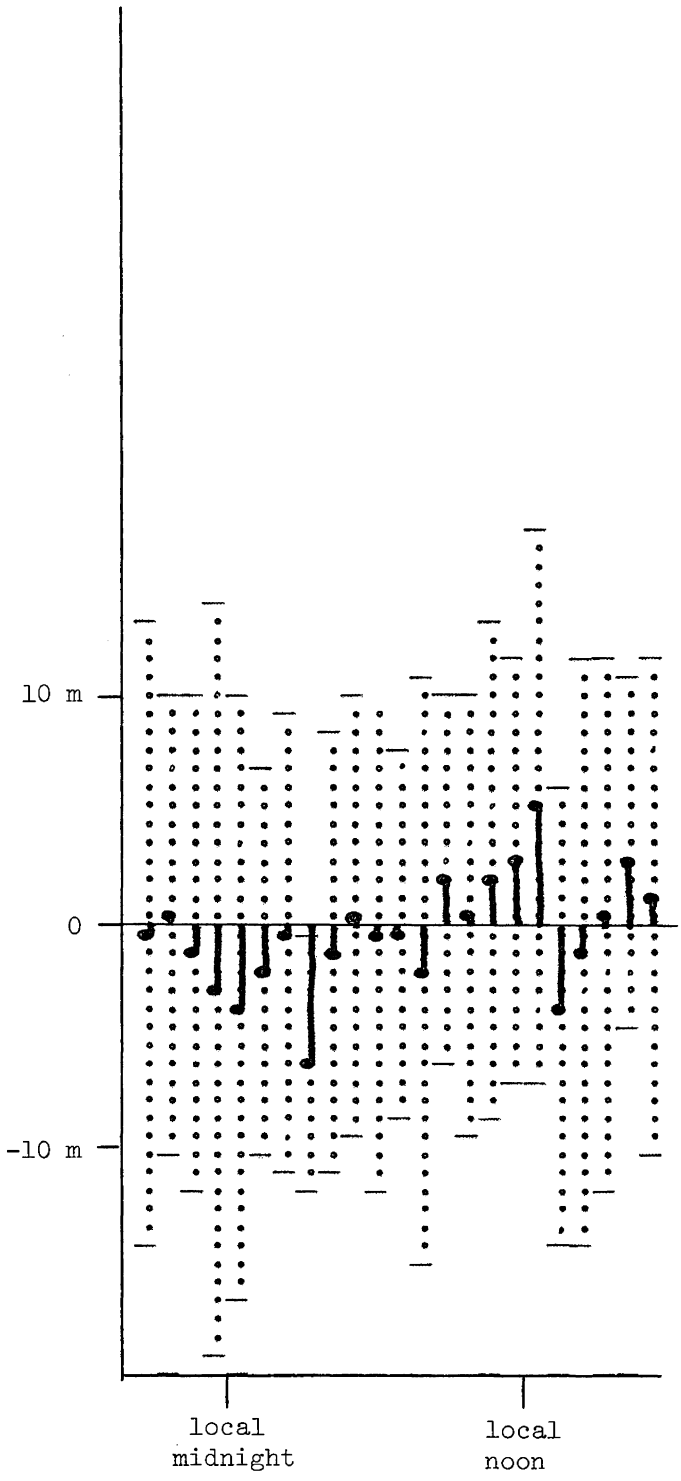

FIGURE 5-6

Analysis of Slant Range Coordinate as a Function of Hour

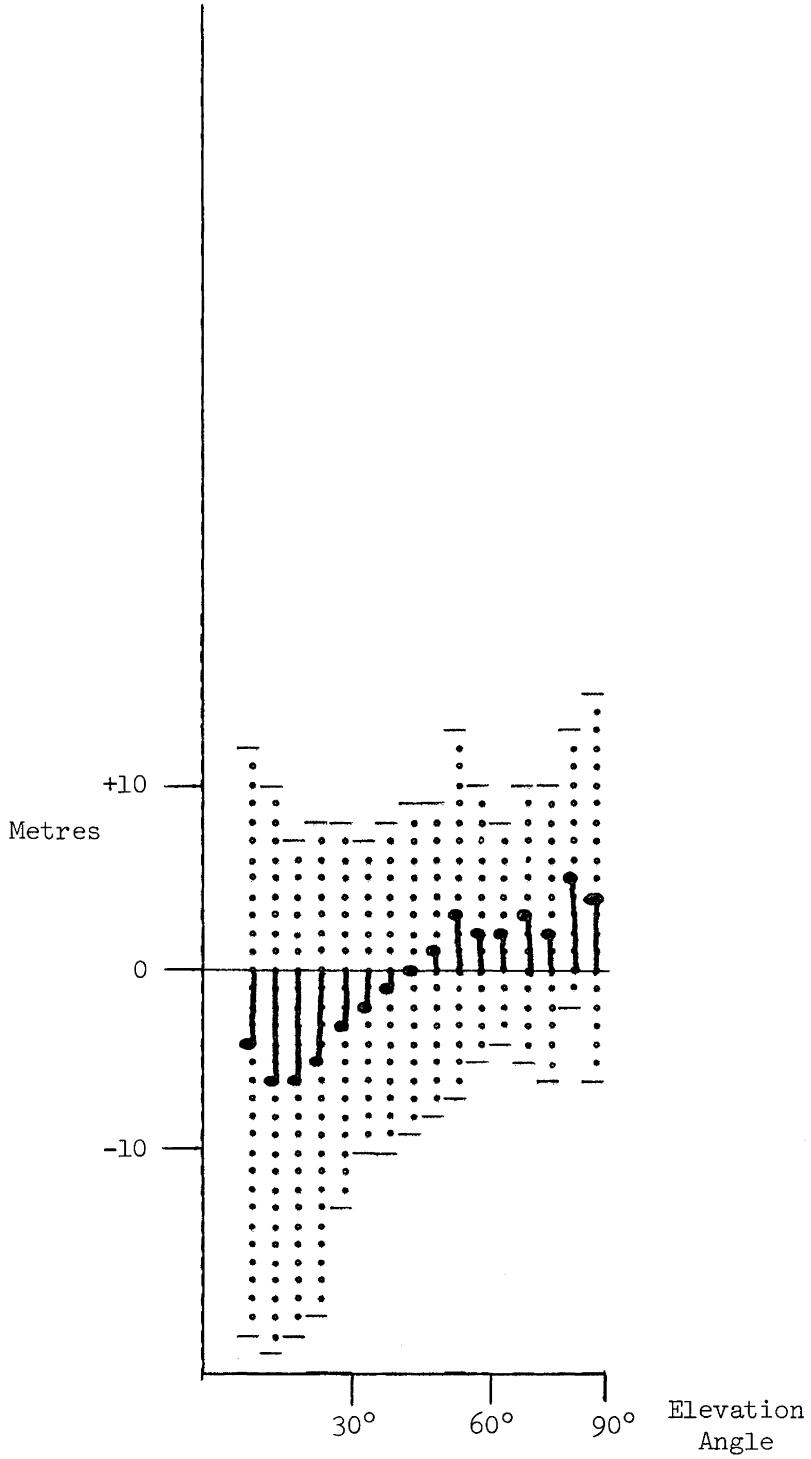

FIGURE 5-7

Analysis of Slant Range Coordinate as a Function of Elevation

5.3.3 Receiver frequency offsets

The hypothesis that the drift of receiver reference oscillators is linear with time was tested by plotting the Guier plane navigation frequency offset results as a function of day of year, and by least squares fitting a linear trend to these values. Figure 5-9 shows the 40 day plot for 1973 Fredericton, indicating that the drift is approximately piecewise linear, that is four different linear fits must be used to approximate the drift. The reason for these changes in drift rate have not been identified. Data from other tracking stations were adequately approximated by one or two linear fits. Table 5-9 summarizes the 1973 fitting results, and indicates that drift rates can vary from less than 1 part in 10^{10} per day to as much as 10 parts in 10^{10} per day, and can be either positive or negative. The receiver frequency offset varied between 100 and 1500 parts in 10^{10} between receivers.

5.3.4 Estimated variance factors

As discussed in section 4.2.2, when navigating in the Guier plane we obtain residuals which are uncontaminated by orbit errors. The effect of other systematic errors, such as residual refraction and frequency offset are, as we have seen, absorbed to some extent by the solution vector as well. Hence we should expect the estimated variance factor to reflect mainly the Doppler measurement precision, free from the three main influences of orbit errors, residual refraction, and oscillator drift. As we have seen from the residual histogram in section 5.3.1 the three receivers have different standard deviations of the residuals. In

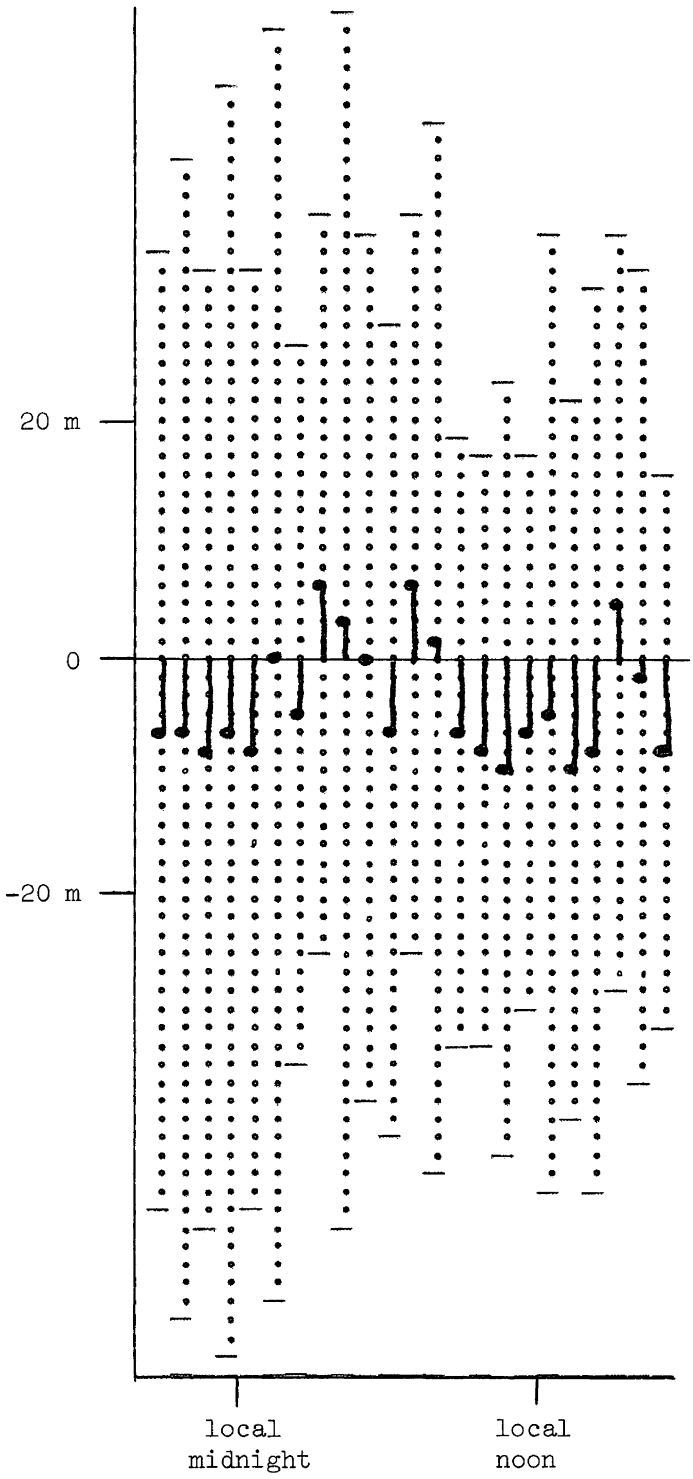

FIGURE 5-8

Analysis of Velocity Coordinate as a Function of Hour

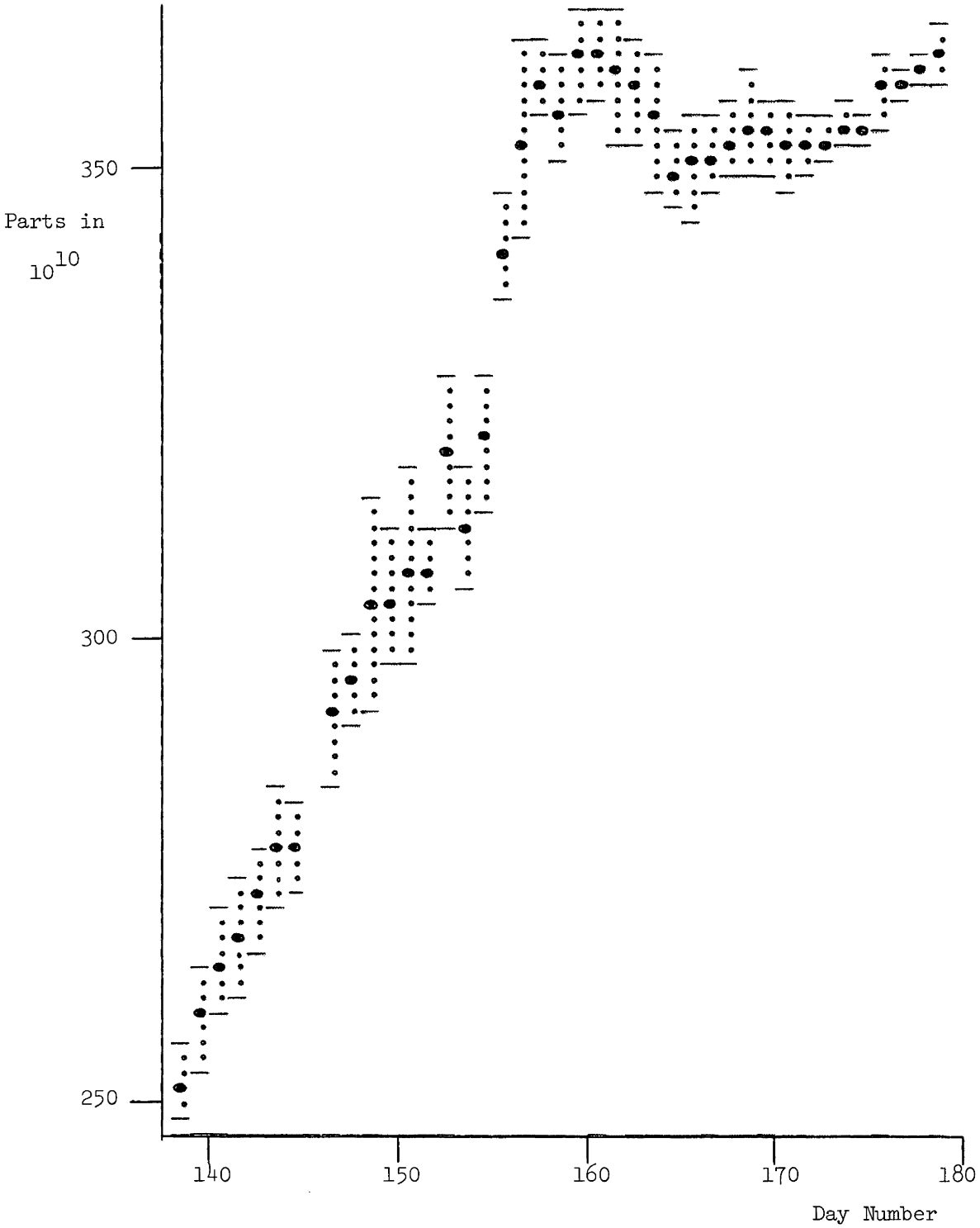

FIGURE 5-9

Analysis of Receiver Frequency Offset as a Function of Day

Receiver	Observing Days (1973)	F = FTO (parts in 10^{10}) + DELF (parts in 10^{10}/day) * (T - TDFO) (day)	σ_F (parts in 10^{10})	Number of Passes Used
ITT	138 - 155	248.2 4.5 138	5.8	259
	155 - 160	174.6 8.9 138	8.2	75
	160 - 165	404.5 -1.7 138	4.7	82
	165 - 180	331.7 0.8 138	3.1	243
MAR101	138 - 148	151.0 2.7 138	3.7	98
	148 - 157	135.2 3.6 138	5.1	157
MAR102	138 - 146	- 469.5 -5.9 138	3.4	72
	148 - 164	- 548.0 -5.2 148	4.5	264
MAR103	138 - 146	-1446.1 -4.7 138	3.4	91
	147 - 163	-1491.7 -3.8 147	4.9	172
MAR104	139 - 146	- 399.7 -9.5 139	4.3	57
	148 - 162	- 482.1 -8.6 148	4.8	247

TABLE 5-9

Receiver Reference Oscillator Offsets and Drifts

essence an analysis of the estimated variance factors is an extension of section 5.3.1, analyzing the residuals according to satellite pass.

Since a unit covariance matrix was assumed for the Doppler measurements, then for the i^{th} pass at a station the single pass estimated variance factor is

$$(\hat{\sigma}_o^2)_i = \sum_{j=1}^{m_i} v_{ij}^2 \; / \; (m_i - 3) \quad , \tag{5-7}$$

where m_i Dopplers are measured ($m_i \; \varepsilon[75,200]$), and 3 parameters are estimated (the Guier plane coordinates and frequency offset). Given a set of n passes we compute the sample mean and standard deviation for $(\hat{\sigma}_o^2)_i$ from

$$\bar{x} = \sum_{i=1}^{n} (\hat{\sigma}_o^2)_i \; / \; n \quad , \tag{5-8}$$

$$s = \left[\sum_{i=1}^{n} ((\hat{\sigma}_o^2)_i - \bar{x})^2 \; / \; (n - 1) \right]^{1/2} \quad . \tag{5-9}$$

Table 5-10 summarizes these results for the 1973 data. Note that the values for $\bar{x}$ in Table 5-10

$$\bar{x} = \frac{1}{n} \sum_{i=1}^{n} \frac{1}{m_i - 3} \sum_{j=1}^{m_i} v_{ij}^2 \simeq \sum_{i=1}^{n} \frac{1}{n} \sum_{j=1}^{m_i} (v_{ij}^2 / m_i) \quad , \tag{5-10}$$

and the values for s^2 in Table 5-7

$$s^2 = \sum_{i=1}^{n} \sum_{j=1}^{m_i} (v_{ij} - \text{mean of all } v_{ij})^2 \; / \; ((\sum_{i=1}^{n} m_i) - 1)$$

$$\simeq \sum_{i-1}^{n} \sum_{j=1}^{m_i} v_{ij}^2 \; / \; \sum_{i=1}^{n} m_i \quad , \tag{5-11}$$

are equal, within the resolution with which they are here presented. That is the mean square residual, averaged over all residuals at a station, is equal to the mean square residual, averaged first over each pass (to

Station	Receiver	$\bar{x}$ (counts^2)	s (counts^2)
1973			
Fredericton	ITT	0.6	0.2
Halifax	MAR101	2.5	0.9
Pleasant	MAR102	2.8	1.0
St. John's	MAR102	2.4	0.8
Hoffman	MAR103	2.5	0.9
Matane	MAR103	2.5	1.1
White	MAR104	2.6	0.7
Goose Bay	MAR104	2.3	0.7
Averages	ITT	0.6	0.2
	MAR	2.5	0.9

TABLE 5-10

Sample mean ($\bar{x}$) and sample standard deviation (s) for estimated variance factors.

obtain approximately $\hat{\sigma}_0^2$), and then averaged over all passes. This is additional evidence that the variances of Doppler measurements are consistent from pass to pass.

5.4 Coordinate Computation Results

In this section we review the results obtained from programs ONESTN, TWOSTN and NETWORK, concentrating principally on the 1973 data. The 1973 network of eight stations was observed in two stages. First the "small" network of five stations (Fredericton, Halifax, Pleasant, Hoffman and White) were simultaneously observed for about eight days. Then the "large" network of five stations (Fredericton, Halifax, St. John's, Matane and Goose Bay) were observed for about fifteen days. Only the Fredericton and Halifax observations interconnect the two sub-networks.

Comparisons between the 1973 small network and the 1972 network of the same stations are made. Comparisons between the 1973 small network and a terrestrial network including these five stations are also made.

5.4.1 1973 Results

As described in section 5.2.2 the network coordinates were computed in three steps, using programs ONESTN, TWOSTN and NETWORK. In this section we review the results after each step, and the differences between them.

Program ONESTN computes the three-dimensional, single-station, multipass coordinates, together with the corresponding covariance matrix, for one station at a time, using all acceptable passes tracked at that station. Table 5-11 lists the final ONESTN outputs for each of the eight 1973 stations. The coordinates are average terrestrial Cartesian, in metres. The covariance matrices are in metres^2. The equivalent network correlation coefficient matrix and coordinate standard deviations are shown

Station	Coordinates (m)	Covariance matrix (m^2)		
	X 1761280.362	0.2088		
Fredericton	Y -4078250.069	0.0588	0.1216	
	Z 4561415.611	0.0188	-0.0529	0.0892
	X 2018847.778	1.2645		
Halifax	Y -4069153.485	0.3611	0.6869	
	Z 4462376.966	0.1553	-0.2427	0.4758
	X 1765437.956	4.2664		
Pleasant	Y -4121697.955	1.4186	2.8731	
	Z 4521331.126	0.2244	-1.2119	1.9552
	X 2612794.802	0.9628		
St. John's	Y -3429076.783	0.3614	0.7755	
	Z 4684923.220	0.1846	-0.2414	0.5074
	X 1909003.017	3.5898		
Hoffman	Y -4093312.872	0.9288	1.9683	
	Z 4488673.238	0.4240	-0.7733	1.4630
	X 1606494.189	1.6314		
Matane	Y -3888719.955	0.3752	0.9601	
	Z 4777520.584	0.1831	-0.4649	0.8434
	X 1848538.507	7.2128		
White	Y -4046222.761	1.9851	3.3276	
	Z 4555692.909	0.5980	-1.3031	2.4579
	X 1888556.658	0.9402		
Goose Bay	Y -3319620.204	0.3473	0.7099	
	Z 5091146.241	0.1196	-0.2981	0.5964

TABLE 5-11

Final ONESTN Coordinates and Covariance Matrices

in Table 5-12.

Program ONESTN also plots the corrections to the a priori coordinate values, the coordinate standard deviations, and the three axes of the 95% confidence region as a function of the number of passes incorporaged in the multipass solution. Table 5-13 shows the final corrections to the a priori coordinates for the 1973 and 1972 data. Figure 5-10 shows the first 60 or so passes for a typical station (Fredericton). The data required (in terms of observing days, number of passes, and number of 4.6 second Doppler counts) for the 95% confidence region semi-major axis to decrease below 10 m, 5 m, 4 m, and 3 m is shown, for all the 1973 and 1972 stations, in Table 5-14. Note that the accuracies in Table 5-14 are estimated from the adjustment, and are measures of internal consistency, rather than repeatability (section 5.4.2) or conformity with an external standard (section 5.4.3). The coordinates and covariance matrices of Table 5-11 are based on the total data values shown in Table 5-14. There is a wide difference in the data required for a given target accuracy, between the three kinds of receivers. On average, to attain 5 m with 95% confidence required about 3 days (35 passes) with the ITT receiver, 5 days (80 passes) with the MAR receivers, and about 20 days (160 passes) with the MVX receiver. Note that the numbers of passes required are in approximately the same proportion as the a priori variances assigned to the three receivers (1.5 to 4 to 10). This indicates that when more precise Doppler measurements are made, the observing time required to attain a given point positioning accuracy is proportionally shortened. The a priori variances enter the computations only as Doppler and pass rejection criteria in PREPARE, since the a priori variance factor for each ONESTN pass (the weight assigned to that pass in the multipass solution)

is the estimated variance factor (based on unit observable covariance matrix) from PREPARE. Therefore the fact that the required numbers of passes is closely proportional to the values chosen for the receiver a priori variance factors is additional evidence as to the relative validity

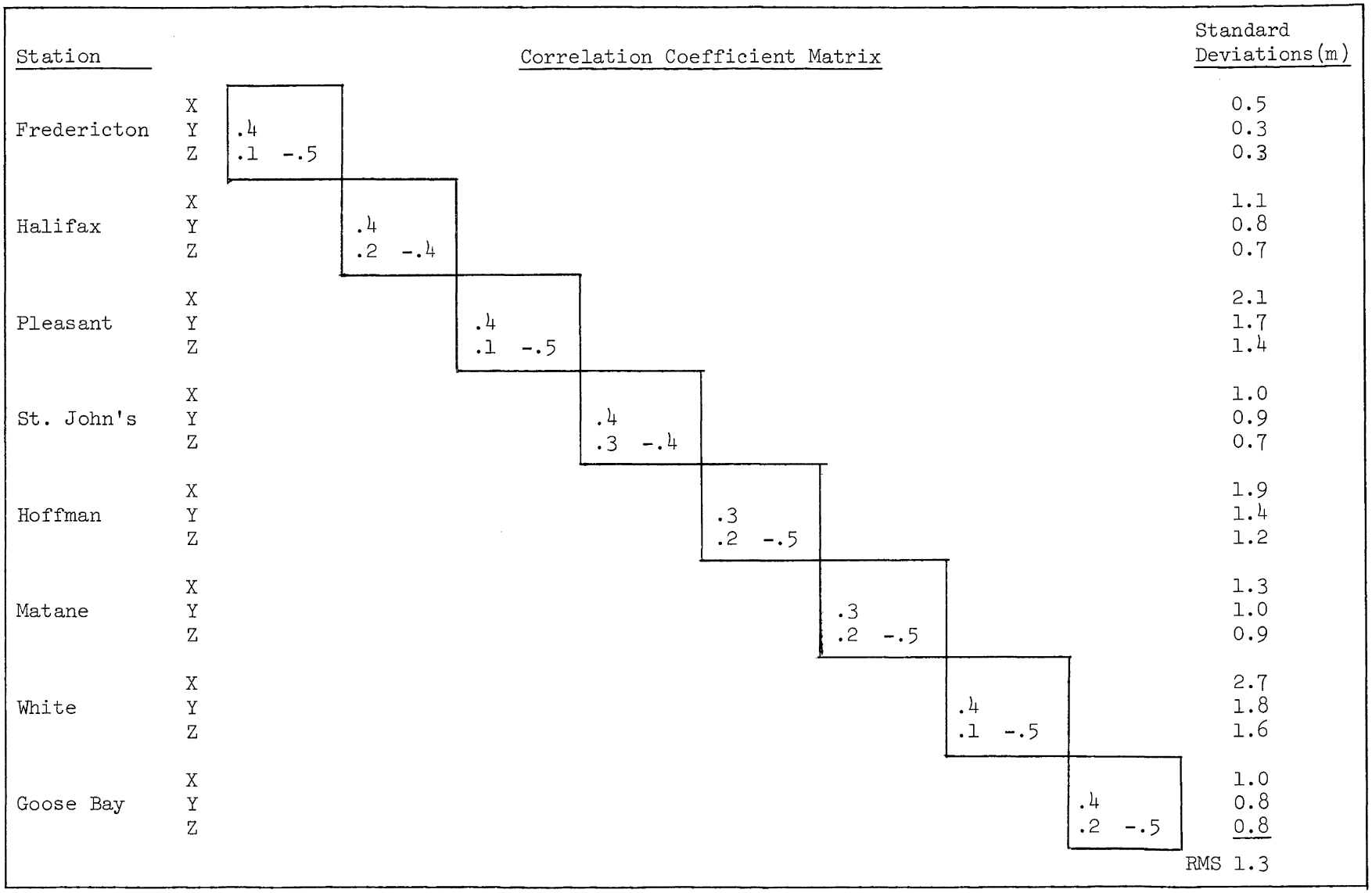

TABLE 5-12
Correlation Coefficient Matrix and Coordinate Standard Deviations for Point Positioning

Station	X(m)	Y(m)	Z(m)
1973			
Fredericton	2	3	2
Halifax	-2	-1	-2
Pleasant	0	-2	0
St. John's	0	-1	-3
Hoffman	3	0	-1
Matane	1	1	3
White	-1	0	-1
Goose Bay	0	1	0
1972			
Fredericton	-1	8	3
Halifax	-1	5	-4
Pleasant	-1	2	0
Hoffman	2	6	1
White	3	-5	8

TABLE 5-13

Final ONESTN Corrections
to a priori coordinates.

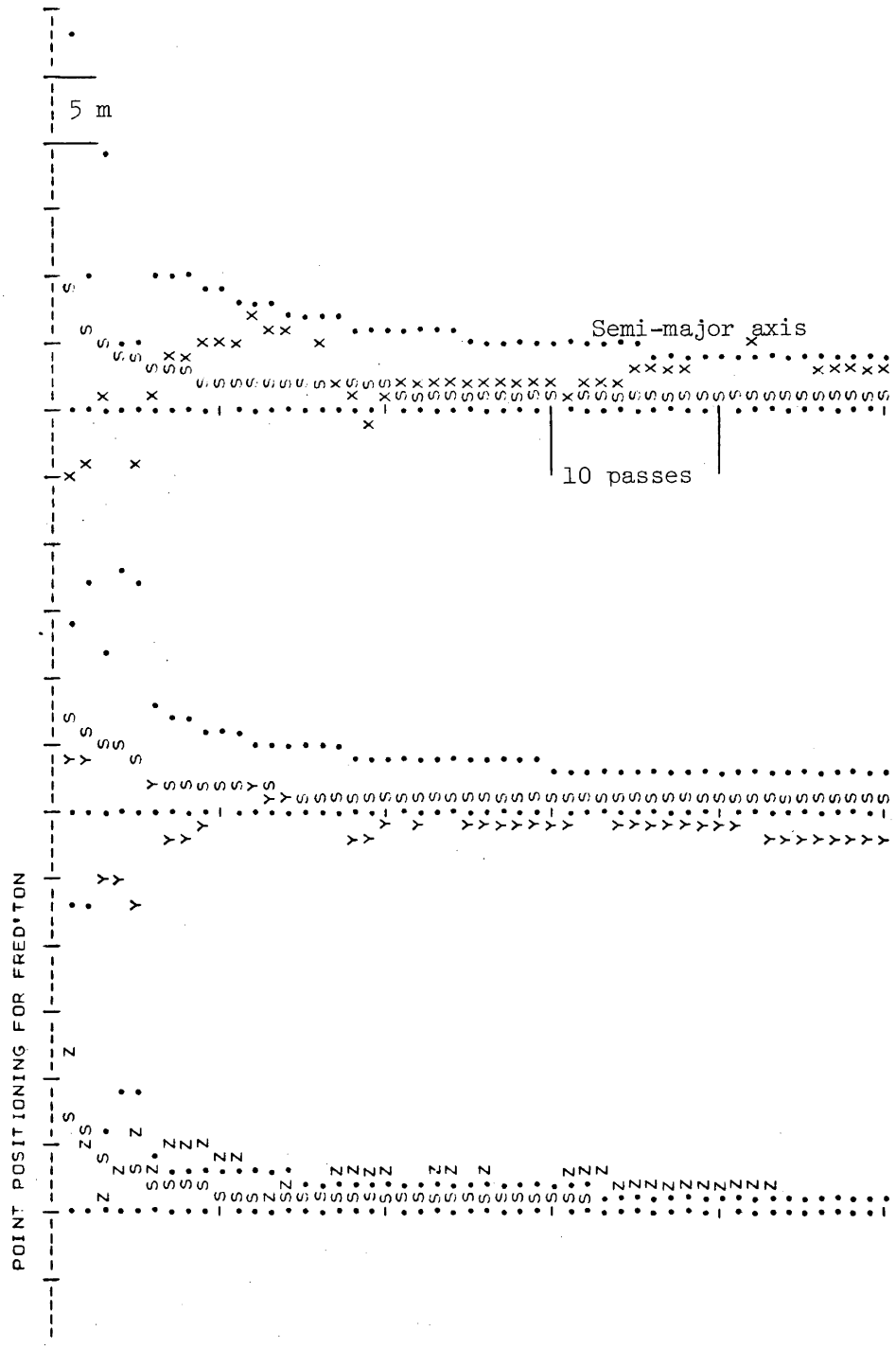

FIGURE 5-10

Typical ONESTN Plot of Coordinate Changes, Standard Deviations 95% Confidence Region Axes.

	to 95% < 10 m			< 5 m			< 4 m			< 3 m			Totals obtained			
Station	Day	Passes	Dops	Day	Pass	Dop	Day	Pass	Dop	Day	Pass	Dop	Day	Pass	Dop	95% Region
1973																
Fredericton	0.5	7	1018	2.5	32	4724	3.5	44	6590	6	76	10935	38	464	62534	1 m
Halifax	2	24	3591	7	92	13411	12	140	20667	17	228	33422	16	248	36293	3
Pleasant	3.5	28	4017										7	71	10376	7
St. John's	1	20	2947	5	84	11986	7	124	17449	12	204	28633	15	252	35683	3
Hoffman	2	24	3390										7	86	12399	6
Matane	1	16	2255	4	76	10311	8	116	16179				10	144	20835	4
White	4	28	3819										6	48	6466	8
Goose Bay	1	24	3295	4	76	10760	5	112	16045	10	184	25855	13	238	33230	3
1972																
Fredericton	8	56	5696	22	164	17079							27	235	24383	5
Halifax	5	41	4092										14	112	11352	6
Pleasant	1	12	1594	3	44	6272	4	60	8619	7	100	14218	10	152	21452	3
Hoffman	0.5	7	1024	2	36	4728	3	52	7057	5	84	11536	14	207	29236	2
White	0.5	7	951	5	41	5527	8	73	9888	12	150	20583	16	197	27280	2
											ITT		78	1020	140502	
											MAR		74	1087	155282	
											MVX		41	347	35735	

TABLE 5-14

Data Required to Obtain Specified Point Positioning Accuracy with 95% Confidence

of the values chosen.

As mentioned in sections 5.1.4 and 5.2.2, for the ONESTN results reported here, the orbit was not relaxed. Three results indicate that the orbit should be relaxed for ONESTN as well as for TWOSTN computations. One of the results is discussed in section 5.4.3. The second result is the rates of chi-square pass rejections given in Table 5-2 for each of the three receivers. Of the passes accepted by PREPARE, 25% were rejected for ITT data, 5% for MAR data and 11% for MVX data. The MAR rejection rate is exactly what should be statistically expected. Since the MVX data is much noisier than the other two, we might suspect that unmodelled systematic contributions exist, and the higher rejection rate should not surprise us. However the 25% ITT rejection rate requires some explanation. The cause postulated here is that since the ONESTN a priori variances (PREPARE estimated variances) were so much smaller for ITT data than for MAR data (averaging 0.6 counts^2 and about 2.5 counts^2 respectively from section 5.3.4), then the ITT solutions were more sensitive than the MAR solutions to unmodelled systematic effects. By holding the orbit fixed the systematic (over one pass) orbit biases are unmodelled. This contaminates the ONESTN estimated variance factor (and so results in more chi-square rejections) more for the ITT than for the MAR data. The solution of course is to relax the orbit for ONESTN computations. To test this hypothesis, the 1973 Fredericton data were recomputed by ONESTN, relaxing the orbit. The 95% confidence level χ^2 rejection rate then dropped from 25% to 3%, confirming the hypothesis.

The third indication that the orbit should be relaxed was obtained by splitting the set of several hundred passes from 1973 Fredericton into subsets of 20 passes each, and computing independent ONESTN solutions for each subset. This was repeated for both fixed and relaxed orbits. Given

the estimated position vector $\hat{X}_i$ and its covariance matrix $\Sigma_{\hat{X}_i}$ from the solution for the i^{th} subset, then the statistic

$$y_i = (X_H - \hat{X}_i)^T \Sigma_{\hat{X}_i}^{-1} (X_H - \hat{X}_i) \quad , \tag{5-12}$$

(where X_H is the 1973 Fredericton position vector from Table 5-11), is distributed as $uF(u, \nu, \alpha)$ (Wells and Krakiwsky, 1971). For $u = 3$ (the number of parameters estimated), $\nu \simeq 2500$ (the number of Dopplers in 20 passes) and $\alpha = 0.95$ (95% confidence level) $3F(3, 2500, 0.95) = 7.8$. Hence we reject at the 95% confidence level the hypothesis

$$\underline{H: \hat{X}_i = X_H}$$

if $y_i > 7.8$. With the orbit fixed, this hypothesis was rejected for 20 of the 24 sets of 20 passes each (over 80% rejection). Relaxing the orbit, this hypothesis was rejected for 14 of the 32 sets of 20 passes each (about 45% rejection). (There were more passes with the orbit relaxed since the χ^2 variance factor rejection rate was much lower, as mentioned earlier.) Furthermore the maximum value of y_i was 464 with the orbit fixed; only 60 with the orbit relaxed.

From the covariance matrix $\Sigma_{\hat{X}_i}$ for the i^{th} subset, estimated standard deviations for $\hat{X}_i$ were computed, and averaged over all subsets to obtain an average estimated standard deviation $\bar{\sigma}$ for each coordinate. From the deviations $(X_H - \hat{X}_i)$, sample standard deviations s for each coordinate were computed. The results for fixed and relaxed orbits are:

	Orbit Fixed			Orbit Relaxed		
	$\bar{\sigma}$(m)	s(m)	s/$\bar{\sigma}$(m)	$\bar{\sigma}$(m)	s(m)	s/$\bar{\sigma}$(m)
x	2.3	5.7	2.5	4.3	6.6	1.5
y	1.7	6.4	3.8	3.2	4.3	1.3
z	1.5	5.8	3.9	4.2	5.0	1.2

These results indicate that $\Sigma_{\hat{X}_i}$ is closer to being the actual covariance matrix of $\hat{X}_i$ when the orbit is relaxed than when the orbit is fixed. However, it appears there remain unmodelled errors in $\hat{X}_i$ even with relaxed orbit. One possibility not investigated is that selecting the passes for each 20 pass subset so that there are equal numbers from all quadrants, and all satellites, may improve the agreement between the $\hat{X}_i$ and X_H. Another possibility is that elimination of such systematic errors as polar motion and residual refraction may improve the agreement between the $\hat{X}_i$ and X_H.

Program TWOSTN computes the six-dimensional, two-station, multipass coordinates, together with the corresponding covariance matrix, for one pair of stations at a time, using all the simultaneous passes tracked at that station. Table 5-15 lists the interstation vectors and distances and their covariance matrices computed from the final TWOSTN outputs, for each of the nineteen 1973 simultaneous pairs.

Program TWOSTN plots the corrections to the a priori values for the interstation vector elements and the interstation distance, their standard deviations, and the three axes of the 95% confidence region of the interstation vector, as a function of the number of simultaneous passes incorporated in the multipass solution. Figure 5-11 shows the first 60 or so passes for a typical simultaneous pair (Fredericton - Halifax). The data required (in terms of number of simultaneous passes and total number of 4.6 second Dopplers from both stations) for the 95% confidence region semi-major axis to decrease below 10 m and 5 m is shown for all the 1973 simultaneous pairs, in Table 5-16. As for Table 5-14, these estimated accuracies reflect internal consistency, not repeatability or conformity with an external standard. The approximate length and azimuth of each line is also shown. Any distance or azimuth dependence which may exist

is overshadowed by the differences in receivers (all pairs containing Fredericton include one ITT and one MAR receiver, all other pairs include two MAR receivers). The data required for a given accuracy is

Stn 1	Stn 2		Interstation Vector (m)	Covariance Matrix (m^2)			Interstation Distance (m)	Variance (m^2)
		X	- 4163.034	6.4458				
Fredericton	Pleasant	Y	43447.401	1.9958	4.5230		59260.914	1.7288
		Z	40085.514	0.5426	- 1.9954	3.1972		
		X	- 87262.895	10.4413				
Fredericton	White	Y	- 32028.644	3.3049	5.4017		93131.257	12.1264
		Z	5725.751	0.8916	- 1.8932	3.5414		
		X	60458.432	16.8270				
Hoffman	White	Y	- 47088.785	5.2536	7.9845		101802.909	4.7125
		Z	- 67016.839	0.8678	- 3.0791	5.7015		
		X	109848.037	8.9909				
Halifax	Hoffman	Y	24159.324	2.3894	5.2184		115506.796	9.0522
		Z	- 26297.446	1.1066	- 2.2096	3.9408		
		X	- 83105.409	16.5336				
Pleasant	White	Y	- 75477.488	5.8109	10.3786		117404.520	17.2272
		Z	- 34357.840	0.6113	- 4.0999	6.8545		
		X	-143562.076	9.9023				
Pleasant	Hoffman	Y	- 28389.321	2.6996	7.3322		149941.972	10.6006
		Z	32658.408	1.0493	- 3.1619	5.2351		
		X	-147724.433	5.1238				
Fredericton	Hoffman	Y	15059.195	1.3176	3.4242		165350.462	3.8037
		Z	72742.613	0.7524	- 1.3344	2.4105		

TABLE 5-15(a)

Stn 1	Stn 2		Interstation Vector (m)	Covariance Matrix (m^2)			Interstation Distance (m)	Variance (m^2)
		X	170304.750	17.7868				
Halifax	White	Y	- 22927.036	4.4736	7.3315		195542.577	11.8442
		Z	- 93314.215	1.9761	-2.9349	5.8673		
		X	253409.707	11.0741				
Halifax	Pleasant	Y	52547.304	3.4261	7.2093		265430.774	11.4649
		Z	- 58955.892	0.8544	-3.3624	5.2741		
		X	-257570.858	2.1869				
Fredericton	Halifax	Y	- 9099.718	0.4654	1.2096		276105.597	1.9036
		Z	99039.128	0.3980	-0.3492	0.8318		
		X	154780.318	3.0599				
Fredericton	Matane	Y	-189530.132	0.7486	1.5122		326465.403	0.6563
		Z	-216104.238	0.2845	-0.7219	1.3201		
		X	412349.580	10.9264				
Halifax	Matane	Y	-180434.554	3.2336	6.9361		549459.357	5.0871
		Z	-315145.649	0.7619	-3.3921	5.5779		
		X	-282061.149	8.9933				
Matane	Goose Bay	Y	-569100.286	0.9405	5.5298		708373.514	5.8868
		Z	-313623.034	2.5020	-2.4959	5.5609		
		X	724240.413	2.8695				
St. John's	Goose Bay	Y	-109455.592	1.7476	2.8337		837568.732	1.8552
		Z	-406222.449	- 0.0655	-1.4897	1.9916		

TABLE 5-15(b)

Stn 1	Stn 2		Interstation Vector (m)	Covariance Matrix (m^2)			Interstation Distance (m)	Variance (m^2)
		X	- 593953.295	7.7069				
Halifax	St. John's	Y	- 640075.199	0.7583	3.8477		901112.422	7.4015
		Z	- 222546.222	2.5847	-0.7969	3.1689		
		X	- 127282.501	2.6116				
Fredericton	Goose Bay	Y	- 758630.138	0.4094	1.5062		933988.401	1.0928
		Z	- 529729.942	0.6273	-0.4549	1.2633		
		X	130288.203	5.4115				
Halifax	Goose Bay	Y	- 749532.757	1.2195	3.2150		986977.471	1.2994
		Z	- 628768.764	0.9992	-1.1048	2.5021		
		X	- 851524.329	3.4025				
Fredericton	St. John's	Y	- 649175.781	0.0193	1.7588		1077857.558	3.6804
		Z	- 123507.242	1.4413	-0.2508	1.4800		
		X	1006302.493	7.9920				
St. John's	Matane	Y	459646.465	4.8129	4.8817		1110177.392	9.6919
		Z	- 92597.309	-0.5853	-2.7244	3.5593		

TABLE 5-15(c)

Final TWOSTN Interstation Vectors and Distances
and their Covariance Matrices.

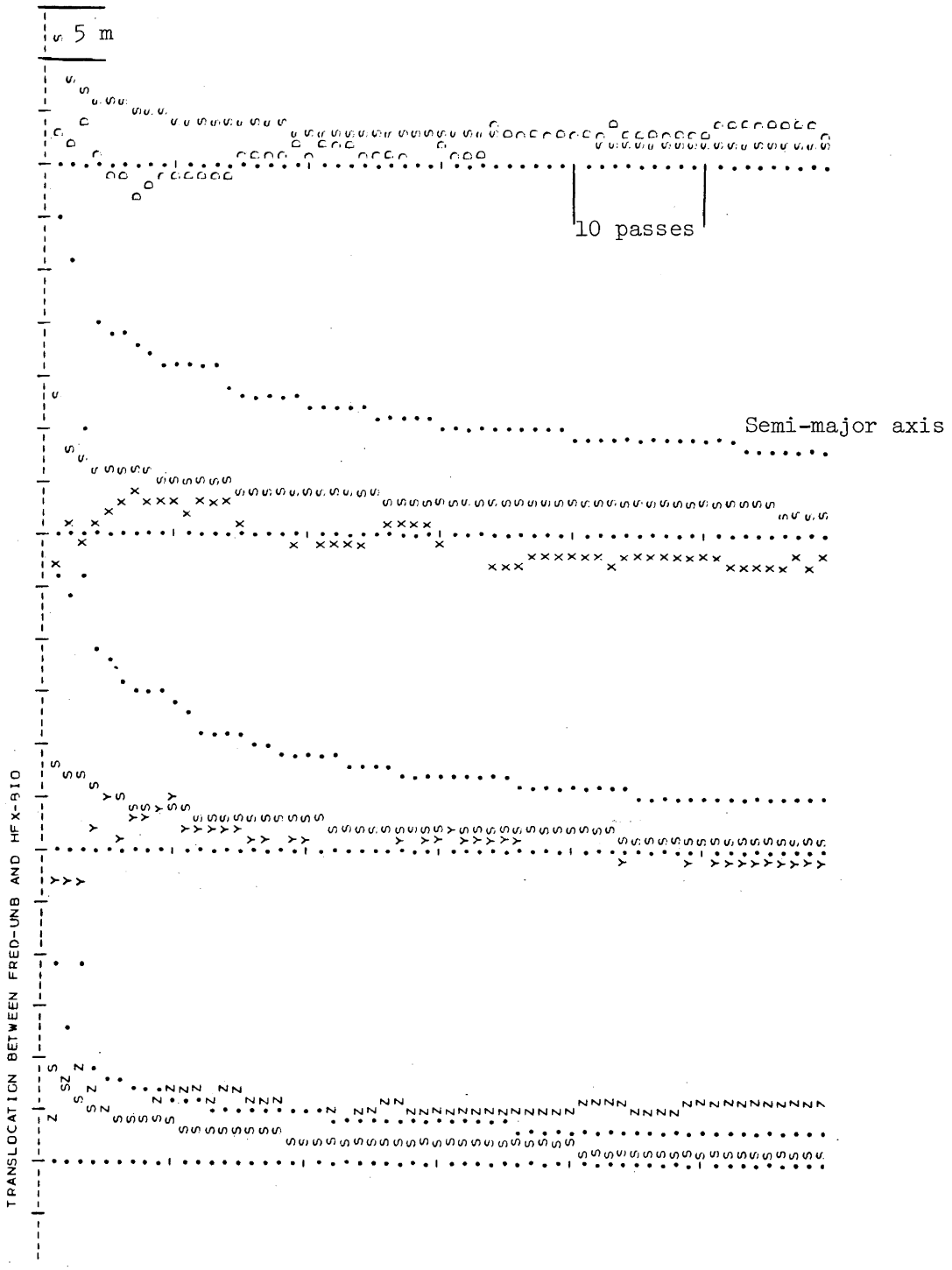

FIGURE 5-11

Typical TWOSTN Plot of Interstation Vector Coordinate and Distance Changes, Standard Deviations and 95% Confidence Region Axes.

Stn 1	Stn 2	Dist (km)	AZ (deg)	To 95% < 10 m		To 95% < 5 m		Totals Obtained		
				Passes	Dops	Passes	Dops	Passes	Dops	95% Region
Fredericton	Pleasant	59	0	31	9047			55	16508	8
Fredericton	White	93	95	31	9120			39	11468	10
Hoffman	White	102	150					38	10972	12
Halifax	Hoffman	116	120	50	14608			65	19066	9
Pleasant	White	117	55					34	9855	13
Pleasant	Hoffman	150	100	45	12892			53	15302	10
Fredericton	Hoffman	165	120	31	8875			73	21314	7
Halifax	White	196	130					37	10731	12
Halifax	Pleasant	265	105	47	13873			50	14706	10
Fredericton	Halifax	276	120	35	10278	123	36163	183	53766	4
Fredericton	Matane	326	170	23	6528	90	26186	106	30831	5
Halifax	Matane	549	145	39	11341			46	13384	10
Matane	Goose Bay	708	45	40	11245			58	16240	9
St. John's	Goose Bay	838	140	51	14811			150	42930	6
Halifax	St. John's	901	70	69	19950			97	28063	8
Fredericton	Goose Bay	934	30	37	10093	111	30932	138	38716	5
Halifax	Goose Bay	987	15	45	13144			99	28984	7
Fredericton	St. John's	1078	80	43	12097			145	41186	6
St. John's	Matane	1110	95	63	18506			83	24636	10

TABLE 5-16

Data Required to Obtain Specified Translocation Accuracy with 95% Confidence

greater for TWOSTN than for ONESTN since the orbit relaxation increases the size of the solution vector covariance matrix.

Program NETWORK combines the coordinates and covariance matrices of Table 5-11 and the interstation vectors and covariance matrices of Table 5-15, into a network adjustment. Three such adjustments were run, one each for the small, large and complete networks. The adjusted coordinates are given in Table 5-17, and the network correlation-coefficient matrices and coordinate standard deviations are in Table 5-18.

The differences between the point positioning and adjusted station coordinates (in the sense adjusted-point positioning) are given in Table 5-19. There are now five sources from which we can compute interstation vectors; the point positioning coordinates, the translocated interstation vectors, and the three adjusted network outputs. Table 5-20 takes the point positioning interstation vectors as standard, and compares the other four to them, resolving the differences into changes in distance (positive if greater than the point positioning interstation distance), and changes in direction (measured in the plane defined by the two interstation vectors). It appears that the differences are about equally divided between distances and direction changes. The point positioning and translocation values differ the most, as expected, since the adjustment model in effect attempts to reconcile the two, and should result in values midway between (for Table 5-20, between zero and the translocation differences).

Since ONESTN holds the orbit fixed, and TWOSTN does not, and since relaxing the orbit increases the estimated covariance matrix, then the point positioning results will be more heavily weighted in the adjustment than the translocation results. Relaxing the orbit for ONESTN will change this relative weighting, and should move the adjusted interstation

ADJUSTED COORDINATES FOR SMALL DOPPLER NETWORK

Station	X(m)	Y(m)	Z(m)
Fredericton	1761279.981	-4078250.349	4561415.724
Halifax	2018849.049	-4069152.197	4462376.666
Pleasant	1765439.674	-4121698.683	4521331.397
Hoffman	1909002.712	-4093311.331	4488673.412
White	1848542.100	-4046222.709	4555691.094

ADJUSTED COORDINATES FOR LARGE DOPPLER NETWORK

Station	X(m)	Y(m)	Z(m)
Fredericton	1761279.145	-4078250.545	4561415.853
Halifax	2018847.847	-4069152.616	4462376.747
St. John's	2612797.629	-3429075.011	4684922.743
Matane	1606496.282	-3888720.490	4777520.640
Goose Bay	1888557.836	-3319619.843	5091145.645

ADJUSTED COORDINATES FOR COMPLETE DOPPLER NETWORK

Station	X(m)	Y(m)	Z(m)
Fredericton	1761279.039	-4078250.606	4561415.892
Halifax	2018847.952	-4069152.456	4462376.692
Pleasant	1765439.157	-4121698.819	4521331.461
St. John's	2612797.611	-3429075.019	4684922.753
Hoffman	1909002.185	-4093311.467	4488673.472
Matane	1606496.260	-3888720.499	4777520.649
White	1848541.574	-4046222.844	4555691.158
Goose Bay	1888557.821	-3319619.845	5091145.652

TABLE 5-17

Adjusted Station Coordinates for Small, Large and Combined Doppler Networks

Station		Correlation Coefficient Matrix												Standard Deviations (m)
	X													0.4
Fredericton	Y	.4												0.3
	Z	.1	.5											0.2
	X	.2	.1											0.7
Halifax	Y	.1	.2	.1	.4									0.5
	Z		.1	.2	.2	.4								0.4
	X	.1	.1		.1	.1								1.0
Pleasant	Y		.1	.1		.1	.1	.4						0.9
	Z		.1	.1		.1	.1	.1	.5					0.7
	X	.1	.1		.2	.1		.2	.1					1.0
Hoffman	Y	.1	.1	.1	.1	.2	.1	.1	.2	.1	.3			0.7
	Z		.1	.1		.1	.1		.1	.1	.2	.5		0.6
	X	.1			.1			.2	.1		.2	.1		1.3
White	Y		.1	.1		.1	.1	.1	.1	.1		.2	.1	0.9
	Z		.1	.1		.1	.1		.1	.2		.1	.2	0.8
													RMS	0.8

TABLE 5-18(a)

Small Doppler Network

Station		Correlation Coefficient Matrix												Standard Deviations(m)
	X													0.5
Fredericton	Y	.3												0.4
	Z	.2	.5											0.3
	X	.2	.1											1.0
Halifax	Y	.1	.2	.1	.3									0.8
	Z		.1	.2	.2	.4								0.6
	X	.2	.1		.1	.1								0.9
St. John's	Y	.1	.2	.1	.1	.2	.1	.4						0.7
	Z		.1	.2		.1	.1	.3	.3					0.7
	X	.2	.1		.1			.1						1.1
Matane	Y	.1	.2	.1		.1			.2		.4			0.8
	Z		.1	.2			.1		.1	.1	.1	.5		0.8
	X	.2	.1		.1	.1		.2		.1	.1			0.9
Goose Bay	Y	.1	.2	.1	.1	.2	.1		.2			.1	.1	0.8
	Z		.1	.2		.1	.1	.1	.1	.2		.1	.1	0.7
													RMS	0.8

TABLE 5-18(b)

Large Doppler Network

Station		Correlation Coefficient Matrix	Standard Deviations (m)
Fredericton	X		0.4
	Y	.3	0.3
	Z	.2 .5	0.3
Halifax	X	.2 .1	0.8
	Y	.1 .2 .1 .3	0.6
	Z	.1 .2 .2 .4	0.5
Pleasant	X	.1 .1	1.4
	Y	.1 .1 .1 .4	1.1
	Z	.1 .1 .1 .1 .5	1.0
St. John's	X	.2 .1 .1 .1	0.8
	Y	.1 .2 .1 .1 .2 .1 .4	0.6
	Z	.1 .2 .1 .1 .3 .4	0.6
Hoffman	X	.1 .1 .2 .1	1.3
	Y	.1 .1 .1 .1 .1 .2 .1 .3	1.0
	Z	.1 .1 .1 .1 .2 .2 .5	0.8
Matane	X	.1 .1 .1 .1 .4	0.9
	Y	.1 .2 .1 .1 .2 .1 .7	0.7
	Z	.1 .2 .1 .1 .1 .5	0.7
White	X	.1 .1 .2 .1 .1 .4	1.7
	Y	.1 .1 .1 .1 .1 .1 .2 .1 .2 .1 .5	1.2
	Z	.1 .1 .1 .1 .2 .1 .2 .1 .5	1.0
Goose Bay	X	.2 .1 .1 .2 .1 .1 .4	0.8
	Y	.1 .2 .1 .1 .1 .1 .2 .1 .1 .1 .1 .4	0.6
	Z	.1 .2 .1 .1 .1 .2 .1 .1 .2 .1 .1 .2 .4	0.6
			RMS 0.9

TABLE 5-18(c)
Correlation Coefficient Matrices and Coordinate Standard Deviations for Small, Large and Combined Networks

CHANGES TO POINT POSITIONING COORDINATES AFTER SMALL NETWORK ADJUSTMENT

Station	ΔX(m)	ΔY(m)	ΔZ(m)	Shift(m)
Fredericton	-0.38	-0.28	0.11	0.48
Halifax	1.27	1.29	-0.30	1.83
Pleasant	1.72	-0.73	0.27	1.89
Hoffman	-0.31	1.54	0.17	1.58
White	3.59	0.05	-1.82	4.03

CHANGES TO POINT POSITIONING COORDINATES AFTER LARGE NETWORK ADJUSTMENT

Station	ΔX(m)	ΔY(m)	ΔZ(m)	Shift(m)
Fredericton	-1.22	-0.48	0.24	1.33
Halifax	0.07	0.87	-0.22	0.90
St. John's	2.83	1.77	-0.48	3.37
Matane	2.09	-0.54	0.06	2.16
Goose Bay	1.18	0.36	-0.60	1.37

CHANGES TO POINT POSITIONING COORDINATES AFTER COMPLETE NETWORK ADJUSTMENT

Station	ΔX(m)	ΔY(m)	ΔZ(m)	Shift(m)
Fredericton	-1.32	-0.54	0.28	1.45
Halifax	0.17	1.03	-0.27	1.08
Pleasant	1.20	-0.86	0.34	1.51
St. John's	2.81	1.76	-0.47	3.35
Hoffman	-0.83	1.41	0.23	1.65
Matane	2.07	-0.54	0.07	2.14
White	3.07	-0.08	-1.75	3.53
Goose Bay	1.16	0.36	-0.59	1.35

TABLE 5-19

Differences Between Point Positioning and Adjusted Coordinates

Stn 1	Stn 2	Length (km)	Azim From North (deg)	Changes in Distance (m)				Changes in Direction (m)			
				Transl-ocation	Small Network	Large Network	Complete Network	Transl-ocation	Small Network	Large Network	Complete Network
Fredericton	Pleasant	59	0	0.7	0.4		0.4	5.5	2.1		2.5
Fredericton	White	93	95	5.1	4.0		4.4	2.8	2.0		2.1
Hoffman	White	102	150	-6.1	-4.3		-4.3	3.3	1.7		1.7
Halifax	Hoffman	116	120	3.4	1.6		1.0	0.9	0.6		0.7
Pleasant	White	117	55	3.8	1.2		1.2	5.5	2.7		2.7
Pleasant	Hoffman	150	100	-1.9	-1.5		-1.5	4.8	2.7		2.7
Fredericton	Hoffman	165	120	1.4	-0.1		0.3	3.8	1.8		2.0
Halifax	White	196	130	-5.2	-2.9		-3.4	3.2	0.9		0.7
Halifax	Pleasant	265	105	0.8	0.1		-0.5	3.2	2.2		2.2
Fredericton	Halifax	276	120	3.5	1.7	1.4	1.7	3.1	1.5	1.3	1.5
Fredericton	Matane	326	170	-3.3		-1.7	-1.8	4.9		2.8	2.9
Halifax	Matane	549	145	-1.5		-1.8	-1.8	4.4		1.7	1.8
Matane	Goose Bay	708	45	-1.3		-0.1	-0.1	3.1		1.4	1.1
St. John's	Goose Bay	838	140	1.6		1.2	1.2	2.0		2.4	1.8
Halifax	St.John's	901	70	3.1		2.4	2.2	5.7		1.7	1.6
Fredericton	Goose Bay	934	30	0.7		0.5	0.6	6.2		2.6	2.7
Halifax	Goose Bay	987	15	-1.1		0.8	-0.8	2.8		1.0	0.9
Fredericton	St.John's	1078	80	9.3		4.5	4.6	4.3		1.4	1.4
St. John's	Matane	1110	95	3.1		1.7	1.7	2.2		1.8	1.8
RMS				3.7	2.3	2.0	2.2	4.0	1.9	1.9	1.9

TABLE 5-20

Changes to Point Positioning Interstation Vectors, Resolved into Changes in Distance and Direction

vectors closer to the translocated values, and away from the point positioning values. Note the TWOSTN covariance matrix is more realistic than that of ONESTN.

5.4.2 Comparison with 1972 results

In this section we investigate the repeatability of Tranit positioning by comparing the 1973 results with results computed from data acquired approximately one year earlier. The 1972 ONESTN results are given in Table 5-21 and TWOSTN results in Table 5-22. Table 5-23 compares the 1972 ONESTN and TWOSTN interstation distances. The shifts between 1973 and 1972 point positions are in Table 5-24, and the differences between 1973 and 1972 interstation distances in Table 5-25.

From Table 5-24 it is clear that differences between the 1973 and 1972 point positioning results contain systematic shifts of the coordinates whose magnitude exceeds the separate internal consistencies of the 1973 and 1972 results. Here we make two postulates concerning these shifts.

(a) The major systematic effect involves polar motion.

(b) The point positioning internal consistencies are too optimistic due to holding the orbit fixed.

For both the 1973 and 1972 data, a transformation from instantaneous to average terrestrial coordinates was made. However from section 5.3.2 it appears that the operational ephemerides are referred to a coordinate system other than the instantaneous terrestrial. The effect of not performing the instantaneous to average terrestrial transformation worsens the disagreement (for example the Fredericton shift becomes approximately 12 m increased from 6.5 m), therefore it is postulated that the z-axis of the operational ephemeris coordinate system is closer to the instantaneous pole than to the average pole.

Station		Correlation Coefficient Matrix	Coordinates (m)	Standard Deviations (m)
	X		1761277.29	1.6
Fredericton	Y	.2	-4078244.35	1.0
	Z	.3 -.6	4561416.09	1.0
	X		2018848.58	2.0
Halifax	Y	.1	-4069147.58	1.5
	Z	.4 -.6	4462374.49	1.5
	X		1765437.11	0.9
Pleasant	Y	.4	-4121693.91	0.7
	Z	.1 -.5	4521330.68	0.6
	X		1909001.38	0.7
Hoffman	Y	.4	-4093307.48	0.6
	Z	.1 -.5	4488675.16	0.5
	X		1848541.48	0.8
White	Y	.3	-4046228.18	0.5
	Z	.2 -.5	4555701.37	0.5
			RMS	1.1

TABLE 5-21

1972 Point Positioning Results

Stn 1	Stn 2		Correlation Coefficient Matrix	Coordinates (m)	Standard Deviations (m)
		X		- 4159.11	3.0
Fredericton	Pleasant	Y	.2	43445.70	1.8
		Z	.3 -.5	40083.52	1.8
		X		- 87270.68	4.0
Fredericton	White	Y	.1	- 32022.67	2.4
		Z	.4 -.5	5711.59	2.5
		X		109837.10	3.6
Halifax	Hoffman	Y	.1	24157.28	2.5
		Z	.4 -.6	- 26298.43	2.6
		X		-147720.57	2.9
Fredericton	Hoffman	Y	.3	15061.66	2.2
		Z	.2 -.6	72740.03	2.0
		X		170302.68	3.6
Halifax	White	Y	0	- 22915.83	2.6
		Z	.4 -.6	- 93324.31	2.7

TABLE 5-22

1972 Translocated Interstation Vectors

		Point Posn		Translocation		
Stn 1	Stn 2	Dist(m)	σ(m)	Dist(m)	σ(m)	Δ(m)
Fredericton	Pleasant	59262.2	0.7	59258.0	1.2	-4.2
Fredericton	White	93127.5	1.8	93135.6	3.9	8.1
Hoffman	White	101805.6	0.6			
Halifax	Hoffman	115506.9	2.0	115496.2	3.4	-10.7
Pleasant	White	117400.0	1.2			
Pleasant	Hoffman	149942.9	1.2			
Fredericton	Hoffman	165349.8	1.5	165346.1	2.4	-3.7
Halifax	White	195549.8	1.9	195544.3	2.8	-5.5
Halifax	Pleasant	265432.3	3.7			
Fredericton	Halifax	276106.7	4.2			

TABLE 5-23

1972 Interstation Distances

Station	ΔX(m)	ΔY(m)	ΔZ(m)	Shift(m)	σ_{shift}(m)	Shift/σ_{shift}
Fredericton	3.07	-5.72	-0.48	6.51	1.17	5.6
Halifax	-0.80	-5.91	2.48	6.46	1.99	3.3
Pleasant	0.85	-4.04	0.45	4.15	1.75	2.4
Hoffman	1.64	-5.39	-1.92	5.95	1.56	3.8
White	2.97	-5.42	8.46	10.48	1.49	7.0
					RMS	4.7

TABLE 5-24

Shifts to 1973 Point Positions to Obtain 1972 Positions

Stn 1	Stn 2	1972 - 1973 Point Posn. Δ(m)	σ_Δ(m)	Δ/σ_Δ	1972 - 1973 Translocation Δ(m)	σ_Δ(m)	Δ/σ_Δ
Fredericton	Pleasant	2.0	1.3	1.6	-2.9	1.7	-1.6
Fredericton	White	1.3	3.4	0.4	4.4	5.2	0.8
Hoffman	White	-3.4	1.8	-1.9			
Halifax	Hoffman	3.4	3.0	1.2	-10.6	4.5	-2.4
Pleasant	White	-0.8	3.5	-0.2			
Pleasant	Hoffman	-1.0	3.1	-0.3			
Fredericton	Hoffman	0.7	2.2	0.3	-4.4	3.1	-1.4
Halifax	White	2.0	3.1	0.7	1.7	4.4	0.4
Halifax	Pleasant	2.4	4.4	0.5			
Fredericton	Halifax	4.6	4.3	1.1			
			RMS	1.0			1.5

TABLE 5-25

Changes to 1973 Interstation Distances to Obtain 1972 Distances

Three inferences are drawn from Table 5-25.

(a) The interstation vectors computed from point positions appear to have a better repeatability than translocated distances. This implies that the rationale for using translocation (because it provides more consistent interstation vectors and distances) is invalid; or that the method of implementing translocation here is incorrect. We return to this point in section 6.1.4.

(b) The point positioning internal consistencies (for distances) appear to be realistic. Thus point positioning network covariance matrices yield optimistic estimates of coordinate repeatability, and realistic estimates of distance repeatability. Note that the correlation between stations (due to use of common passes, or even different passes drawn from the same operational ephemeris solution) is not modelled in the point positioning network covariance matrices (Tables 5-12 and 5-21). Therefore an appropriate increase in the magnitude of single station covariance matrices (obtained for example by relaxing the orbit for ONESTN runs), balanced by the introduction of interstation correlations, would result in less optimistic coordinate confidence regions, and essentially unchanged distance confidence regions.

(c) The translocation internal consistencies are too optimistic.

5.4.3 Comparison with terrestrial network

To investigate the external consistency of Transit positioning the 1972 and 1973 results for the "small" network were compared with a terrestrial network containing the same five stations. This terrestrial network extended from Fredericton to Halifax, was observed by the Geodetic Survey of Canada, and was adjusted accounting for the effect of geoid heights on observed distances, and for the effect of deflections of the

vertical on observed directions (Thomson, Nassar and Merry, 1974). Minimum constraints were used, and the Fredericton Doppler tracking station was held fixed. Adjusted terrestrial coordinates were computed for the Transit antenna locations, to faciltate the comparisons. Terrestrial interstation distances are compared with 1973 Transit distances in Table 5-26, and with 1972 Transit distances in Table 5-27. The terrestrial distances agree best with the 1973 point positioning distances (rms discrepancy of 1.7 m) and the 1972 point positioning distances (rms discrepancy of 2.2 m). Again the translocation distances appear to be worse than the point positioning distances, if their agreement with the terrestrial distances is taken as a measure of quality.

The rms value for Δ/σ_{Δ} is a scalar measure of external consistency (Wells, Krakiwsky and Thomson, 1974), which indicates the extent to which the distances and standard deviations from one network are consistent with the distances and standard deviations from the other network. The networks are inconsistent to the extent that this rms value differs from unity. According to this criterion, both 1973 point positoning and translocation are consistent with the terrestrial network, whereas the 1973 small adjusted network and the 1972 point positioning and translocation are all somewhat inconsistent, in the sense that the network covariance matrices are too optimistic.

Stn 1	Stn 2	Terrestrial Dist(m)	σ(m)	Terr - Point Posn. Δ(m)	σ_Δ(m)	Δ/σ_Δ	Terr - Trans. Δ(m)	σ_Δ(m)	Δ/σ_Δ	Terr - Small Network Δ(m)	σ_Δ(m)	Δ/σ_Δ
Fredericton	Pleasant	59258.4	0.3	-1.8	1.1	-1.6	-2.5	1.3	-1.9	-2.2	0.6	-3.8
Fredericton	White	93127.3	0.2	1.1	2.9	0.4	-4.0	3.5	-1.1	-2.8	1.4	-2.0
Hoffman	White	101805.6	0.4	-3.4	1.7	-2.0	2.7	2.2	1.2	0.9	0.9	1.0
Halifax	Hoffman	115504.1	0.2	0.7	2.2	0.3	-2.7	3.0	-0.9	0.9	1.1	0.8
Pleasant	White	117398.1	0.3	-2.7	3.3	-0.8	-6.5	4.2	-1.5	-3.9	1.5	-2.6
Pleasant	Hoffman	149943.3	0.3	-0.6	2.9	-0.2	1.4	3.3	0.4	0.9	1.3	0.7
Fredericton	Hoffman	165349.4	0.4	0.3	1.7	0.2	-1.1	2.0	-0.6	0.4	0.9	0.4
Halifax	White	195547.2	0.5	-0.6	2.4	-0.3	4.6	3.4	1.4	2.3	1.1	2.1
Halifax	Pleasant	265430.0	0.5	0.1	2.4	0.0	-0.8	3.4	-0.2	0.0	1.2	0.0
Fredericton	Halifax	276103.9	0.6	1.8	1.1	1.6	-1.7	1.5	-1.1	0.0	0.8	0.0
					RMS	1.0			1.1			1.8

TABLE 5-26

Terrestrial Interstation Distances Compared to 1973 Doppler Distances

Stn 1	Stn 2	Terr - Point Posn. Δ(m)	σ_Δ(m)	Δ/σ_Δ	Terr - Trans. Δ(m)	σ_Δ(m)	Δ/σ_Δ
Fredericton	Pleasant	-3.8	0.8	-4.8	0.4	1.2	0.3
Fredericton	White	-0.2	1.8	-0.1	-8.3	3.9	-2.1
Hoffman	White	0.0	0.7	0.0			
Halifax	Hoffman	-2.8	2.0	-1.4	7.9	3.4	2.3
Pleasant	White	-1.9	1.2	-1.6			
Pleasant	Hoffman	0.4	1.2	0.3			
Fredericton	Hoffman	-0.4	1.6	-0.3	3.3	2.4	1.4
Halifax	White	-2.6	2.0	-1.3	2.9	2.8	1.0
Halifax	Pleasant	-2.3	3.7	-0.6			
Fredericton	Halifax	-2.8	4.2	-0.7			
			RMS	1.7			1.6

TABLE 5-27

Terrestrial Interstation Distances Compared to 1972 Doppler Distances

CHAPTER 6

DISCUSSION AND CONCLUSIONS

In section 6.1 we first re-examine the a priori decisions listed in section 5.1. Options and alternatives to each decision are discussed and evaluated with regard to the results presented in Chapters 4 and 5.

The results of Chapters 4 and 5 and the discussions of section 6.1 are summarized as a set of conclusions (section 6.3). A list of suggestions for future work based on these conclusions completes the chapter.

6.1 Re-examination of Assumptions and Decisions

In this section we follow the structure of section 5.1, and discuss the assumptions and decisions under the same four headings: The measurement and correction of the Doppler counts; the satellite ephemeris; filtering of noisy measurements and passes; and computation of the station coordinates. In each case we first restate the decision from section 5.1, and then discuss it.

6.1.1 Doppler measurements and corrections

In section 5.1.1 nine decisions were listed affecting the Doppler measurements, and their corrections.

The first decision is to use navigation-type Transit receivers. In section 2.2.2 we defined navigation receivers as those which use the satellite time base exclusively, and geodetic receivers as those which also

use the receiver time base. When the test data of Chapter 5 was collected in 1972 and 1973, the only alternative to navigation receivers was the Geoceiver (Magnavox, 1971), which is expensive and difficult for civilian agencies to acquire. Since then two new, less expensive geodetic receivers, the Marconi 722-B (Marconi, 1974) and the JMR-1 (JMR, 1973) have become available.

The operation of these three geodetic receivers is discussed and compared with navigation receivers in section 2.2.2. Geodetic receiver Doppler measurements are more precise due to reducing or eliminating the effect of some of the measurement noise sources such as

(a) non-uniformity of the satellite time base as received at the receiver antenna, due to uncorrected propagation effects,

(b) non-uniformity of the satellite time base as detected by the receiver, due to variable propagation delays within the receiver,

(c) noise on the measurements due to the different signal paths (and propagation delays) through the receiver for the received frequency, and for the time signals,

(d) noise on the measurements due to the fact that navigation receivers record only the integral number of positive zero crossings of the Doppler beat frequency, occurring between detection of successive time signals, whereas, given the supplementary timing information available in geodetic receivers, a more precise correspondence between the actual integration interval, and the interval defined by successive time marks can be made.

On the other hand use of a local clock requires accounting for a number of effects on the observations which do not influence navigation receiver measurements, such as

(a) differences between the satellite and receiver time bases,

(b) special and general relativity effects, (see page 45).

The second decision is to use the Transit navigation observation equation (2-43). Derivation of this equation in section 2.2.2 required five assumptions, discussed in section 2.2.3, which are

(a) that the integration interval is defined by the epochs at which the satellite time marks are received. Actually the integration interval is between the first positive zero crossings of the Doppler beat frequency following detection of the time marks. In section 2.2.3 it is shown that if standard deviations of 30μs, 10μs and $1/\sqrt{12}(f_g - f_s)$ are assumed for the short period receiver time variations, the receiver Doppler delay, and the zero crossing delay respectively, they will contribute to two minute integrated Doppler counts a bias of about 1 count at closest approach and zero at the horizons, and a standard deviation of about 1.5 counts.

(b) that at the epoch at which the satellite transmits a two minute time mark, it occupies the position defined by the operational ephemeris for that epoch. In section 2.2.3 we noted that this required that the satellite time marks be synchronized to the ephemeris epochs, and that the ephemeris describe the actual satellite trajectory. There is evidence to indicate synchronization errors of typically 50 μs (equivalent to about 0.4m along track ephemeris error) is achieved. In Chapter 4 we determined that ephemeris prediction error is typically 25 m along track, which is therefore the dominant effect.

(c) that the propagation time from satellite to receiver is s/c where s is the geometric distance and c the vacuum velocity. This does not account for the effects of ionospheric and tropospheric refraction on the propagation velocity (see below) or on the curvature of the signal path. Rather than attempt to correct for this curvature, measurements made below a threshold elevation angle (where curvature is pronounced)

are deleted.

(d) that special and general relativistic effects can be ignored.

(e) that the satellite and receiver oscillator frequencies can be assumed constant for the duration of a pass (20 minutes). If the measured long term drift rates (0.5 and up to 10 parts in 10^{10} per day for satellite and receiver oscillators respectively) are assumed also to be the short term drift rates, biases of 0.02 and 0.3 counts are introduced into two-minute integrated Doppler counts.

Equation 2-43 is a range-difference observation equation. Alternatives are the asymptotic ranging equation of Brown and Trotter (1969), and the frequency equation of Anderle (1973a), both of which are described in section 2.2.2. There seems to be no compelling reason to choose one of these alternatives. Note however the discussion below concerning correlations between Dopplers.

The third decision is to correct for tropospheric and ionospheric refraction using reduction equations. The alternative is to incorporate these corrections in the observation equation (equation 2-64). If this approach is taken, the corrections no longer need be considered as perfect, as when the reduction equation approach is taken.

The results of sections 5.3.1 and 5.3.2 indicate that in fact the tropospheric refraction correction used here is not complete, and some residual tropospheric refraction remains.

The fourth decision is to compute the tropospheric correction using the Hopfield model (section 2.3.1), with meteorological observations from the nearest weather station. Alternatives are

(a) to make no correction,

(b) to use the same or a simpler model incorporating average meteorological values for the station and season,

(c) to use meteorological observations made at the tracking station rather than at the nearest weather station, and

(d) to use a simpler model without observed meteorological values, but to include a tropospheric refraction scaling factor as a parameter of the position fix (Brown, 1971; Kouba, 1974; Anderle, 1973). This last alternative is particularly attractive, since

(i) it eliminates the necessity of acquiring and time-synchronizing meteorological observations, and

(ii) as noted above, the results of sections 5.3.1 and 5.3.2 indicate that residual refraction effects are contained in the data, even after the Hopfield reduction applied here.

The fifth decision is to make a first order ionospheric correction based on dispersion by comparing the Doppler measurements at two different frequencies (requiring dual channel receivers) (section 2.4.1). Alternatives are

(a) to ignore ionospheric refraction (single channel receivers), and

(b) to make a higher order correction (requiring three or more channels) as described in Willman and Tucker (1968). Since the Transit system is based on dual frequency broadcasts, it is not possible to make a higher order correction with this system, at the present time.

The sixth decision is to use the shortest possible Doppler integration interval (approximately 4.6 seconds). Alternatives are any multiple of 4.6 seconds, usually no greater than 120 seconds. The advantage of using the 4.6 second interval is the capability of filtering and testing the measurements so that a minimum of data is rejected. The disadvantage is the larger number of data points which must be stored and processed, and the size of the associated covariance and design matrices involved. In particular it was necessary for this reason to assume the

covariance matrix of the observables to be diagonal, and to adopt the network adjustment strategy described in sections 5.1.4 and 6.1.4. The processing costs (section 5.2.4) are also higher than they would be for longer integration intervals.

The seventh decision is to assume individual Doppler measurements are uncorrelated. There are arguments both for and against correlation between consecutive Dopplers. The argument in favour is based on the fact that the epoch ending one integration interval also starts the next integration interval, so that an epoch error will affect both integrations (Brown and Trotter, 1969; Kirkham, 1972; Krakiwsky, Wells and Kirkham, 1972). The argument countering this contends that when measurements are made at two frequencies, the epochs of integration at one frequency are uncorrelated with the epochs of integration at the other frequency, and therefore the correction for ionospheric refraction, which combines the two frequency measurements, in effect uncorrelates the measurements (Anderle, private communication, 1974). In any event, the point is adademic here, since introducing correlated measurements when using 4.6 second integration would have overtaxed the computer facilities which were available.

The eighth decision is to assume all Doppler measurements to have equal variances. In section 5.3.1 we examined the dependence of Doppler residual sample standard deviations upon elevation angles (Figures 5-4 and 5-5). From these results it appears that high elevation Doppler measurements should be assigned variances up to twice the mid-range or average value, and, pending the results of incorporating a residual refraction parameter into the estimation process, low elevation Doppler measurements should be assigned variances somewhat higher than the mid-range or average value.

The ninth decision is to assume particular values for the Doppler variances, depending on the receiver model used. These values (scales

for the Doppler covariance matrix) were determined from two investigations. The sample variances of Table 5-7 for several hundred thousand residuals indicated the following variances for 4.6 second Doppler counts:

ITT 5001	0.8 counts^2
Marconi 722	2.6 counts^2
Magnavox 702	4.0 counts^2

However when these values were used for the rejection criteria of section 5.2.3, far too many measurements and passes (up to 50% on a 95% confidence level Chi-square test) were rejected. Hence the higher values of section 5.1.1 were adopted:

ITT 5001	1.5 counts^2
Marconi 722	4.0 counts^2
Magnavox 702	10.0 counts^2

It should be noted that the Marconi receivers used were the first four serial numbers off their assembly line (in 1973). Three of these have subsequently been converted from model 722 to model 722-B, which incorporates several modifications designed to reduce the measurement noise. Similarly the Magnavox receiver was serial number 5 off their assembly line (in 1968), and a later, redesigned version of the model 702 has been marketed since 1971. Therefore these figures should not be taken as a comparison of currently marketed models from the various manufacturers.

6.1.2 Satellite ephemerides

In section 5.1.2 four decisions were listed concerning the satellite ephemerides.

The first decision is to use the operational ephemeris. The alternative is to use the precise ephemeris post-computed by the U.S. Naval Weapons Laboratory (section 4.4.1). The operational ephemeris is less precise, however it is available in real time for all satellites,

whereas the NWL precise ephemeris is available only after some delay, and at present is routinely computed for only one satellite.

The second decision is to approximate the variable orbit parameters of the operational ephemeris. The decision (section 5.1.1 and 6.1.1) to use a 4.6 second integration interval necessitates some method of obtaining satellite positions between the (two minute) operational ephemerides. The method chosen was to least-squares fit generalized polynomials to each of the three sets of variable orbit parameters ΔE, Δa and η (defined in Table 4-2), specifically to find the best least squares approximations to each of ΔE, Δa and η given the base functions {1, cos2nt, sin2nt, t}, where n is the satellite mean motion (defined in Table 4-1), and t is time (section 4.5.4). Alternatives to the best least squares approximation are

(a) best approximations based on other criteria, for example the Chebyshev (minimax) criterion, and

(b) interpolation, for which many techniques could be chosen, the simplest being a linear interpolation between data points. The least squares approximation was chosen because

(i) it utilizes software already required elsewhere in the processing,

(ii) none of the alternatives appear to provide any great advantage, and

(iii) the results (using the given base function) are satisfactory, and indeed much more satisfactory than some of the alternatives (for example linear interpolation). The specific base functions chosen were used because they appear to be the set of four functions which best model the shape of the variable orbit functions ΔE, Δa and η (section 4.5). An alternative would be to use more than four base functions, however it is

desirable to minimize the number of base functions, so that fewer values of ΔE, Δa and especially η are required for the approximations. However, omitting any of the four base functions adopted creates significant errors in the approximants.

The third decision is to allow the orbit to relax parallel to itself. The alternatives are

(a) holding the orbit fixed, or

(b) allowing the orbit to relax without the restriction of maintaining parallelism. The orbit was not held fixed in order that some of the known systematic errors in the operational ephemeris (section 4.4) could be absorbed. The orbit was kept parallel as a consequence of Guier's theorem (section 4.2).

The orbit relaxation was also restricted in the sense that a priori weights were assigned to each of the orbit bias components (section 4.6). The values chosen (equivalent to standard deviations of 2, 0.5 and 1 broadcast units, or 26, 5 and 10 metres, in the along track, radial and cross track directions respectively) were based on a comparison between sets of operational and precise ephemerides for passes tracked over Fredericton, N.B. (section 4.4). It should be noted that Fredericton is within 200 km of one of the four NNSS operational network stations (at Winter Harbour, Maine). Since the operational ephemerides are predicted based on tracking data from these four stations, it may be that less favourable agreements between the operational and precise ephemerides would be obtained at locations more remote from the four operational tracking stations.

The fourth decision presumes the operational ephemeris to be referred to the instantaneous terrestrial coordinate system of some epoch. From the results of section 5.3.2 and from Kouba (private communication, 1974), it would appear that this is not the case, and the polar motion

correction made to the operational ephemeris is incomplete. Since 27 January 1974 the operational ephemeris is claimed to be referred to the average terrestrial system (Piscane et al, 1973), so that the question of the incompleteness of the pole motion correction is no longer relevant.

6.1.3 Data filtering

In section 5.1.3 eight decisions were listed concerning data filtering.

The first decision is to examine and edit the observed data as thoroughly as possible. Alternatives are

(a) not to edit the data, and

(b) to use less rigorous testing than was used here. One of the main contentions of this investigation is that the quality of the results obtained here can be directly attributed to the rigour of the data filtering which was used. However, one of the consequences of this rigorous editing policy was greatly increased computing costs (section 5.2.4).

The second decision is to use the majority voting process as the first data filter.

There is no alternative to majority-voting, since the digits of the operational ephemeris must be recovered from the received messages absolutely error free. However here we have assumed in addition that any inconsistency between one or more digits in a particular message word and its majority voted equivalent indicates noisy reception, and therefore contaminated Doppler data, which is therefore rejected. This assumption may not be valid in all cases, but is consistent with the policy of rejecting when in doubt. There is some evidence that this assumption is often valid, however, since in many cases the few message words proceeding a loss of lock do contain noisy digits. A more sophisticated alternative to this method is provided by the JMR receiver (JMR, 1973) which outputs

a "quality factor" digit, derived from the AGC voltage, under the assumption that this voltage indicates signal strength, and hence is related to signal noise.

The third decision is to use Guier plane navigation as the second data filter. Guier plane navigation as a filtering technique is not new (Guier, 1967; Anderle, 1973). However in these other applications the data was filtered for use in computing orbit trajectories and new earth gravity model, rather than for the relatively simple task undertaken here of computing tracking station coordinates. Alternatives to this method of filtering would be

(a) to compute two dimensional, single pass filtering fixes in some other coordinate system (say latitude and longitude, or topocentric X and Y), however note that the error component in the direction suppressed by the Guier plane is nearly singular. Coordinate corrections in the Guier plane can be physically interpreted since they are bounded by actual ephemeris and station coordinates. Latitude and longitude navigation, on the other hand, gives unbounded $\Delta\lambda$ as the elevation angle approaches 90°.

(b) To incorporate the filtering into the final three dimensional, multipass computation.

The reasons that Guier plane navigation was chosen over these alternatives is duscussed in section 4.2. The Guier plane is the two dimensional coordinate system in which

(a) the Doppler residuals and the estimated variance factor are uncontaminated (to first order) by satellite orbit errors, and

(b) the solution vector consists of the three parameters (frequency offset, and Guier plane X and Y coordinates) which can be accurately estimated from a single pass. There are two consequences of (a). The first is that since the estimated variance factor is uncontaminated, it can be

used to scale the observable covariance matrices in three dimensional multipass solutions. That is, it is assumed that the variance of a Doppler observation will vary from pass to pass (due for example, to differing refractive variability, differing signal strength, differing signal interference from ground reflection and other sources), and that the effect of these influences are incorporated in the Guier plane estimated variance factor, which should be used to appropriately weight each pass in a multipass solution. The second consequence is that since the Doppler residuals are here reduced to their experimental noise level, this is the best place to individually examine them for rejection or non-rejection. A normality test is used (section A.1).

There are also two consequences of (b). The first is that since one of the estimated parameters is the frequency offset, and since the value obtained here will be more accurately determined (less contaminated by systematic errors of geometrical origin) than for any other coordinate system, then the frequency offset should be held fixed at this value (very heavily weighted) in subsequent multipass solutions. Note that the argument can be made that separately estimating frequency offset and position from the same data suppresses any correlation between them, and is therefore statistically unsound. For this reason, while the Guier plane estimate for frequency offset is kept as the corrected determination, the NWL programs leave it as an undetermined parameter in later solutions (Anderle, personal communication). However here the frequency offset value was held fixed and weighted according to an assigned standard deviation of 0.0001 parts in 10^{10}. A more appropriate alternative would be to use the standard deviation computed for the Guier plane frequency offset solution, which was usually between 1 and 10 parts in 10^{10}.

The second consequence is that the other two estimated parameters

(the Guier plane X and Y coordinates) can be considered to be either

(a) the correction to the satellite orbit (resolved into the Guier plane) assuming perfect a priori tracking station coordinates, or

(b) the correction to the tracking station coordinates (resolved into the Guier plane) assuming a perfectly known orbit. In reality neither the tracking station coordinates nor the satellite orbit are perfect, so that these two coordinates will reflect imperfections from both sources. However, presuming reasonably well-known tracking station coordinates (errors of the same magnitude as the orbit errors - say 10 to 20 m), then anomalously large values (say over 100 m) for the Guier plane X and Y indicate a problem pass, which should be rejected. (Note that this does not imply that the a priori station coordinates must be known to within 10 or 20 m in order to be able to use the filtering and coordinate computation methods described in Chapter 5. However when they are known to this precision, usually from preliminary processing of the data, then an effective Guier plane filter with tight threshold values can be used.) Similarly large standard deviations for the estimates of either frequency offset or Guier plane coordinates are also an indication that the pass has not yielded a well-determined solution, and should be rejected.

The results of section 5.3 indicate that not only is Guier plane navigation a useful filtering tool, but that it also can be effectively used to detect and identify residual systematic influences in the data.

The fourth, fifth and sixth decisions are to examine both individual and single pass sets of Doppler measurements, to make as minute an examination of the individual Dopplers as possible (by using the shortest possible integration interval), and to reject a piece of data if the results for any test on that data fall below specified thresholds. An alternative would be to introduce some system of graduated weighting in which all pieces

of data would be conditionally accepted, some with higher weights than others. In this context the accept-reject policy in effect restricts these weights to be either 0 or 1. One of the reasons graduated weighting was not chosen is that it is not at all obvious how such a weighting scheme should be designed. It would have to account for the results of several different tests on the same data. Some of the reasons for rejection are related to the data noise level (which might be amenable to graduated weighting). Other reasons for rejection are due to blunders (for example a majority vote failure, or a Doppler count out of its correct sequence), and these are not consistent with a scheme of graduated weighting. The decision to entirely discard questionable data was also based on the abundance of available data. From section 5.4.1 we note that it is possible to achieve point positioning with a 95% confidence of 5 metres with data accumulated in five days or less (at latitude 45°, with five operational satellites and using operational ephemerides). The fraction of data actually rejected, even with the most rigorous of tests, was of order 50%, relative to the total number of alerted passes (section 5.2.3). The duration of tracking station occupation times would not be significantly shortened, even if a sizeable portion of the rejected data were to be salvaged through some graduated weighting scheme and were to leave the required number of data points unchanged.

The seventh decision enumerates specific thresholds for rejection of individual Doppler counts. Some of these thresholds are absolute, such as the existence of non-numeric or majority vote failure characters, loss of lock in either channel, or balancing about closest approach. Others are to some extent arbitrary, such as 8° elevation cutoff ,

100 count misclosure cutoff (if the a priori

station coordinates are less well known than they were here, this threshold must be broadened to reflect the accuracy in their knowledge), and 95% confidence level normality test on the residuals (which could be chosen at some other confidence level, but with marginal difference in the rejection rate).

The eighth decision enumerates specific thresholds for rejection of passes. In this case most of the thresholds are somewhat arbitrary, such as at least 75 Doppler counts (to begin with this was set at 50, but this resulted in several anomalous passes at each station not being rejected), closest approach elevation 10° (the usual cutoff is 15°, but was reduced here in the expectation that other tests, such as the 75 count minimum, and the Hopfield correction would adequately filter anomalous passes down to 10°), the alert computation threshold (five units as described in section 4.3), the orbit approximation threshold (95% confidence level rejection on the estimated variance factor using an a priori value of 0.25 broadcast units^2), and the Guier plane navigation thresholds (again some of these must be broadened when the station coordinates are less well known).

6.1.4 Coordinate computation

In section 5.1.4 we outlined the network computation strategy of separately computing position vectors and interstation vectors, then combining them in a network adjustment. Here we discuss this more fully.

As we have seen, the Transit system, in contrast to other geodetic tools, is capable of providing tracking station position vectors using only observations made at the particular tracking station. However such independently determined position vectors for a network of tracking stations will be affected by certain systematic errors (principally errors in the assumed satellite trajectory, and uncorrected refraction) which will create inconsistencies between the coordinates of various stations, that is

the network will not be homogeneous. The magnitude of these inconsistencies may be several metres, and for many purposes (for example navigation) are negligible. However to fully utilize the capabilities of the Transit system, it is necessary to reduce as much as possible the effect of these systematic errors, by somehow combining the observations from different stations to improve the internal consistency (homogeneity) of the network coordinates.

Three approaches taken to obtain network coordinates have been labelled point positioning (the position vectors already mentioned), translocation (the interstation vectors also mentioned), and short arc determination (DOD, 1972). Let us differentiate these three approaches according to the sparseness of the covariance matrix of the coordinates of all stations in the tracking network (which we will call the network covariance matrix). By allowing the satellite ephemeris to relax slightly during the adjustment (in accordance with the results established in Chapter 4) covariances are introduced between tracking stations.

In the short arc method, the orbit is relaxed consistently with observations from all stations in the network, and the network covariance matrix is fully populated. In translocation, the orbit is relaxed consistently with observations from one pair of stations at a time, and only the covariances between these pairs of stations are nonzero. In point positioning either the orbit is not relaxed, or else it is relaxed consistently with the observations from just one station at a time, in either case the covariances between stations are zero. In this context translocation can be considered the general method, with the short arc method being a kind of "multistation" translocation, and point positioning being the limiting case either in the sense that only one station is involved, or in the sense that the orbit is held fixed.

Note that the "translocation" described in DOD (1972) was actually performed by making two separate point positioning computer runs, both holding the orbit (defined by the precise ephemeris) fixed.

The short arc method is the most rigorous approach, however it has two disadvantages. Since for each pass data from all stations simultaneously tracking the pass must be simultaneously processed, the arrays containing this data can become large for networks of many stations. This is particularly true in the present case, having chosen to use 4.6 second Doppler integration intervals, thus having larger data arrays per station than for longer integration intervals. The straightforward solution to the problem of non-simultaneous data is to accept only passes tracked by all stations, however the disadvantage here is that a high proportion of the data will be rejected.

More efficient data utilization can be accomplished by merging the results from various patterns of simultaneous tracking stations into one solution. One method of identifying these various patterns is pass by pass - that is each pass would have its own subnetwork of simultaneous tracking stations, and this pattern would shift from pass to pass in a multipass short arc adjustment. Another alternative is to identify these various patterns subnetwork by subnetwork - that is each subnetwork would have its own set of simultaneous passes. The limiting case of this latter method is subnetworks consisting of only two stations - that is translocation pairs. Therefore one way of approximating the results of the rigorous short arc method, but without the disadvantages of large arrays and high data rejection rates, is to translocate between all pairs of stations, and to combine the results of all translocations in a network adjustment.

In theory these alternatives are less rigorous than a short arc

adjustment of only passes observed at all network stations. Since we are attempting to eliminate systematic errors by combining data from all stations in one short arc adjustment, theoretically we will reintroduce these systematic errors to the same extent that we use passes which were tracked by less than the full network. However the practical consequences of adopting one of these less rigorous alternatives is likely to be somewhat lessened by the inclusion of a much higher percentage of the observed data than is possible with the rigorous method. To finally resolve this matter of practical consequences will require comparisons between results obtained using both the rigorous and less rigorous methods.

The method decided upon for use here was the last alternative given above; to combine the results of point positioning and translocation in a network adjustment.

The three steps of the coordinate computations are to:

(a) compute a three dimensional, single station (point positioning), multipass set of coordinates (and their corresponding covariance matrix) for each tracking station, holding the orbit fixed, and using all available passes at each station.

(b) compute a six dimensional, two station, multipass (translocation) set of coordinates (and their corresponding covariance matrix) for each pair of stations for which passes were tracked simultaneously, using all simultaneous passes, and allowing the orbit to relax parallel to itself (as described in Chapter 4) consistently with the observations from both stations. The six coordinates and covariance matrix from each translocation solution are then propagated into three coordinate differences (the components of the interstation vector) and the corresponding covariance matrix.

(c) compute a network adjustment using the model

$$\Delta x_{ij} = x_i - x_j$$

where x_i and x_j are the coordinates of stations i and j computed in step (a), and Δx_{ij} are the components of the interstation vector between i and j computed in step (b). The inference upon which the use of this model is based, is that x_i and Δx_{ij} are different observables , albeit ultimately traceable to intersecting sets of Doppler measurements. However the rationale for using this approach is strictly pragmatic; and no claim of rigour is made. All quantities are weighted in accordance with the covariance matrices computed in steps (a) and (b). The network adjustment merges the single station (point positioning) coordinates with the translocated interstation vectors to obtain a set of adjusted station coordinates, and the corresponding network covariance matrix.

This method of coordinate computation was chosen because the size of the already large arrays (due to the use of 4.6 second Dopplers) are kept small relative to the alternative methods. An additional advantage of this approach is that individual sets of station coordinates and interstation vectors can be examined, recomputed, added to or deleted from the network without having to recompute anything else but the network adjustment of step (c) (which from section 5.2.4 is a trivial contribution to the overall computing costs). On the other hand this same feature requires many more computer runs to perform all the point positioning and translocation solutions prior to the network adjustment, and therefore may be more expensive in computer time than a method of coordinate computation which required only one run per network.

Note that while the orbit was allowed to relax in the translocation solutions (step (b)), it was held fixed in the single station solutions

(step (a)). The reasoning behind this decision was based on the concept of "lines of position". In translocation, the magnitude of the orbit relaxation is constrained not only by the a priori weights assigned to the three orbit bias parameters, but also by the fact that the orbit must relax in a way that is consistent with observations from two stations. In other words there are two "lines of position" which together constrain the magnitude of the relaxation. However in the single station solution the magnitude of the orbit relaxation is constrained only by the a priori weights, and in this case allowing orbit relaxation in effect partitions the misclosures into residuals and orbit biases solely according to the relative magnitudes of the observable and orbit weights. One consequence of holding the orbit fixed for point positioning is that the resulting covariance matrices are smaller in magnitude than they would be had the orbit been relaxed.

There are alternative reasons for not holding the orbit fixed in point positioning, however. The systematic errors we are trying to absorb by relaxing the orbit are still there, and are unmodelled when the orbit is held fixed. Evidence supporting this is given is section 5.4.1. The smaller covariance matrix obtained by holding the orbit fixed should therefore be too optimistic. Evidence supporting this is given in section 5.4.2.

Conversely there may be arguments for not relaxing the orbit for the two-station translocation solution used here. The results of section 5.4 indicate that

(a) there is a significant discrepancy between point positioning distances and translocation distances (Table 5-20),

(b) the repeatability of point positioning distances is better than for translocation distances (Table 5-25),

(c) the conformity of point positioning distances to terrestrial

distances is better than for translocation distances (Tables 5-26 and 5-27).

These results do not support the arguments advanced earlier justifying the three step method of obtaining final coordinates. If the point positioning results are superior to the translocation results, then merging the two will degrade the point positioning rather than enhance it. However, validity of the translocation concept has been demonstrated by Westerfield and Worsley (1966); in the DOD Geoceiver test (DOD, 1972); by Gloeckler (1973), and elsewhere. Possible causes for the negative results encountered here are

(a) separately relaxing the orbit for each pair of tracking stations may bias the results, that is two station translocation may be incompatible with relaxing the orbit,

(b) both the translocation concept, and orbit relaxation have the same purpose - to reduce the effect of orbit errors. The effect of trying to do both translocation and orbit relaxation at the same time may be destructive rather than constructive, that is even multistation translocation may not be compatible with relaxing the orbit, and

(c) rigorous translocation requires rigorously identical data points from the translocation stations. Here we adopted the looser requirement (following the approach in DOD, 1972), that equal numbers of data points for each pass be selected from each station, rather than enforcing the more rigorous requirement for exactly identical data points. The data points at each station were required to be balanced about closest appraoach, which in general occurs at different times for different stations. It may be that enforcing identical data points would have improved the translocation results.

We mentioned at the beginning of this section that there are likely two principle sources of systematic errors causing inhomogeneity. One is orbit biases, which we have discussed. The other is residual refraction. This problem is not so clearly resolved as orbit biases. Part of the residual refraction is likely to be a local effect (indicating the use of individual scaling parameters for each station), and part may affect all stations equally (indicating a common scaling factor for all stations). In addition to systematic residual refraction (which can be modelled by a scaling factor), there will of course be some random residual refraction, which we can not model, and which will show up as part of the irreducible system noise. What relative weights should be assigned to

these two components of the residual refraction is not clear. In any case, no refractive scaling parameters were used at all in the work reported here.

6.2 Conclusions

The conclusions are divided into three groups: Those pertaining to the accuracy with which measurements are made; those concerning the consistency of the coordinates computed from these measurements; and those relevant to the operational aspects of the system.

6.2.1 Measurement accuracy

The three major contributions to errors in the measurements are from

(a) operational ephemeris errors

(b) ionospheric and tropospheric refraction

(c) receiver contributions.

The magnitude of the first of these, from Tables 4-7 and 4-8, determined from biases between the operational and NWL precise ephemerides and expressed as satellite position errors, has standard deviations of about 2, 0.5 and 1 broadcast units (26, 5 and 10 m) respectively along track, radially and cross track. From Table 5-8 multipass sets of orbit errors are biased by between 0 and 10 m along track and between 0 and 6 m in the slant range direction (the sum of the radial and cross track components), and are scattered by 30 to 50 m along track, and 10 to 15 m in slant range. One systematic source of orbit errors in the test data used here which has since been eliminated (Piscane et al, 1973) is that the operational ephemeris was not referred either to the average terrestrial (CIO) pole or instantaneous terrestrial pole (Figure 5-8).

The operational ephemeris functions $\Delta E(t)$, $\Delta a(t)$ and $\eta(t)$

(defined in Table 4-2) can be well represented by the base functions $\Phi = \{1, \cos 2nt, \sin 2nt, t\}$, where n is the mean motion (defined in Table 4-1). The fit of Φ to NWL precise ephemeris coordinates is within the roundoff error in these coordinates, and $\dot{\Phi}$ then also fits the precise ephemeris velocities within ten times the roundoff error in these velocities (Tables 4-9 and 4-10). The fit of Φ to the operational ephemeris is within the roundoff error in $\Delta E(t)$, $\Delta a(t)$, $\eta(t)$ (Tables 4-11 and 4-12). Biases between the Φ approximants to the operational ephemeris and the precise ephemeris are substantially the same as biases between the operational ephemeris itself and the precise ephemeris (Tables 4-13 and 4-14).

Modelling ionospheric refraction by a two-frequency dispersive model (section 2.4) and tropospheric refraction by the Hopfield model (section 2.3), and rejecting data within 8° of the horizon, leaves some residual tropospheric refraction errors in the data (Figures 5-6 and 5-7), affecting single pass station coordinates by up to 5 m.

The receiver contribution to measurement precision varies considerably from receiver to receiver. From Table 5-7 multipass sets of measurement residuals had sample standard deviations of 0.9, 1.6 and 2.0 counts respectively for ITT 5001, Marconi 722 and Magnavox 702 receivers. All such sample standard deviations closely fitted the standard deviation of the best fitting normal curve. All such sets of residuals were skewed (moment coefficients of skewness between -0.27 and +0.05) and leptokurtic (moment coefficients of kurtosis between 3.3 and 5.3). The biases (sample means) of these sets were 0, 0.05 and 0.06 counts respectively for the ITT, Marconi and Magnavox receivers.

The sample standard deviation of these residuals exhibits an elevation angle dependence (Figures 5-4 and 5-5) which may indicate the presence of residual refraction at low angles, and reflect the decreased

sensitivity of the dipole antenna at high angles.

The satellite reference oscillator frequency drift rates, averaged over one year, are between 0.04 and 0.6 parts in 10^{10} per day (Table 2-2). The receiver reference oscillator frequency drift rates, averaged over about one month, are between 1 and 10 parts in 10^{10} per day. The receiver frequencies are offset from their nominal values by between 100 and 1500 parts in 10^{10} (Figure 5-9 and Table 5-9).

6.2.2 Consistency of station coordinates

The point positioning coordinates obtained for the test data have an rms estimated standard deviation of 1.3 m (Table 5-12). However in these computations the satellite orbit was held fixed. Three results indicate the orbit should be relaxed:

(a) the multipass point positioning 95% confidence level chi-square test on estimated variance factors results in 25% rejection for ITT data with the orbit fixed, and 3% with the orbit relaxed (section 5.4.1).

(b) using 20 pass subsets of the 659 passes obtained at 1973 Fredericton to compute independent point positioning coordinates, the ratio of the sample standard deviations of these coordinates to the average of the estimated standard deviations resulting from the point positioning solutions is 2.5 to 4.0 when the orbit is fixed and 1.2 to 1.5 when the orbit is relaxed (section 5.4.1).

(c) the external consistency between Transit and terrestrial interstation distances indicates that the Transit estimated covariance matrices are too optimistic. Relaxing the orbit increases the estimated variances of the Transit coordinates, and hence of the interstation distances.

For the 1972 and 1973 data, the point positioning repeatability in the coordinates was between 4 and 10 m (Table 5-24), and in distance was between 1 and 5 m, with external consistency index 1.0 (Table 5-25). The coordinate shifts are attributed in large part to pole motion effects.

The conformity of point positioning distances to terrestrial distances was better than 4 m, with external consistency indices 1.0 and 1.7 for 1973 and 1972 data (Tables 5-26, 5-27). Translocated interstation distances differed from point positioning distances with an rms value of 3.7 m (Table 5-20). Repeatability between 1972 and 1973 was from 2 to 11 m (Table 5-24). Conformity with terrestrial distances ranged from 1 to 8 m (Table 5-26, 5-27). The poor translocation results may be due to attempting to relax the orbit while translocating; to non-rigorous data point matching; or to other unidentified causes.

6.3.3 Operational considerations

The observing time to obtain a point positioning 95% confidence region smaller than 5 m is 3 days (35 passes), 5 days (80 passes) and 20 days (160 passes) respectively for the ITT, Marconi and Magnavox receivers (Table 5-14). To obtain translocated interstation vectors with a 10 m 95% confidence region requires between 20 and 70 simultaneous passes (Table 5-16).

The data rejection rate for the test data is about 65%, composed of 24% passes not tracked, 10% fail majority voting, 10% elevation below 10°, 10% less than 75 Doppler measurements per pass, 6% other filtering rejects, and 6% multipass chi-square rejections (section 5.2.3).

The cost of processing the test data using the methods described in section 5.2.2 is $4000, broken into $2.23 per accepted pass, or $36 per observing day.

6.3 Suggestions for Future Work

It is recommended that

(a) a test set of measurements obtained using geodetic receivers be analyzed and compared with the results presented here.

(b) a test set of measurements obtained since January 27, 1974 (since which time the operational ephemeris is referred to the average terrestrial pole) be analyzed and compared with the results presented here.

(c) the operational ephemeris be relaxed in point positioning solutions.

(d) a residual tropospheric refraction correction be incorporated into the observation equation.

(e) the Doppler integration interval of 4.6 seconds be retained for data filtering, but that the filtered data be compressed for coordinate computation, either by combining the filtered data into longer integration intervals, or by using some other set of parameters to represent the single pass contribution to a multipass solution (for example the Guier plane coordinates).

(f) the correlation between Doppler measurements be taken into account.

(g) alternatives to the network adjustment strategy used here be investigated, particularly computing adjusted coordinates in one step rather than three (Kouba, 1974), perhaps facilitated by adoption of (e).

(h) the application of the methods described here to networks of moving stations (Thorndike 1973; 1974) be investigated.

(i) alternative methods of implementing translocation (orbit fixed, rigorous data point matching) be tested and compared with the results obtained here.

REFERENCES

Abramowitz, M. and Stegun, I.A. (1965). "Handbook of mathematical functions". Dover.

Anderle, R.J. (1972). "Pole position for 1971 based on Doppler satellite observations". Technical report TR-2734, U.S. Naval Weapons Laboratory.

Anderle, R.J. (1973a). "Determination of polar motion from satellite observations". Geophysical Surveys, 1, 147-161.

Anderle, R.J. (1973b). "Pole position for 1972 based on Doppler satellite observations". Technical report TR-2952, U.S. Naval Weapons Laboratory.

Anderle, R.J. (1974). "Transformation of terrestrial survey data to Doppler satellite datum". Journal of Geophysical Research (in press).

Barrell, H. and Sears, J.E. (1939). "The refraction and dispersion of air for the visible spectrum". Royal Society of London, Philosophical Transactions, Series A, 238, 1-64

Brouwer, D. (1963). "Minor secular and long-period effects" in Proceedings of the first international symposium on the use of artificial satellites for geodesy. North Holland, Amsterdam.

Brown, D.C. and Trotter, J.E. (1969). "SAGA, a computer program for short arc geodetic adjustment of satellite observations". U.S. Air Force Cambridge Research Laboratories report.

Brown, D.C. (1970). "Near term prospects for positional accuracies of 0.1 to 1.0 metres from satellite geodesy". U.S. Air Force Cambridge Research Laboratories report AFCRL-70-0501.

Brown, D.C. and Trotter, J.E. (1973). "Extensions to SAGA for the geodetic reduction of Doppler operations". U.S. Air Force Cambridge Research Laboratories report AFCRL-TR-73-0177.

CGPM (1960). Resolution 6. 11th General Conference of Weights and Measures.

CGPM (1967). Resolution 1. 13th General Conference of Weights and Measures.

Chauvenet, W. (1891). "A manual of spherical and practical astronomy". Dover reprint, 1960.

Cheney, E.W. (1966). "Introduction to approximation theory". McGraw-Hill.

CSA (1973). "The international system of units". Canadian Standards Association Standard Z234.2.

Dixon, W.J. (1962). "Rejection of observations", in Sarhan, A.E. and Greenberg, B.G. Contributions to order statistics. Wiley.

Dunnell, C.A. (1967). "TRANET Doppler tracking system". APL Technical Digest, 6, No. 4, 17-23.

Edlen, B. (1966). "The refractive index of air". Metrologia, 2, 71.

Essen, L. and Froome, K.D. (1951). "The refractive indices and dielectric constants of air and its principal constituents at 24,000 mc/s". Proceedings of the Physical Society of London, B64, 862-875.

Evenson, K.M., Wells, J.S., Petersen, F.R., Danielson, B.L., Day, G.W., Barger, R.L., and Hall, J.L. (1972). "Speed of light from direct frequency and wave length measurements of the methane-stabilized laser". Physical Review Letters, 29, 1346-1349.

Gill, T.P. (1965). "The Doppler effect". Academic.

Goff, J.A. and Gratch, S. (1946). "Low-pressure properties of water from -160 to 212 F". Transactions of the American Society of Heating, Refrigerating and Air-conditioning Engineers, 52, 95-122.

Grant, S.T. (1973). "Rho-rho Loran-C combined with satellite navigation for offshore surveys". International Hydrographic Review, 50, No. 2, 35-54.

Guier, W.H. and Weiffenbach, G.C. (1960). "A satellite Doppler navigation system". Proceedings of the Institute of Radio Engineers, 48, 507-516.

Guier, W.H. (1963). "Studies on Doppler residuals - 1: Dependence on satellite orbit error and station position error". Report TG-503, The Johns Hopkins University Applied Physics Laboratory.

Guier, W.H. (1965). "Satellite geodesy". APL Technical Digest, 4, No. 3, 2-12.

Guier, W.H. (1967). "Data and orbit analysis in support of the U.S. Navy satellite Doppler system". Philosophical Transactions of the Royal Society of London, Series A, 262, 89-99.

Hadgigeorge, G. (1972). "The geodetic positioning capability of the geoceiver". Proceedings of the symposium on satellite and terrestrial triangulation, Graz, p.117-133.

Hagglund, J.E. (1974). "The effect of course and speed errors on a satellite fix position". B.Sc. report, Surveying Engineering Department, University of New Brunswick.

Hald, A. (1952). "Statistical theory with engineering applications". Wiley.

Hamilton, W.C. (1964). "Statistics in physical science". Ronald.

Hirvonen, R.A. (1971). "Adjustment by least squares in geodesy and photogrammetry". Ungar.

Hogg, R.V. and Craig, A.T. (1971). "Introduction to mathematical statistics". McMillan.

Hopfield, H.A. (1969). "Two-quartic tropospheric refractivity profile for correcting satellite data". Journal of Geophysical Research, 74, 4487-4499.

Hopfield, H.S. (1971). "Tropospheric effect on electromagnetically measured range: prediction from surface weather data". Radio Science, 6, 357-367.

Hopfield, H.S. (1972). "Tropospheric refraction effects on satellite range measurements". APL Technical Digest, 11, No. 4, 11-19.

Hopfield, H.S. and Utterback, H.K. (1973). "Tropospheric effect on electromagnetic range measurement at oblique angles". Transactions of the American Geophysical Union, 54, 232 (abstract).

IEEE (1972). "IEEE standard dictionary of electrical and electronics terms". Wiley.

IUGG (1958). Resolution 1. Compte Rendu of the XI General Assembly of the International Union of Geodesy and Geophysics, Bulletin Geodesique, 47, 91.

Jenkins, F.A. and White, H.E. (1957). "Fundamentals of optics". McGraw-Hill.

JMR (1973). "The JMR-1 Doppler survey set description and application". Document No. 73288, JMR Instruments Inc., Granada Hills, Cal.

Kaula, W.M. (1966). "Theory of satellite geodesy". Blaisdell.

Kerslake, R.W. (1973). "The economics of geodetic control from Doppler satellite observations". B.Sc. report, Surveying Engineering Department, University of New Brunswick.

Kirkham, B.P. (1972). "An improved weighting scheme for satellite Doppler observations". B.Sc. thesis, Surveying Engineering Department, University of New Brunswick.

Korn, G.A. and Korn, T.M. (1968). "Mathematical handbook for scientists and engineers". McGraw-Hill.

Kouba, J. (1970). "Generalized sequential least squares expressions and MATLAN programming". M.Sc. thesis, Surveying Engineering Department, University of New Brunswick.

Kouba, J. (1972). "Principal property and least squares adjustment design". The Canadian Surveyor, 26, 136-145.

Kouba, J. (1974). "Reduction of Doppler satellite data observed in Canada in 1973". The Canadian Surveyor, 28.

Krakiwsky, E.J. (1968). "Sequential least squares adjustment of satellite triangulation and trilateration in combination with terrestrial data". Report 114, Department of Geodetic Science, The Ohio State University.

Krakiwsky, E.J. and Kouba, J. (1970). "An exploratory investigation into satellite positioning techniques to be employed in Canadian continental shelf and arctic areas". Technical Report 4, Surveying Engineering Department, University of New Brunswick.

Krakiwsky, E.J. and Wells, D.E. (1971). "Coordinate systems in geodesy". Lecture Notes 16, Surveying Engineering Department, University of New Brunswick.

Krakiwsky, E.J., Wells, D.E., and Kirkham, B.P. (1972). "Geodetic control from Doppler satellite observations". The Canadian Surveyor, 26, 146-162.

Krakiwsky, E.J., Wells, D.E. and Thomson, D.B. (1973). "Geodetic control from Doppler satellite observations for lines under 200 km". The Canadian Surveyor, 27, 141-148.

Krakiwsky, E.J. and Thomson, D.B. (1974). "Mathematical models for the combination of terrestrial and satellite networks". The Canadian Surveyor, 28.

Laidet, L.M. (1972). "Worldwide synchronization using the Transit satellite system". Proceedings of the Institute of Electrical and Electronic Engineers, 60, 630-632.

Luenberger, D.G. (1969). "Optimization by vector space methods". Wiley.

Magnavox (1971). "Radio receiver set AN/PRR-14". Part No. 709478-801, Magnavox Research Laboratories, Torrance, Cal.

Marconi (1974). "Satellite position location/navigation system CMA-722B". Publication 722-2, Canadian Marconi Company, Montreal, Que.

Moffett, J.B. (1971). "Program requirements for two minute integrated Doppler satellite navigation solution". Technical Memorandum TG-819-1. Applied Physics Laboratory, The Johns Hopkins University, Silver Spring, Maryland.

Nassar, M.M. (1972). "Least squares adjustment of Doppler satellite observations". M.Sc. thesis, Technical Report 21, Surveying Engineering Department, University of New Brunswick.

Nassar, M.M. (1972). "Program DOPSATS - phased least squares adjustment of Doppler satellite observations for a single motionless tracking station". Technical Report 18, Surveying Engineering Department, University of New Brunswick.

Newton, R.R. (1967). "The Navy Navigation Satellite System". Space Research VII, 2, 735 - 763

Ogunbayo, E.A. (1971). "Geodetic positioning by Doppler satellite observations". B.Sc. thesis, Surveying Engineering Department, University of New Brunswick.

Piscane, V.L., Holland, B.B. and Black, H.D. (1973). "Recent (1973) improvements in the navy navigation satellite system". Navigation, 20, 224-229.

Rindler, W. (1969). "Essential relativity." Van Nostrand

Romanowski, M. (1970). "The theory of random errors based on the concept of modulated normal distributions". Report NRC-11432, Division of Physics, National Research Council of Canada.

Rowley, W.R.C. and Hamon, J. (1963). "Some measurements of asymmetry of spectral line profiles". Revue d'Optique, 42, 519-531.

Saastamoinen, J.J. (1973). "Contributions to the theory of atmospheric refraction". Bulletin Geodesique, 107, 13-34.

Schmid, H.H. and Schmid, E. (1965). "A generalized least squares solution for hybrid measuring systems". The Canadian Surveyor, 19, 27-41.

Sims, T. (1972). "The NWL precise ephemeris". Technical report TR-2872, U.S. Naval Weapons Laboratory.

Smith, E.K. and Weintraub, S. (1953). "The constants in the equation for atmospheric refractive index at radio frequencies". Proceedings of the Institute of Radio Engineers, 41, 1035-1037.

Smithsonian (1971). "Smithsonian meteorological tables". Sixth edition, Fifth reprint, Smithsonian Institution Press, Washington.

Stansell, T.H. (1971). "Transit, the navy navigation satellite system". Navigation, 18, 93-109.

Terrien, J. (1974a). "International agreement on the value of the velocity of light". Metrologia, 10, 9.

Terrien, J. (1974b). "News from the Bureau International des Poids et Mesures". Metrologia, 10, 75-77.

Tienstra, J.M. (1956). "Theory of the adjustment of normally distributed observations". Argus, Amsterdam.

Thomson, D.B., Nassar, M.M. and Merry, C.L. (1974). "Distortions of Canadian geodetic networks due to the neglect of deflections of the vertical and geoidal heights". The Canadian Surveyor, 28.

Thomson, D.B. and Krakiwsky, E.J. (1974). "Combination of geodetic networks" Technical Report 28, Surveying Engineering Department, University of New Brunswick (in preparation).

Thorndike, A.S. (1973). "An integrated system for measuring sea ice motions". Proceedings of the 1973 IEEE International Conference on Engineering in the Ocean Environment, p.490-499.

Thorndike, A.S. (1974). "Strain calculations using AIDJEX 1972 position data". Arctic Ice Dynamics Joint Experiment Bulletin 24, University of Washington, Seattle.

Udoffa, I.M. (1973). "The application of four radio positioning systems in the 1972 hydrographic survey of the Labrador coast". M.Eng. report, Surveying Engineering Department, University of New Brunswick.

URSI (1957). Resolution 6. Proceedings of the XII General Assembly of International Union of Radio Science, VOL XI, Part 1, Commission I, On Radio Measurements and Standards, p. 78.

Vaníček, P. (1971). "Further development and properties of the spectral analysis by least squares". Astrophysics and Space Sciences, 12, 10-73.

Vaníček, P. (1972). "Tensors". Lecture Notes 27, Surveying Engineering Department, University of New Brunswick.

Vaníček, P. and Wells, D.E. (1972). "The least squares approximation and related topics". Lecture Notes 22, Surveying Engineering Department, University of New Brunswick.

Vaníček, P. (1973). "Introduction to adjustment calculus (second edition)". Lecture Notes 35, Surveying Engineering Department, University of New Brunswick.

Wade, R.L. (1973). "Three dimensional adjustment and analysis of Doppler translocation networks". B.Sc. report, Surveying Engineering Department, University of New Brunswick.

Weiffenbach, G.C. (1967). "Tropospheric and ionospheric propagation effects on satellite radio Doppler geodesy". pp.339-352 in Electromagnetic Distance Measurement, University of Toronto Press.

Wells, D.E. and Krakiwsky, E.J. (1971). "The method of least squares". Lecture Notes 18, Surveying Engineering Department, University of New Brunswick.

Wells, D.E. (1972). "Fast and simple alert computations for Transit satellites". Technical Report 19, Surveying Engineering Department, University of New Brunswick.

Wells, D.E., Krakiwsky, E.J. and Thomson, D.B. (1974). "Internal and external consistency of networks". The Canadian Surveyor, 28.

Wells, D.E. and Vaníček, P. (1975). "Least squares spectral analysis". Submitted to Communications of the Association for Computing Machinery.

Wells, D.E. (1975). "Doppler satellite programs description and documentation". (in preparation).

Westerfield, E.E. and Worsley, G. (1966). "Translocation by navigation satellite". APL Technical Digest, 5, No. 5, 2-10.

Willke, T.A. (1965). "Useful alternatives to Chauvenet's rule for rejection of measurement data". U.S. National Bureau of Standards Statistical Engineering Laboratory mimeographed report.

Willman, J.F. and Tucker, A.J. (1968). "Accuracy of satellite Doppler data for ionospheric study, navigation and geodesy". Journal of Geophysical Research, 73, 385-392.

Wonnacott, T.H. and Wonnacott, R.J. (1972). "Introductory statistics", second edition, Wiley.

Ying Chung-Chi (1972). "On phased adjustment". Survey Review, 20, 282-288 and 298-309.

Yionoulis, S.M. (1970). "Algorithm to compute tropospheric refraction effects on range measurements". Journal of Geophysical Research, 75, 7636-7637.

DOD, (1972). "Report of the DOD Geoceiver test program". DMA Report 0001, Defense Mapping Agency, U.S. Department of Defense, Washington.

Vanicek, P. (1973). "Dynamic satellite geodesy". Lecture notes 32, Surveying Engineering Department, University of New Brunswick.

Moller, P. (1952). "The theory of relativity". Oxford.

Gloeckler, F.M. (1973). "Recent translocation results using navigation satellites". Preprint.

APPENDIX A

STATISTICAL TESTS

In this appendix we outline three statistical tests used in Chapters 4 and 5. These are a normality test, used to reject individual observations; a chi-square test, used to reject sets of observations; and a chi-square goodness-of-fit test between a histogram of observed frequencies and predicted frequencies given by a hypothetical distribution. The discussion of this last test leads to an algorithm for finding the normal distribution which best fits a set of observed frequencies.

A.1 Rejection of Individual Observations

Assume we are given a sample of n observations (or residuals) x_i which have been drawn from a normally distributed population $N(\mu,\sigma)$. We suspect that the sample is contaminated by one or more values x_i which do not come from this population, since they are far removed from the remaining values (that is we suspect them to be gross errors or blunders). We require some criterion with which we can decide to accept or reject these values as part of the sample.

There are four cases distinguished by our knowledge of the population from which the sample has been drawn.

(a) both μ and σ are known

(b) only σ is known

(c) neither μ or σ is known, however an independent (uncontaminated) estimate of the sample standard deviation is available.

(d) neither μ or σ is known, and no independent estimate of the sample standard deviation is available.

If our sample consists of residuals resulting from a least squares estimation, the population mean is zero, and the population variance is given by the a priori variance factor. Assuming the latter is known the problem belongs to case (a) above. A complete answer to the question of how to select a rejection criterion, particularly for cases (b), (c), (d), is not available, but a considerable literature exists. See for example the review by Dixon (1962). Here we consider only case (a).

Let us draw a sample z_i of only one element from a population distributed N(0,1). The probability that the value of z_1 exceeds some value B is

$$P(z_1 > B) = \int_B^\infty \phi(t)\, dt = \alpha_1 \quad , \tag{A-1}$$

where $\phi(t)$ is the normal distribution probability density function. Let us draw another sample y_i of n elements from the same population and order them in increasing value from y_1 to y_n. The probability that any particular element of y_i exceeds B is

$$P(y_i > B) = \alpha_1 \quad . \tag{A-2}$$

The probability that <u>at least one</u> of the elements of y_i (i.e. at least the n^{th}-ordered element y_n) exceeds B is the sum of the individual probabilities

$$\alpha_n = P(y_n > B) = 1-(1-\alpha_1)^n = 1-1 + n\alpha_1 + \text{h.o.t.} \simeq n\alpha_1 \tag{A-3}$$

We now make a basic assumption: for an appropriately small α_1 we interpret the existance of a value $z_1 > B$ (where B is from $P(z_1 > B) = \alpha_1$) as indicating that z_1 did not come from N(0,1). Similarly for an appropriately small α_n we interpret the existance of any value $y_i > B$ (where B is from $P(y_i > B) = \alpha_1 = \frac{\alpha_n}{n}$) as indicating that it did not come from N(0,1).

Under this assumption, for a sample x_i of n elements drawn from a

population distributed $N(\mu,\sigma)$, we reject at the $100(1 - \alpha)\%$ confidence level the hypothesis

$$\underline{\text{H: a particular } x_i \text{ comes from the population } N(\mu,\sigma)} \ ,$$

if for that particular x_i

$$y_i = \left| \frac{x_i - \mu}{\sigma} \right| > B \quad , \tag{A-4}$$

where B is computed from

$$P(y_i > B) = \int_B^{\infty} \phi(t)dt = \frac{\alpha}{n} \quad , \tag{A-5}$$

or

$$P(-\infty \leq y_i \leq B) = \int_{-\infty}^{B} \phi(t)dt = 1 - \frac{\alpha}{n} \quad . \tag{A-6}$$

The observation or observations corresponding to any residual value or values which fail this test are deleted from the set of observations and the least squares estimation is repeated without it or them.

For $\alpha = 0.25$ (75% confidence level) this rejection criterion has been called Chauvenet's Rule (Chauvenet, 1891; Willke, 1965; Hirvonen, 1971). Here we have used $\alpha = 0.1$ (90% confidence level).

An algorithm for computing B, the abscissa value of $N(\mu,\sigma)$ corresponding to probability α from

$$\alpha = \int_{-\infty}^{B} \phi(t)dt \quad , \tag{A-7}$$

is, if $\alpha > 0.5$, (Abramowitz and Stegun, 1965, equation 26.2.23)

$$B = \mu + \sigma \left[t - \frac{c_1 + c_2 t + c_3 t^2}{1 + c_4 t + c_5 t^2 + c_6 t^3} \right] \tag{A-8}$$

where

$$t = \left[\ell n \left(\frac{1}{(1 - \alpha)^2} \right) \right]^{1/2} \tag{A-9}$$

and

$$c_1 = 2.515517$$

$$c_2 = 0.802853$$

$$c_3 = 0.010328 \qquad \text{(A-10)}$$

$$c_4 = 1.432788$$

$$c_5 = 0.189269$$

$$c_6 = 0.001308$$

The value of B computed from (A-8) is accurate to within $\sigma/2000$.

A.2 Rejection of a set of Observations

Let v_i be a sample of n residuals resulting from the least squares estimation of u parameters. Letting V be the vector whose elements are v_i, we assume that V is drawn from a multivariate normal distribution $N(\theta,\Sigma)$, with zero vector of means θ, and covariance matrix Σ. Given the a priori weight matrix $P = \sigma_o^2 \Sigma^{-1}$, then the estimated variance factor is

$$\hat{\sigma}_o^2 = V^T P V /(n - u) \quad . \qquad \text{(A-11)}$$

The statistic $(n - u)\hat{\sigma}_o^2/\sigma_o^2$ is distributed $\chi^2(n - u)$ (Wells and Krakiwsky, 1971).

We reject at the 100 α% confidence level the hypothesis

$$\underline{\text{H: V is distributed N}(\mu,\sigma)} \quad ,$$

if

$$y = (n - u)\, \hat{\sigma}_o^2/\sigma_o^2 > c \quad , \qquad \text{(A-12)}$$

where c is computed from

$$P(y > c) = \int_c^\infty \phi(t)dt = \alpha \quad , \qquad \text{(A-13)}$$

and $\phi(t)$ is the chi-square probability density function with $(n - u)$ degrees of freedom.

The set of observations corresponding to the residuals forming V in (A-11) are deleted if this hypothesis is rejected.

An algorithm for computing c, the abscissa value of $\chi^2(\nu)$ corresponding to probability α is (Abramowitz and Stegun, 1965, equation 26.4.17)

$$c = \nu \left[1 - \frac{2}{9\nu} + B \sqrt{\frac{2}{9\nu}} \right]^3 \quad , \tag{A-14}$$

where B is the abscissa value of N(0,1) corresponding to probability α, given by (A-8). The accuracy of c given by (A-14) is within 0.04 for $\nu > 1$.

A.3 Chi-square Goodness-of-fit Test

Given a set of observed frequencies f_i, $i = 1,2,\ldots,n$, $\sum_i f_i = N$ and a distribution function $\phi(t)$, $\int_{-\infty}^{\infty} \phi(t)dt = 1$, we wish to determine whether the observed frequencies adequately approximate $\phi(t)$ or not.

To obtain a discrete function from $\phi(t)$ we use the approximation

$$\int_a^b \phi(t)dt \simeq \int_a^b \phi\left(\frac{a+b}{2}\right)dt = (b-a)\,\phi\left(\frac{a+b}{2}\right) \quad , \tag{A-15}$$

then

$$\int_{-\infty}^{\infty} \phi(t)dt \simeq \sum_i (b_i - a_i)\,\phi\left(\frac{a_i + b_i}{2}\right) = \sum_i p_i = 1 \quad , \tag{A-16}$$

where the (a_i, b_i) are determined from the boundaries of the classes having the frequencies f_i.

Since $\Sigma f_i = N$ and $\Sigma p_i = 1$, we must scale one or the other of these in order to compare them. Multiplying the p_i by N we compute the differences $(f_i - Np_i)$. For sufficiently large N the chi-square goodness-of-fit statistic

$$y = \sum_{i=1}^{n} \frac{(f_i - Np_i)^2}{Np_i} \quad , \tag{A-17}$$

is distributed approximately as $\chi^2(\nu)$, where $\nu = n - 1 - u$, n being the number of classes, and u being the number of parameters of $\phi(t)$ which have been estimated from the observed data (Hogg and Craig, 1971; Hamilton, 1964).

We reject at the 100 α% confidence level the hypothesis

H: the f_i are distributed as $\phi(t)$,

if

$$y > c \quad , \tag{A-18}$$

where c is computed from (A-14).

If $Np_i < 5$ that class is either omitted from the comparison or combined with adjacent classes so that their sum exceeds 5 (in which case n is reduced accordingly) (Hogg and Craig, 1971; Hamilton, 1964).

As pointed out by Wonnacott and Wonnacott (1972), the above hypothesis can always be rejected by making N large enough. In fact this is the case here, where N ranged from 7500 to 90000 residuals per tracking station. The chi-square goodness-of-fit statistic was used, however, in fitting normal distributions to observed frequencies, as described in the next section.

A.4 Best Fitting Normal Distribution

Given a set of observed frequencies f_i, one best fitting normal distribution is defined by those values of μ and σ for which the chi-square goodness-of-fit statistic (A-17) is a minimum. However, in our case the f_i are based on residuals from least squares estimations, so we will specify $\mu = 0$ a priori. Then the best fitting normal distribution is defined by that value of σ for which the chi-square goodness-of-fit statistic is a minimum.

This is a nonlinear least squares approximation problem (section 3.1.6). The known function is composed of the observed frequencies f_i which we want to approximate by the function Np_i, which in our case is nonlinear in the parameter σ (or more generally in both μ and σ). We want to minimize the mean quadratic distance $\rho(f_i, Np_i)$. If we select $1/Np_i$ as the weight function, then

$$\rho(f_i, Np_i) = \sum_i \frac{(f_i - Np_i)^2}{Np_i} \quad , \tag{A-19}$$

and minimizing $\rho(f_i, Np_i)$ is equivalent to minimizing the chi-square

goodness-of-fit statistic. Of course we are free to choose other weight functions (for example the unit function), and we then obtain the best fitting normal distribution in some other sense than being the one to minimize the chi-square goodness-of-fit statistic.